PAPR and ICI Reduction Techniques for OFDM Based Satellite Communication Systems

Emad Al-Dalakta

Newcastle University

Newcastle upon Tyne, UK.

A thesis submitted for the degree of

Doctor of Philosophy

June 2012

Declaration

I declare that this thesis is my own work and it has not been previously submitted, either by me or by anyone else, for a degree or diploma at any educational institute, school or university. To the best of my knowledge, this thesis does not contain any previously published work, except where another person's work used has been cited and included in the list of references.

Emad Yacoub Qeryaqos Al-Dalakta

I dedicate this thesis to my precious wife, Hiyam, and children, Astefanos and Irene, who have supported me throughout the years of my study, especially in the years that I was working on this thesis.

With all my love

Acknowledgements

Foremost, I would like to express my sincere gratitude to my first supervisor, Prof. Bayan Sharif, for the continuous support of my PhD study and research, for his patience, motivation, enthusiasm and immense knowledge. His guidance helped me throughout the research and writing of this thesis. I would like to thank my second supervisor Dr. Charalampos Tsimenidis whose encouragement, guidance and support from the initial to the final level enabled me to develop an understanding of the subject. Dr. Tsimenidis has always encouraged me to work in new areas and he has been patient and tolerant of my weaknesses in written English. I would like to thank my third supervisor, Dr. A. Arafat, as his support of this project was greatly needed and deeply appreciated. Dr. Arafat was particularly helpful in assessing the technical concepts of this research. I owe my deepest gratitude to Dr. A. Hazmi for his help in checking my simulation codes and polishing the figures for the Journal papers. I would like also to show my gratitude to Dr. Robert Baxley for his guidance and help on complexity calculation. It is a pleasure to thank our lovely postgraduate research coordinator, Mrs. Gill Webber, for her assistance in numerous ways.

I offer my regards and blessings to all those who supported me in any respect during the completion of the project; I would especially like to thank my parents, who have supported me throughout my life. I thank them from the bottom of my heart for giving birth to me in the first place and supporting me spiritually throughout my life. I would also like to show my gratitude to my brother and my sisters for their moral support.

Lastly, I would like to express my sincere gratitude to my sponsor the Ministry of Higher Education in Iraq who have given me the opportunity of an education at the best universities in the UK.

Abstract

Multi-carrier systems such as orthogonal frequency division multiplexing (OFDM) are significantly affected by peak-to-average-power ratio (PAPR). Unfortunately, the high PAPR inherent to OFDM signals envelopes will occasionally drive high power amplifiers (HPAs) to operate in the nonlinear region of their characteristic curve. The nonlinearity of the HPA exhibits amplitude and phase distortions, which cause loss of orthogonality among the subcarriers (SCs), and hence, inter-carrier interference (ICI) is introduced in the transmitted signal. The ICI power is proportional to the amplitude of the signal at the amplifier input and it may cause a considerable bit error rate (BER) degradation.

A plethora of research has been devoted to reduce the performance degradation due to the PAPR problem inherent to OFDM systems. Some of the reported techniques such as amplitude clipping have low-complexity; on the other hand, they suffer from various problems such as in-band distortion and out-of-band expansion. Signal companding methods have low-complexity, good distortion and spectral properties; however, they have limited PAPR reduction capabilities. Advanced techniques such as coding, partial transmit sequences (PTS) and selected mapping (SLM) have also been considered for PAPR reduction. Such techniques are efficient and distortionless, nevertheless, their computational complexity is high and requires the transmission of several side information (SI) bits.

In this thesis, a new low-complexity scheme is proposed based on the PTS that employs two inverse fast Fourier transforms (IFFTs) and two circulant transform matrices, in order to reduce complexity and improve the system performance. Furthermore, the low-complexity scheme is simplified by omitting one of the circulant transform matrices in order to reduce both the computational complexity and the number of SI bits at the cost of a small reduction in PAPR and BER performance.

It is well known that, accurate PAPR estimation requires oversampling of the transmitted signal, which in turn results in increased complexity. More importantly, minimising the PAPR does not necessarily minimise the distortion produced by the nonlinearity of the HPA. Therefore, minimising PAPR does not necessarily imply that the BER will be minimised too. Efficient and less complex schemes for BER reduction of OFDM systems in the presence of nonlinear HPA and/or carrier frequency offset (CFO) are proposed. These proposed techniques are based on predicting the distortion introduced by the nonlinearity of HPA and/or CFO. Subsequently, techniques such as the PTS and SLM are invoked to minimise the distortion and BER. Three distortion metrics are adopted in this thesis: inter-modulation distortion (IMD), peak interference-to-carrier ratio (PICR) and distortion-to-signal power ratio (DSR). Monte Carlo simulations will confirm that the DSR and PICR are more reliable than the PAPR and IMD for selecting the coefficients of the PTS and SLM to minimise the BER. Furthermore, complexity analyses demonstrate that the proposed schemes offer significant complexity reduction when compared to standard PAPR-based methods.

A closed form solution for accurate BER for the OFDM signals perturbed by both the HPA nonlinearity and CFO was derived. Good agreement between the simulation results and the theoretical analysis can be obtained for different HPA parameters and CFOs.

Finally, efficient approaches to reduce the impact of nonlinear power amplifiers with respect to the BER of OFDM systems are proposed. These are approaches based on: the well-established PAPR schemes, a power amplifier model and a simple single point cross correlator. The optimum phase sequence within the proposed approaches is selected by maximising the correlation between the input and output of the power amplifier model. Simulation results have confirmed that the BER using the proposed approaches is almost identical to the DSR, while the complexity is reduced significantly for particular system configurations.

Contents

List of Figures

List of Tables

Nomenclature

Acronyms

3G	Third-Generation
4G	Fourth-Generation
ABC	Artificial Bee Colony
ACE	Active Constellation Extension
AM/AM	Amplitude/Amplitude distortion
AM/PM	Amplitude/Phase distortion
AWGN	Additive White Gaussian Noise
BER	Bit Error Rate
BL	Basic-Layer
BO	Back-Off
BPSK	Binary Phase Shift Keying
CA	Complex Addition
CCDF	Complementary Cumulative Distribution Function
CCRR	Computational Complexity Reduction Ratio
CE	Cross Entropy
CFO	Carrier Frequency Offset
CM	Complex Multiplication
CP	Cyclic Prefix

CPS	Complex Phase Shift
CPSC	Complex Phase Shift Compensation
CPTS	Conventional Partial Transmit Sequences
CSLM	Conventional Selected Mapping
DAC	Digital-to-Analogue Converter
DPTS	Decomposition Partial Transmit Sequences
DSP	Digital Signal Processing
DSR	Distortion-to-Signal power Ratio
DVB-S2	Digital Video Broadcasting over Satellites
DVB-SH	Digital Video Broadcasting Satellite services to Handheld
DVB-T	Digital Video Broadcasting-Terrestrial
EL	Enhancement-Layer
EP	Excess Power
ESNR	Effective Signal-to-Noise Ratio
ETSI	European Telecommunications Standards Institute
FEQ	Frequency-Domain Equaliser
FFT	Fast Fourier Transform
FPGA	Field Programmable Gate Array
GA	Genetic Algorithm
GEO	Geostationary Earth Orbit
HM	Hierarchical Modulation
HPA	High Power Amplifier
IBO	Input Back-Off
ICI	Inter-Carrier Interference

IFFT	Inverse Fast Fourier Transform
ILI	Inter-Layer Interference
IMD	Inter-Modulation Distortion
IPTS	Iterative Partial Transmit Sequences
ISI	Inter-Symbol Interference
LC-IPTS	Low-Complexity Iterative Partial Transmit Sequences
LEO	Low Earth Orbit
LMS	Land Mobile Satellite
LOS	Line-Of-Sight
LTE	long term evolution system
MEO	Medium Earth Orbit
MIMO	Multiple-Input Multiple-Output
ML	Maximum Likelihood
MMSE	Minimum Mean Squared Error
MSE	Mean Square Error
MSM	Multi-points Square Mapping
NCT	Nonlinear Companding Transforms
OBO	Output Back-Off
OFDM	Orthogonal Frequency Division Multiplexing
PAPR	Peak-to-Average-Power Ratio
PIAR	Post-IFFT Amplitude Randomising
PICR	Peak Interference-to-Carrier Ratio
PSD	Power Spectrum Density
PSK	Phase Shift Keying

PSO	Particle Swarm Optimisation
PTS	Partial Transmit Sequences
QAM	Quadrature Amplitude Modulation
QPSK	Quadrature Phase Shift Keying
RA	Real Addition
RM	Real Multiplication
SA	Simulated Annealing
SC	Subcarrier
SI	Side Information
SISO	Single-Input Single-Output
SLC-IPTS	Simplified Low-Complexity Iterative Partial Transmit Sequences
SLM	Selected Mapping
SNR	Signal-to-Noise Ratio
SPS	Subblock Partition Scheme
SPW	Subblock Phase Weighting
SSPA	Solid-State Power Amplifier
TD	Total Degradation
TI	Tone Injection
TR	Tone Reservation
TWTA	Travelling Wave Tube Amplifier

List of Symbols

N	Number of subcarriers
λ	Ratio of the minimum distances in QPSK/16-QAM modulation
$\mathbf{d}$	Signal constellations sequence
d_k	Frequency-domain samples of $\mathbf{d}$
$\mathbf{D}$	Binary data matrix
$\mathbf{x}$	Data sequence
x_n	Time-domain data samples of $\mathbf{x}$
$\mathbf{s}$	OFDM symbol
s_n	Time-domain OFDM samples of $\mathbf{s}$
$\mathbf{y}$	Amplifier output vector
y_n	Time-domain samples of $\mathbf{y}$
$\mathcal{F}$	Nonlinear characteristics of the HPA
$\mathbf{z}$	Received sequence
z_n	Time-domain samples of $\mathbf{z}$
$\mathbf{r}$	Frequency-domain sequence
r_k	Frequency-domain samples of $\mathbf{r}$
$\hat{\mathbf{D}}$	Estimated binary data
$\boldsymbol{\eta}$	Noise vector
σ_η^2	Noise variance
$E\{.\}$	Expected value
σ_x^2	Variance of x_n
N_g	Cyclic prefix length
T_u	Time of the useful part of the OFDM symbol in seconds
T_s	Receiver sample rate
$(.)^T$	Transpose matrix
$(.)^{-1}$	Inverse matrix

$(.)^H$	Hermitian transpose matrix
$(.)^*$	Conjugate matrix
$\|\|.\|\|$	Euclidean norm of a vector
$\mathbf{W}$	Normalised $N \times N$ IFFT matrix
$\mathbf{W}^{-1}$	Normalised $N \times N$ FFT matrix
$j^2 = -1$	Imaginary unit
ρ_n	Absolute value of the time-domain samples at the HPA input
θ_n	Angle of the time-domain samples at the HPA input
$A(.)$	AM/AM conversion of the nonlinear amplifier
$\phi(.)$	AM/PM conversion of the nonlinear amplifier
G	Amplifier gain
A_{sat}	Amplifier input saturation voltage
A_0	Maximum amplifier output due to maximum input A_{sat}
p	Smoothness factor of the SSPA
K	Nonlinearity order
α_1, α_3	1^{st} and 3^{rd} order polynomial coefficients
$\mathcal{P}_{in}$	Average power of the OFDM symbol at the input of the amplifier
$\mathcal{P}_{out}$	Average power of the OFDM symbol at the output of the amplifier
a^i	i-th point constellation
c^i	Average r_k^i at i-th point constellation
t_{SG}	Time delay from satellite to ground
A_{SG}	Propagation path loss from satellite to ground
f_{SG}	Doppler shift due to satellite motion
$\triangle\tau_n$	n-th tap-delay related to the multipath propagation
G_n	n-th tap-gain related to the multipath propagation
f_d	Maximum Doppler shift related to the mobile motion
v	Speed of the mobile motion
f_c	Carrier frequency
c	Speed of light
θ	Elevation angle
P_e	Probability of error
γ_b	SNR per bit for each subcarrier
γ_s	SNR per symbol

$x(t)$	Continuous time-domain signal
L	Oversampling factor
$\|.\|$	Absolute value of a complex variable
$F(z)$	Cumulative distribution function
$P_r(\text{PAPR})$	Probability of the PAPR
α	Certain number
R	Coding rate
$b^{(v)}$	Complex weighting phase factors for the PTS scheme
V	Number of partition in PTS scheme
$\mathbf{d}^{(v)}$	Disjoint sets before the IFFT for the PTS scheme
$\mathbf{x}^{(v)}$	Time-domain samples after the IFFT for the PTS scheme
U	Number of partition in SLM scheme
$\mathbf{a}^{(u)}$	Complex weighting phase sequence for the SLM scheme
$\mathbf{d}^{(u)}$	Alternative input sequence for the SLM scheme
$\circ$	Hadamard product
$x_n^{(u)}$	Time-domain samples after the IFFT for the SLM scheme
$\mathbf{B}$	Frequency-domain peak reduction vector for the TR scheme
$\mathbf{T}_r$	Circulant transform matrix
$\hat{\mathbf{b}}$	Adjacent periodic weighting vector of $\mathbf{b}$
$\mathbf{R}$	Diagonal matrix of $\hat{\mathbf{b}}$
$\mathbf{t}_r$	The IFFT of $\hat{\mathbf{b}}$
$\mathbf{F}$	Normalised $LN \times LN$ IFFT matrix
$\mathbf{F}^{-1}$	Normalised $LN \times LN$ FFT matrix
$\mathbf{t}_r^{\langle k \rangle}$	Circularly right shifted version of the row vector $\mathbf{t}_r$ by element k
$\mathbf{d}^{(l)}$	Disjoint sets for the LC-IPTS and SLC-IPTS schemes, $l = 1, 2$
$\mathbf{x}^{(l)}$	Time-domain signals for the LC-IPTS and SLC-IPTS schemes, $l = 1, 2$
$\mathbf{x}_T$	Addition of the $\mathbf{x}^{(l)}$ after multiplication by the $\mathbf{T}_r^{(l)}$
$\mathbf{Y}_b$	Received signal after the FFT for the LC-IPTS and SLC-IPTS schemes
$\mathcal{I}$	Number of iterations for the PTS scheme
$\mathcal{I}_l$	Number of iterations for the LC-IPTS and SLC-IPTS schemes, $l = 1, 2$
g	Number of RAs required for each RM
A	Addition instructions
M	Multiplication operations

C	Equivalent complexity in terms of A and M
β	Useful part of the OFDM symbol
ψ_k	Nonlinear noise of the OFDM symbol
IBO_l	Linear IBO
Re{.}	Real part of a complex variable
Im{.}	Imaginary part of a complex variable
$\boldsymbol{\psi}$	Vector of nonlinear noise samples
$\overline{\text{DSR}}$	Normalised DSR
$\psi_{k,PTS}$	Nonlinear noise of the proposed PTS scheme
$\psi_k^{(v)}$	Nonlinear noise for each partition of the proposed PTS scheme
$\overline{\text{DSR}}_{PTS}$	Normalised DSR for the proposed PTS scheme
$\psi_{k,SLM}$	Nonlinear noise of the proposed SLM scheme
$\overline{\text{DSR}}_{SLM}$	Normalised DSR for the proposed SLM scheme
f_m	Mean number of multiplications
f_a	Mean number of additions
C_r	Relative complexity of the DSR criterion over the other schemes
σ_{ICI}^2	Variance of the ICI
$\Delta\varepsilon$	CFO
f	SC spacing
ε	Normalised CFO
η_n	Noise samples of $\boldsymbol{\eta}$
ω_k	The FFT of η_n
β_0	Complex phase shift of the useful part owing to CFO
β_{l-k}	Nonlinear noise component owing to CFO
ε_{wc}	Worst-case CFO
P	Variance of d_k

Chapter 1

Introduction

1.1 Background

Satellite communication systems comprising fixed and mobile systems are currently utilised to provide high data rate transmissions for broadcasting and multimedia services by employing efficient modulation schemes such as quadrature amplitude modulation (QAM). The main motivations for using QAM in mobile satellite systems are the power and spectral efficiencies. Consequently, QAM deployed in third-generation (3G) systems has become a robust candidate for fourth-generation (4G) wireless transmission systems [1]. In such applications, the performance of the satellite system is mainly dominated by the additive white Gaussian noise (AWGN). Thus, transmitting QAM symbols using single carrier systems is a reasonable approach. However, for emerging satellite technologies such as digital video broadcasting satellite services to handhelds (DVB-SH) [2], the mobility of the receiver causes time varying multipath propagation that requires high complexity receivers to combat its effects. To overcome this problem, multicarrier techniques such as orthogonal frequency division multiplexing (OFDM) have been adopted [2]. Although OFDM proved to be efficient for combating the multipath distortion introduced by the land mobile satellite (LMS) channels, other limitations such as the peak-to-average-power ratio (PAPR) may reduce the gain that can be achieved by using OFDM due to the use of high power amplifiers (HPAs) such as the travelling wave tube amplifier (TWTA). The nonlinearity of the TWTA exhibits AM/AM amplitude and AM/PM phase distortion, which cause loss of orthogonality among the subcarriers (SCs), and hence, inter-carrier interference (ICI) is introduced in the

transmitted signal [3]. The ICI power is proportional to the amplitude of the signal at the amplifier input and it may cause a considerable bit error rate (BER) degradation. On the other hand, quadrature phase shift keying (QPSK) modulation is utilised for low data rate communication due to its robustness against the nonlinear distortion caused by the amplifier, therefore the BER degradation is less than the QAM modulation.

To implement the OFDM for high data rate transmission, a noticeable increase in cost and complexity is added to the mobile satellite systems. The main advantages of the OFDM transmission scheme are as follows [4]:

- OFDM is an efficient technique for eliminating the multipath distortion; the complexity of channel equalisation in OFDM systems is significantly lower than that of single-carrier systems. As a result of the narrow bandwidth of each subchannel, the channel distortion in OFDM systems can be eliminated by utilising one-tap frequency-domain equalisers (FEQs).

- OFDM is robust against the narrowband interference; the interference of the SCs increase only by a small percentage due to narrowband interference.

- OFDM is attractive for broadcasting applications because it makes single-frequency networks possible.

However, the significant disadvantages of the OFDM transmission scheme are as follows:

- Its sensitivity to the ICI caused by carrier frequency mismatch between the transmitter and receiver and/or the Doppler shift.

- OFDM has relatively high PAPR; owing to the OFDM, the envelope can have extreme variations, where rare peaks may contain a power that exceeds the saturation range of the HPA, resulting in a clipping of the signal.

1.2 Aim of the Thesis

The operating points of the HPA have to be selected within the linear region to mitigate the effects of the ICI generated by the HPA, and hence, improve the BER performance. However, the power efficiency of the amplifier will be reduced due to

the high back-off (BO) required. To reduce the ICI by applying well-known PAPR techniques, the computational complexity of the system will be increased. Therefore, three factors have to be taken into account: system computational complexity, HPA efficiency and BER performance. The aim of this thesis is to achieve a compromise among these factors, i.e. propose new techniques with low computational complexity, low error rate and high power efficiency.

1.3 Contributions of the Thesis

There are four main significant objectives for this thesis. The first objective is to design low-complexity schemes based on the partial transmit sequences (PTS) technique using circulant transform matrices. These schemes require only two inverse fast Fourier transforms (IFFTs). The overall computational complexity for the proposed schemes will be derived and formulated, and compared with the complexity of PTS and selected mapping (SLM) schemes. Moreover, the complementary cumulative distribution function (CCDF) and BER performances will be simulated and compared with well-established schemes.

The second objective is to propose efficient and less complex schemes for BER reduction of OFDM systems in the presence of HPA nonlinearity. The proposed techniques, based on predicting the distortion introduced by the HPA nonlinearity, and techniques such as the PTS and SLM, will be invoked to minimise the distortion and consequently the BER. The computational complexity and system performances for the proposed schemes will be compared to other techniques, which are optimised to reduce the PAPR.

The third objective is to add the effect of carrier frequency offset (CFO) to the proposed techniques based on predicting the distortion introduced by HPA nonlinearity. This will also require the computational complexity for proposed schemes to be compared with conventional PAPR reduction techniques. Finally, a closed form solution for accurate BER of the OFDM signals perturbed by the amplifier nonlinearity and CFO will be derived, and the accurate BER will be compared with the simulation results for various BOs and CFOs.

The fourth objective is to propose new approaches to reduce the complexity of the proposed techniques that are based on predicting the distortion. In the proposed approaches, the transmitted phase vector will be selected to maximise the

cross correlation between the input and output of the nonlinear HPA model. The computational complexity and BER performances for the proposed approaches will be compared to other state-of-the-art techniques.

In summary, the following points indicate the contribution of this work:

1. To design low-complexity schemes based on the PTS technique.
2. To propose efficient schemes for BER reduction of OFDM systems in the presence of the HPA nonlinearity.
3. To add the effect of CFO to the proposed techniques in (2).
4. To derive a closed form solution for accurate BER of the OFDM signals perturbed by the HPA nonlinearity and CFO.
5. To propose efficient and less complex approaches to reduce the impact of nonlinear power amplifiers on the BER of OFDM systems using correlation metric.

1.4 Publications Arising From This Research

1. **E. Q. Al-Dalakta**, C. C. Tsimenidis, B. S. Sharif and A. Al-Dweik, "Interference Cancellation for OFDM Systems with Hierarchical Modulation over Non-linear Satellite Channels," *Int. Conf. on Acoustics, Speech and Signal Processing*, pp: 3560-3563, May 2011.
2. **E. Q. Al-Dalakta**, A. Al-Dweik, A. Hazmi, C. C. Tsimenidis and B. S. Sharif, "Efficient BER Reduction Technique for Nonlinear OFDM Transmission Using Distortion Prediction," *IEEE Trans. Veh. Technol.*, vol. 61, no. 5, pp. 2330-2336, Jun. 2012.
3. **E. Q. Al-Dalakta**, C. C. Tsimenidis, B. S. Sharif, A. Al-Dweik and A. Hazmi, "Efficient ICI Reduction Technique for OFDM Systems Distorted by TWTA and CFO," *accepted in 2nd Int. Conf. on Communications and Information Technology*, Hammamet, Tunisia, 2012.
4. **E. Q. Al-Dalakta**, C. C. Tsimenidis, B. S. Sharif and A. Al-Dweik, "Computationally Efficient PAPR Reduction schemes in OFDM-Based Satellite Communication Systems," *accepted to 76th IEEE Vehicular Technology Conf.*, Quebec City, Canada, Sep. 2012.

5. **E. Q. Al-Dalakta**, A. Al-Dweik, A. Hazmi, C. C. Tsimenidis and B. S. Sharif, "Low Complexity Partial Transmit Sequence using Maximum Cross Correlation," *submitted to IEEE Commun. Lett. and under review.*

1.5 Thesis Outline

The thesis is organised as detailed below:

Chapter 2 demonstrates the constellations used in OFDM systems. These constellations are introduced in satellite digital broadcasting and adopted in DVB-SH standard. Furthermore, the chapter presents the effects of the HPAs nonlinearities on OFDM signals. Finally, an overview is provided of the satellite mobile channel models that have been utilised in 3G mobile communication systems.

Chapter 3 introduces the main PAPR reduction techniques in OFDM systems. Five conventional techniques for PAPR reduction in the OFDM systems are investigated: amplitude clipping and filtering, coding schemes, tone reservation (TR) and tone injection (TI), nonlinear companding transforms (NCT) and multiple signal representation techniques such as PTS and SLM. Moreover, the criteria for selecting the reduction technique that can reduce the PAPR effectively and simultaneously maintain the BER performance are studied. Finally, a comprehensive literature review for PTS and SLM schemes is presented.

Chapter 4 proposes low-complexity and simplified low-complexity schemes using circulant transform matrices. In these schemes, only two IFFTs are required. Furthermore, the equations of the proposed schemes are derived. The overall computational complexity for the PTS, SLM and proposed schemes are also formulated. The proposed low-complexity (odd-cases) can reduce the complexity and improve the system performance. Moreover, the proposed simplified low-complexity (odd-case) can reduce both the computational complexity and the number of side information (SI) bits, however, at the cost of a reduction in PAPR and BER performance.

Chapter 5 presents efficient techniques to improve the BER performance degradation due to the nonlinear characteristics of HPAs utilised in OFDM-based systems. Extensive simulation results have demonstrated that minimising the amplifier distortion provides significant BER reduction in comparison to state-of-the-art techniques, which are optimised to reduce the PAPR. Moreover, measuring the distortion of the proposed techniques is less complex than the PAPR, as the distortion estimation

does not require oversampling.

Chapter 6 demonstrates efficient techniques to reduce the BER for distorted OFDM systems via the HPA and CFO. The proposed techniques are less complex than PAPR-based techniques and can achieve an improvement in BER performance. Also in this chapter, a closed form solution for the BER is derived theoretically and an accepted agreement of the BER is achieved when the simulation results are compared with the analytical calculations.

Chapter 7 presents new low-complexity approaches to reduce the BER performance degradation that is based on maximising the correlation between the input and output of the HPA. Complexity analyses have demonstrated that the proposed techniques are less complex than the current leading techniques proposed in chapter 5. Furthermore, the complexity reduction within the results was achieved without any noticeable BER degradation.

Finally, conclusions are summarised in chapter 8 and the thesis ends with possible suggestions of future work.

Chapter 2

System Model

This chapter demonstrates the constellations used in OFDM systems. These constellations are introduced in satellite digital broadcasting and adopted in DVB-SH standard. Furthermore, it presents two main models of HPAs: the memoryless and the polynomial models. Moreover, the effects of the HPAs nonlinearities on OFDM signals are presented. Finally, it provides an overview of the satellite mobile channel models that have been utilised in 3G mobile communication systems.

2.1 Modulation Schemes

Wireless communication systems use various categories of phase shift keying (PSK) and QAM modulation schemes to achieve high bandwidth efficiency at the cost of high power efficiency. For example and for same bit rate, a 16-QAM system requires half as much bandwidth as a 4-QAM system; however its BER performance is drastically worse than 4-QAM.

The envelope amplitude and/or phase of the RF carrier can be varied by utilising M-ary modulation schemes usually considered in digital baseband communications. Two degrees of freedom can be offered by varying the envelope amplitude and phase. For example, the QPSK modulation schemes map baseband data into four possible RF carrier signals. Therefore, depending on the change in either the amplitude and/or phase of the carrier, the modulation scheme is called M-ary QAM or M-ary PSK.

2.1.1 M-PSK scheme

In this type of modulation scheme, M possible phase angles are represented that is $\theta_i = (2i-1)\pi/M$, where $i = 1, 2, \cdots, M$, with constant amplitude [5]. For example, QPSK modulation scheme, $M = 4$ with signal constellations $d_{k,i} \in \{A\mathrm{e}^{j\theta_i}; \theta = \pi/4, 3\pi/4, 5\pi/4, 7\pi/4\}$, where $A = 1$, is used mainly for satellite and mobile communications owing to: its easy form, realistic power and spectral efficiencies as well as immunity to noise and interference. The QPSK has been adopted for digital video broadcasting satellite (DVB-S) [1] and for DVB terrestrial services [6] systems.

2.1.2 M-QAM scheme

In QAM modulation schemes, two orthogonal carriers, in-phase and quadrature carriers, are utilised for sending data over a known channel. Different constellations of QAM can be shaped by selecting several amplitudes and phases [5]. For example, in a 16-QAM modulation scheme, $M = 16$ with signal constellations $d_k \in \{\pm 1 \pm j1, \pm 1 \pm j3, \pm 3 \pm j1, \pm 3 \pm j3\}$, has gained significant attention in high data rate applications owing to its spectral and power efficiencies, as well as its additional flexibility of using various amplitudes and phases [1].

2.1.3 Hierarchical modulation scheme

Besides the conventional modulation schemes, the M-ary PSK and M-ary QAM, hierarchical modulation (HM) has been introduced in satellite digital broadcasting [2] and for DVB terrestrial services [6]. In the DVB-SH standard, the HM is selected as an alternative to the conventional modulation schemes [2]. The HM is one of the promising technologies that will upgrade existing systems with backward compatibility, i.e. the receivers that have been designed to use the conventional modulation schemes will remain functional by detecting the data in the high priority constellation points [7], [8] and [9]. Furthermore, the additional complexity and cost for HM-based systems are relatively low [10] and [11]. However, HM usually suffers from the interference between the enhancement-layer (EL) and basic-layer (BL) streams, which is denoted as the inter-layer interference (ILI) [12] and [13].

Fig. 2.1 shows the block diagram of the hierarchical QPSK/16-QAM modulation. The HM is designed using two separate data streams, namely the basic and enhancement streams that are combined into a single stream. The basic and enhancement

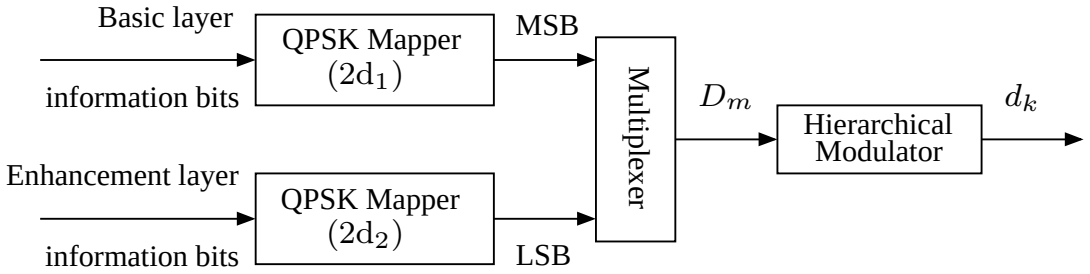

Figure 2.1: Block diagram of QPSK/16-QAM hierarchical modulation.

information bits are mapped to 16-QAM symbols similar to the conventional 16-QAM systems. The minimum distance between the BL and EL constellation points is equal to $2d_1$ and $2d_2$, respectively.

At the receiver, basic demmaping algorithms are required. The matched filtered output is taken by the absolute value through the AWGN channel. Consequently, only the first qardrant of 16-QAM constellation is required to extract the EL information 2-bits in accordance with distance d_1. In contrast, the BL stream can be detected like QPSK constellation using the Euclidean demmaping algorithm according to λ.

The mapping of both information bits streams is performed using a Karnaugh map approach to incorporate Gray mapping. The constellation scheme of QPSK/16-QAM modulation is depicted in Fig. 2.2. The ratio of the minimum distances is defined as $\lambda = d_2/d_1$ [7], where λ is a factor that determines the performance of the BL and EL layers. In this work, $\lambda = 0.5$ is considered, therefore the EL constellation is a uniform 16-QAM.

2.2 OFDM Signalling

The discrete-time complex-baseband model of the considered OFDM system is depicted in Fig. 2.3. The OFDM signal consists of N SCs modulated by M-QAM symbols that are constructed from the binary data set $\mathbf{D}$,

$$\mathbf{D} = \begin{bmatrix} D_{1,0} & D_{1,1} & \cdots & D_{1,N-1} \\ D_{2,0} & D_{2,1} & \cdots & D_{2,N-1} \\ \vdots & \vdots & \ddots & \vdots \\ D_{m,0} & D_{m,1} & \cdots & D_{m,N-1} \end{bmatrix}, \tag{2.1}$$

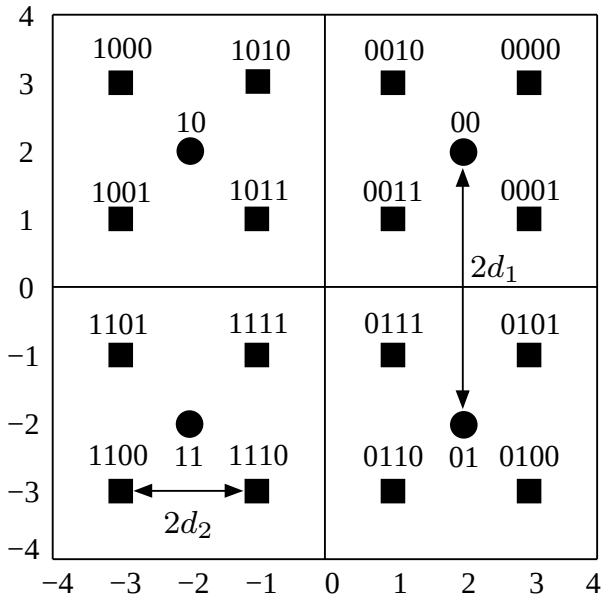

Figure 2.2: QPSK/16-QAM hierarchical constellation with $\lambda = d_2/d_1 = 0.5$. The circles are BL information and the squares are EL information.

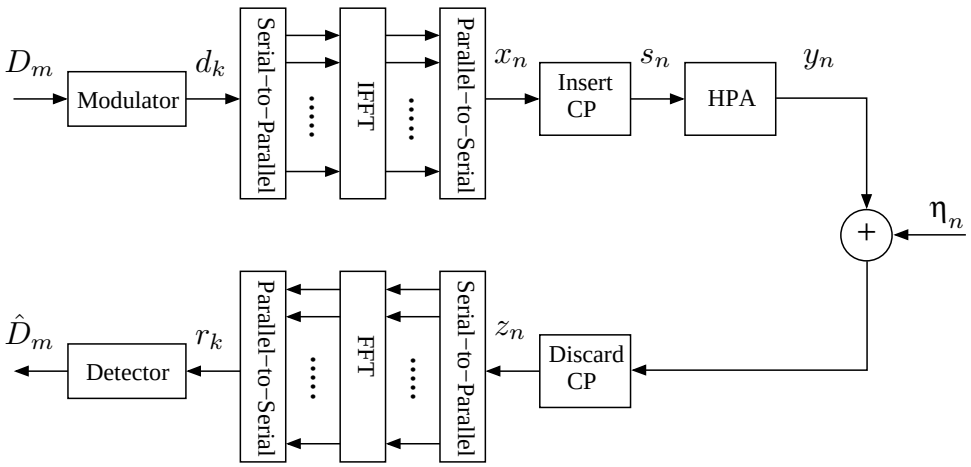

Figure 2.3: Block diagram of OFDM system in the presence of the HPA.

where $D_{p,q} \in \{0, 1\}$. Each column in $\mathbf{D}$ is mapped to one of $M \triangleq 2^m$ possible QAM constellation points using Gray mapping to produce the data sequence $\mathbf{d} = [d_0, d_1, \cdots, d_{N-1}]^T$, which modulates the N SCs by means of the IFFT,

$$\mathbf{x} = \mathbf{W}\,\mathbf{d}, \tag{2.2}$$

where $\mathbf{W}$ is the normalised $N \times N$ IFFT matrix. The elements of $\mathbf{W}$ are defined as $W_{i,k} = (1/\sqrt{N}) \exp(j2\pi ik/N)$, where i and k denote the row and column numbers $\{i, k\} = 0, 1, \cdots, N-1$, respectively. Consequently, the nth sample in the sequence $\mathbf{x}$ can be expressed as

$$x_n = \frac{1}{\sqrt{N}} \sum_{k=0}^{N-1} d_k \mathrm{e}^{j2\pi kn/N}, \quad n = 0, 1, \cdots, N-1. \tag{2.3}$$

where $j^2 = -1$ is the imaginary unit. After parallel-to-serial conversion, a time-domain guard band denoted as the cyclic prefix (CP) is added by copying the last N_g samples of $\mathbf{x}$ and appending them at the beginning of the IFFT output to form the time-domain OFDM symbol $\mathbf{s} = [x_{N-N_g}, x_{N-N_g+1}, \cdots, x_N, \mathbf{x}]$. The CP length N_g should be selected to be larger than the delay spread of the channel to prevent inter-symbol interference (ISI). The useful part of the OFDM symbol does not include the N_g prefix samples and has a duration of T_u seconds. The samples of $\mathbf{s}$ are then amplified by the HPA, which produces the set of samples $\mathbf{y} = [y_{N-N_g}, y_{N-N_g+1}, \cdots, y_0, \cdots, y_{N-1}]$, where $\mathbf{y} = \mathcal{F}(\mathbf{s})$, with $\mathcal{F}$ representing the nonlinear characteristics of the HPA.

At the receiver front-end, the received signal is applied to a matched filter and it is then sampled at a rate $T_s = T_u/N$. After dropping the first N_g CP samples, the received sequence $\mathbf{z} = [z_0, z_1, \cdots, z_{N-1}]^T$ can be expressed as

$$\mathbf{z} = \mathcal{F}(\mathbf{W}\,\mathbf{d}) + \boldsymbol{\eta}, \tag{2.4}$$

where the noise samples $\boldsymbol{\eta} = [\eta_0, \eta_1, \cdots, \eta_{N-1}]^T$ are independent normally distributed random variables with zero mean and variance $\sigma_\eta^2 = E\{|\eta_n|^2\}$, and $E\{.\}$ denotes the expected value. Subsequently, the sequence $\mathbf{z}$ is fed to fast Fourier trans-

form (FFT) that produces the frequency-domain sequence $\mathbf{r} = [r_0, r_1, \cdots, r_{N-1}]^T$,

$$\mathbf{r} = \mathbf{W}^H \mathbf{z}. \tag{2.5}$$

Note that $\mathbf{W}^{-1} = \mathbf{W}^H$ because $\mathbf{W}$ is a unitary matrix. The kth element of $\mathbf{r}$ can be expressed as

$$r_k = \frac{1}{\sqrt{N}} \sum_{n=0}^{N-1} z_n \, \mathrm{e}^{-j2\pi kn/N}, \quad k = 0, 1, \cdots, N-1. \tag{2.6}$$

Finally, the estimated binary data, $\hat{\mathbf{D}}$, can be obtained from $\mathbf{r}$ by means of the maximum likelihood (ML) detection. It is worth noting that the demodulation process, in chapters 4, 5, 6 and 7, is performed based on the assumption of perfect: channel knowledge, symbol timing, carrier frequency and phase synchronisation.

2.3 High Power Amplifier Models

2.3.1 Memoryless models

Usually, HPAs are characterised as memoryless nonlinear amplifiers. By noting that the polar representation of the time-domain samples at the HPA input is $s_n = \rho_n \mathrm{e}^{j\theta_n}$, the amplifier output using memoryless model can be expressed as [3]

$$y_n = A(\rho_n)\mathrm{e}^{j[\theta_n + \phi(\rho_n)]}, \tag{2.7}$$

where $\rho_n \triangleq |s_n|$ and $\theta_n \triangleq \arg(s_n)$. The operators $A(.)$ and $\phi(.)$ represent the AM/AM and AM/PM conversion of the nonlinear amplifier, respectively. Generally, two types of amplifier have been presented in the literature, TWTA with severe AM/PM conversion and solid-state power amplifier (SSPA) with zero AM/PM conversion.

2.3.1.1 TWTA Saleh's model

The TWTA model is commonly used to emulate the nonlinear behaviour of satellite transponders. In this work, the memoryless Saleh's TWTA model is considered,

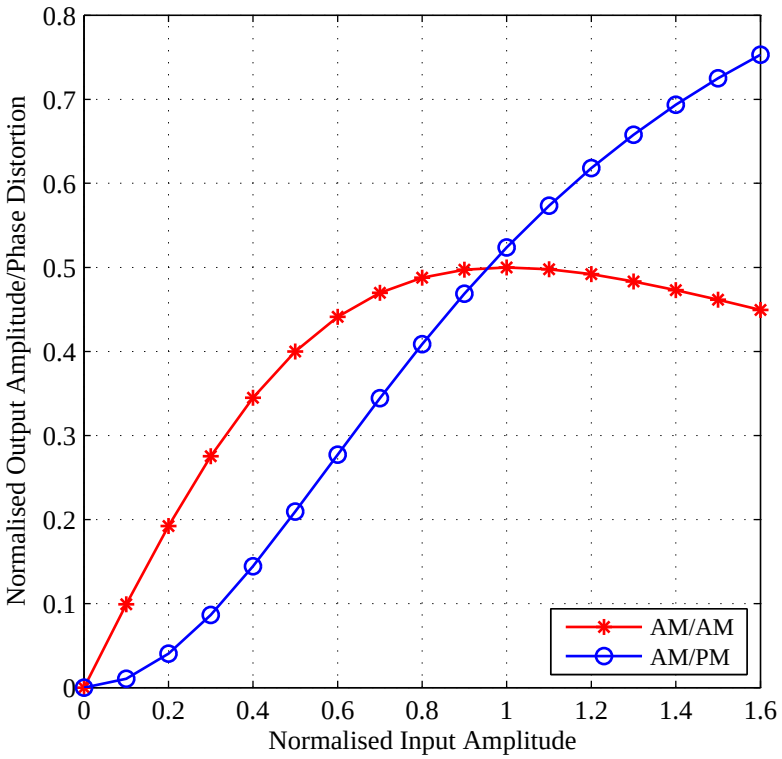

Figure 2.4: The normalised AM/AM and AM/PM transfer curves of TWTA.

where the AM/AM and AM/PM profiles are described by [14]

$$A(\rho_n) = G\frac{A_{sat}^2\rho_n}{\rho_n^2 + A_{sat}^2}, \tag{2.8}$$

$$\phi(\rho_n) = \frac{\pi}{3}\frac{\rho_n^2}{\rho_n^2 + A_{sat}^2}, \tag{2.9}$$

here A_{sat} denotes the amplifier input saturation voltage and G is the amplifier gain, duo to the normalisation G should be equal to one. The normalised characteristics of the TWTA model are illustrated in Fig. 2.4.

2.3.1.2 SSPA Rapp's model

The SSPA model is commonly used in mobile and cellular communications. The AM/AM and AM/PM profiles of memoryless Rapp's SSPA model are described by [15]

$$A(\rho_n) = G\frac{\rho_n}{\left[1 + \left(\frac{\rho_n}{A_0}\right)^{2p}\right]^{1/2p}}, \tag{2.10}$$

$$\phi(\rho_n) = 0, \tag{2.11}$$

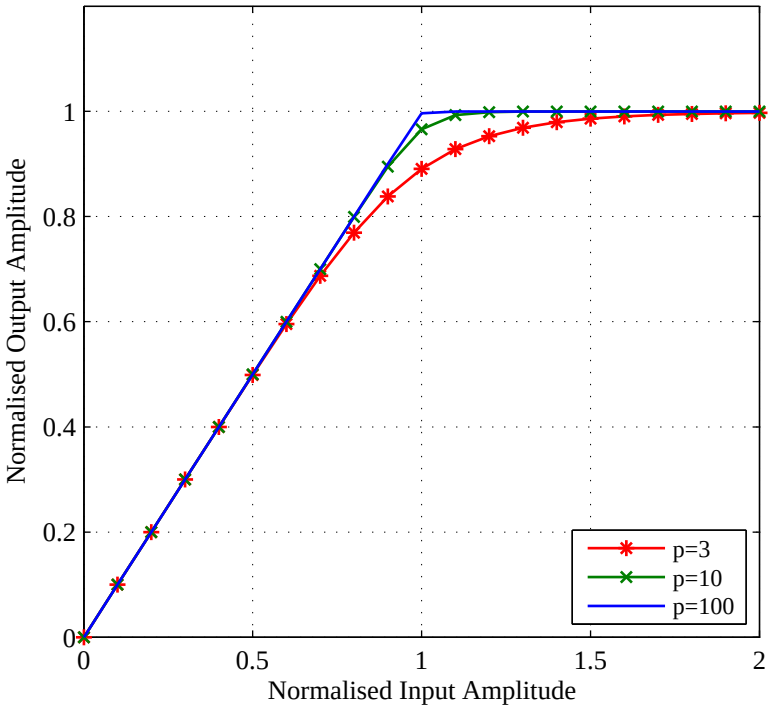

Figure 2.5: The normalised AM/AM transfer curve of SSPA for $p = 3$, 10 and 100 (soft limiter).

where A_0 denotes the maximum amplifier output due to maximum input A_{sat} and the smoothness of the transition from the linear region to limiting region can be controlled by the parameter p. Fig. 2.5 depicts the AM/AM characteristic of the SSPA model for various values of p.

2.3.2 Polynomial model

The output of the HPA y_n using the equivalent polynomial model with normalised input saturation amplitude A_{sat} can be expressed as [16]

$$y_n = \sum_{k=1}^{K} \alpha_k s_n |s_n|^{(k-1)}, \tag{2.12}$$

where K is the order of nonlinearity and $\alpha_1, \cdots, \alpha_K$ are the polynomial coefficients. In the polynomial model, odd order nonlinearity produces the maximum intermodulation. Moreover, most of the intermodulation power is produced by orders less or equal to 3. Consequently, representing the nonlinearity model by a third order nonlinearity is sufficiently accurate. Therefore, the HPA output can be approximated

as

$$y_n \approx \alpha_1 s_n + \alpha_3 |s_n|^2 s_n. \tag{2.13}$$

2.4 Effects of Nonlinearities on OFDM Signal

The amplified OFDM signal is affected by two types of distortion. The first distortion is due to AM/PM conversion which causes interference between the in-phase and quadrature components; this distortion is called an in-band distortion. The second, known as out-of-band distortion, occurs between the OFDM SCs causing spectral spreading of the transmitted signal and adjacent symbols.

The operating point of the amplifier is set by choosing either the input back-off (IBO) or the output back-off (OBO). These two parameters can be defined as

$$\text{IBO} = 10 \log_{10} \frac{A_{sat}^2}{\mathcal{P}_{in}}, \tag{2.14}$$

$$\text{OBO} = 10 \log_{10} \frac{A_0^2}{\mathcal{P}_{out}}, \tag{2.15}$$

where $\mathcal{P}_{in}$ and $\mathcal{P}_{out}$ are the average power of the OFDM symbol at the input and output of the amplifier, respectively. High back-off's are required to reduce the effects of the HPA nonlinearities. Consequently, the operating point of the amplifier is moved far from the saturation region. However, the power efficiency of the HPA is reduced [17].

By using memoryless Saleh's TWTA model described in (2.8), for maximum input, $\rho_n = A_{sat}$, the maximum output is $A(\rho_n) = A_{sat}/2$. The amplifier input power, $\mathcal{P}_{in}$, should be equal to the output power of the amplifier, $\mathcal{P}_{out}$, to achieve the normalisation. Consequentially, the relation between IBO and OBO in dB is IBO = OBO + 6. However, when memoryless Rapps SSPA model described in (2.10) is used, the maximum input, $\rho_n = A_{sat}$, is equal to the maximum output $A(\rho_n) = A_{sat}$. Therefore, the IBO is equal to the OBO in dB [18].

2.4.1 Effect on constellation points

Figs. 2.6 and 2.7 depict the received constellation diagram for the TWTA and the SSPA, respectively, at signal-to-noise ratio (SNR) = 20 dB, $N = 1024$ SCs and various OBOs. It can be seen from these figures that for low OBOs, received con-

stellation points are more scattered than that of the high OBOs for both amplifiers. Therefore, due to this scattering, severe degradation in the BER performance will occur. Furthermore, the received constellation shape for the TWTA appears as a rotated and attenuated cloud.

2.4.2 Effect on power spectrum

Fig. 2.8 shows the power spectrum density (PSD) of an OFDM signal measured at the output of the TWTA and SSPA for various values of OBOs with number of SCs, $N = 1024$ and 5 MHz bandwidth. It can be clearly noted from this figure that the out-of-band emission decreases with increasing OBO power. For example in Fig. 2.8(a), comparing the PSD of OBO = 1 dB with OBO = 9 dB case, the out-of-band emission reduces approximately 20 dB. Moreover, the operating point of the TWTA, which is the OBO, should be greater than 5 dB, and the SSPA should be greater than 3 dB. Owing to the low level of the side lobes for the out-of-band emission, this will conform to the spectrum mask limits defined by the European Telecommunications Standards Institute (ETSI) [19].

2.4.3 Total degradation effect

The efficiency of the HPA is decreased due to the large OBO. Therefore, to balance the output power and the nonlinear distortion, an optimum selection for the operating point of HPA, total degradation (TD) curve is particularly helpful for estimating the optimum operating OBO. The TD for a certain BER threshold is defined in [20] as

$$\mathrm{TD} = \mathrm{OBO} + \mathrm{SNR}_{\mathrm{HPA}} - \mathrm{SNR}_{\mathrm{AWGN}} \text{ [in dB]}, \tag{2.16}$$

where $\mathrm{SNR}_{\mathrm{AWGN}}$ is the corresponding required SNR to obtain the certain BER in an ideal system (without HPA nonlinearity) and $\mathrm{SNR}_{\mathrm{HPA}}$ is the required SNR when distortion caused by the HPA is taken into account at a specified OBO. Nevertheless, the efficiency of the HPAs will be decreased due to large OBOs. As a result, an optimum operating point be existent which can balance the nonlinear distortion and the output power.

Fig. 2.9 depicts simulated TD curves for 16-QAM-OFDM and QPSK-OFDM using either the TWTA or the SSPA. The threshold BER is 10^{-4}. It is clear that

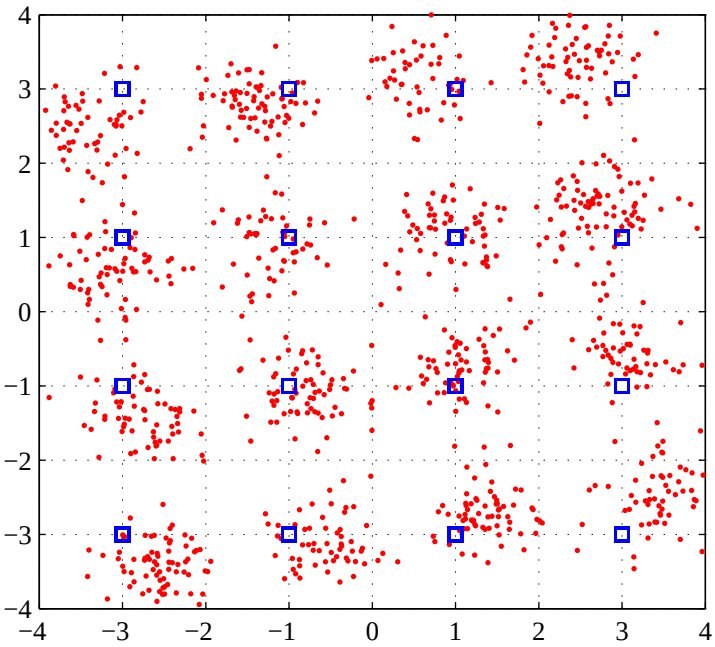

(a) TWTA with OBO=5 dB

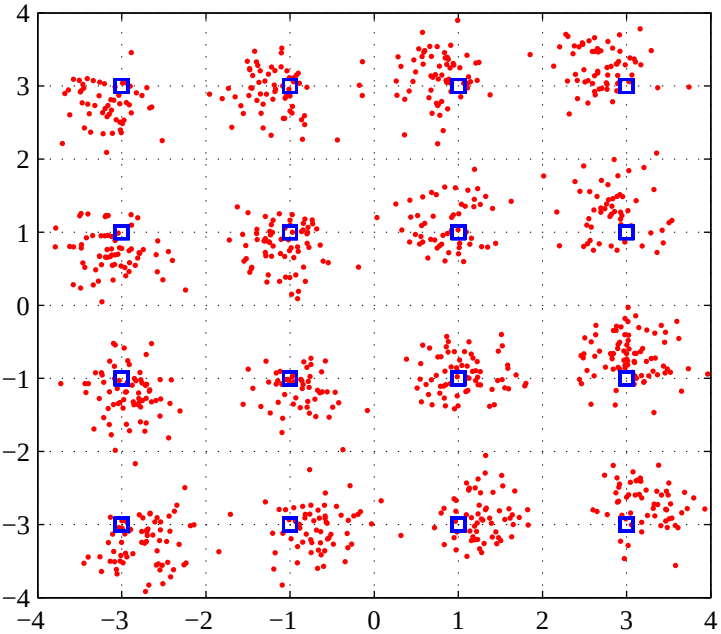

(b) TWTA with OBO=7 dB

Figure 2.6: Effect of OBO on 16-QAM constellation points for the TWTA at SNR = 20 dB, $N = 1024$ SCs.

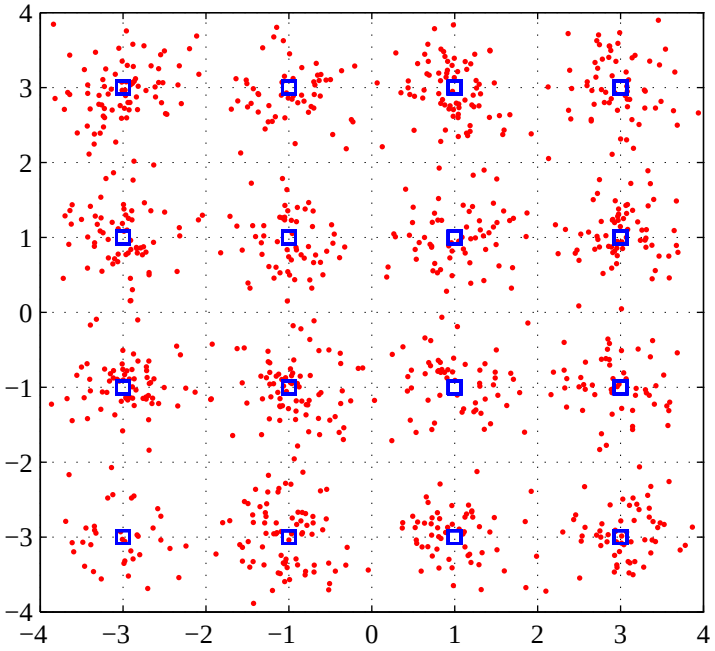

(a) SSPA with OBO=3 dB

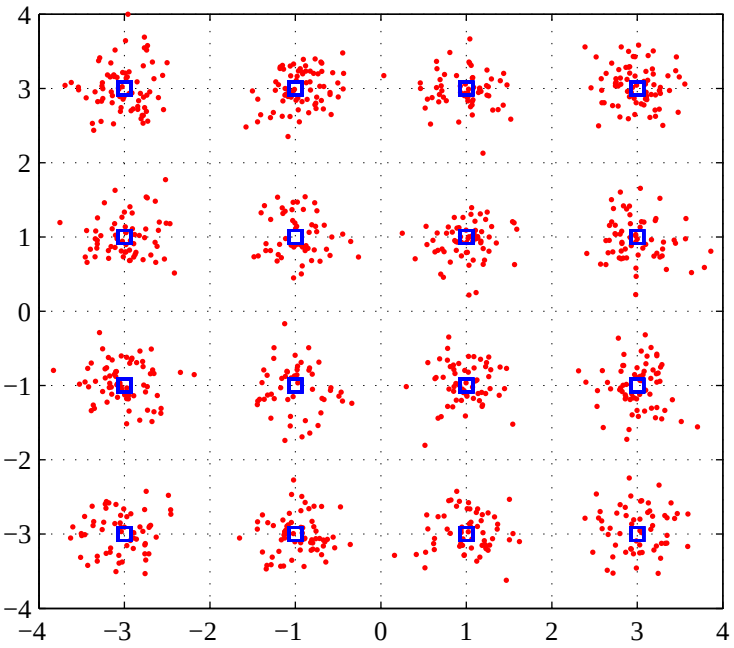

(b) SSPA with OBO=5 dB

Figure 2.7: Effect of OBO on 16-QAM constellation points for the SSPA at SNR = 20 dB, $N = 1024$ SCs and $p = 3$.

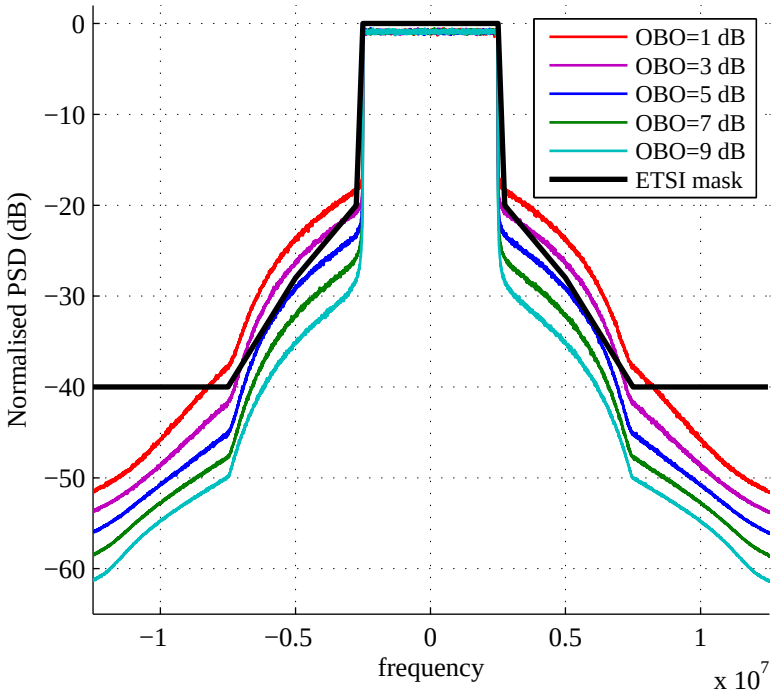

(a) TWTA case

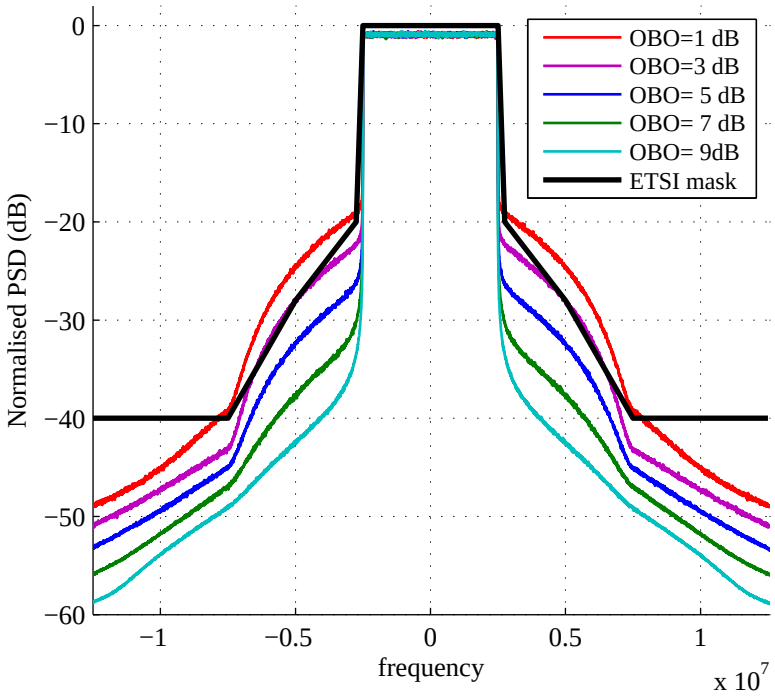

(b) SSPA case

Figure 2.8: Effect of OBO on spectrum plot of OFDM signal using either the TWTA or the SSPA ($p = 3$) with $N = 1024$ SCs.

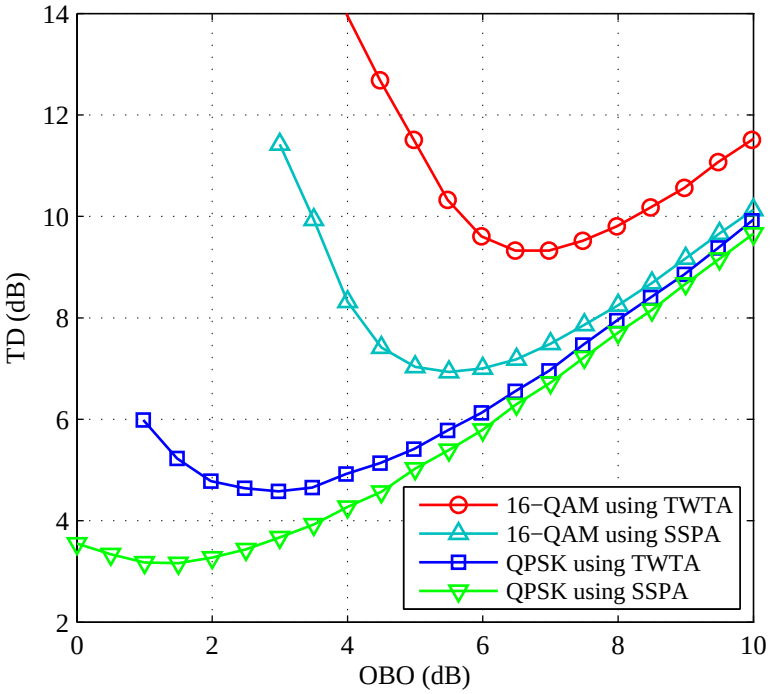

Figure 2.9: TD versus OBO for 16-QAM-OFDM and QPSK-OFDM using either the TWTA or the SSPA at target BER $= 10^{-4}$, $N = 1024$, $p = 3$.

the TWTA has much higher TD than SSPA for both constellations. Furthermore, the TWTA and SSPA have an optimum of OBO = 6.5 and 5.5 dB respectively, for 16-QAM-OFDM. For QPSK-OFDM, using either the TWTA or the SSPA, the optimum OBO is 3 and 1.5 dB respectively. However, for QPSK-OFDM with optimum values of OBOs, filters are required to significantly reduce the out-of-band frequency components in the nonlinearly distorted OFDM signal as shown in Fig. 2.9.

2.5 Phase Synchronisation

The mathematical analysis of the OFDM systems in the presence of nonlinear distortions due to the TWTA is complicated; consequently, the use of numerical simulations is unavoidable. One of the techniques to estimate the complex phase shift (CPS) can be achieved by sending one OFDM symbol and estimating the CPS at receiver at high SNR. The estimated CPS can then be applied to all of the OFDM symbols. Fig. 2.10 illustrates the signal-space representation of the received symbol. The CPS estimation can be summarised from [17] as follows:

1. Send OFDM symbol as shown in Fig. 2.3 at high SNR, to eliminate the effects of the AWGN.

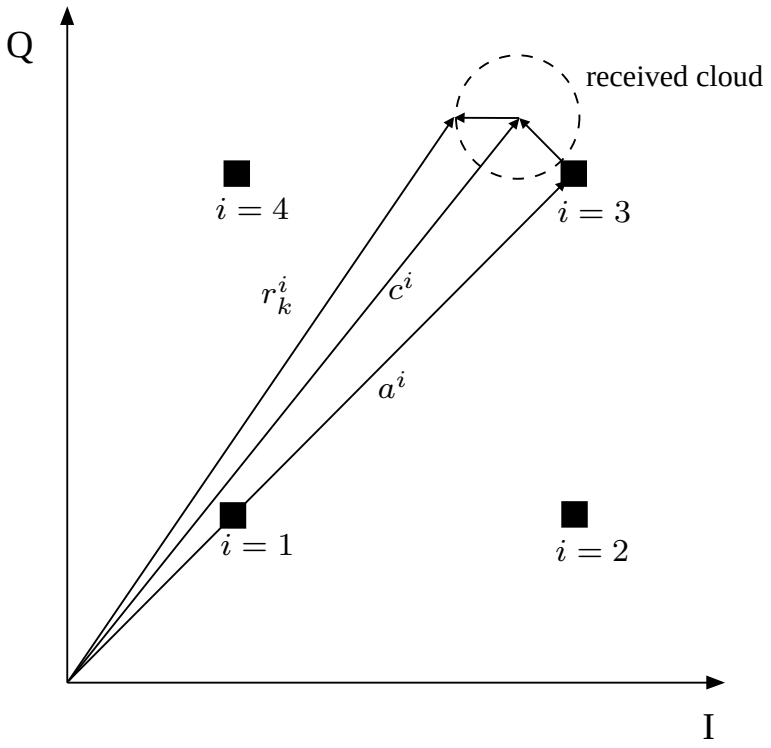

Figure 2.10: Signal-space representation of the received symbol with neglected Gaussian noise.

2. After the FFT, demodulate and modulate the received OFDM symbol, r_k for $k = 0, 1, \cdots, N-1$.

3. Separate the constellation points, r_k^i for $i = 1, 2, \cdots, M$, which lie in the vicinity of the i-th point, a^i.

4. Evaluate c^i by averaging r_k^i.

5. Calculate the CPS by using $\text{CPS} = \dfrac{c^i}{a^i}$.

6. Rotate the received constellation to its correct orientation by dividing each SCs, r_k by CPS value.

Fig. 2.11 depicts the constellation before and after CPS compensation (CPSC) at the output of FFT demodulator using TWTA for 16-QAM-OFDM systems at OBO = 6.5 dB and $N = 1024$ SCs in the absence of AWGN. The CPS should be compensated properly through channel estimation before detection of the OFDM symbol.

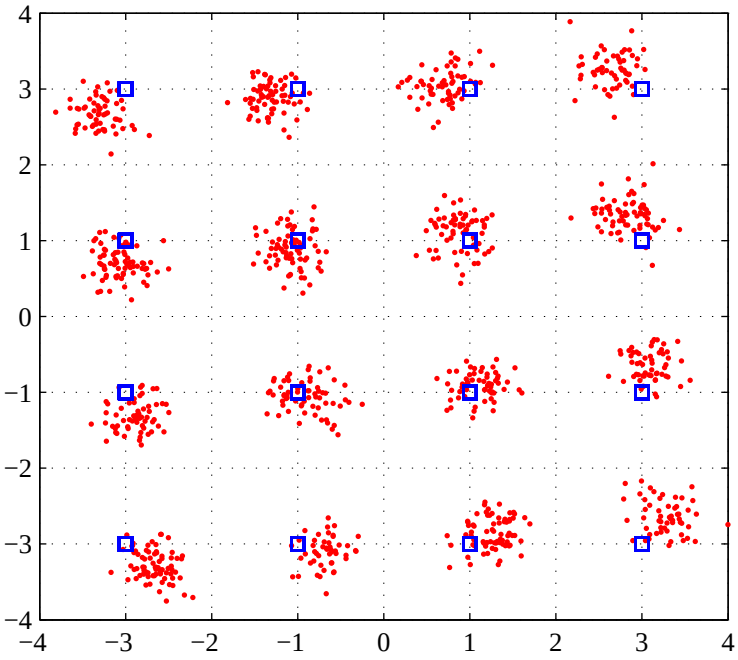

(a) Constellation before CPSC

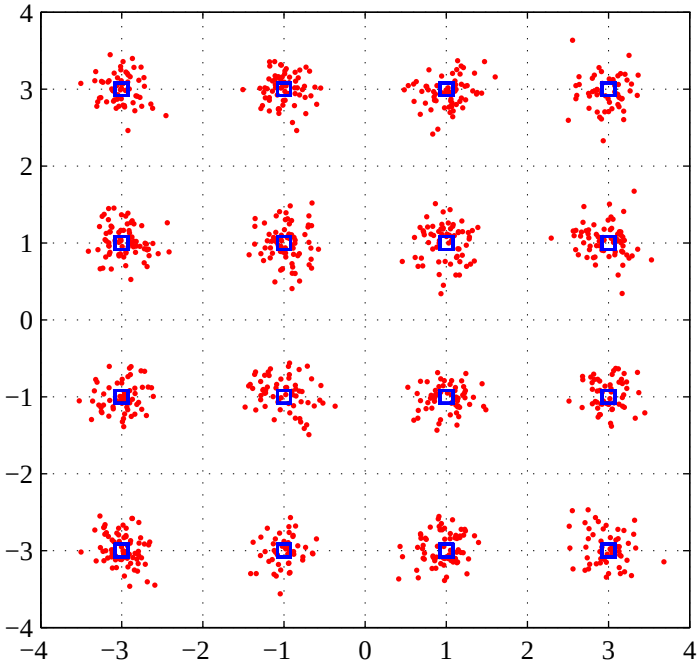

(b) Constellation after CPSC

Figure 2.11: Constellation at the output of FFT demodulator using TWTA for 16-QAM-OFDM systems at OBO = 6.5 dB, $N = 1024$ SCs and SNR = 40 dB.

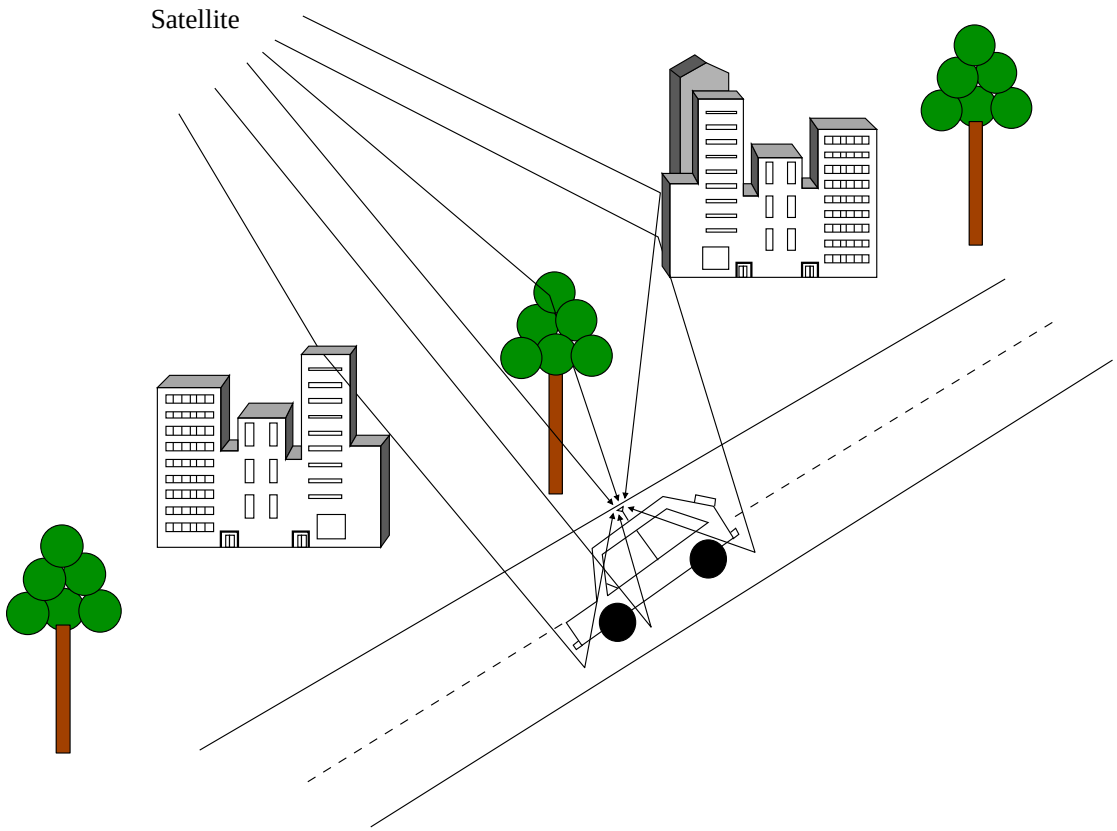

Figure 2.12: Multipath propagation.

2.6 Mobile Satellite Systems

Generally, satellite services can be classified into three significant categories: fixed service satellites which provide point to point communication, broadcast service satellites that supply satellite television/radio and mobile service satellites used for satellite phones. Fig. 2.12 illustrates the propagation process and multipath fading for mobile satellite systems.

Different frequency bands have been used for various kinds of satellites. These bands are [21]:

- L-Band, 1 to 2 GHz, used by mobile service satellites.
- S-Band, 2 to 4 GHz, used by mobile service satellites, NASA and deep space research.
- C-Band, 4 to 8 GHz, used by fixed service satellites.
- X-Band, 8 to 12.5 GHz, used by fixed service satellites.
- Ku-Band, 12.5 to 18 GHz, used by fixed service satellites, broadcast service satellites and in terrestrial imaging.

- K-Band: 18 to 26.5 GHz, used by fixed service satellites and broadcast service satellites.

- Ka-Band: 26.5 to 40 GHz, used by fixed service satellites.

The 3G mobile communication systems are currently designed to offer very wide area coverage using low (LEO) and medium (MEO) earth orbit satellites. A typical coverage area for a single satellite in LEO is 1000 km in diameter. Mobile satellite systems that operate at L and S-Bands can provide voice and low data rate services, however systems that operate at Ka-Band can provide high data rates, such as internet access, over narrow areas. Atmospheric effects may be considerable in such systems that operate at higher frequencies [22].

Mobile satellite systems are typically categorised according to their orbit type [22] and [21] as follows:

- LEOs satellite systems are used mainly for data communication such as e-mail and voice quality. LEOs include satellites at a height of 500-2000 km and a large number of satellites to provide global coverage are required. For example, 66 satellites are required at an altitude 780 km of the Iridium system.

- MEO satellites are used typically for geographical positioning systems. MEO entailed satellites are at an elevation of approximately 5000-12000 km and for wide area coverage, required fewer and slower moving satellites. The Odyssey system, for example, comprises of 12 satellites at an altitude of 10370 km.

- Geostationary satellites (GEOs) are used essentially for wideband applications and data transmissions at high speed. GEOs include satellites at a particular altitude of 36000 km. Only three satellites are required for global coverage, where these satellites revolve once during their orbit for each rotation of the earth.

2.7 Channel Modelling

The authors in [22], [23] and [24] reviewed the satellite mobile channel models carried out in the literature. Two main categories of LMS propagation channel models have been conducted for the 3G mobile communications, narrowband and wideband

models. Three main modelling approaches for the narrowband have been investigated: empirical, statistical and analytical approaches. The statistical approach is flexible and has efficient performance, as well as having less complexity compared to the other approaches. For wideband approaches, two main types of modelling have been studied: the Jahn [25] and Parks [26] models. The latter is adopted in this work owing to this model being more sophisticated and applicable to five various propagation circumstances: urban, suburban, open/highway, lightly and heavily wooded. The Parks, wideband satellite mobile channel, consists of two cascaded processes: satellite process and terrestrial process. The channel parameters are illustrated below.

2.7.1 Satellite process

Fig. 2.13 shows the block diagram of the satellite process. The effects between the satellite and the globe's surface are known as the satellite process. These effects include:

- Time delay, t_{SG}, which is due to the propagation path length from satellite to ground.

- Propagation path loss, A_{SG}, which consists of free space, antenna radiation pattern and all atmospheric effects. For example, in LEO satellite, the free space loss is 164 dB at 10 degree elevation angle and frequency of 1.625 GHz [22].

- Doppler shift, f_{SG}, which occurs due to the relative motion of the satellite and a fixed point on the earth near to the mobile device. For frequencies in the L and S-Bands, the maximum Doppler shift is approximately ±30-60 kHz for LEO constellations depending on the orbital altitude [26]. The compensation of this shift can be either at the transmitter or receiver [22]. It is worth noting that in this work, the Doppler compensation is performed at the transmitter based on the assumption of perfect phase synchronisation. For further information, a various phase estimation schemes for LEO satellite at receiver can be seen in [27].

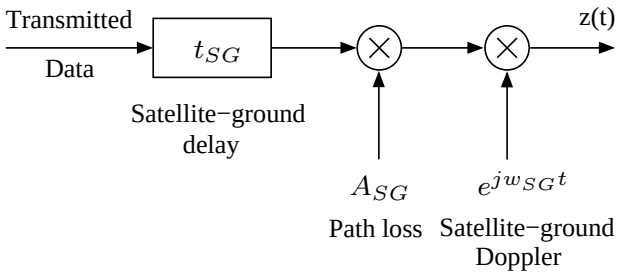

Figure 2.13: Block diagram of satellite process.

2.7.2 Terrestrial process

The terrestrial process is patterned as a tapped delay line that is shown in Fig. 2.14, with $\triangle\tau_1, \triangle\tau_2, \cdots, \triangle\tau_n$ denoting the tap-delays related to the multipath propagation in the terrestrial circumstances and the tap-gain processes $G_0, G_1, \cdots, G_n$ relating to the terrestrial circumstances. The construction of each tap-gain has the following parameters [26]:

- Rician (Rice) k factor which can be defined as the ratio of the coherent and incoherent powers in tap-gain process. The k factor for Rayleigh (Ray) taps is equal to 0 dB. Note that for low delay taps the Rice factor is larger than that of the Ray taps.
- Maximum Doppler shift, f_d, which can be expressed as $f_d = \frac{v f_c}{c}$, relates to the mobile motion relative to the fixed point on the earth near to the mobile, where v is the speed of the mobile motion, f_c is the carrier frequency at L or S-Band and c is the speed of light ($3 * 10^8$ m/s). In this work, the effect of the f_d is not taken into account when the receiver has perfect phase synchronisation.
- Relative mean power due to shadowing and multipath fading.

The terrestrial process parameters for urban environments at L-Band are illustrated in Table 2.1 [26] for different elevation angles. It is clear from this table that the first two paths are coherent components: line-of-sight (LOS) which has the highest power, followed by specular reflection from the ground to mobile. Other propagation impairment paths, which are non-coherent components, the result of delay and attenuation from buildings and terrains that can be represented as Rayleigh fading paths. The relative tap delay in this example is approximately 100 ns.

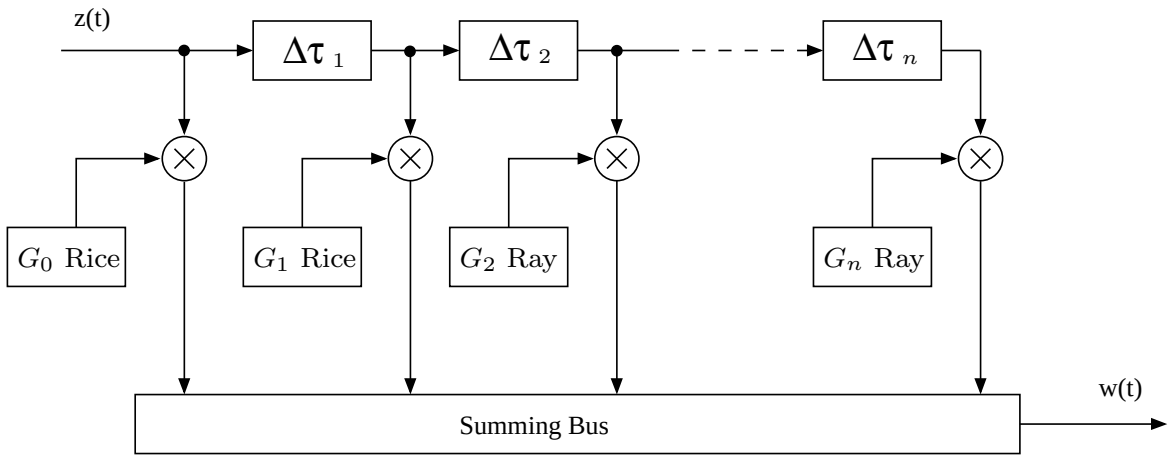

Figure 2.14: Block diagram of terrestrial process.

Table 2.1: Terrestrial process parameters for urban circumstances.

	$\theta > 45$		$\theta \leq 45$	
Relative delay (ns)	Relative mean power (dB)	Rice k factor (dB)	Relative mean power (dB)	Rice k factor (dB)
0	0	12	0	16
100	-9.7	3	-15	6
200	-19.2	0	-20	0
300	-22.8	0	-26	0
400	-	-	-28	0
500	-	-	-30	0

Table 2.2: System parameters for simulations.

System Item	Parameter
Modulation	QPSK, 16-QAM and HM
Synchronisation	Complete
Channel type	Parks wideband satellite mobile channel
Equalisation	One-tap FEQ
Number of SCs	1024
Duration of CP	$T_u/4$
Bit rate	5 Mbps
Carrier frequency	at L or S-Band
Application	Mobile TV

2.8 BER Performance of Different Modulation Constellation

The system performance is introduced for OFDM systems with different types of modulation. The simulation parameters are chosen from DVB-SH specification and can be shown in Table 2.2. Initially, the BER performance is investigated over an AWGN channel and subsequently, the scenario is developed for practical mobile satellite channel communications.

The optimum OBOs obtained from subsection 2.4.3 are used. Moreover, the CPS as illustrated in section 2.5 is estimated. The estimation of the CPS is equal to $0.991 - j0.233$ and $0.9993 - j0.105$ for QPSK and 16-QAM constellations, respectively.

2.8.1 Theoretical probability of error

The probability of an error in uncoded OFDM systems within an AWGN channel can be expressed as

$$P_e = P_{err}\left(\gamma_b\right), \tag{2.17}$$

where γ_b is the signal to noise ratio per bit for each SC and can be expressed by

$$\gamma_b = \frac{\gamma_s}{m}, \tag{2.18}$$

where m is the number of bits per symbol transmitted over each SC and γ_s is signal to noise ratio per symbol. The symbol probability of error of M-ary PSK is given

by [5]

$$P_s = 2Q\left(\sqrt{2\gamma_s}\sin\left(\frac{\pi}{M}\right)\right), \tag{2.19}$$

where the function $Q(x)$ is defined as

$$Q(x) = \frac{1}{2}\text{erfc}\left(\frac{x}{\sqrt{2}}\right), \tag{2.20}$$

and the function $\text{erfc}(x)$ is the complementary error function, while the equivalent bit error probability for this constellation can be approximated as

$$P_b \approx \frac{1}{m}P_s. \tag{2.21}$$

The P_e for M-ary QAM mapping can be expressed as [5]

$$P_e = 2\left(\frac{\sqrt{M}-1}{\sqrt{M}}\right)Q\left(\sqrt{\frac{3\gamma_s}{M-1}}\right), \tag{2.22}$$

whereas the P_s for this constellation can be given as

$$P_s = 1-(1-P_e)^2, \tag{2.23}$$

and can be approximated as [28]

$$P_s \approx\ 2P_e. \tag{2.24}$$

Finally, a similar expression to (2.21) can be used for BER calculations using M-ary QAM.

The probability of a bit error in HM systems for BL is given by [7]

$$P_b = \frac{1}{2}Q\left(\frac{1-\lambda}{\sqrt{1+\lambda^2}}\sqrt{\gamma_s}\right) + \frac{1}{2}Q\left(\frac{1+\lambda}{\sqrt{1+\lambda^2}}\sqrt{\gamma_s}\right), \tag{2.25}$$

while, the P_b for EL can be expressed by [7]

$$P_b = \frac{1}{2}Q\left(\frac{\lambda}{\sqrt{1+\lambda^2}}\sqrt{\gamma_s}\right) + \frac{1}{2}Q\left(\frac{2-\lambda}{\sqrt{1+\lambda^2}}\sqrt{\gamma_s}\right) - \frac{1}{2}Q\left(\frac{2+\lambda}{\sqrt{1+\lambda^2}}\sqrt{\gamma_s}\right). \tag{2.26}$$

2.8.2 Performance over an AWGN channel

Fig. 2.15 depicts the BER versus SNR for OFDM systems using QPSK and 16-QAM constellations in the presence of either the TWTA or the SSPA nonlinearity over an AWGN channel. It can be noted from Fig. 2.15(a) that the CPSC is required to improve the BER performance for QPSK and 16-QAM constellations. Furthermore, the BER degradation in terms of SNR at 10^{-4} BER is approximately 4.5 and 2.5 dB for 16-QAM and QPSK schemes after CPSC, respectively, compared to the theoretical cases. As shown in Fig. 2.15(b) and in comparison to the theoretical cases, the BER degradation is approximately 1.5 and 3 dB for 16-QAM and QPSK schemes, respectively.

The BER for HM-OFDM systems in the presence of either the TWTA or the SSPA is shown in Fig. 2.16. The SSPA outperforms the TWTA in BER performance. In comparison to the theoretical case, the BER degradation in terms of SNR is approximately 2.5 and 1 dB for TWTA and SSPA cases, respectively.

2.8.3 Performance in mobile satellite channel

After the knowledge of the BER performance over an AWGN channel, the system is examined in the mobile satellite fading channel to observe its performance under feasible channel degradations. The BER performance for QPSK, 16-QAM and HM modulation schemes in the presence of the TWTA nonlinearity and a wideband channel with elevation angles, $\theta > 45$ and $\theta \leq 45$, is depicted in Fig. 2.17. A similar scenario of the BER performance over an AWGN is achieved for the mobile satellite fading channel, except for an extra impairment owing to multipath fading. As expected, if the elevation angle decreases, the BER will increase owing to the increase in multipath effects. Note that the compensation of channel impairment and the CPS in OFDM systems can be achieved by utilising one-tap FEQ and CPSC, respectively after the FFT at receiver.

2.9 Chapter Summary

This chapter demonstrates three types of constellations: QPSK, 16-QAM and HM based OFDM systems, which were introduced in satellite digital broadcasting and consequently, adopted into the DVB-SH standard. Furthermore, two main models of

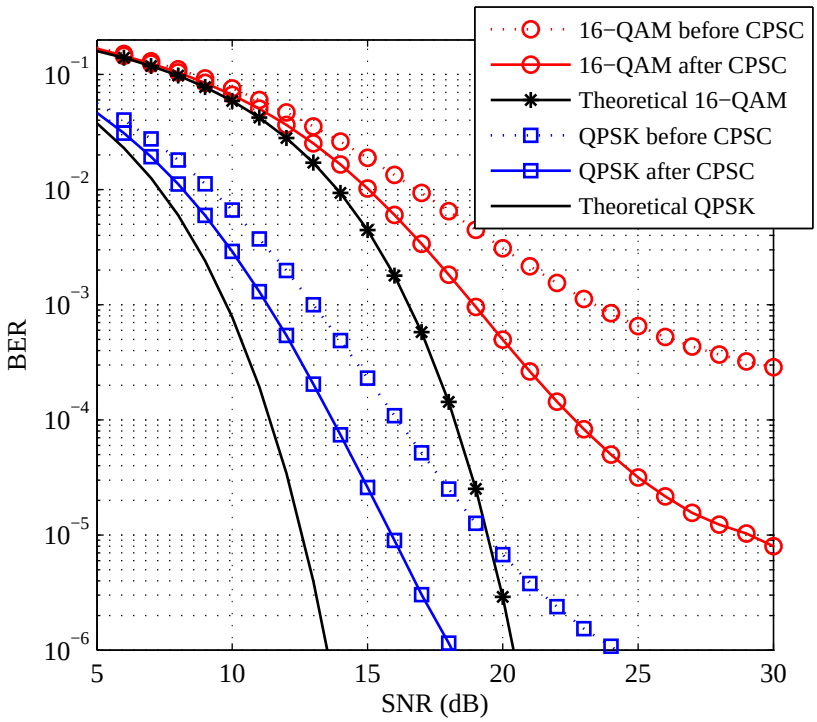

(a) TWTA case

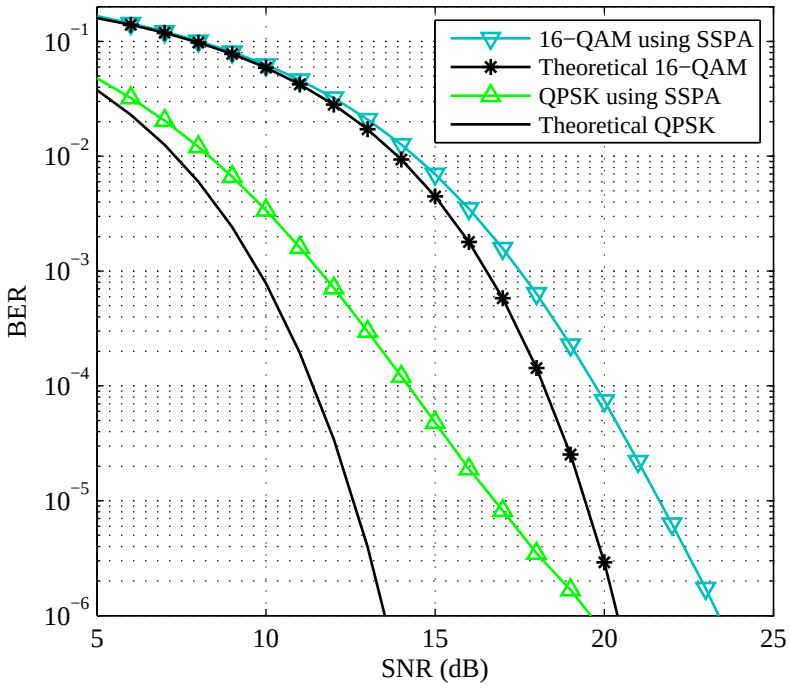

(b) SSPA case

Figure 2.15: BER versus SNR for OFDM systems using QPSK, 16-QAM constellation in the presence of either the TWTA or the SSPA nonlinearity over an AWGN with optimum OBOs and $N = 1024$ SCs.

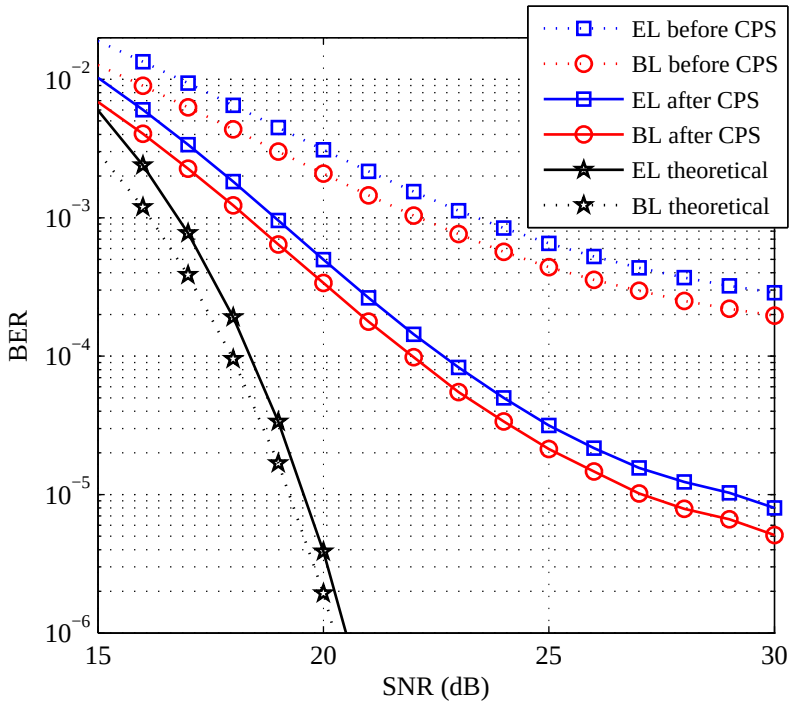

(a) TWTA case

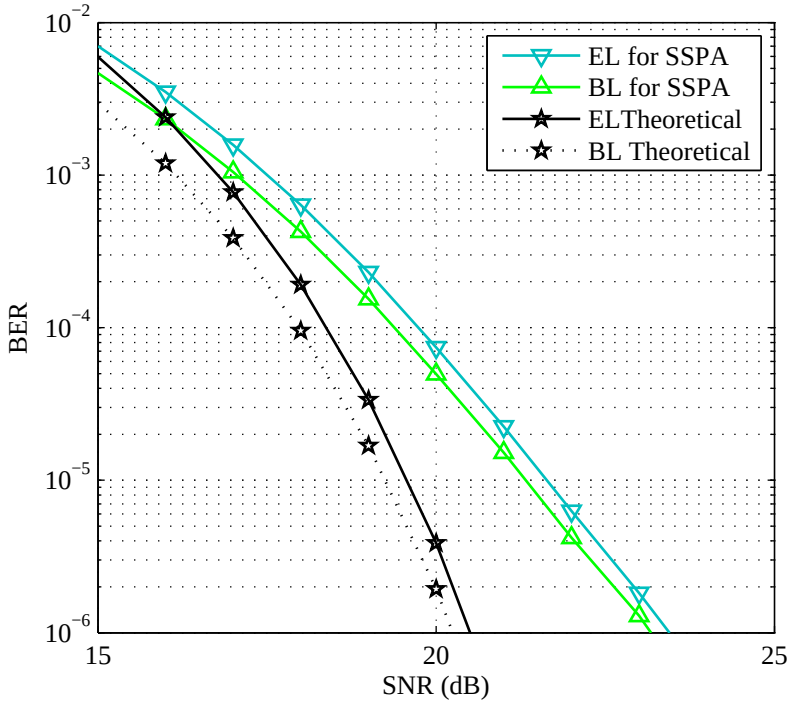

(b) SSPA case

Figure 2.16: BER versus SNR for HM-OFDM systems in the presence of either the TWTA or the SSPA nonlinearity over an AWGN with optimum OBOs and $N = 1024$ SCs.

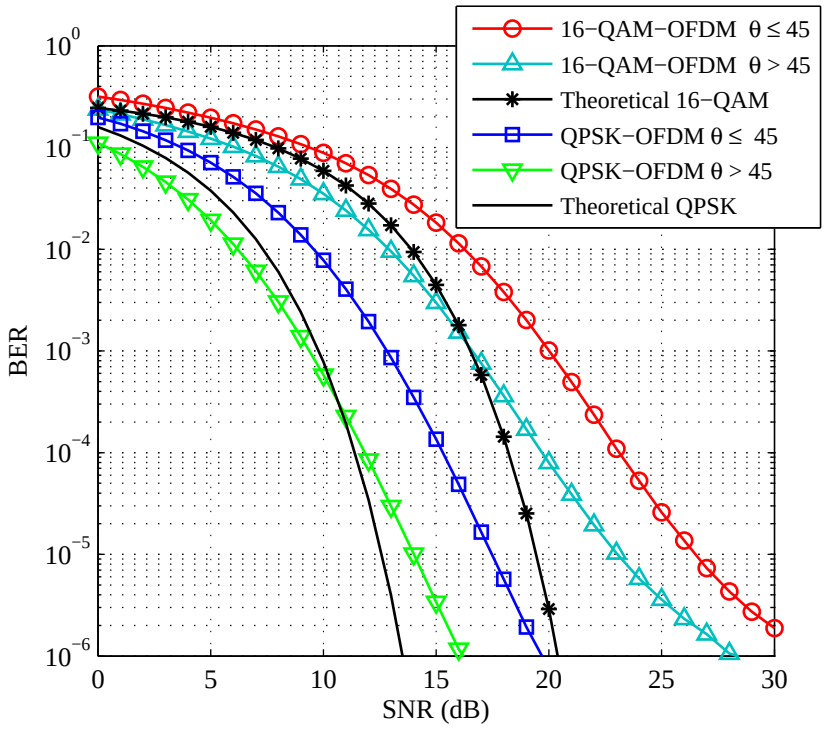

(a) QPSK and 16-QAM-OFDM

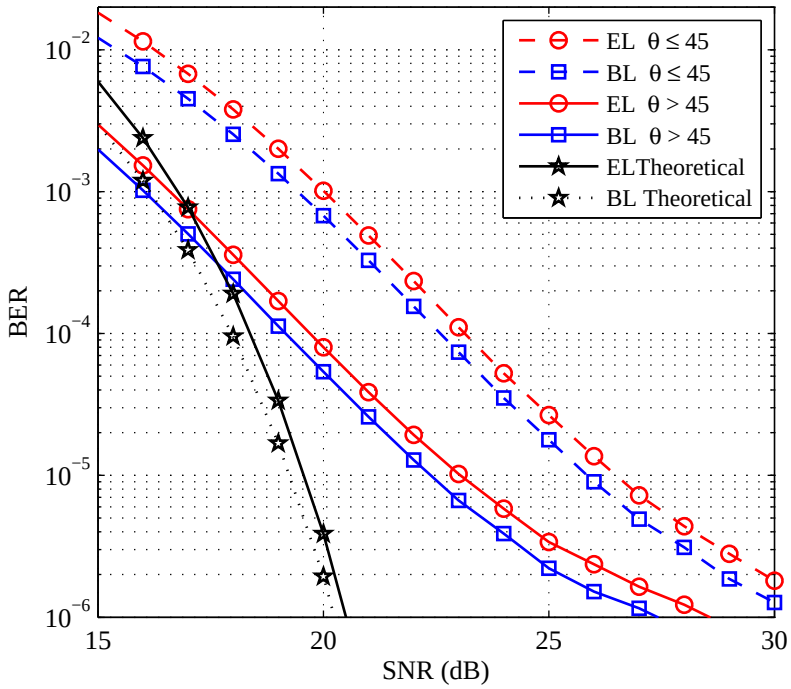

(b) HM-OFDM

Figure 2.17: BER versus SNR for OFDM systems in the presence of the TWTA nonlinearity and a wideband channel with optimum OBO and $N = 1024$ SCs.

HPAs are presented: the memoryless and the polynomial models. The nonlinearities of HPAs in OFDM signals have three essential effects on: the constellation points, the power spectrum and the total degradation. From these effects the optimal OBO can be obtained for different types of amplifiers and constellations. Moreover, this chapter provides an overview of the satellite mobile channel models that have been utilised in the 3G mobile communication systems. Finally, the BER is used to assess the system performance over an AWGN and Parks wideband channel for different modulation schemes.

Chapter 3

PAPR Reduction Techniques

This chapter introduces the main PAPR reduction techniques in OFDM systems. several conventional techniques for PAPR reduction in the OFDM systems are investigated. Moreover, the criteria for selecting the reduction technique that can reduce the PAPR effectively and simultaneously maintain the high-quality performance are studied. Finally, it presents the literature review of the recent research scenarios in PAPR reduction based on the PTS and SLM schemes.

3.1 PAPR in OFDM

One of the main disadvantages of the OFDM systems is the high PAPR of the transmitted signal due to the combination of N modulated SCs. The PAPR for a continuous-time signal, $x(t)$, is defined as [29] and [30]

$$\text{PAPR} = \frac{\max\{|x(t)|^2\}}{E\{|x(t)|^2\}}, \quad 0 \leqslant t < T_u. \tag{3.1}$$

On the other hand, the PAPR for discrete-time signals can be estimated by oversampling the data sequence $\mathbf{d}$ depicted in Fig. 2.3 by a factor L and computing LN-points IFFT of the data block with $(L-1)N$ zero-padding. The PAPR in this case is defined as [29] and [30]

$$\text{PAPR} = \frac{\max\{|x_n|^2\}}{E\{\|\mathbf{x}\|^2\}}, \quad n = 0, 1, \cdots, LN-1, \tag{3.2}$$

where $\|\mathbf{x}\|$ is the Euclidean norm of $\mathbf{x}$, $\|\mathbf{x}\| \triangleq \sqrt{|x_0|^2 + |x_1|^2 + \cdots + |x_{LN-1}|^2}$. The denominator in (3.2) represents the average power per OFDM symbol at the HPA

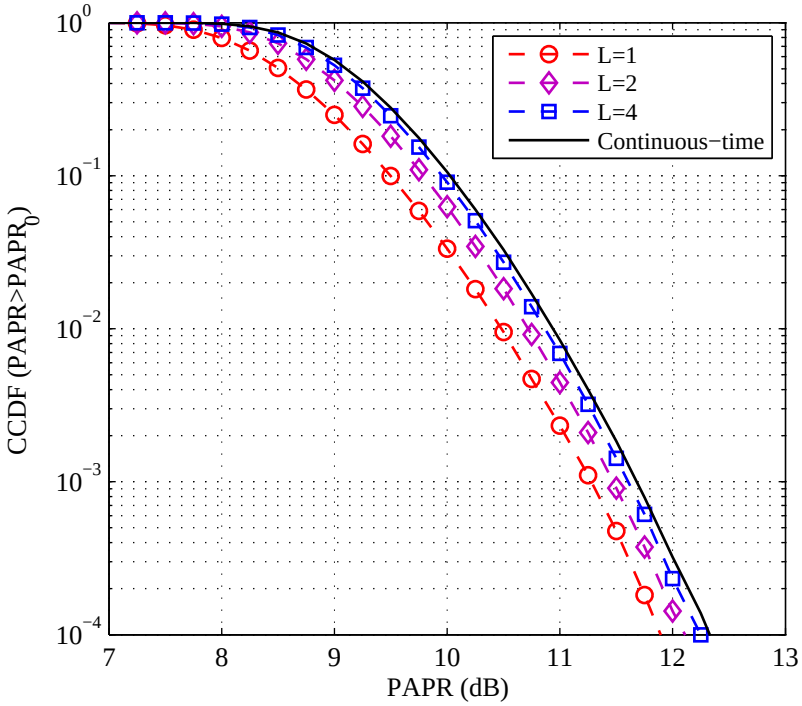

Figure 3.1: CCDF of the PAPR for OFDM systems oversampled by different L with $N = 1024$ SCs.

input, which is denoted as $\mathcal{P}_{in}$.

3.2 CCDF of the PAPR

The CCDF is widely used to assess the performance of PAPR reduction techniques which is defined as the probability that the PAPR is greater than a reference value denoted as PAPR_0. Fig. 3.1 depicts the CCDF of the PAPR of the OFDM signals with $N = 1024$ SCs and different oversampled factor, $L = 1$, 2 and 4. It is clear that the PAPR does not increase considerably after $L = 4$. Therefore, an accurate PAPR estimation for the discrete model requires an oversampling factor $L \geqslant 4$. It has been shown that the difference between the continuous-time and discrete-time PAPR is negligible for $L = 4$ [31].

A straightforward estimated expression for the CCDF of the PAPR of an OFDM signal with Nyquist rate sampling was derived in [32]. For an OFDM signal with a large number of SCs and from the central limit theorem, the real and imaginary parts of N-point IFFT output samples have a mutually independent and uncorrelated Gaussian probability distribution function with zero mean and a variance of $\sigma^2 = E\{|x_n|^2\}/2$.

Furthermore, the amplitude of the OFDM signal has a Rayleigh distribution, whereas the power distribution can be characterised by a central chi-square distribution with two degrees of freedom. The cumulative distribution function (CDF) of this distribution is given by

$$F(z) = 1 - \exp(-z). \tag{3.3}$$

The probability of the PAPR for a non-oversampling data block can be written as

$$P_r(\text{PAPR} \leqslant z) = F(z)^N = (1 - \exp(-z))^N. \tag{3.4}$$

Furthermore, the CCDF of the PAPR can be given by

$$\text{CCDF} = P_r(\text{PAPR} > \text{PAPR}_0) = 1 - F(\text{PAPR}_0)^N = 1 - (1 - \exp(-\text{PAPR}_0))^N, \tag{3.5}$$

while the CCDF for oversampled data block can be approximated by adding a certain constant, α, to (3.5)

$$\text{CCDF} = P_r(\text{PAPR} > \text{PAPR}_0) = 1 - (1 - \exp(-\text{PAPR}_0))^{\alpha N}. \tag{3.6}$$

Fig. 3.2 depicts the CCDF of the PAPR of the 16-QAM-OFDM signals with different SCs given $\alpha = 1.8$. From this figure it can be seen that the CCDF expression is not precise for a small number of SCs; for large values of $N > 128$ this expression is more precise.

3.3 Significant PAPR Reduction Schemes

Various techniques have been proposed to reduce the PAPR comprising amplitude clipping [33], clipping and filtering [34], coding schemes [35], phase optimisation [36], NCT [37], TR and TI [38], active constellation extension (ACE) [39], multiple signal representation techniques such as PTS and SLM [40] and interleaving [41]. In this section, five conventional techniques for PAPR reduction in the OFDM systems are investigated.

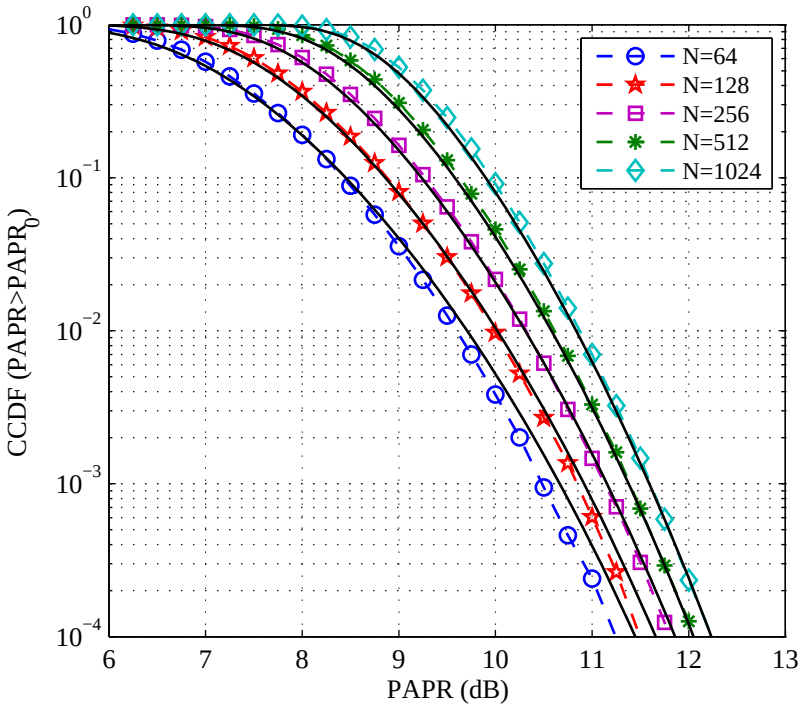

Figure 3.2: CCDF of the PAPR for OFDM systems for different number of SCs. Dotted lines are simulated; solid lines are calculated.

3.3.1 Clipping and filtering

The most straightforward and widely used technique of PAPR reduction is amplitude clipping. This technique can be implemented by either clipping parts of the signals that are greater than a threshold level or by transmitting the input signal below the threshold level without clipping. In the clipping technique, the BER performance of the OFDM systems is deteriorated due to the in-band distortion, while the spectral efficiency is degraded owing to the out-of-band radiation [33].

The out-of-band radiation can be decreased by filtering the signal after clipping it, while the in-band distortion can not be decreased. On the other hand, several peaks of re-growth may be produced by clipping, therefore the signal at these peaks will be greater than the clipping threshold after clipping and filtering. The peak re-growth can be decreased by duplicating the clipping and filtering stage to achieve the required PAPR reduction at the expense of increasing the computational complexity [34].

Table 3.1: All possible data blocks and corresponding PAPR for an OFDM signal with coding rate $R = 3/4$.

Data block	PAPR (dB)	Data block	PAPR (dB)
[1,1,1,1]	6.0	[-1,1,1,1]	2.3
[1,1,1,-1]	2.3	[-1,1,1,-1]	3.7
[1,1,-1,1]	2.3	[-1,1,-1,1]	6.0
[1,1,-1,-1]	3.7	[-1,1,-1,-1]	2.3
[1,-1,1,1]	2.3	[-1,-1,1,1]	3.7
[1,-1,1,-1]	6.0	[-1,-1,1,-1]	2.3
[1,-1,-1,1]	3.7	[-1,-1,-1,1]	2.3
[1,-1,-1,-1]	2.3	[-1,-1,-1,-1]	6.0

3.3.2 Coding schemes

Coding can be employed as well in the PAPR reduction for OFDM systems. The main idea of the coding is to select the code word that minimises the PAPR for transmission. Table 3.1 illustrates all possible data blocks and corresponding PAPR for an OFDM signal with coding rate $R = 3/4$ using binary PSK (BPSK) [29]. From this table it can be shown that eight data blocks with odd parity code can achieve approximately 2.3 dB PAPR reduction.

On the other hand, for a large number of SCs, an extensive search to obtain the optimal code word that minimises the PAPR is required, also huge lookup tables are needed for encoding and decoding, however the error correction problem in this scheme is not solved. A simple implemented scheme for both PAPR reduction and error correction problems was proposed by [42]. To decrease the PAPR in this scheme, the codes for error corrections and offsets of the resultant coded signals are selected. However, this scheme requires comprehensive computation to choose the code word that has superior codes for error corrections and offsets.

To achieve 3 dB PAPR reduction, a Golay complementary sequence [43] and Reed-Muller codes [44] have been proposed as code words. However, the transmission rate is reduced drastically for practical multicarrier systems with a large number of SCs. Furthermore, these techniques require a comprehensive search for a code word that has a minimum PAPR and good error correction.

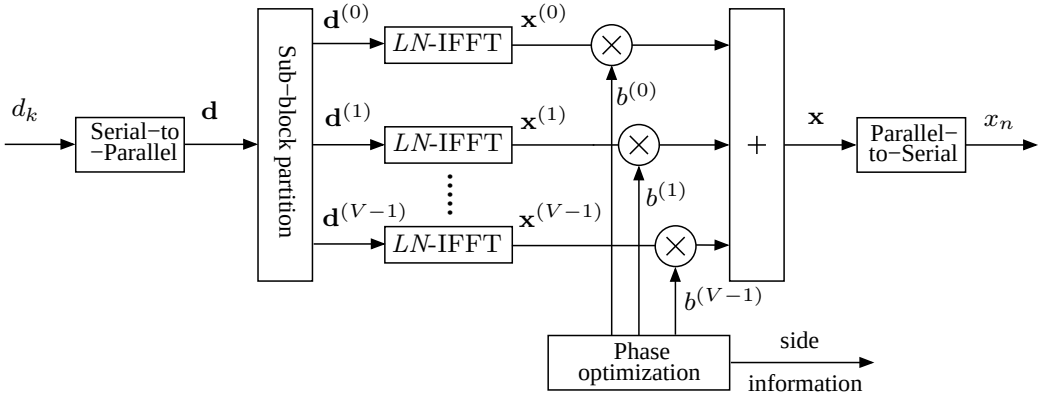

Figure 3.3: Block diagram of CPTS scheme.

3.3.3 Partial transmit sequences scheme

Fig. 3.3 depicts the block diagram of the conventional PTS (CPTS) scheme [40]. In this technique, the input data block $\mathbf{d}$, which consists of N symbols, is partitioned into V disjoint sets $\mathbf{d}^{(v)}$, $v = 0, 1, \cdots, V-1$ and zero padded left and right to obtain

$$\mathbf{d}^{(v)} = \left[\mathbf{0}^{1\times vN/V}, \{\mathbf{d}\}_{vN/V}^{(v+1)N/V-1}, \mathbf{0}^{1\times[N-(v+1)N/V]}\right]. \tag{3.7}$$

The time-domain vector, $\mathbf{x}^{(v)}$, is obtained by applying a LN-point IFFT on each of the disjoint sets. The time-domain samples, $x_n^{(v)}$, can be expressed as

$$x_n^{(v)} = \frac{1}{\sqrt{LN}} \sum_{k=0}^{N-1} d_k^{(v)} \mathrm{e}^{j2\pi kn/LN}, \quad n = 0, 1, \cdots, LN-1. \tag{3.8}$$

Subsequently, the complex weighting phase factors, $b^{(v)} = \{\pm 1, \pm j\}$, are introduced to scramble the IFFT outputs. Finally, the V signals are added to produce the overall time-domain samples

$$x_n = \sum_{v=0}^{V-1} b^{(v)} x_n^{(v)}. \tag{3.9}$$

The main idea of this scheme is to select the optimal combination of phase factors that minimise the PAPR and transmit these factors as SI.

3.3.4 Selected mapping scheme

The block diagram of the conventional SLM (CSLM) scheme is shown in Fig. 3.4 [40]. The data symbols are copied into U sections, each multiplied by U different phase sequences $\mathbf{a}^{(u)} = [a_0^{(u)}, a_1^{(u)}, \cdots, a_{N-1}^{(u)}]$ with $u = 0, 1, \cdots, U-1$, to generate

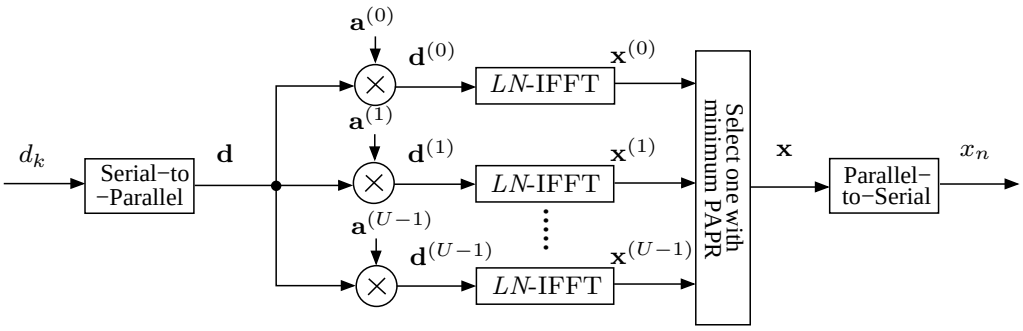

Figure 3.4: Block diagram of CSLM scheme.

alternative input sequences that can be represented as

$$\mathbf{d}^{(u)} = \mathbf{d} \circ \mathbf{a}^{(u)}, \quad u = 0, 1, \cdots, U-1, \tag{3.10}$$

where $\mathbf{a}^{(0)}$ is set as a unity vector, while $\mathbf{a}^{(u)}, u = 1, 2, \cdots, U-1$ are selected randomly with phase values $\{\pm 1, \pm j\}$. The operation $\circ$ denotes the Hadamard product (element-wise product). Subsequently, each of the U branches is applied to a LN-point IFFT. The resulting sample of the u-th sequence can be expressed as

$$x_n^{(u)} = \frac{1}{\sqrt{LN}} \sum_{k=0}^{N-1} d_k a_k^{(u)} \mathrm{e}^{j2\pi kn/LN}, \quad n = 0, 1, \cdots, LN-1. \tag{3.11}$$

The PAPR is computed for the U branches using the set of phase vectors $\mathbf{a}^{(0)}, \cdots, \mathbf{a}^{(U-1)}$ and the branch with the minimum PAPR is selected for transmission.

3.3.5 Nonlinear companding transforms

One of the interesting PAPR reduction approaches are NCT. These transforms have two main advantages in addition to high capability to the PAPR reduction: low implementation complexity and no bandwidth expansion [37]. An example of the NCT is an exponential transform [45] that expands the small amplitude signals and compresses the high amplitude signals; as a result, the average power of the transmitted signals is increased, and consequently, the PAPR will decrease. The increase in the average power causes the HPA to operate in vicinity to the saturation region; subsequently the system BER performance will degrade.

Four conventional companding approaches have been presented in [37]: linear symmetrical transform, linear nonsymmetrical transform, nonlinear symmetrical transform and nonlinear nonsymmetrical transform. Among the presented

approaches, the second approach presents the best compromise between the PAPR and BER performance.

3.3.6 Tone reservation and tone injection schemes

TR and TI are two well-known schemes to reduce the PAPR of OFDM systems. The OFDM signal peaks can be reduced by inserting a subset of tone-dependent time-domain signals to the original OFDM signal. The time-domain signal can be calculated easily using different algorithms at the transmitter and discarded at the receiver. Note that the inserted signals have no effect on the data carrying SCs as the SCs are orthogonal in the OFDM systems.

The transmitter of the TR scheme sends data on a large subset of SCs to minimise the PAPR reduction [38]. The key point of this scheme is to generate time-domain peak reduction vector, $\mathbf{b}$; subsequently, to insert this vector to the original time-domain vector, $\mathbf{x}$. The frequency-domain peak reduction vector $\mathbf{B} = [B_0, B_1, \cdots, B_{N-1}]^T$ is added to the original frequency-domain vector, $\mathbf{X}$, the entire vector can be characterised as $\mathbf{x} + \mathbf{b} = \text{IFFT}\{\mathbf{X} + \mathbf{B}\}$. The peak reduction signal, $B_k = 0,\ k \notin \{l_1, l_2, \cdots, l_Q\}$, is inserted in the original data block, $X_k = 0,\ k \in \{l_1, l_2, \cdots, l_Q\}$, where Q is the non-zero positions in vector $\mathbf{B}$. Two algorithms have been proposed to obtain the non-zero values of the vector $\mathbf{B}$ that can reduce the PAPR, convex optimisation and simple gradient algorithm.

The main objective of a PAPR reduction based TI scheme is to increase the constellation size, where each of the points in the typical basic constellation is mapped into a number of corresponding points [38]. The real and/or imaginary parts of the basic constellation points, X_k, are modified to obtain $\hat{X}_k$. The modified transmitted signal can be expressed as, $\hat{X}_k = X_k + (m + jn)F$, where m and n are integer values and F is a positive real number. These parameters should be known at the receiver. The selection of these parameters depends on the required PAPR reduction, to avoid degrading the BER performance.

The TI scheme has two significant disadvantages compared to the TR scheme. Firstly, same frequency band is used for both the modified signal and information signal. Secondly, the transmit power signal is increased owing to the injected signal in the TI scheme.

3.4 Factors for Selecting the PAPR Reduction Technique

Several factors should be considered for selecting the technique that can reduce the PAPR effectively while simultaneously maintaining the high-quality performance. These factors are as follows from [29] and [30]:

1. High capability PAPR reduction: clearly, this is the major factor to be taken into account for selecting the PAPR reduction method. In particular methods such as the amplitude clipping and NCT, the destructive effects of the in-band distortion and out-of-band radiation should be considered.

2. Low average power in transmit signal: the average power of the transmit signals is increased after utilising some PAPR reduction methods such as TR and TI. The average power must be normalised after the PAPR reduction to the power level before the PAPR reduction. This normalisation causes degradation in the BER performance.

3. No BER performance degradation at the receiver: the main idea of the PAPR reduction in OFDM signals is to achieve an improvement in the BER performance. This performance degrades due to the in-band distortion in clipping and NCT schemes. Furthermore, recovering the side information incorrectly at the receiver side in the PTS and SLM schemes is another cause of BER performance degradation.

4. No loss in data rate: in consequence of sending the SI, the signal bandwidth expands in a few schemes such as PTS, SLM and coding. The data rate will reduce due to the bandwidth expansion. To perform the original data rate of the OFDM signal, the SI should be embedded.

5. Low computational complexity: commonly, more complex schemes can achieve superior PAPR reduction. However, a scheme such as PTS reduces the PAPR by exhaustive searching of weighing phase factors. Therefore, the desired time and hardware for the PAPR reduction should be reduced to the minimum possible.

6. No spectral spillage: OFDM is immune to the multipath fading; consequently,

Table 3.2: Comparison of PAPR reduction schemes.

	Power increase	Computational complexity	Data rate loss	BER degradation	HPA power efficiency
Clipping	No	Low	No	**Yes**	**Low**
Coding	No	**High**	**Yes**	No	High
PTS/SLM	No	**High**	**Yes**	No	High
NCT	No	Low	No	**Yes**	High
TR/TI	**Yes**	**High**	**Yes**/No	No	High

in order not to defeat this feature in any PAPR reduction scheme, the spectral spillage should be prevented.

7. HPA efficiency: the operating point of the HPA must be near to the saturation region to increase the HPA efficiency; this will increase the error rate. Consequently, utilising PAPR reduction schemes can improve the BER performance, and hence, increase the amplifier efficiency.

8. Other factors: the effect of nonlinear devices such as digital-to-analogue converters (DACs) and mixers require careful scrutiny. Furthermore, the cost of these devices is a significant factor in respect of PAPR reduction methods.

Most PAPR techniques achieve high PAPR reduction at the expense of increased transmit signal power, data rate, BER and implementation complexity. It has been shown in [46] that the relationship between power efficiency of the HPA and PAPR reduction should be considered, and hence, the PAPR level is selected to obtain the lowest possible BER, not minimum PAPR value. This technique is known as an efficient-PAPR selection.

Table 3.2 shows the summary of the five standard PAPR reduction schemes [29] and [30]. It can be seen from this table that the PTS and SLM schemes are efficient and distortionless for PAPR reduction. However, these schemes are more complex than other schemes and the data rate is reduced due to the transmission of the SI bits. The CSLM can be implemented with less complexity than the CPTS. Furthermore, the required bits for SI are fewer. On the other hand, the CPTS can achieve more PAPR reduction. Generally, more complex techniques have better PAPR reduction capability.

3.5 Literature Review for PTS Scheme

S. H. Muller and J. B. Huber, 1997 [40], proposed a new significant useful and flexible PAPR reduction technique for OFDM named CPTS. The main objective of this scheme is from scrambling the partitioned sets by using rotation phase factors, $\{\pm 1, \pm j\}$, after the IFFT within the transmitter, then selecting the optimal sequences with minimum the PAPR as shown in Fig. 3.3.

In particular, there are two major disadvantages of the PTS when compared with well-known PAPR reduction techniques. Firstly, high complexity is required when searching for an optimal solution. This scheme requires an exhaustive search over all combinations of the allowed phase weighting factors; the search complexity increases exponentially with the number of subblocks. Secondly, efficient transmit and recover side information at the receiver is required.

3.5.1 Computational complexity reduction techniques

3.5.1.1 Low-complexity techniques

S. G. Kang et al, 1999 [47], presented a novel subblock partition scheme (SPS) for the PTS technique. Three categories of partitioning can be classified: interleaved, adjacent and pseudo-random partition. In the proposed scheme, to create each subblock, signals are repetitively copied and concatenated instead of zero-padding concatenation. The proposed concatenated pseudo-random SPS demonstrated PAPR reduction performance similar to the conventional pseudo-random PTS. Furthermore, computational complexity can be reduced significantly. Therefore, this scheme is suitable for high speed data rate applications.

L. J. Cimini and N. R. Sollenberger, 2000 [48], proposed suboptimal scheme for combining the PTS with $\{\pm 1\}$ weighting factors only. The proposed scheme is less complex than the CPTS and more simply realised, however, with minor performance degradation. This scheme described a suboptimal iterative algorithm called the iterative PTS (IPTS).

A. D. S. Jayalath and C. Tellambura, 2000 [49], presented an adaptive PTS technique for PAPR reduction in OFDM system. This technique stopped iterations as soon as the PAPR was reduced to below the threshold. The proposed technique can achieve high complexity reduction, however with trivial degradation in performance.

The same authors, in [50], developed the adaptive PTS by adding an interleaver. In this technique, the PAPR is computed for the original data sequence without interleaving and PAPR minimisation stops immediately when the PAPR is less than a certain threshold as in [49]. Otherwise, the data sequence is interleaved and the PAPR re-computed. The minimisation process is stopped when the PAPR is lower than the threshold.

W. S. Ho et al, 2003 [51], proposed a suboptimal dual-layered approach to reduce the computational complexity of the CPTS. In the first layer, the subblocks are grouped into divisions. Each division carried out all possible combinations of $\{\pm 1\}$ that should be examined to achieve minimum PAPR. For further PAPR reduction, each independently optimised division is presented as a block in the second layer. The simulation results show that this approach can achieve efficient PAPR reduction.

O. Kwon and Y. Ha, 2003 [52], presented a new suboptimal PTS that can obtain specific bits in phase factors that manage smaller PAPR in each procedure using a fixed threshold. Compared with the CPTS technique, the computational complexity can be reduced at the cost of a slight degradation to the PAPR performance.

L. Yang et al, 2006 [53], proposed a novel reduced complexity PTS approach by considering the correlation between the weighting factors and the transmitted bit vectors using suboptimal PTS with a fixed threshold. This approach outperforms the proposed PTS scheme in [52].

P. Boonsrimuang et al, 2007 [54], presented new weighting factor method for the PTS scheme which can improve the PAPR reduction performance and achieve less computational complexity. The proposed method divided each partition into two parts, each part scrambled by different weighting phase factors. The proposed scheme can improve both PAPR and BER performances.

S. J. Ku et al, 2010 [55], proposed a new reduced complexity PTS scheme. In this scheme, a new cost function is created, which can be defined as the sum of the power samples after the IFFT in each subblock. The samples with cost function that are greater than or equal to a fixed threshold are selected. Consequently, the signal with lowest PAPR for transmission is chosen from the selected candidates. The proposed scheme can achieve approximately the same PAPR reduction compared to the CPTS scheme, with less computational complexity.

J. Hou et al, 2011 [56], presented a novel scheme based on the PTS to reduce the computational complexity, tacking into account the correlation among the weighting

phase factors. In this scheme, instead of decreasing the number of candidate signals, simplifying the computation for each candidate signal is required. Since the number of candidates is not decreased, the proposed scheme can achieve similar PAPR reduction compared to the CPTS scheme, with lower computational complexity.

3.5.1.2 Non-uniform factors techniques

P. Foomooljareon et al, 2003 [57], presented a new technique based on the PTS scheme. The input envelope of the OFDM signal is scaled by using different scaling factors in this technique. The scaling factors used are $\{0.5, 1\}$ instead of $\{\pm 1\}$ within the IPTS. Simulation results demonstrated that the proposed technique outperforms the adaptive PTS presented in [49].

Y. R. Tsai, and S. J. Huang, 2008 [58], proposed a modified PTS scheme by applying non-uniform phase factors. The phases used are $\{0, 0.64\pi, \pi, 1.36\pi\}$ instead of the uniform phases, $\{0, 0.5\pi, \pi, 1.5\pi\}$. The proposed scheme outperforms the CPTS scheme in PAPR reduction performance, without increasing the computational complexity.

3.5.1.3 Various techniques

N. T. Hieu et al, 2005 [59], presented a low-complexity method for PAPR reduction based on the PTS by using only one IFFT and interleaving the weighting phase factors in matrix form. The simulation results show a similar PAPR reduction in the proposed method compared to the CPTS.

D. W. Lim et al, 2006 [60], presented a new PTS approach with low computational complexity by dividing the IFFTs into two stages, l and $n - l$. The first l stages produce a signal vector and this signal vector is partitioned into signal sub-vectors. The second $n - l$ stages are applied to each of the signal sub-vectors and the results, after being multiplied by a set of rotating phase factors, are added. The lowest PAPR among these signal sequences is selected for transmission. By comparing the performance of the proposed approach to the CPTS, similar PAPR reduction can be achieved.

A. Ghassemi and T. A. Gulliver, 2008 [61], proposed a new technique to reduce the computational complexity, named decomposition PTS (DPTS). In this technique, signals are considered at the middle stages of an N-point radix FFT.

The DPTS decreases the multiplicative and additive complexity, whilst presenting similar PAPR reduction to the CPTS.

3.5.1.4 Advanced techniques

Most recently, novel algorithms for optimisation problem solving were launched through the evolution of computation. The conventional computation systems are correct for accurate computation; however these systems have high computational complexity. Evolutionary algorithms have further robustness and efficiency to solve complicated real problems. Several evolutionary algorithms have been adopted to reduce the computational complexity of the PTS scheme, such as Genetic algorithm (GA) [62], particle swarm optimisation (PSO) [63], simulated annealing (SA) [64], cross entropy (CE) [65] and artificial bee colony (ABC) [66]. These algorithms can achieve similar PAPR reduction when compared with the various techniques developed in the literature discussed above. Furthermore, the BER performance does not degrade.

3.5.2 Different metrics

As can be seen, major research has focused on minimising the PAPR metric of OFDM signals to improve the BER performance. On the other hand, the effects of the HPA characteristics are taken into account in recent studies, where new metrics are proposed. These metrics depend on the amplifier parameters and are applied to either the SLM or the PTS scheme. The new technique can mitigate the effects of the ICI generated by the amplifier, and hence, improve the BER performance.

X. Lei et al, 2003 [67], combined the PTS with the clipping technique to introduce a new scheme. The criterion adopted in this scheme is the estimation of the clipping noise power. For the PTS technique, the candidate with the lowest clipping noise power (not the lowest PAPR) is selected for transmission. The simulation results demonstrate that this scheme can achieve a reduction in both clipping noise and BER.

M. R. D. Rodrigues and I. J. Wassell, 2006 [68], proposed a new metric to reduce the BER of OFDM systems distorted by amplifier nonlinearity. This metric named as IMD is used with either the SLM or the PTS scheme. Simulation results show that the IMD outperforms the conventional schemes utilising PAPR metric. On the other

hand, further computational complexity is required for IMD metric calculation.

D. H. Park and H. K. Song, 2007 [3], introduced a new technique based on the PTS scheme that used an adaptive nonlinear estimator to estimate nonlinear distortion generated by the amplifier. Instead of the PAPR metric calculation, the mean square error (MSE) between the OFDM signals before and after the amplifier is adopted. The candidate with the minimum MSE (MMSE) is selected for transmission among OFDM scrambled signals. The proposed technique can achieve marginal BER performance improvement compared to the IPTS scheme, at the expense of additional complexity.

3.5.3 Side information issue (PTS)

L. J. Cimini and N. R. Sollenberger, 2000 [69], embedded the SI within the transmitted data and recovered it at the receiver using the PTS technique. To recover the data accurately, the receiver must know which inversion sequence is used to modify the transmitted data. The simple algorithm is used to generate a marker at the transmitter when $b^{(v)} = -1$, which subsequently rotates the disjoint set $\mathbf{d}^{(v)}$ in that subblock by $\pi/4$. This algorithm is designed to remove standard QPSK modulation by raising the frequency-domain symbols to the power of four. At the receiver, the subblock is multiplied by $b^{(v)} = -1$ when the partition is rotated by $\pi/4$. Simulation results indicate that there is no degradation in the BER performance when the marking algorithm is utilised.

C. C. Feng et al, 2003 [70], proposed two low-complexity schemes for the protection and transmission of the SI for the PTS approach. The first included frequency-domain marking algorithms and decision statistics for PSK modulation, whereas the second presented time-domain marking algorithm for QAM modulation. The latter demonstrated better system performance compared to the conventional approach.

A. D. S. Jayalath and C. Tellambura, 2003 [71], presented a new approach to embed the SI into PTS-OFDM signals without deterioration to the PAPR performance. The objective of this approach is to append the SI of the current OFDM symbol in the beginning subblock of the next OFDM symbol. Simulation results showed that the BER performance of the system can be improved. Moreover, the same authors in [72], proposed a new ML decoder for the SLM and PTS without SI. The main idea is to increase the diversity at the receiver by using U sets of the

symbols and consequently derive the ML decoder for SLM then utilising optimum hard decision for each SC. The proposed scheme does not degrade the BER due to errors in SI at the expense of an increase of the receiver complexity.

T. Giannopoulos and V. Paliouras, 2006 [73], proposed a new decoder for embedding the SI. This decoder used the known values of pilot tones and searched all possible combinations of weighting factors at the receiver to obtain the factor combination that has been utilised at the transmitter. No additional pilot tones are required for the proposed scheme, and hence, no bandwidth expansion is needed. Simulation results indicated that the proposed decoder can achieve similar BER compared to the OFDM systems without PAPR reduction. Furthermore, the proposed scheme can reduce the PAPR drastically.

H. G. Ryu et al, 2007 [74], proposed a new technique on the SI transmission based on the PTS scheme. In this technique, the input data block is partitioned into disjoint sets as in the CPTS method. Subsequently, the SI referring to the weighting factors is inserted in each cluster. The proposed technique can achieve similar PAPR reduction performance as the CPTS scheme, without degradation of the BER performance.

Y. Zhou and T. Jiang, 2009 [75], proposed a new multi-points square mapping (MSM) method and joined the proposed method with the CPTS technique in order to reduce the PAPR of OFDM systems. In this method, four constellation points that are apexes of a square have been used to represent one datum. The proposed method produced similar performance of PAPR reduction to the CPTS technique without transmitting the side information. Furthermore, this method has better bandwidth efficiency and BER performance.

L. Guan et al, 2010 [76], inserted the SI of the PTS into channel frequency response. Moreover, a new pilot arrangement is proposed, in which the pilots are independently appended into each PTS subblock to accomplish perfect channel estimation. Extensive simulations showed that the BER and PAPR reduction performances can be improved using the proposed pilot arrangement.

H. Kim et al, 2011 [77], proposed a new data recovery technique without transmitting the SI, based upon PTS-OFDM systems. In this technique, extra pilots are appended at the end of each subblock; consequently, effective data decoding using channel estimation can be carried out with known pilots. Compared to the CPTS, the proposed technique did not require the SI to be transmitted, yet still achieved

similar performance of PAPR reduction as the perfect SI and ML decoding scheme.

L. Yang, et al, 2011 [78], proposed a low-complexity PTS-based scheme by utilising cyclical shifting for each subblock sequence after the IFFT at the transmitter, while, at the receiver, after employing the FFT, the partitions are interleaved then demodulated and combined. This enabled the receiver to effectively detect the transmitted signal without SI. Simulation results demonstrated that the proposed scheme achieves similar BER performance as the CPTS with perfect SI detection.

3.6 Literature Review for SLM Scheme

R. W. Bauml el al, 1996 [79], proposed a new scheme for the PAPR of multicarrier systems referred to as SLM. This scheme offers considerable advantages at a marginal increase in complexity. In the SLM scheme, the data is multiplied by the rotated phase factor sets, $\{\pm 1, \pm j\}$, before IFFT at transmitter, then the sequences with minimum PAPR after the IFFT are selected, as shown in Fig. 3.4.

3.6.1 Computational complexity reduction techniques

C. L. Wang and Y. Ouyang, 2005 [80], introduced two novel low-complexity techniques based on the SLM scheme. In these schemes, a number of IFFTs are replaced by several types of conversion matrices. In the first scheme, only a single IFFT is required to produce the set of candidate signals, whereas in the second scheme, two IFFT operations are required. Simulation results have illustrated that the second proposed technique has approximately similar PAPR reduction performance to the CSLM, however, with degradation in the BER performance. Subsequently, C. L. Wang and S. J. Ku, 2009 [81], modified a new set of conversion matrices for the SLM scheme to reduce the complexity without degradation to the BER performance. On the other hand, the new scheme can achieve less PAPR reduction compared to the previous schemes.

D. W. Lim et al, 2005 [82], proposed a new low computational complexity SLM approach. The objective of the proposed scheme is similar to [60] using two stages of IFFTs. Similar performance of PAPR reduction is achieved when comparing the proposed approach to the CSLM.

S. J. Heo et al, 2007 [83], presented a low-complexity SLM-based method by

increasing the number of phase sequences and decreasing the number of IFFTs. The proposed method is suitable for high data rate OFDM systems. Comparing the proposed method to the CSLM, their simulation results demonstrated that the PAPR reduction performance is not compromised.

E. Alsusa and L. Yang, 2006 [84], presented a new low-complexity PAPR reduction technique using a single IFFT and a pool of random sequences. This technique, denoted as post-IFFT amplitude randomising (PIAR) technique, where a unique set of time-domain sequences per OFDM block is selected using an appropriate selection approach to minimise the PAPR. Compared to the CSLM, the PIAR can significantly reduce the PAPR and computational complexity.

L. Yang et al, 2008 [85], proposed a low-complexity SLM scheme utilising the time-domain sequence superposition technique. The proposed scheme requires only two IFFTs operations; in contrast the CSLM requires several IFFT operations. Simulation results illustrated that the proposed scheme can achieve similar PAPR reduction to that of the CSLM scheme.

A. Ghassemi and T. A. Gulliver, 2008 [86], presented a new technique named partial SLM with the same low-complexity IFFTs used in DPTS [61]. This technique can achieve huge computational complexity reduction compared to the CSLM, while attaining similar PAPR reduction.

C. P. Li et al, 2010 [87], proposed three novel low-complexity SLM schemes. In these schemes, three types of sequence are proposed, each sequence involving certain vectors and their cyclically shifted versions. The three schemes can achieve significantly less computational complexity than the CSLM, however, at a cost which impacts upon PAPR reduction.

3.6.2 Side information issue (SLM)

M. Breiling et al, 2001 [88], employed a scrambling approach combined with the SLM-PAR reduction for coded OFDM systems. By using label insertion and the scrambling approach, the SI transmission is embedded and protected within this scheme. However, an additional complexity is required to achieve an improvement in the BER performance.

N. Chen and G. T. Zhou, 2006 [89], proposed a novel approach which joined channel estimation and SLM-PAPR reduction technique, named "blind selected pilot

tone modulation". The index for the SLM can be blindly detected at the receiver which is performed according to the position of the pilot tones. The proposed approach is both power and bandwidth efficient. Simulation results showed that the proposed approach can achieve both PAPR and BER reduction over frequency-selective fading channels.

E. Alsusa and L. Yang, 2008 [90], embedded the SI at the transmitter side for both coded and uncoded systems. Simply recognised phase randomising vectors are used in order to avoid sending the SI in this technique. Compared to the CSLM technique, the proposed technique can achieve identical PAPR reduction performance; furthermore, it can provide considerably BER performance improvement.

S. Y. Le Goff et al, 2008 [91], presented a novel SLM scheme for embedding the SI at the transmitter. In this scheme, each SI index of the modulation symbols is extended by a specific set of positions; at the receiver, the SI detection block attempts to identify the positions of the extended symbols. Simulation results demonstrated that the proposed scheme can reduce the PAPR. However, a trivial degradation in BER performance is accomplished in addition to a minor increase in complexity at the receiver side.

3.7 Chapter Summary

From the literature review, it can be concluded that the low computational complexity trend is the main scenario in PAPR reduction topics. Furthermore, there is a shortcoming in the investigations for including the amplifier parameters with either the PTS or the SLM schemes. Only two metrics, IMD and MSE, have been adopted for selecting the weighting phase factors that depend on amplifier parameters to lower the effects of the ICI produced by the amplifier, and consequently, reduce the BER. However, the computational complexity of these metrics is higher than the PAPR metric. As a result, it is crucial to find new low-complex techniques for PAPR reduction by utilising different metrics that depend on amplifier parameters.

3.8 Conclusion

This chapter introduces the main PAPR reduction techniques in OFDM systems. The PTS and SLM schemes are the most important schemes used for PAPR reduc-

tion. These schemes are efficient and distortionless but more complex than other techniques and require recovering the SI at the receiver efficiently. Moreover, this chapter presents the literature review of the recent research scenarios in PAPR reduction based on the PTS and SLM schemes.

Chapter 4

New PAPR Reduction Low-Complexity Schemes in OFDM Systems

In this chapter, a new low-complexity scheme based on the IPTS (LC-IPTS) that employs two IFFTs and two circulant transform matrices is proposed, in order to reduce the complexity and improve the system performance. Furthermore, the low-complexity scheme is simplified (SLC-IPTS) by omitting one of the circulant transform matrices in order to reduce both the computational complexity and the number of the SI bits, at the cost of a small reduction in PAPR and BER performance.

4.1 PTS Flipping Algorithm

As shown in Fig. 3.3, the CPTS scheme requires an exhaustive search over all combinations of allowed phase weighting factors, $b^{(v)} = \{\pm 1, \pm j\}$, the search complexity increases exponentially with the number of subblocks. In contrast, for the IPTS only two phase factors, $b^{(v)} = \{\pm 1\}$, are applied to achieve low-complexity [48].

For further complexity reduction, the IPTS flipping algorithm described in [3] is adopted in this work. This algorithm can be summarised in the following steps:

1. Suppose that $b^{(v)} = 1$, for $v = 0, 1, \cdots, V-1$ and calculate the PAPR_1 of the overall time-domain samples in (3.9).

2. Modify the first phase factor ($b^{(0)} = -1$) and recalculate the new PAPR, PAPR_2.

3. If the PAPR_2 is lower than in the PAPR_1, keep $b^{(0)} = -1$ as an element of the final phase sequence; otherwise, go back to the previous value of $b^{(0)}$.

4. Investigate all V alternatives, and finally, transmit the phase sequence with minimum PAPR.

For the CPTS flipping algorithm repeat steps 2 to 4 for $b^{(v)} = -j$ and $b^{(v)} = j$. Consequently, the number of iterations in the flipping algorithm based on the IPTS and CPTS is $V + 1$ and $3V + 1$, respectively.

4.2 Circulant Transform Matrix

There are two methods to obtain the circulant transform matrix, $\mathbf{T}_r$. In the first method which is used for implementation, the phase factors can be expressed as $\mathbf{b} = [b^{(0)}, b^{(1)}, \cdots, b^{(V-1)}]_{1\times V}$, while the vector $\hat{\mathbf{b}}$ is the adjacent periodic weighting factors of $\mathbf{b}$ that can be described as $\hat{\mathbf{b}} = [b^{(0)}, b^{(1)}, \cdots, b^{(V-1)}, \cdots, b^{(0)}, b^{(1)}, \cdots, b^{(V-1)}]_{1\times LN}$. Let

$$\mathbf{t}_r = \hat{\mathbf{b}}\mathbf{F}, \tag{4.1}$$

where the transformation $\mathbf{F}$ of size $LN \times LN$ is defined as

$$\mathbf{F} = \frac{1}{\sqrt{LN}} \begin{bmatrix} 1 & 1 & \cdots & 1 \\ 1 & e^{j2\pi/LN} & \cdots & e^{j2\pi(LN-1)/LN} \\ \vdots & \vdots & \ddots & \vdots \\ 1 & e^{j2\pi(LN-1)/LN} & \cdots & e^{j2\pi(LN-1)(LN-1)/LN} \end{bmatrix}, \tag{4.2}$$

therefore, the circulant transform matrix can be written as [80]

$$\mathbf{T}_r = \begin{bmatrix} \mathbf{t}_r \\ \mathbf{t}_r^{\langle 1\rangle} \\ \mathbf{t}_r^{\langle 2\rangle} \\ \vdots \\ \mathbf{t}_r^{\langle LN-1\rangle} \end{bmatrix}_{LN\times LN}, \tag{4.3}$$

where $\mathbf{t}_r^{\langle k\rangle}$ is a circularly right shifted version of the row vector $\mathbf{t}_r$ by element k.

The $\mathbf{T}_r$ matrix, used for analysis, can be written using second method. The idea of the proposed $\mathbf{T}_r$ matrix is depicted in Fig. 4.1 [80] and [92]. As shown from this

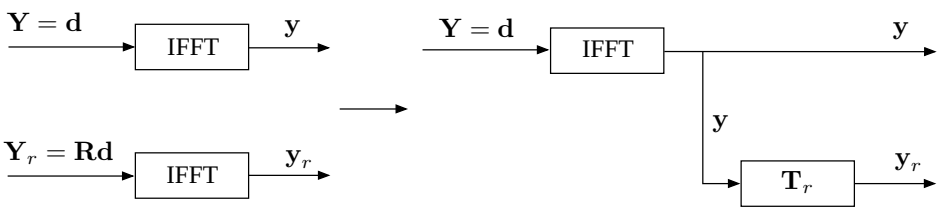

Figure 4.1: The $\mathbf{T}_r$ matrix idea.

figure, the output of the two IFFTs, $\mathbf{y}$ and $\mathbf{y}_r$, respectively, can be expressed as

$$\mathbf{y} = \mathbf{FY} = \mathbf{Fd}, \tag{4.4}$$

$$\mathbf{y}_r = \mathbf{FY}_r = \mathbf{FRd}, \tag{4.5}$$

where $\mathbf{R}$ can be written as

$$\mathbf{R} = \begin{bmatrix} b^{(0)} & 0 & \cdots & 0 \\ 0 & b^{(1)} & \cdots & 0 \\ \vdots & \vdots & \ddots & \vdots \\ 0 & 0 & \cdots & b^{(V-1)} \end{bmatrix}_{LN \times LN}. \tag{4.6}$$

Furthermore, by performing the FFT in (4.4), and substituting $\mathbf{d}$ into (4.5), $\mathbf{y}_r$ can be written as

$$\mathbf{y}_r = \mathbf{FRF}^{-1}\mathbf{y}, \tag{4.7}$$

where the transformation $\mathbf{F}^{-1}$ of size $LN \times LN$ can be expressed as

$$\mathbf{F}^{-1} = \frac{1}{\sqrt{LN}} \begin{bmatrix} 1 & 1 & \cdots & 1 \\ 1 & e^{-j2\pi/LN} & \cdots & e^{-j2\pi(LN-1)/LN} \\ \vdots & \vdots & \ddots & \vdots \\ 1 & e^{-j2\pi(LN-1)/LN} & \cdots & e^{-j2\pi(LN-1)(LN-1)/LN} \end{bmatrix}. \tag{4.8}$$

Finally, the matrix $\mathbf{T}_r$ can be obtained directly from (4.7)

$$\mathbf{T}_r = \mathbf{FRF}^{-1}. \tag{4.9}$$

For $N = 4$ SCs, $L = 4$ oversampling factor and $V = 4$ partitions, four cases of phase factors can be determined: odd-case (1), odd-case (2), even-case (1) and even-case (2). In the odd-cases the number of 1's is odd, while in the even-cases the

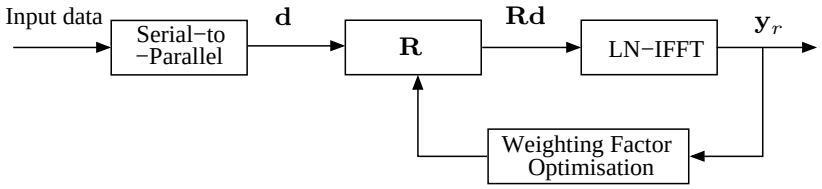

Figure 4.2: Block diagram of SPW technique.

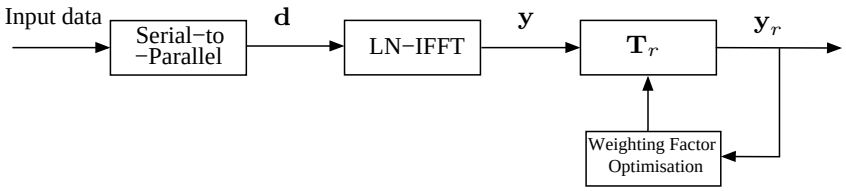

Figure 4.3: Block diagram of low-complexity SPW technique.

number of 1's is even. Therefore, each case has four vectors. The circulant matrices for these vectors are shown in Appendix A. The $\mathbf{T}_r$ matrices corresponding to the phase factors $\mathbf{b}$ for even and odd-case vectors can be computed off-line and saved in memory.

4.3 Literature Review

H. G. Ryu and K. J. Youn, 2002 [93] introduced a new subblock phase weighting (SPW) technique for PAPR reduction. The PTS and SLM schemes used V and U-IFFTs, respectively. In contrast, this technique utilises only one IFFT block is at any time. However, due to the sequential processing, a time delay in the SPW technique is introduced. Furthermore, this technique has less computational complexity than the conventional schemes. Fig. 4.2 depicts the block diagram of the SPW technique.

N. T. Hieu et al, 2005 [59] proposed a low-complexity phase weighting method as shown in Fig. 4.3. In the proposed scheme, only one IFFT and one phase weighting matrix are utilised to reduce the system complexity. However, no PAPR reduction can be found in comparison to the IPTS technique.

C. Wang and Y. Ouyang, 2005 [80] replaced the IFFT blocks applied in the CSLM scheme by a particular type of low-complexity matrices. Based on the proposed matrices, two novel schemes with low-complexities were proposed. The first method applies a single IFFT, while the second method applies two IFFTs. The simulation shows that the first scheme has worse PAPR reduction performance, while the second

scheme has the same reduction as the CSLM method.

4.4 New Schemes for PAPR Reduction

In this section, a new low-complexity based on IPTS technique named as LC-IPTS is proposed for PAPR reduction. In this technique, only two IFFTs and two circulant transform matrices, $\mathbf{T}_r$, are employed to reduce complexity and to achieve better performance than the PTS and the SLM techniques. Fig. 4.4 shows the new proposed LC-IPTS scheme for PAPR reduction. In this scheme the input data block $\mathbf{d} = [d_0, d_1, \cdots, d_{N-1}]$ with N SCs is partitioned into two disjointed sets $\mathbf{d}^{(1)} = [d_0, d_1, \cdots, d_{\frac{N}{2}-1}, 0, \cdots, 0]$ and $\mathbf{d}^{(2)} = [0, \cdots, 0, d_{\frac{N}{2}}, d_{\frac{N}{2}+1}, \cdots, d_{N-1}]$. In this figure, only two IFFTs blocks can be observed. The time domain signals $\mathbf{x}^{(l)}$, $l = 1, 2$, are obtained by computing an IFFT of length NL; subsequently, the two disjointed sets are concatenated with $(L-1)N$ zeros. Thus, $\mathbf{x}^{(l)}$ can be written as

$$\mathbf{x}^{(l)} = \mathbf{X}^{(l)}\mathbf{F}, \tag{4.10}$$

where $\mathbf{x}^{(l)} = [x_0^{(l)}, x_1^{(l)}, \cdots, x_{LN-1}^{(l)}]$. The time domain signals are multiplied by the circulant transform matrices $\mathbf{T}_r^{(l)}$ and added together to obtain $\mathbf{x}_T$ which can be represented by

$$\mathbf{x}_T = \mathbf{x}^{(1)}\mathbf{T}_r^{(1)} + \mathbf{x}^{(2)}\mathbf{T}_r^{(2)} = \mathbf{x}_T^{(1)} + \mathbf{x}_T^{(2)}. \tag{4.11}$$

Fig. 4.5 shows the proposed SLC-IPTS scheme. The main difference between the LC-IPTS and SLC-IPTS schemes is that the upper branch in the latter scheme does not include $\mathbf{T}_r$. Therefore, the transmitted signal can be simplified to

$$\mathbf{x}_T = \mathbf{x}^{(1)} + \mathbf{x}^{(2)}\mathbf{T}_r = \mathbf{x}^{(1)} + \mathbf{x}_T^{(2)}. \tag{4.12}$$

Finally, the optimum circulant transform matrices that minimise PAPR are selected for transmission.

In order to recover the information from the transmitted signal, SI is required on which $\mathbf{T}_r$ is utilised in the first and second branches. Firstly, an LN-point FFT on the received data is performed. The received signal in the absence of noise after

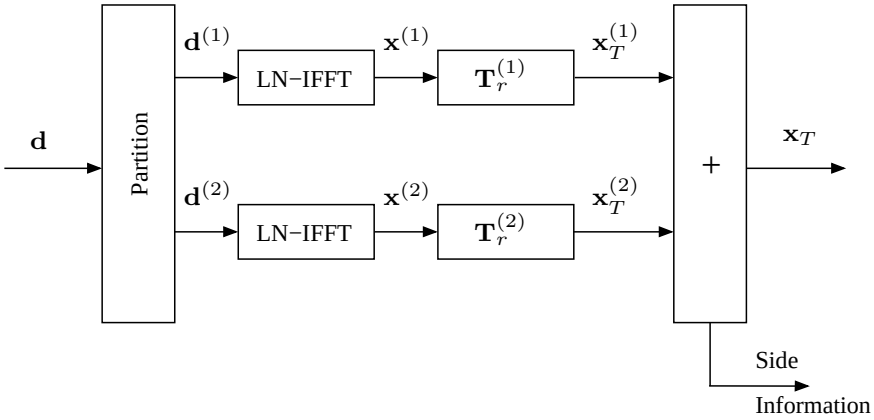

Figure 4.4: Block diagram of the proposed LC-IPTS technique.

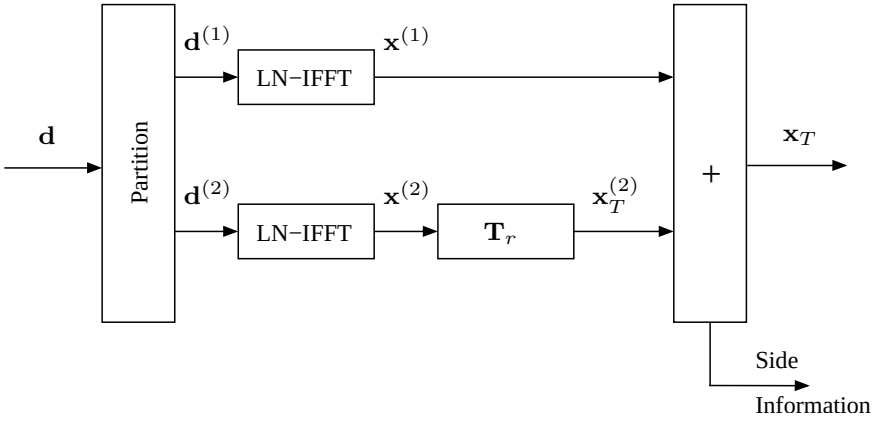

Figure 4.5: Block diagram of the proposed SLC-IPTS technique.

the FFT for the LC-IPTS scheme can be given as

$$\mathbf{Y}_b = \left[\mathbf{d}^{(1)}\mathbf{F}\mathbf{T}_r^{(1)} + \mathbf{d}^{(2)}\mathbf{F}\mathbf{T}_r^{(2)}\right]\mathbf{F}^{-1}, \tag{4.13}$$

substituting $\mathbf{R}^{(l)} = \mathbf{F}\mathbf{T}_r^{(l)}\mathbf{F}^{-1}$ for $l = 1, 2$ in (4.13), therefore, $\mathbf{Y}_b$ can be rewritten as

$$\mathbf{Y}_b = \mathbf{d}^{(1)}\mathbf{R}^{(1)} + \mathbf{d}^{(2)}\mathbf{R}^{(2)}. \tag{4.14}$$

Similarly, the received signal after the FFT for the SLC-IPTS scheme can be expressed as

$$\begin{aligned}\mathbf{Y}_b &= \left[\mathbf{d}^{(1)}\mathbf{F} + \mathbf{d}^{(2)}\mathbf{F}\mathbf{T}_r\right]\mathbf{F}^{-1}, \\ &= \mathbf{d}^{(1)} + \mathbf{d}^{(2)}\mathbf{R}.\end{aligned} \tag{4.15}$$

Finally, the signal $\mathbf{Y}_b$ is multiplied by the conjugate matrices of $\mathbf{R}$ to recover the transmitted signal.

4.5 Computational Complexity Calculations

In this section, the computational complexity of the PTS, SLM, LC-IPTS and SLC-IPTS techniques will be discussed. Generally, the complexity of one LN-point IFFT is $(LN/2)\log_2(LN)$ complex multiplications (CMs) and $(LN)\log_2(LN)$ complex additions (CAs) when zero-padding is not considered [78] and [80]. The computational complexity of the considered PAPR reduction techniques is assessed in terms of the equivalent complexity C, which is a function of the number of real additions (RAs) and real multiplications (RMs) required to select the coefficients for each technique. In general, one CM requires four RMs and two RAs, whereas, a CA requires two RAs.

4.5.1 Complexity analysis of the PTS and SLM techniques

To prevent a CM operation, the phase factors are selected uniformly from $b^{(v)} = \{\pm 1, \pm j\}$ for CPTS and $b^{(v)} = \{\pm 1\}$ for the IPTS. Whereas for SLM the phase factors are chosen from $a_i^{(u)} \in \{\pm 1, \pm j\}$, $i \in \{0, 1, \cdots, N-1\}$. It is worth noting that the multiplication by ± 1 or $\pm j$ is considered as a trivial multiplication in this chapter as highlighted in [80] and [94].

The computational complexity of the PTS scheme is considered by the following operations

- $(VLN/2)\log_2(LN)$ CMs and $(VLN)\log_2(LN)$ CAs are required for implementing a VLN-point IFFT.
- $(V-1)\mathcal{J}LN$ CAs are required to generate the overall time-domain samples, x_n, in (3.9), where $\mathcal{J}$ is the number of iterations.
- $2\mathcal{J}LN$ RMs and $\mathcal{J}LN$ RAs are required to calculate the PAPR metric.

Note that in practice, $\mathcal{J} = V + 1$ and $\mathcal{J} = 3V + 1$ are selected for the IPTS and CPTS, respectively. The computational complexity operations for the SLM scheme are characterised as follows:

- $(ULN/2)\log_2(LN)$ CMs and $(ULN)\log_2(LN)$ CAs are required for implementing ULN-point IFFT.
- $2ULN$ RMs and ULN RAs are required to calculate the PAPR metric.

Table 4.1: 16 types of $\mathbf{b}$ and $\mathbf{B}$ for $V = 4$ partitions.

SLC-IPTS		LC-IPTS	$\mathbf{b}$	$\mathbf{B} = \text{IFFT}\{\mathbf{b}\}$
full-case	odd-case	odd-case (1)	[1,1,1,-1]	0.5 × [1,j,1,-j]
			[1,1,-1,1]	0.5 × [1,1,-1,1]
			[1,-1,1,1]	0.5 × [1,-j,1,j]
			[-1,1,1,1]	0.5 × [1,-1,-1,-1]
		odd-case (2)	[-1,-1,-1,1]	0.5 × [-1,-j,-1,-j]
			[-1,-1,1,-1]	0.5 × [-1,-1,1,-1]
			[-1,1,-1,-1]	0.5 × [-1,j,-1,j]
			[1,-1,-1,-1]	0.5 × [-1,1,1,1]
	even-case	even-case (1)	[1,1,-1,-1]	0.5 × [0,1+j,0,1-j]
			[-1,1,1,-1]	0.5 × [0,-1+j,0,-1-j]
			[1,-1,-1,1]	0.5 × [0,1-j,0,1+j]
			[-1,-1,1,1]	0.5 × [0,-1-j,0,-1+j]
		even-case (2)	[1,-1,1,-1]	0.5 × [0,0,1,0]
			[-1,1,-1,1]	0.5 × [0,0,-1,0]
			[1,1,1,1]	0.5 × [1,0,0,0]
			[-1,-1,-1,-1]	0.5 × [-1,0,0,0]

4.5.2 Complexity analysis of the proposed techniques

Four cases of phase factors (for $V = 4$ partitions) can be determined (each case has four vectors) as shown in Table 4.1. In the odd-cases of the circulant transform matrix, $3LN$ CAs are required. The first even-case has $2LN$ CMs and LN CAs. The second even-case has no added computational complexity.

In the LC-IPTS technique, two LN-point IFFTs are required (i.e. $(LN)\log_2(LN)$ CMs and $(2LN)\log_2(LN)$ CAs). In addition, in the odd-cases, $3\mathcal{V}LN$ CAs are required, where $\mathcal{V} = 4$ is the number of circulant transforms performed in each case. In the even-case (1), $2\mathcal{V}LN$ CMs and $\mathcal{V}LN$ CAs are needed. Furthermore, the combination of the two sub-blocks requires $\mathcal{I}LN$ CAs, where $\mathcal{I} = 16$ iteration operations are used for all cases mentioned above. Finally, $2\mathcal{I}LN$ RMs and $\mathcal{I}LN$ RAs are required for power calculation for these cases.

In the SLC-IPTS technique, two LN-point IFFTs are required similar to the LC-IPTS technique. As shown in Table 4.1, in the odd-case, $\mathcal{I}_1 = 8$ circulant transform matrices are utilised; therefore, $3\mathcal{I}_1LN$ CAs are needed. In the even-case, $\mathcal{I}_2 = 8$ circulant transform matrices are utilised; therefore, $\mathcal{I}_2LN$ CMs and $\mathcal{I}_2LN/2$ CAs are required. In the full-case, $\mathcal{I} = \mathcal{I}_1 + \mathcal{I}_2$ circulant transform matrices are utilised, $\mathcal{I}_2LN$ CMs and $3\mathcal{I}_1LN + \mathcal{I}_2LN/2$ CAs are required. Furthermore, the combination of the two subblocks requires $\mathcal{I}_1LN$, $\mathcal{I}_2LN$ and $\mathcal{I}LN$ CAs for the odd-case, even-

Table 4.2: Analysis of the Computational Complexity in the PTS, SLM and Proposed Techniques.

PAPR Reduction Technique	Number of RAs (A)	Number of RMs (M)
PTS [94]	$VLN\{3\log_2(LN)+2\mathcal{I}\}-LN\mathcal{I}$	$2VLN\log_2(LN)+2LN\mathcal{I}$
SLM [94]	$ULN\{3\log_2(LN)+1\}$	$2ULN\{\log_2(LN)+1\}$
Proposed LC-IPTS odd-case (1) and (2)	$3LN\{2\log_2(LN)+4\mathcal{V}+\mathcal{I}\}$	$2LN\{4\log_2(LN)+\mathcal{I}\}$
Proposed LC-IPTS even-case (1)	$3LN\{2\log_2(LN)+16/3\mathcal{V}+\mathcal{I}\}$	$2LN\{4\log_2(LN)+6\mathcal{V}+\mathcal{I}\}$
Proposed LC-IPTS even-case (2)	$3LN\{2\log_2(LN)+\mathcal{I}\}$	$2LN\{4\log_2(LN)+\mathcal{I}\}$
Proposed SLC-IPTS odd-case	$3LN\{2\log_2(LN)+3\mathcal{I}_1\}$	$2LN\{4\log_2(LN)+\mathcal{I}_1\}$
Proposed SLC-IPTS even-case	$6LN\{\log_2(LN)+\mathcal{I}_2\}$	$2LN\{4\log_2(LN)+3\mathcal{I}_2\}$
Proposed SLC-IPTS full-case	$3LN\{2\log_2(LN)+2\mathcal{I}_2+3\mathcal{I}_1\}$	$2LN\{4\log_2(LN)+3\mathcal{I}_2+\mathcal{I}_1\}$

case and full-case, respectively. Finally, $2\mathcal{I}_1LN$, $2\mathcal{I}_2LN$ and $2\mathcal{I}LN$ RMs as well as $\mathcal{I}_1LN$, $\mathcal{I}_2LN$ and $\mathcal{I}LN$ are required to calculate the power for odd-case, even-case and full-case, respectively.

4.5.3 Overall computational complexity

The overall computational complexity in terms of the total number of RAs and RMs for the PTS, SLM and all proposed cases mentioned above can be formulated in Table 4.2. Although additions and multiplications are implemented differently in hardware, their relative complexity can be roughly set to g, where one RM is equivalent to g RAs [95]. Therefore, the equivalent complexity can be calculated as

$$C = A + gM, \tag{4.16}$$

where the g parameter is the number of addition instructions required for each multiplication operation. From this table the number of RAs in terms of the number of SCs can calculated for $V = U = 4$ partitions using $g = 4$ [95]. Fig. 4.6(a) depicts the total number of RAs for the LC-IPTS, IPTS, CPTS and SLM techniques. It is clear that the proposed even-case (2) and odd-cases have the lowest complexity than other schemes. On the other hand, even-case (1) is more complex than IPTS

Table 4.3: The CCRR of the proposed schemes over the SLM, IPTS and CPTS for $N = 128$, $L = 4$ and $V = U = 4$.

Proposed Technique	Case	CCRR-SLM	CCRR-IPTS	CCRR-CPTS
LC-IPTS	odd-cases	8%	16%	33%
	even-case (1)	-22%	-12%	11%
	even-case (2)	13%	21%	37%
SLC-IPTS	odd-case	23%	30%	43%
	even-case	-1%	7%	26%
	full-case	-33%	-22%	3%

and SLM techniques. In addition, CPTS has the worst computational complexity. The total number of RAs for the SLC-IPTS, IPTS, CPTS and SLM techniques are illustrated in Fig. 4.6(b). It can be observed from this figure that the odd-case has lowest computational complexity. In contrast, the full-case is more complex than IPTS and SLM techniques.

The computational complexity reduction ratio (CCRR) of the proposed schemes over the PTS or SLM can be defined as [59]

$$\text{CCRR} = \left(1 - \frac{x}{y}\right) \times 100\%, \tag{4.17}$$

where x is the number of RAs for one of the proposed scheme case and y is the number of RAs for the PTS or SLM scheme.

Table 4.3 shows the calculated CCRR for the LC-IPTS and SLC-IPTS over SLM, IPTS and CPTS techniques for $N = 128$ SCs and $V = U = 4$ partitions. The minus sign in this table means that the proposed technique is more complex than the conventional one. It can be observed that the SLM has less CCRR than the PTS for all cases. Furthermore, even-case (1) and full-case are more complex compared with other cases in LC-IPTS and SLC-IPTS, respectively. For example, in LC-IPTS, the CCRR is equal to 16% and 21% in comparison to the IPTS with odd-cases and even-case (2), respectively, has a 12% increase in complexity in comparison to the IPTS. In SLC-IPTS, the CCRR is equal to 30% and 7% in comparison to the IPTS with odd-case and even-case, respectively. The IPTS has a 22% reduction in complexity in comparison to the full-case.

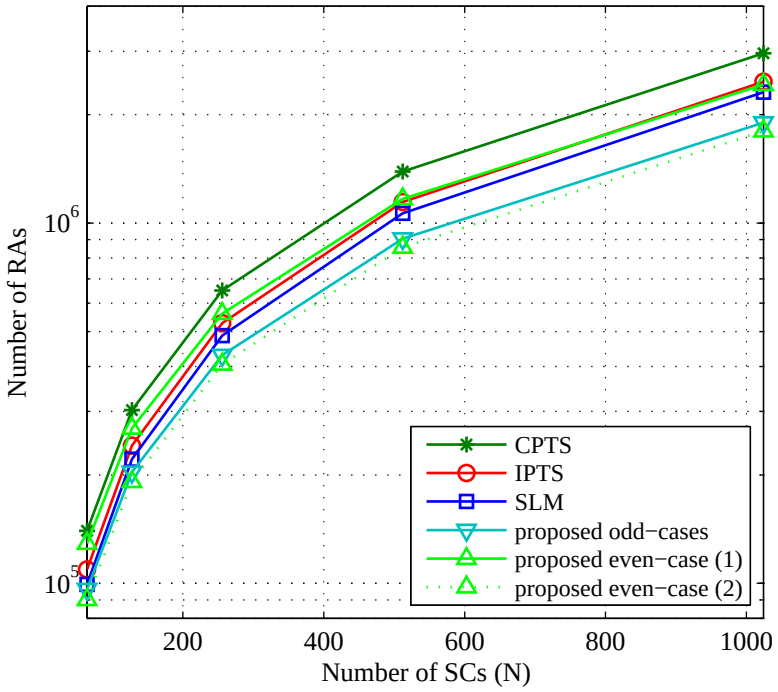

(a) Proposed LC-IPTS

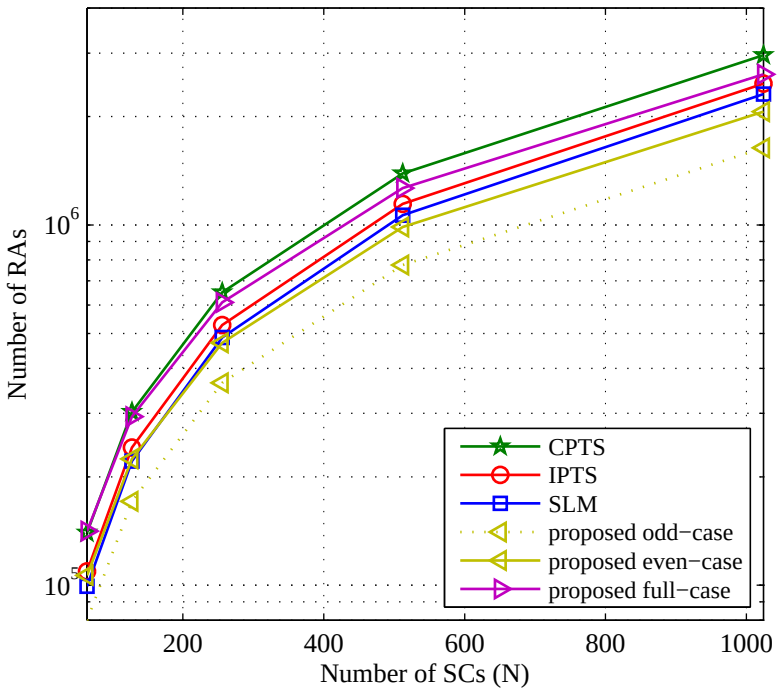

(b) Proposed SLC-IPTS

Figure 4.6: Total number of RAs for the proposed (LC-IPTS and SLC-IPTS), IPTS, CPTS and SLM techniques.

4.6 Simulation Results

In this section simulation results are presented, 10^5 OFDM blocks are randomly generated with 128 SCs, ($N = 128$), using 16-QAM, QPSK and HM data symbols constellations. In addition, the PTS, SLM and proposed techniques are utilised for PAPR reduction. For the IPTS and proposed techniques, the number of allowed phase factors are two with random phase values (± 1), while, for the CPTS and SLM techniques, the number of allowed phase factors are four with random phase values ($\pm 1, \pm j$).

4.6.1 Power amplifiers operating points

Lower values of OBOs are required when PAPR reduction techniques are utilised. Fig. 4.7 depicts the simulated TD curves using either the TWTA or the SSPA for 16-QAM-OFDM and QPSK-OFDM systems at a threshold BER of 10^{-4}. It is clear from this figure that the TD of the TWTA is higher than SSPA for both constellations. Moreover, the TWTA and SSPA have an optimum OBO = 5 and 4 dB, respectively, for 16-QAM-OFDM. While, for QPSK-OFDM the optimum OBO is 0 dB using both TWTA and SSPA.

4.6.2 Time-domain OFDM symbol

Fig. 4.8 illustrates time-domain signals of a single random OFDM symbol at the output of the IFFT and TWTA with $N = 128$ using 16-QAM-modulated SCs without and with PAPR reduction. It can be noted that, the PAPR reduction techniques can lower the magnitudes of the OFDM symbol peaks. Consequently, these low level magnitudes should minimise the effect of clipping due to the amplifier, and hence, reduce the BER.

4.6.3 Power spectrum performance

The PSD of an OFDM signal with and without PAPR reduction measured at the output of the TWTA is shown in Fig. 4.9. It can be noted from this figure that the out-of-band power produced by the different reduction techniques is approximately identical. In particular, the out-of-band power produced by the conventional PAPR reduction techniques (PTS and SLM) is a little lower than that produced by the

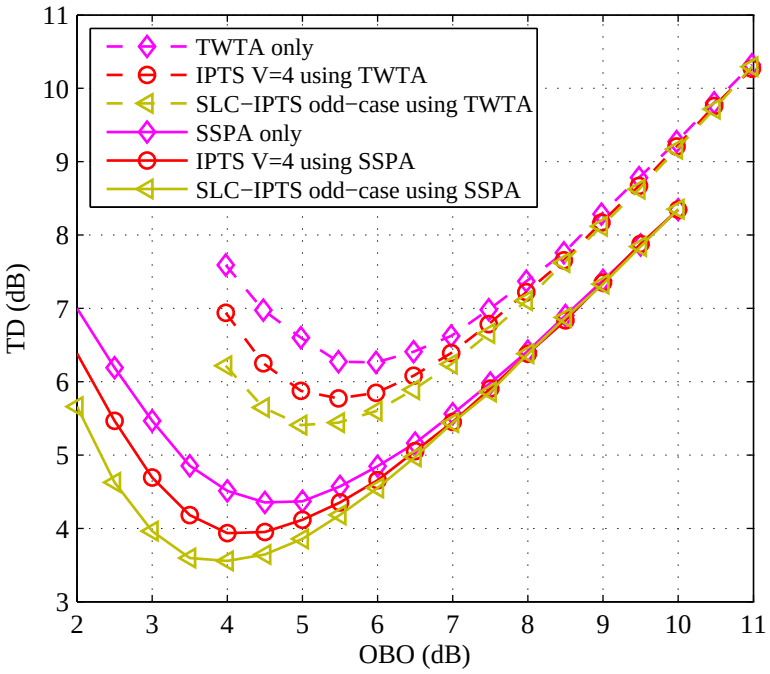

(a) 16-QAM-OFDM

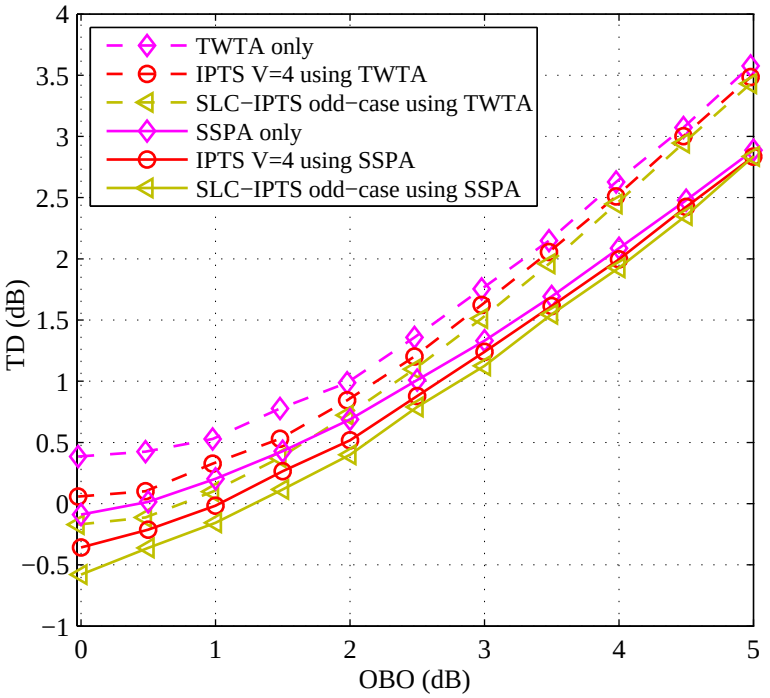

(b) QPSK-OFDM

Figure 4.7: TD versus OBO for 16-QAM-OFDM and QPSK-OFDM systems using either the TWTA or the SSPA for target BER $= 10^{-4}$, $N = 128$.

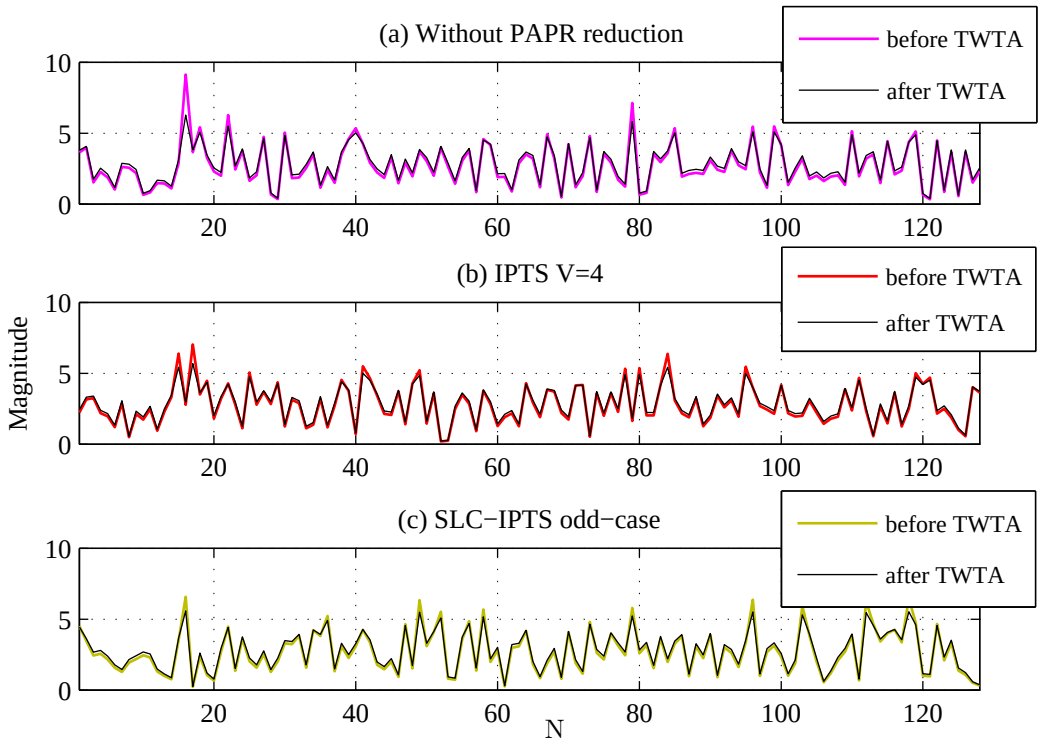

Figure 4.8: Time-domain signals at the IFFT output with $N = 128$ using a single 16-QAM-OFDM symbol, with and without PAPR reduction.

TWTA only case with OBO = 5 dB. In contrast, the out-of-band power given by the PAPR reduction techniques is slightly higher than that produced by the proposed reduction schemes (LC-IPTS and SLC-IPTS). Finally, it is clear from this figure that there is no sacrificing in the out-of-band power spectrum when the proposed techniques are utilised.

4.6.4 CCDF performance

Fig. 4.10(a) shows the CCDF of PAPR for the PTS, SLM and LC-IPTS techniques. It can be seen that the CCDF curve for odd-cases is the best. For example, the odd-cases can achieve 2, 1.4 and 1.2 dB PAPR reduction at 10^{-4} CCDF, compared with the IPTS, CPTS and SLM techniques respectively. Due to the inclusion of vector $\mathbf{t}_r$ in the odd-cases, there is a variety of phase weighting factors in comparison to the even-cases; the PAPR reduction of the former is better than the latter. The CCDF curves of PAPR for the PTS, SLM and SLC-IPTS techniques are shown in Fig. 4.10(b). From these curves, the PAPR reduction for the full-case is better than odd-case or even-case. In addition, the full-case can achieve 2.2, 1.5 and 1.4 dB PAPR reduction, whereas odd-case or even-case can achieve 1.8, 1.1 and 1 dB

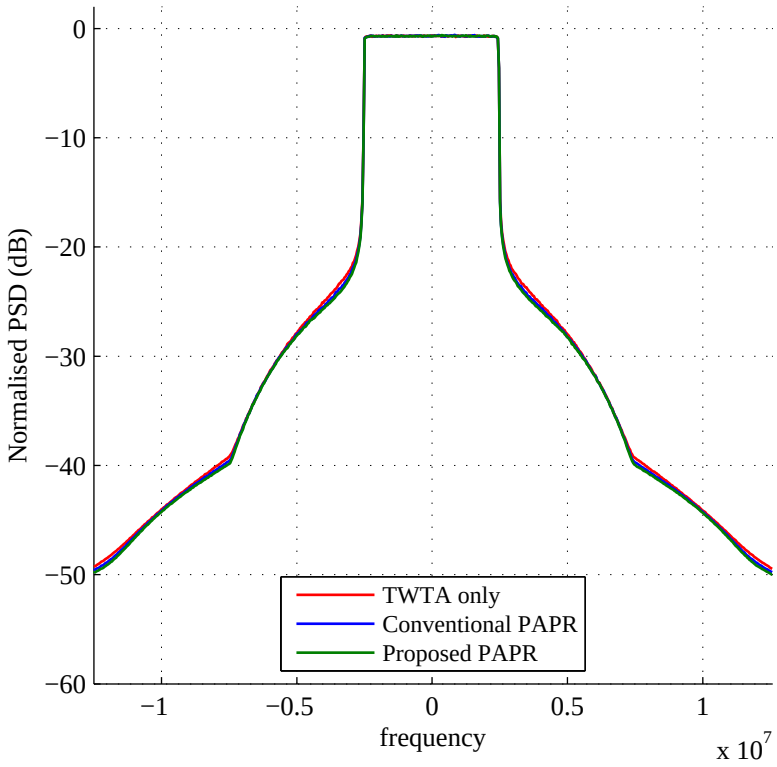

Figure 4.9: The out-of-band power spectrum plot of an OFDM signal, with and without PAPR reduction, $N = 128$ SCs, using the TWTA with OBO = 5 dB.

PAPR reduction compared to the IPTS, CPTS and SLM, respectively. The full-case scheme can achieve better PAPR reduction than the odd or even-case due to the wide range of phase weighting factors of the vector $\mathbf{t}_r$.

4.6.5 BER performance

The BER performance is assessed over an AWGN and wideband satellite channels in this chapter.

4.6.5.1 BER performance over an AWGN channel

Figs. 4.11, 4.12 and 4.13 depict the BER performance for: 16-QAM, HM and QPSK constellations, respectively, of the following schemes: IPTS, SLM, CPTS and the proposed techniques using either the TWTA or the SSPA. We can observe that there is a trend reflected throughout these figures which will now be discussed. The LC-IPTS even-case schemes have the worst BER performance, while the SLC-IPTS full-case scheme has the best BER performance. The reason for this phenomenon is that the generated vectors of the full-case are double in comparison with the odd

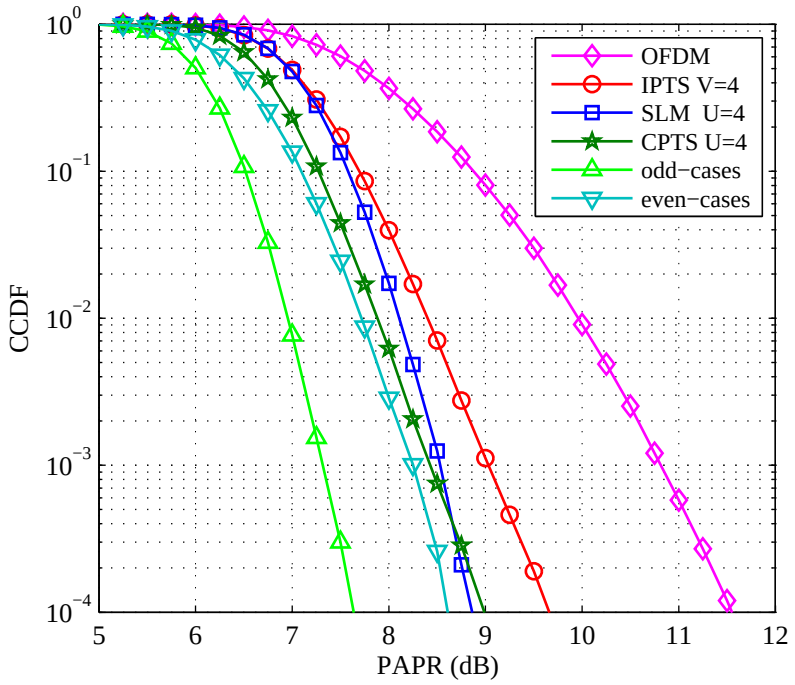

(a) Proposed LC-IPTS technique

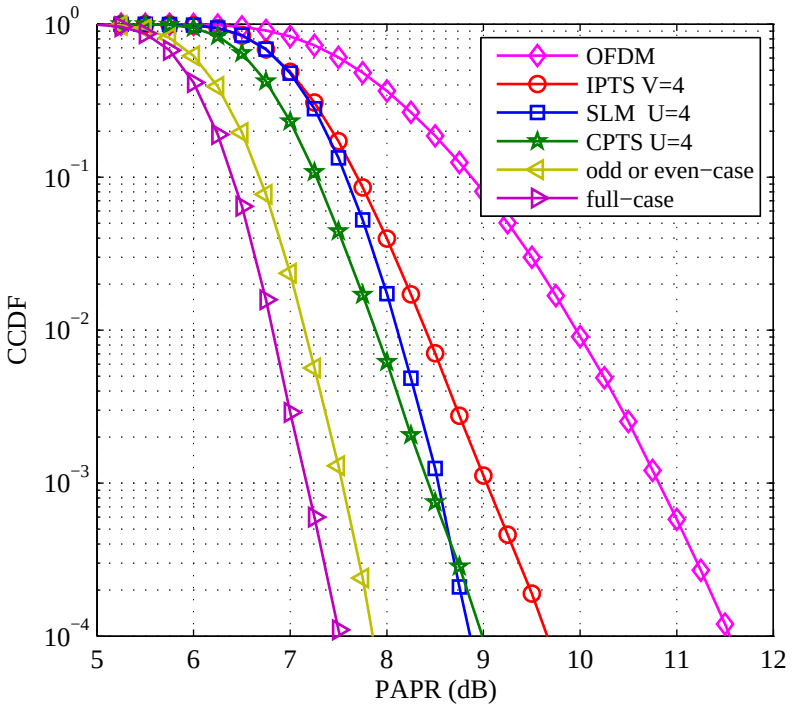

(b) Proposed SLC-IPTS technique

Figure 4.10: CCDF of PAPR for the proposed (LC-IPTS and SLC-IPTS), IPTS, CPTS and SLM techniques.

Table 4.4: The SNR improvement of the proposed LC-IPTS and SLC-IPTS schemes over the IPTS, SLM and CPTS techniques.

Proposed Technique	Case	Constellation (HPA)	SNR improvement in dB (IPTS)	SNR improvement in dB (SLM)	SNR improvement in dB (CPTS)
LC-IPTS	odd-cases	16-QAM (TWTA)	1.4	1	0.1
		16-QAM (SSPA)	0.8	0.6	0.1
		EL-HM (TWTA)	1.1	0.8	0.1
		EL-HM (SSPA)	0.7	0.6	0.1
		QPSK (TWTA)	1	0.8	0.2
		QPSK (SSPA)	0.5	0.4	0.1
SLC-IPTS	full-case	16-QAM (TWTA)	1.6	1.2	0.3
		16-QAM (SSPA)	0.9	0.8	0.2
		EL-HM (TWTA)	1.3	1	0.3
		EL-HM (SSPA)	0.8	0.7	0.2
		QPSK (TWTA)	1.2	1	0.3
		QPSK (SSPA)	0.6	0.5	0.2

or even-case. Furthermore, the LC-IPTS odd-case schemes have better performance than the even-cases; this is due to the fact that the elements of the phase rotation, vector $\mathbf{B}$, for the odd-cases have the same amplitude but with no zero elements. It should be noted that BL can achieve a similar improvement in BER performance to that shown in the 16-QAM constellation.

Due to he LC-IPTS with the odd-case scheme and SLC-IPTS with the full-case scheme have the best BER performance for: 16-QAM, HM and QPSK constellations using either the TWTA or the SSPA, therefore, the SNR improvement of the proposed LC-IPTS (odd-cases) and SLC-IPTS (full-case) schemes with the IPTS, SLM and CPTS techniques is compared in Table 4.4. It is apparent from this table that the improvement in SNR is less than 1 dB when SSPA is used, while a higher improvement can be achieved when TWTA is utilised.

4.6.5.2 BER performance in mobile satellite channel

The BER performance using QPSK and 16-QAM modulation schemes in the presence of the TWTA nonlinearity and the wideband channel with elevation angle, $\theta \leq 45$, is depicted in Fig. 4.14. The analogous trend of the BER performance is achieved for mobile satellite fading channel compared to the AWGN, except an extra degradation due to multipath fading is introduced.

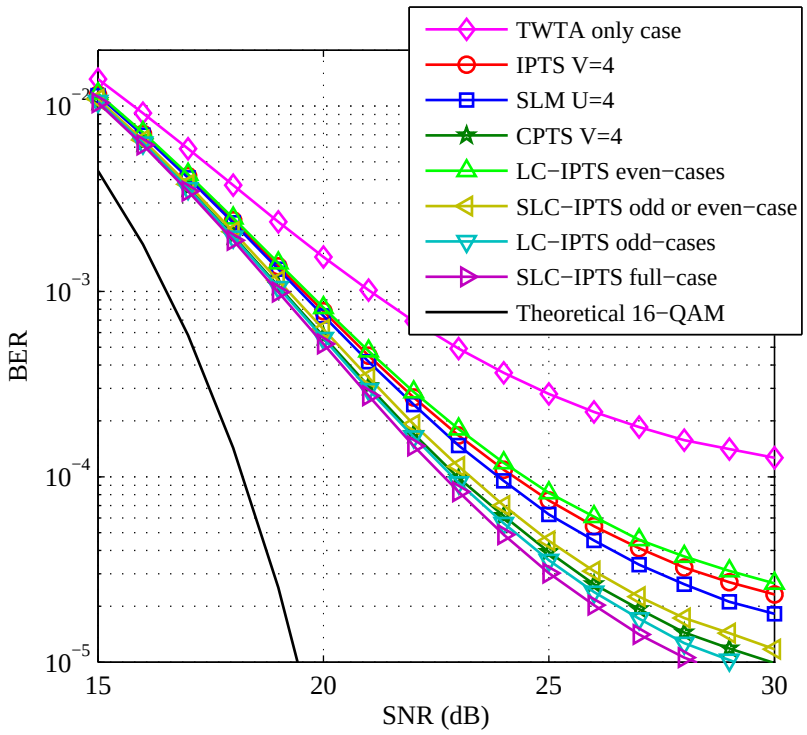

(a) TWTA case

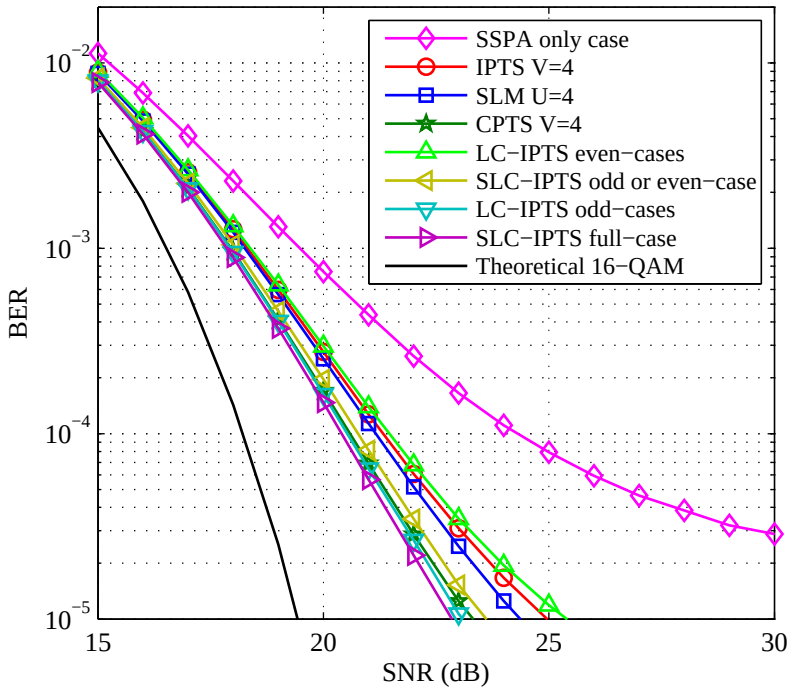

(b) SSPA case

Figure 4.11: BER performance for the LC-IPTS, SLC-IPTS, IPTS, CPTS and SLM techniques using either the TWTA or the SSPA with 16-QAM constellation.

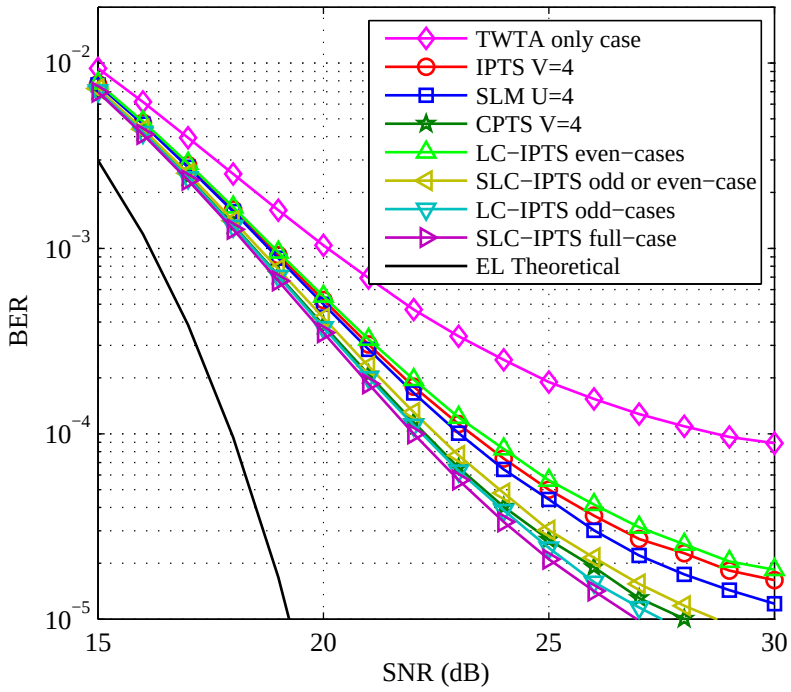

(a) TWTA case

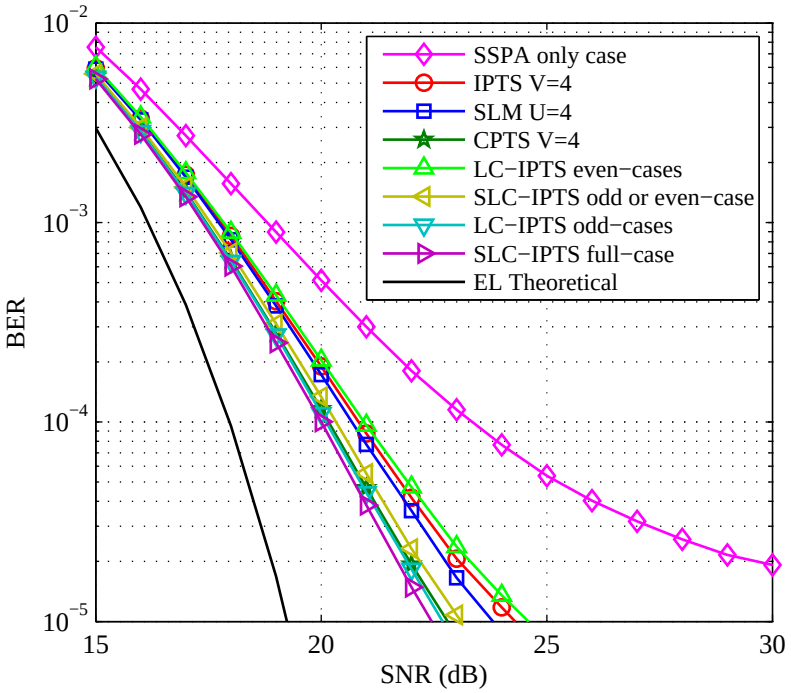

(b) SSPA case

Figure 4.12: BER performance of EL for the LC-IPTS, SLC-IPTS, IPTS, CPTS and SLM techniques using either the TWTA or the SSPA with HM-OFDM systems.

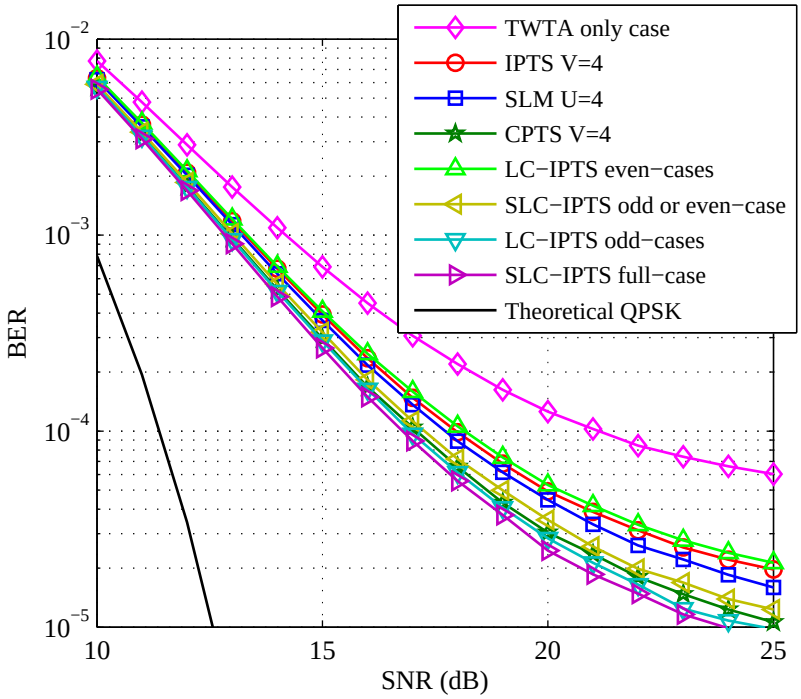

(a) TWTA case

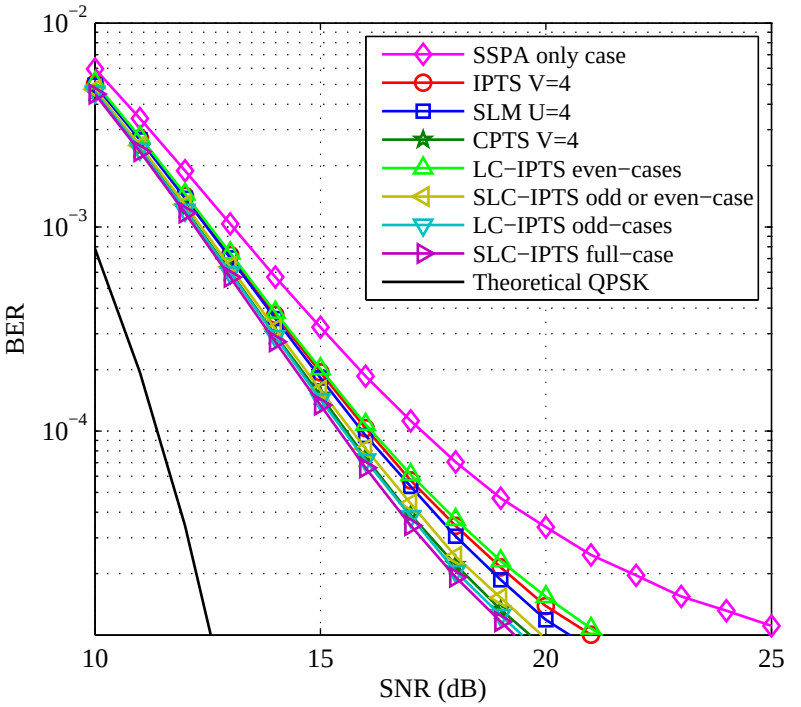

(b) SSPA case

Figure 4.13: BER performance of EL for the LC-IPTS, SLC-IPTS, IPTS, CPTS and SLM techniques using either the TWTA or the SSPA with QPSK-OFDM systems.

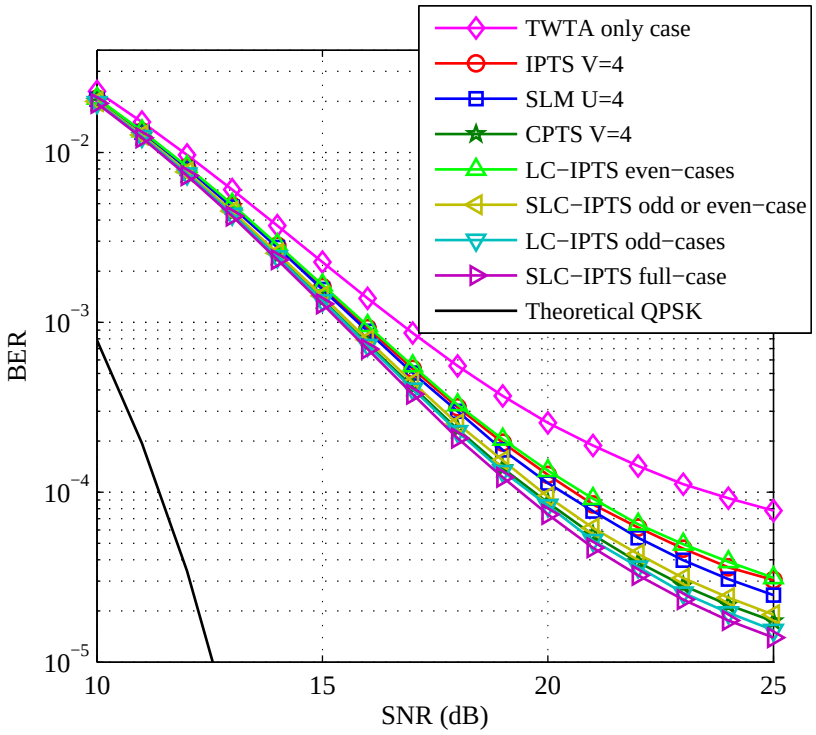

(a) QPSK-OFDM

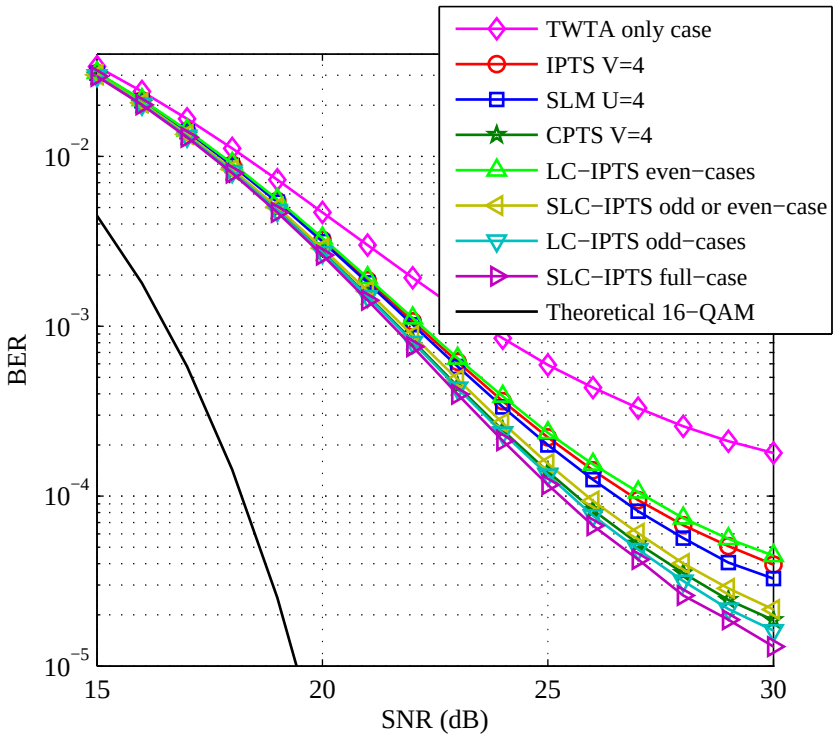

(b) 16-QAM-OFDM

Figure 4.14: BER performance for the LC-IPTS, SLC-IPTS, IPTS, CPTS and SLM techniques using the TWTA and wideband channel.

Table 4.5: The overall comparison of the proposed schemes over the IPTS for $N = 128$, $L = 4$ and $V = U = 4$ using either the TWTA or the SSPA with 16-QAM-OFDM systems.

Proposed Technique	Case	CCRR-IPTS in %	PAPR Reduction in dB	SNR Improvement in dB	Side Information Bits
LC-IPTS	**odd-cases**	16	**2**	**1.4** for TWTA **0.8** for SSPA	4
	even-case (1)	-12	1.1	-0.2 for TWTA -0.1 for SSPA	4
	even-case (2)	21	1.1	-0.2 for TWTA -0.1 for SSPA	4
SLC-IPTS	**odd-case**	**30**	1.8	1 for TWTA 0.6 for SSPA	**3**
	even-case	7	1.8	1 for TWTA 0.6 for SSPA	3
	full-case	-22	2.2	1.6 for TWTA 0.9 for SSPA	4

4.7 Chapter Summary

Table 4.5 compares the performance and complexity of the proposed LC-IPTS and SLC-IPTS schemes over the IPTS using either the TWTA with OBO = 5 dB or the SSPA with OBO = 4 dB and 16-QAM constellation. In view of the odd-cases from the two proposed techniques, it is clear to see that the SLC-IPTS has a significant improvement in CCRR-IPTS and SI. However, this is at a cost of 0.2 dB for PAPR reduction as well as 0.4 dB degradation in SNR performance for the TWTA case.

4.8 Conclusion

In this chapter, new low-complexity and simplified low-complexity schemes using circulant transform matrices have been proposed. In these schemes, only two IFFTs are required. Furthermore, the equations for the proposed schemes were derived. The overall computational complexity for the PTS, SLM and proposed schemes were also formulated. The proposed LC-IPTS (odd-case (1) and (2)) has shown to reduce the complexity and improve the system performance. Moreover, the proposed SLC-IPTS (odd-case) has shown to reduce both the computational complexity and the number of side information bits. However, this is at the cost of a minor reduction in both PAPR and BER performance.

Chapter 5

Efficient BER Reduction Techniques for Nonlinear OFDM Transmission Using Distortion Prediction

This chapter presents efficient techniques to reduce the BER of the OFDM signals transmitted over a nonlinear HPA. The proposed techniques are based on predicting the distortion power that an HPA would generate due to the nonlinear characteristics of such devices. In a method similar to the SLM or PTS schemes, the predicted distortion is used to select a set of phases that minimise the actual HPA distortion. Simulation results have confirmed that an SNR reduction of ~ 4.5 dB using the TWTA at a BER of $\sim 10^{-4}$ can be achieved when the proposed technique is compared to the standard PTS utilising 16 partitions. The most important findings are the proposed techniques for the 16 partitions, which can eliminate the error floor caused by the ICI when SSPA is used. Moreover, complexity analysis has demonstrated that the proposed system offers a significant complexity reduction of approximately 60% when compared to state-of-the-art methods.

5.1 Introduction

Wireless communication systems are currently required to provide high data rate transmission with strict constraints on power consumption and bandwidth occu-

pancy. Consequently, the adoption of power and spectrally efficient M-ary modulation schemes such as QAM in conjunction with OFDM is indispensable. The QAM-OFDM combination offers unpreceded power and bandwidth efficiency that enables data rates up to 1 Gbps, as in the case of the downlink of the advanced implementation of the long term evolution (LTE) system [96]. Consequently, OFDM has been adopted in many digital communication standards such as digital video broadcasting-terrestrial (DVB-T) [97], Wimax technologies [98] and digital video broadcasting over satellites (DVB-S2) [99] to name a few.

In general, the HPAs that are deployed in wireless communication systems are often configured to operate near-saturation limits in order to maximise the amplifier power efficiency. Unfortunately, the high PAPR inherent to the OFDM signals' envelope will occasionally drive the HPA to operate in the nonlinear region of its characteristics curve. The nonlinearity of the HPA exhibits AM/AM amplitude and AM/PM phase distortions, which cause a loss of orthogonality among the SCs, and hence, ICI is introduced [68]. The ICI power is proportional to the amplitude of the signal at the amplifier input and may cause a considerable degradation in terms of its BER performance.

In the literature, extensive research has been devoted to reduce the degradation due to the PAPR problem inherent to OFDM systems. Some of the reported techniques such as amplitude clipping have low-complexity, but they suffer from various problems such as in-band distortion and out-of-band expansion. Signal companding methods have low-complexity, good distortion and spectral properties; however they have limited PAPR reduction capabilities. Advanced techniques such as coding, PTS and SLM [40] have been considered for PAPR reduction too. Such techniques are efficient and distortionless, however their computational complexity is high and requires the transmission of several bits of side information [91]. A comprehensive overview of the main PAPR reduction techniques is reported in [29] and [30].

The standard SLM and PTS methods are based on modifying the phases of the SC data symbols at the transmitter side to minimise the PAPR. This goal is achieved by multiplying the data symbols with several pre-designed phase vectors, and then selecting the phase vector which produces the minimum PAPR. The receiver should be informed of the phase vector that has been selected in order to reverse the operation at the receiver side. Such approaches are effective only if the number of trial phase vectors is large. Consequently, the complexity of these techniques is

high, particularly when the number of tested phase vectors is large. Furthermore, accurate PAPR estimation requires oversampling of the transmitted signal, which introduces further complexity to such techniques. However, it is worth noting that minimising the PAPR does not necessarily minimise the distortion produced by the nonlinearity of the HPA, and hence, it does not necessarily minimise the BER [100].

In order to reduce the computational complexity of the CPTS and CSLM schemes, numerous modified versions were proposed such as [60], [80], [86] and [87]. In contrast to these methods, it was demonstrated in [68] that using other less-direct indicators such as the inter-modulation distortion (IMD) to select the coefficients of the PTS and SLM results in a noticeable improvement. However, the high computational complexity is the main limitation of the IMD approach. Similarly, the excess power (EP) is proposed in [100] to measure the nonlinearity of transmission systems, which can also be used to minimise the PAPR too. In general, IMD-based systems outperform EP systems, however, with higher complexity. In such techniques, the PAPR is minimised by reducing metrics such as the IMD and EP.

In this chapter, efficient and computationally less complex schemes are proposed to reduce the BER within OFDM systems in the presence of nonlinear HPA. The proposed techniques are based on the prediction of the distortion, which is introduced by the nonlinearity of an HPA, followed by techniques such as the PTS and SLM are invoked, to minimise the distortion and consequently the BER. The adopted distortion metrics are referred to as the distortion-to-signal power ratio (DSR) and the peak interference-to-carrier ratio (PICR). The DSR and PICR metrics of measurement were first introduced in [100] and [101], respectively, to assess the impact of the HPA nonlinearity in OFDM systems at the receiver side. However, they were never used in the context of nonlinear amplifier distortion minimisation. The DSR, which is usually evaluated at the receiver side, is predicted at the transmitter side using a simple equivalent mathematical model after the IFFT. Both metrics are analytically derived by taking into consideration the nonlinear distortion due to the HPA. Monte Carlo simulations have confirmed that the DSR and PICR metrics are more reliable than those of the PAPR and IMD, for selecting the coefficients of the PTS and SLM to minimise the BER. Furthermore, complexity analysis of the new schemes demonstrates that the proposed schemes offer a significant complexity reduction when compared to standard PAPR-based methods.

In this work, two HPA models are required. The first model will be used to mimic

the actual memoryless model used in the transmission process. Thus, this model should accurately model the HPA nonlinearity. For such purposes, [17] demonstrated that the memoryless model is highly accepted for describing the nonlinearity of HPAs. The second amplifier model, polynomial, is required to predict the resulting distortion when high signal peaks occur. Using this model, it should be relatively simple to reduce the computation complexity of the distortion prediction process. Furthermore, the use of two different models is pivotal, since accurate knowledge of the HPA characteristics is not usually available.

5.2 The Distortion Metrics

In this section, the distortion metrics for the AWGN channel are estimated. Assuming a third order polynomial HPA model, the effect of nonlinearity on the signal quality can be evaluated by computing the FFT of the HPA output. Based on (2.6) and (2.13), r_k can be expressed as

$$r_k = \frac{1}{\sqrt{N}} \sum_{n=0}^{N-1} \alpha_1 x_n \mathrm{e}^{-j2\pi kn/N} + \frac{1}{\sqrt{N}} \sum_{n=0}^{N-1} \alpha_3 |x_n|^2 x_n \mathrm{e}^{-j2\pi kn/N}. \tag{5.1}$$

Substituting (2.3) into (5.1), r_k can be rewritten as [16]

$$\begin{aligned} r_k \;=\; & \frac{1}{\sqrt{N}} \sum_{n=0}^{N-1} \alpha_1 \left[\frac{1}{\sqrt{N}} \sum_{l=0}^{N-1} d_l \mathrm{e}^{j2\pi ln/N} \right] \mathrm{e}^{-j2\pi kn/N} \\ & + \frac{1}{\sqrt{N}} \sum_{n=0}^{N-1} \alpha_3 |x_n|^2 \left[\frac{1}{\sqrt{N}} \sum_{l=0}^{N-1} d_l \mathrm{e}^{j2\pi ln/N} \right] \mathrm{e}^{-j2\pi kn/N}, \end{aligned} \tag{5.2}$$

then

$$r_k = \underbrace{d_k \left[\alpha_1 + \frac{\alpha_3}{N} \sum_{n=0}^{N-1} |x_n|^2 \right]}_{\text{Useful Signal}} + \underbrace{\frac{\alpha_3}{N} \sum_{\substack{l=0 \\ l \neq k}}^{N-1} d_l \left[\sum_{n=0}^{N-1} |x_n|^2 \mathrm{e}^{j2\pi n(l-k)/N} \right]}_{\text{ICI}}, \tag{5.3}$$

and finally, r_k can be expressed in compact form as [16]

$$r_k = \beta d_k + \psi_k, \tag{5.4}$$

where the first term on the RHS of (5.4) represents the useful part of the symbol, β is a phase shift given by

$$\begin{aligned}\beta &= \alpha_1 + \frac{\alpha_3}{N}\sum_{n=0}^{N-1}|x_n|^2 \\ &= \alpha_1 + \frac{\alpha_3}{\mathrm{IBO}_l},\end{aligned} \tag{5.5}$$

and ψ_k is the nonlinear noise component that can be described as

$$\psi_k = \frac{\alpha_3}{N}\sum_{\substack{l=0\\ l\neq k}}^{N-1} d_l \sum_{n=0}^{N-1}|x_n|^2 \mathrm{e}^{j2\pi n(l-k)/N}, \tag{5.6}$$

and $\mathrm{IBO}_l = 10^{\mathrm{IBO}/10}$.

The IMD-reduction metric proposed in [68] can be written as

$$\mathrm{IMD} = \max\left\{\max_{0\leqslant k\leqslant N-1}\left\{-\frac{\mathrm{Re}\{\psi_k\}}{\mathrm{Re}\{\beta d_k\}}, -\frac{\mathrm{Im}\{\psi_k\}}{\mathrm{Im}\{\beta d_k\}}\right\}\right\}, \tag{5.7}$$

where Re{.} and Im{.} denote the real and imaginary parts of a complex variable, respectively.

In contrast, the PICR introduced by [101] can be defined as

$$\mathrm{PICR} = \max_{0\leqslant k\leqslant N-1}\left\{\frac{|\psi_k|^2}{|\beta|^2|d_k|^2}\right\}. \tag{5.8}$$

The DSR at the receiver with negligible AWGN can be defined as [100]

$$\mathrm{DSR} = \frac{E\{|\boldsymbol{\psi}|^2\}}{|\beta|^2 E\{|\mathbf{d}|^2\}}, \tag{5.9}$$

where $\boldsymbol{\psi} = \{\psi_0, \psi_1, \cdots, \psi_{N-1}\}$ is the vector of the nonlinear noise component samples. The normalised DSR can be obtained by dividing (5.9) by $|\beta|^2 E\{|\mathbf{d}|^2\}$, which is a constant of a given OFDM symbol

$$\overline{\mathrm{DSR}} = \|\boldsymbol{\psi}\|^2 = \sum_{i=0}^{N-1}|\psi_i|^2. \tag{5.10}$$

It is worth noting, that accurate evaluation of the PAPR and IMD require an oversampling factor of $L \geqslant 4$ [31] and [68], whereas no oversampling is required for the DSR and PICR estimation [101].

5.2.1 Proposed DSR reduction using PTS scheme

Fig. 5.1 depicts the block diagram of the PTS scheme combined with DSR. In this technique and similar to the CPTS, V disjoint sets $\mathbf{d}^{(v)}$, $v = 0, 1, \cdots, V-1$ are obtained by partitioning the input data block $\mathbf{d}$ in (3.7). The time-domain vector $\mathbf{x}^{(v)}$ is obtained by applying an N-point IFFT on each of the disjoint sets, such that

$$\mathbf{x}^{(v)} = \mathbf{W}\,\mathbf{d}^{(v)}. \tag{5.11}$$

The time-domain samples of the $\mathbf{x}^{(v)}$ vector can be expressed as

$$x_n^{(v)} = \frac{1}{\sqrt{N}} \sum_{k=0}^{N-1} d_k^{(v)} \mathrm{e}^{j2\pi kn/N}, \quad n = 0, 1, \cdots, N-1. \tag{5.12}$$

Subsequently, the IFFT outputs are scrambled by the complex weighting phase factors, $b^{(v)} = e^{j\phi_v}$, $v = 0, 1, \cdots, V-1$. Finally, the overall time-domain samples in (3.9) can be obtained by adding the V signals.

The FFT of the HPA output can be expressed as

$$r_k = \underbrace{\sum_{v=0}^{V-1} d_k^{(v)} b^{(v)} \left[\alpha_1 + \frac{\alpha_3}{N} \sum_{n=0}^{N-1} |x_n|^2\right]}_{\text{Useful Signal}} + \underbrace{\frac{\alpha_3}{N} \sum_{v=0}^{V-1} b^{(v)} \sum_{\substack{l=0 \\ l\neq k}}^{N-1} d_l^{(v)} \sum_{n=0}^{N-1} |x_n|^2 \mathrm{e}^{j2\pi n(l-k)/N}}_{\text{ICI}}. \tag{5.13}$$

The frequency domain symbol on SC k can be presented in compact form as

$$r_k = \sum_{v=0}^{V-1} d_k^{(v)} b^{(v)} \beta + \psi_{k,PTS}, \tag{5.14}$$

where the factor β is identical to (5.5) and the nonlinear noise component can be written as [101]

$$\psi_{k,PTS} = \sum_{v=0}^{V-1} b^{(v)} \psi_k^{(v)}. \tag{5.15}$$

The term $\psi_k^{(v)}$ is given by

$$\psi_k^{(v)} = \frac{\alpha_3}{N} \sum_{\substack{l=0 \\ l\neq k}}^{N-1} d_l^{(v)} \sum_{n=0}^{N-1} |x_n|^2 \mathrm{e}^{j2\pi n(l-k)/N}. \tag{5.16}$$

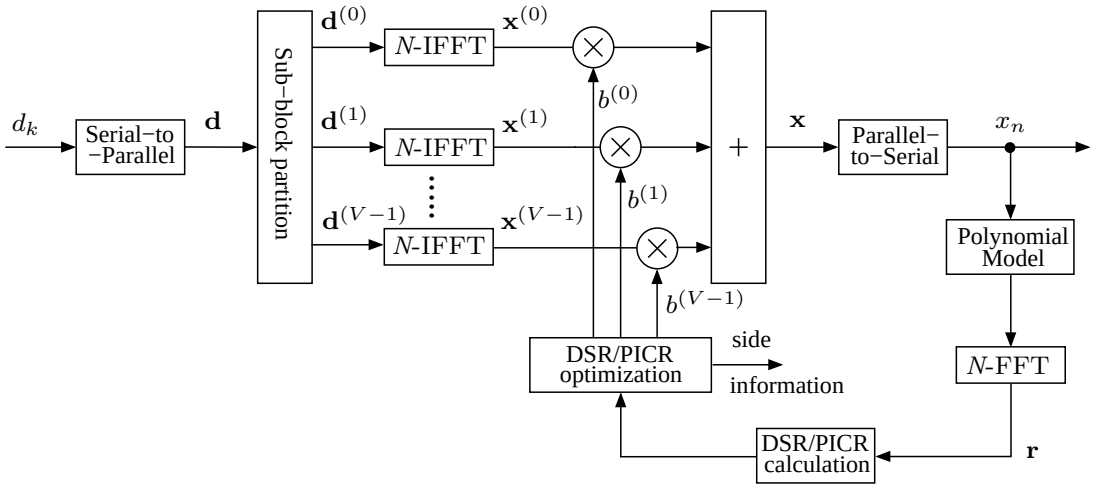

Figure 5.1: Block diagram of the proposed PTS scheme based on distortion sensing.

The minimum normalised DSR for PTS scheme can be defined as

$$\overline{\mathrm{DSR}}_{PTS} = \min_{b^{(0)},\cdots,b^{(V-1)}} \|\boldsymbol{\psi}_{PTS}\|^2 . \tag{5.17}$$

In the IPTS, two phase flipping values $\{\pm 1\}$ are utilised in order to minimise the number of trial values [3].

5.2.2 Proposed DSR reduction using SLM scheme

The block diagram of the SLM-based DSR method is shown in Fig. 5.2. Similar to the CSLM, the data symbols are copied into U sections, where each of the data symbols are multiplied by U different phase sequences in order to generate alternative the input sequences that are represented in (3.10). Subsequently, each of the U branches is applied to an N-point IFFT. The resulting sample of the u-th sequence can be expressed as

$$x_n^{(u)} = \frac{1}{\sqrt{N}} \sum_{k=0}^{N-1} d_k a_k^{(u)} \mathrm{e}^{j2\pi kn/N}, \quad n = 0, 1, \cdots, N-1. \tag{5.18}$$

Hence, after the HPA and FFT, r_k can be expressed as

$$r_k = \underbrace{d_k a_k^{(u)} \left[\alpha_1 + \frac{\alpha_3}{N} \sum_{n=0}^{N-1} |x_n|^2 \right]}_{\text{Useful Signal}} + \underbrace{\frac{\alpha_3}{N} a_k^{(u)} \sum_{\substack{l=0 \\ l \neq k}}^{N-1} d_l \left[\sum_{n=0}^{N-1} |x_n|^2 \mathrm{e}^{j2\pi n(l-k)/N} \right]}_{\text{ICI}} . \tag{5.19}$$

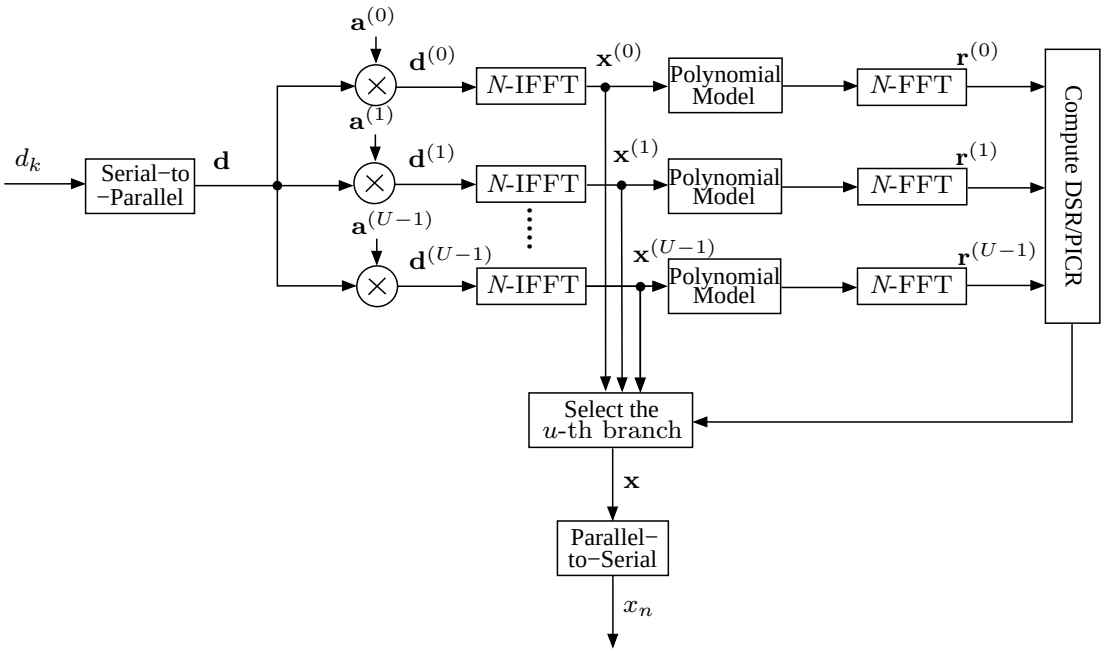

Figure 5.2: Block diagram of the proposed SLM scheme based on distortion sensing.

The frequency domain symbol on SC k can be presented in compact form as

$$r_k^{(u)} = d_k a_k^{(u)} \beta + \psi_{k,SLM}^{(u)}, \tag{5.20}$$

where β is given by (5.5) and

$$\psi_{k,SLM}^{(u)} = \frac{\alpha_3}{N} a_k^{(u)} \sum_{\substack{l=0 \\ l \neq k}}^{N-1} d_l \sum_{n=0}^{N-1} |x_n|^2 \mathrm{e}^{j2\pi n(l-k)/N}. \tag{5.21}$$

The normalised DSR is computed for the U branches using the set of phase vectors $\mathbf{a}^{(0)}, \cdots, \mathbf{a}^{(U-1)}$ and the branch with the minimum normalised DSR is selected for transmission

$$\overline{\mathrm{DSR}}_{SLM} = \min_{u=0,\cdots,U-1} \left\| \boldsymbol{\psi}_{SLM}^{(u)} \right\|^2, \tag{5.22}$$

where $\boldsymbol{\psi}_{SLM}^{(u)} = \left[\psi_{0,SLM}^{(u)}, \cdots, \psi_{N-1,SLM}^{(u)} \right]$.

5.3 Power Amplifiers Operating Points

Fig. 5.3 depicts the simulated TD curves using either the TWTA or the SSPA for 16-QAM-OFDM systems at a BER of $\sim 10^{-4}$. The optimum OBOs for the TWTA and the SSPA cases are 5 and 3.5 dB, respectively, whereas it is shown in Fig. 4.7 that for QPSK-OFDM, the optimum OBO is 0 dB for both the TWAT and the

SSPA cases.

5.4 Polynomial Model Coefficients Calculation

It is necessary to be knowledgeable about the sign of the third order nonlinearity parameters for the polynomial model. In particular, the model demonstrates expansive nature in performance, when α_3/α_1 has a positive value. In contrast, the model demonstrates a compressive nature in performance, when α_3/α_1 is negative. On the other hand, it can be observed from Figs. 2.4 and 2.5, that the practical nonlinearities demonstrate compression performance for the TWTA and the SSPA, respectively [68].

In practice, the coefficients representing nonlinearities that demonstrate both AM/AM and AM/PM characteristics are complex values [68]. The complex coefficients are obtained by equating memoryless Saleh's model equations with (2.13) and utilising the minimax criterion [102]. The coefficients used for the TWTA polynomial model are $\alpha_1 = 0.9920 + j0.0340$ and $\alpha_3 = -0.9100 + j0.5755$. In contrast, for nonlinearities which exhibit only AM/AM characteristics, the coefficients are real values [68]. Thus, the coefficients α_1 and α_3 can be obtained by equating the memoryless Rapp's model equations with (2.13) and using curve fitting methods. The coefficients used for an SSPA polynomial model are $\alpha_1 = 1$ and $\alpha_3 = -0.132$. Figs. 5.4 and 5.5 depict the output of the TWTA and SSPA, respectively, versus the amplifier's input using the obtained coefficients α_1, α_3 and optimum OBOs. Acceptable agreements between the memoryless and polynomial models are shown in these figures.

5.5 Computational Complexity

In this section, the computational complexity of the PTS, SLM and proposed techniques is discussed. Generally, the complexity of one LN-point IFFT is $(LN/2)\log_2(N)+$ $LN/2$ CMs and $(LN)\log_2(N)$ CAs for zero-padded systems [80].

The PAPR and IMD are implemented using an oversampling factor used $L = 4$ [31] and [68]. Although using smaller oversampling factors is possible, this is the smallest value that can produce reliable PAPR or IMD estimates. The effect of L can be evaluated by comparing the selected phase sequence for the continuous and

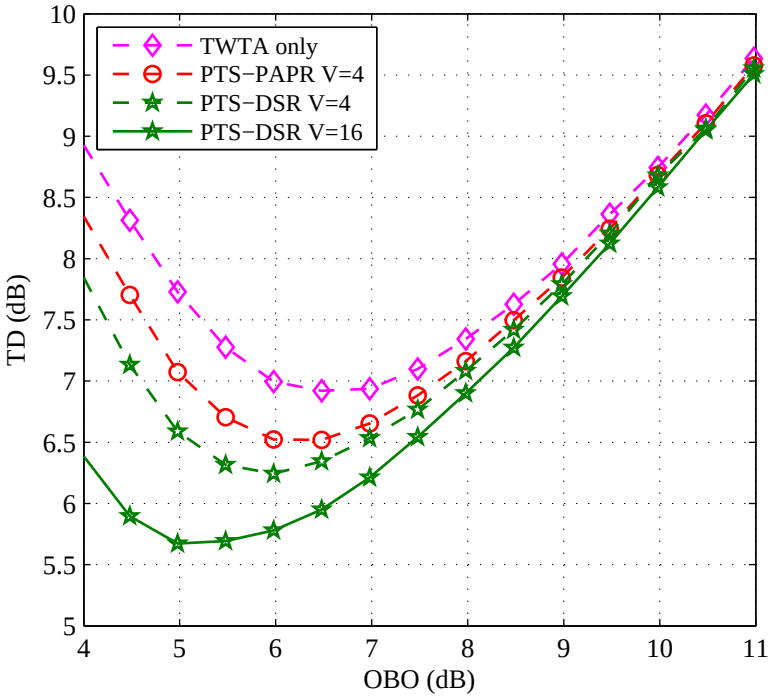

(a) TWTA case

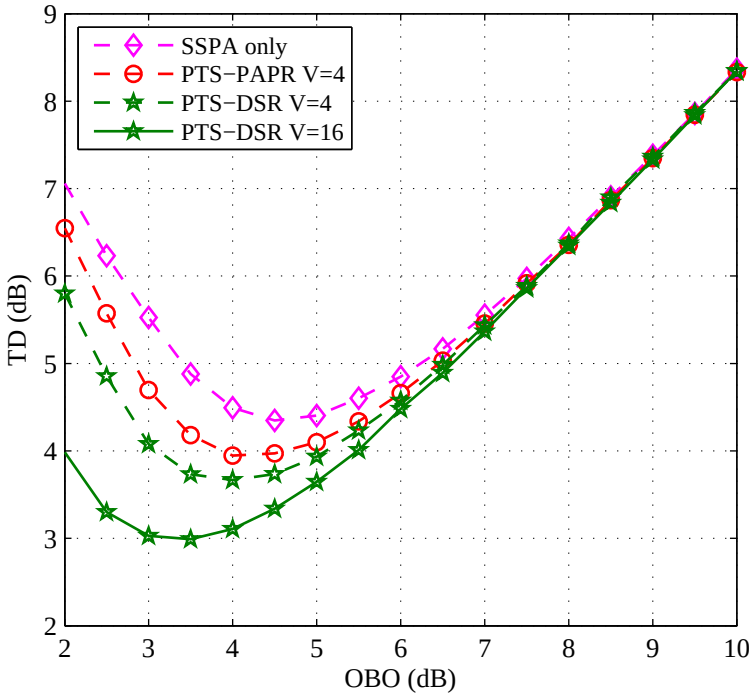

(b) SSPA case

Figure 5.3: TD versus OBO for 16-QAM-OFDM at target BER $= 10^{-4}$, $N = 128$.

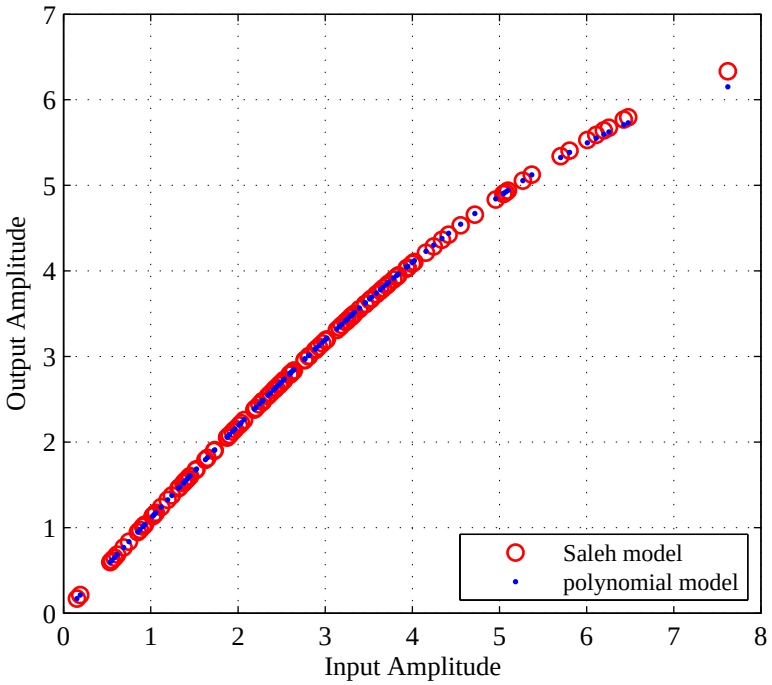

(a) Output amplitude

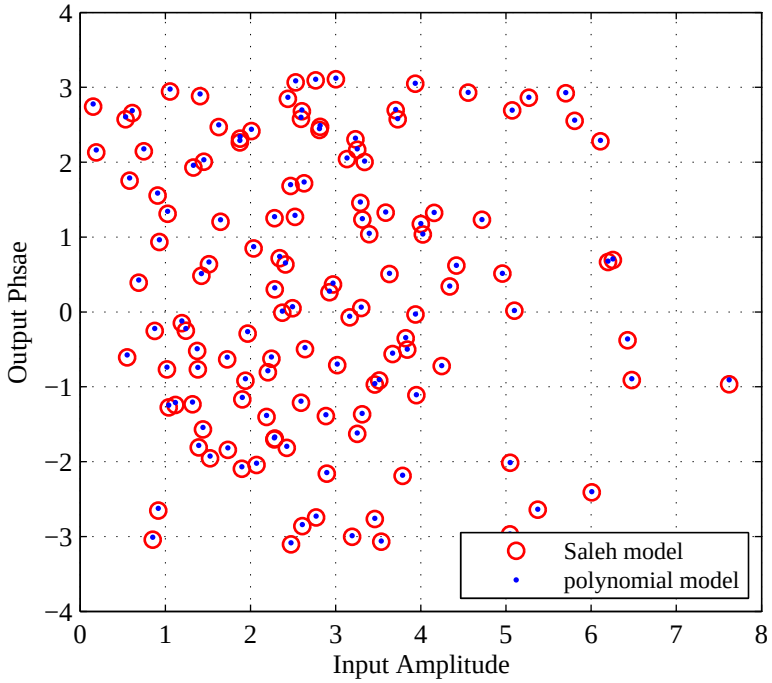

(b) Output phase

Figure 5.4: Output of the TWTA versus input amplitude for 16-QAM-OFDM using OBO = 5 dB, $\alpha_1 = 0.9920 + j0.0340$ and $\alpha_3 = -0.9100 + j0.5755$.

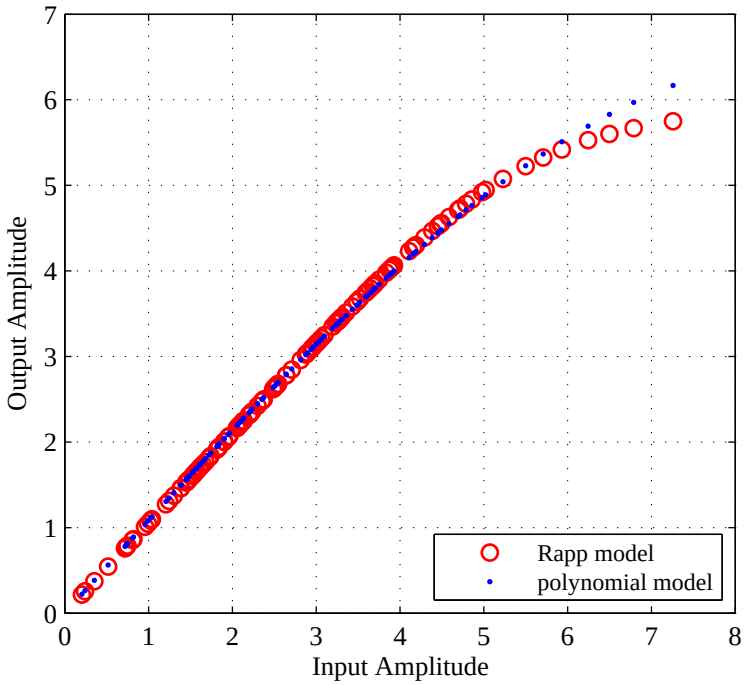

(a) Output amplitude

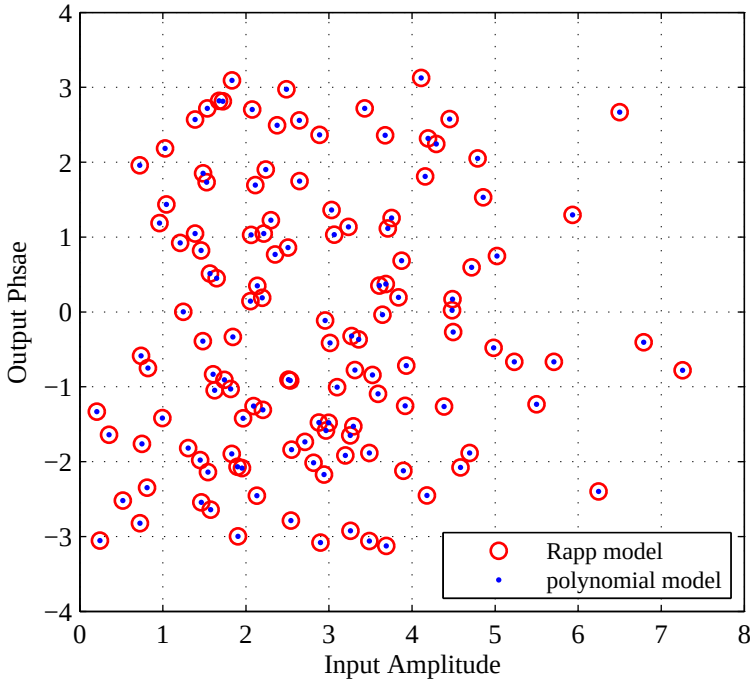

(b) Output phase

Figure 5.5: Output of the SSPA versus input amplitude for 16-QAM-OFDM using OBO = 3.5 dB, $\alpha_1 = 1$ and $\alpha_3 = -0.132$.

discrete OFDM systems. For example, in the case of $\{U, V\} = 16$, the probability of selecting the same phase sequence is approximately 0.038, 0.24, 0.48 and 0.65, for $L = 1$, 2, 3 and 4, respectively, while it is always 1.0 for the DSR irrespective of the value of L.

5.5.1 Complexity analysis of the PTS and SLM techniques

The computational complexity of the PTS-PAPR scheme is considered by the following operations:

- $Vf_m(LN/2\log_2(N) + LN/2)$ CMs and $Vf_a(LN\log_2(N))$ CAs are required for implementing a VLN-point IFFT, where f_m and f_a are the mean number of multiplications and additions, respectively, in respect of the sparseness of the partitions [95]. These parameters can be calculated using the Markov model presented in [103].
- $VLN(\mathcal{I} - 1)$ CMs are required for scrambling the IFFT output by $b^{(v)}$.
- $(V - 1)\mathcal{I}LN$ CAs are required to generate the overall time-domain samples, x_n, in (3.9).
- $2\mathcal{I}LN$ RMs and $\mathcal{I}LN$ RAs are required to calculate the PAPR metric.

The computational complexity operations for the SLM scheme are characterised as follows:

- $N(U - 1)$ CMs are required to create $\mathbf{d}^{(u)}$ in (3.10).
- $U(LN/2\log_2(N) + LN/2)$ CMs and $U(LN\log_2(N))$ CAs are required for implementing a ULN-point IFFT.
- $2ULN$ RMs and ULN RAs are required to calculate the PAPR metric.

The computational complexity equations of the PTS-PAPR and SLM-PAPR were derived [95] and formulated in Table 5.1.

5.5.2 Complexity analysis of the proposed techniques

The computational complexity of the PTS and SLM schemes based on distortion sensing is dominated by the following operations:

- An N-point IFFT/FFT requires $(N/2)\log_2(N)$ CMs and $(N)\log_2(N)$ CAs.
- The HPA output y_n using (2.13) requires $12N$ RMs and $6N$ RAs for the TWTA model, and $6N$ RMs and $3N$ RAs for the SSPA model.
- The $\psi_{k,PTS}$ and $\psi_{k,SLM}$ terms can be calculated by subtracting the frequency domain symbol from the corresponding useful signal using (5.14) and (5.20), respectively. Each term requires $8N$ RMs and $6N$ RAs for the TWTA model and $6N$ RMs and $4N$ RAs for the SSPA model. The DSR metric calculation using (5.10) requires $2N$ RMs and N RAs, thus, the overall DSR metric requires $10N$ RMs and $7N$ RAs for the TWTA, with $8N$ RMs and $5N$ RAs for the SSPA.

For the PTS scheme, the sparse VN-point IFFT requires $Vf_m(N/2)\log_2(N)$ CMs and $Vf_a(N)\log_2(N)$ CAs. Furthermore, $VN(\mathcal{J}-1)$ CMs are required for scrambling the IFFT outputs by $b^{(v)}$. Finally, $(V-1)N\mathcal{J}$ CAs are required to generate the overall time-domain samples, x_n, in (3.9). However, for the SLM scheme, $N(U-1)$ CMs are required to generate alternative input sequences, $\mathbf{d}^{(u)}$, in (3.10).

5.5.3 Overall computational complexity

It can be noted that from (5.8), the PICR criterion has higher computational complexity than the DSR where an additional $2N$ RMs and N RAs are required in the denominator calculation. On the other hand, the IMD approach has a higher computational complexity than the PAPR [68]. The computational complexity formulae are calculated for the IMD approach that is used with the PTS and SLM schemes, and hence, Table 5.1 lists these formulae. Therefore, the proposed DSR metric introduces in the lowest complexity when combined with SLM and PTS schemes.

The equations for $A_{PTS-DSR}$, $M_{PTS-DSR}$, $A_{SLM-DSR}$ and $M_{SLM-DSR}$ are listed in Table 5.1 using either of the TWTA or the SSPA models. The relative complexity (C_r) of the DSR criterion over the other schemes can be defined as the ratios of C_{DSR} metric divided by the equivalent complexity, C, of the other technique, where C is defined in (4.16). For example, given that $N = 128$, $V = U = 4$, $g = 4$, $f_a = 65\%$, $f_m = 75\%$ and $\mathcal{J} = V+1$, the relative complexity using the TWTA model is 60% and 71% for the PTS-PAPR and SLM-PAPR techniques, respectively. However, when the SSPA model is used, the C_r is 55% and 65% for the PTS-PAPR and SLM-PAPR

Table 5.1: Analysis of the Computational Complexity for the PTS and SLM Schemes Based on the PAPR, IMD and DSR Criteria in Terms of Number of Real Operations using either the TWTA or the SSPA models.

Number of Real Operations	Equivalent Complexity (C) using TWTA polynomial model	Equivalent Complexity (C) using SSPA polynomial model
$A_{PTS-PAPR}$ [95]	$2V\{f_m(NL/2\log_2(N)+NL/2)+f_a(NL\log_2(N))\}$ $+4(\mathcal{I}-1/2)VNL-\mathcal{I}NL$	$2V\{f_m(NL/2\log_2(N)+NL/2)+f_a(NL\log_2(N))\}$ $+4(\mathcal{I}-1/2)VNL-\mathcal{I}NL$
$M_{PTS-PAPR}$ [95]	$4Vf_m(NL/2\log_2(N)+NL/2)$ $+4(\mathcal{I}-1)VNL+2\mathcal{I}NL$	$4Vf_m(NL/2\log_2(N)+NL/2)$ $+4(\mathcal{I}-1)VNL+2\mathcal{I}NL$
$A_{SLM-PAPR}$ [95]	$UNL\{3\log_2(N)+2\}+2N(U-1)$	$UNL\{3\log_2(N)+2\}+2N(U-1)$
$M_{SLM-PAPR}$ [95]	$2UNL\{\log_2(N)+2\}+4N(U-1)$	$2UNL\{\log_2(N)+2\}+4N(U-1)$
$A_{PTS-IMD}$	$2V\{f_m(NL/2\log_2(N)+NL/2)+f_a(NL\log_2(N))\}$ $+3\mathcal{I}N\log_2(N)+2(\mathcal{I}-1)VNL+(2V+7)\mathcal{I}NL+6\mathcal{I}N$	$2V\{f_m(NL/2\log_2(N)+NL/2)+f_a(NL\log_2(N))\}$ $+3\mathcal{I}N\log_2(N)+2(\mathcal{I}-1)VLN+2(V-1)\mathcal{I}NL+9\mathcal{I}N$
$M_{PTS-IMD}$	$4Vf_m(NL/2\log_2(N)+NL/2)+2\mathcal{I}N\log_2(N)$ $+4(\mathcal{I}-1)VNL+14\mathcal{I}NL+10\mathcal{I}N$	$4Vf_m(NL/2\log_2(N)+NL/2)+2\mathcal{I}N\log_2(N)$ $+4(\mathcal{I}-1)VNL+4\mathcal{I}VNL+19\mathcal{I}N$
$A_{SLM-IMD}$	$2U\{3NL/2\log_2(N)+NL/2\}+3UN\log_2(N)$ $+2N(4U-1)+9UNL$	$2U\{3NL/2\log_2(N)+NL/2\}+3UN\log_2(N)$ $+2N(3U-1)+5UNL$
$M_{SLM-IMD}$	$4U\{NL/2\log_2(N)+NL/2+N/2\log_2(N)\}$ $+2N(7U-1)+14UNL$	$4U\{NL/2\log_2(N)+NL/2+N/2\log_2(N)\}$ $+4N(3U-1)+11UNL$
$A_{PTS-DSR}$	$\{V(f_m+2f_a)+3\mathcal{I}\}\{N\log_2(N)\}$ $+2VN(2\mathcal{I}-1)+12N\mathcal{I}$	$\{V(f_m+2f_a)+3\mathcal{I}\}\{N\log_2(N)\}$ $+2VN(2\mathcal{I}-1)+6N\mathcal{I}$
$M_{PTS-DSR}$	$2(Vf_m+\mathcal{I})\{N\log_2(N)\}$ $+4VN(\mathcal{I}-1)+22N\mathcal{I}$	$2(Vf_m+\mathcal{I})\{N\log_2(N)\}$ $+4VN(\mathcal{I}-1)+14N\mathcal{I}$
$A_{SLM-DSR}$	$UN\{6\log_2(N)+16\}-2N$	$2UN\{3\log_2(N)+5\}-2N$
$M_{SLM-DSR}$	$2UN\{2\log_2(N)+13\}-4N$	$UN\{4\log_2(N)+18\}-4N$

schemes, respectively.

The relative complexity C_r versus the number of SCs, N, for the PTS and SLM techniques based on the PAPR, IMD and PICR criteria using $V = U = 4$ is given in Fig. 5.6. The curves in the figure demonstrate that C_r is almost independent of N, particularly for $N \geq 256$ for both the TWTA and SSPA cases. In terms of performance, the DSR has a slightly lower complexity than the PICR, where $C_r \sim 97\%$ for the TWTA case; whereas for the SSPA case, the $C_r \sim 97\%$ and $\sim 98.5\%$ for the SLM and PTS, respectively. This scenario is different for the PAPR, where C_r drops significantly to $\sim 65\%$ and 59% for the SLM and PTS, respectively using the TWTA; while $C_r \sim 61\%$ and 55% for the SLM and PTS, respectively, using the SSPA. The major reduction was recorded for the IMD case, where $C_r \sim 36\%$ for both the SLM and PTS using the TWTA; whereas $C_r \sim 38\%$ and 44% for the SLM and PTS, respectively, using the SSPA.

The relative complexity as a function of V and U for $N = 128$ SCs is presented in Fig. 5.7. Similar to the results in Fig. 5.6, it is apparent that C_r is almost independent of the values of V/U except for the PTS-PAPR and PTS-IMD, where C_r decreases substantially to less than 30% by increasing V/U to 64 for both the TWTA and the SSPA cases. Consequently, using the DSR with the PTS at high

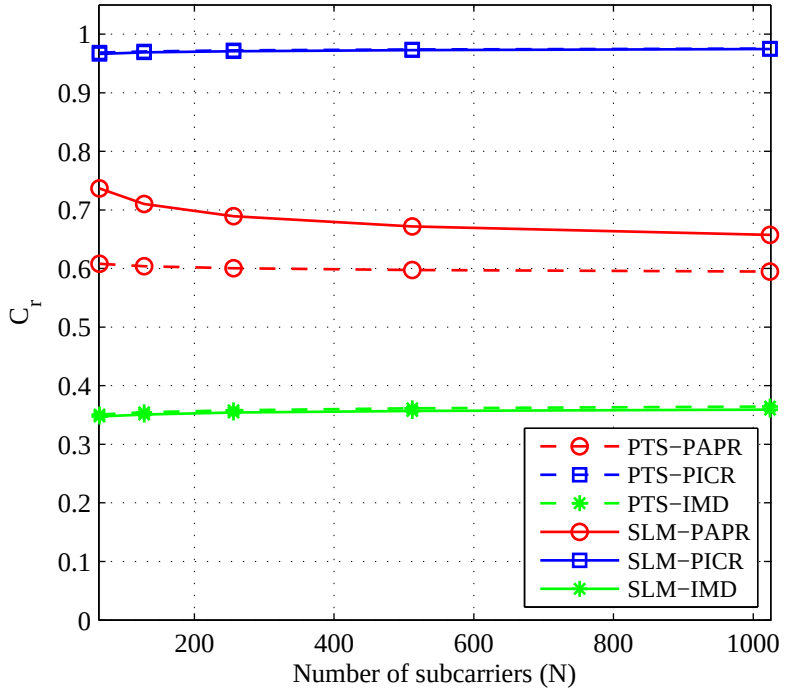

(a) TWTA case

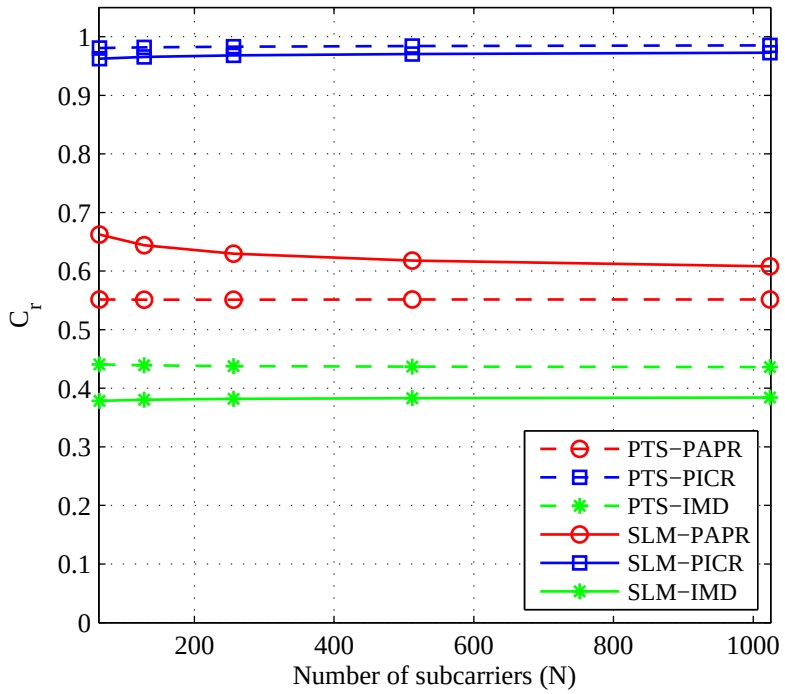

(b) SSPA case

Figure 5.6: Relative complexity for the PTS and SLM techniques based on the PAPR, IMD and PICR criteria.

V/U values becomes more attractive as the complexity reduction, $(1 - C_r)$, is more than 70%.

The relative complexity for the DSR with respect to PAPR based on the SLM using the SSPA for $g = 4$ can be expressed as

$$C_r = \frac{U[22\log_2(N) + 82] - 18}{UL[11\log_2(N) + 18] + 18U - 18}. \tag{5.23}$$

Since the constant term "18" in the numerator and denominator is much smaller than the other terms, C_r can be approximated as

$$C_r = \frac{22\log_2(N) + 82}{L[11\log_2(N) + 18] + 18}. \tag{5.24}$$

It is interesting to note that C_r in (5.24) is independent of U. Moreover, the dependency of C_r on N can be obtained by computing the derivative of (5.24) with respect to N,

$$\frac{\partial C_r}{\partial N} = \frac{-506L + 396}{N\ln(2)[11L\log_2(N) + 18L + 18]^2}. \tag{5.25}$$

Typically $N \geq 64$ and $L \geq 4$, hence the derivative described in (5.25) is approximately zero. Consequently, C_r can be considered to be independent of both U and N for the PAPR-SLM case.

It has been demonstrated that the local emulation of the HPA polynomial model with the FFT are required to calculate distortion metrics. As a result, the schemes utilising these metrics are more hardware complex than PAPR reduction-based techniques.

5.6 Numerical Results

Monte Carlo simulation is used to assess the performance of the proposed system and compare it to other well-established PAPR reduction techniques. The simulation results are obtained using 10^5 OFDM blocks generated using $N = 128$. The data symbols are selected uniformly from a Gray coded 16-QAM, QPSK and HM symbol constellation. The PTS and SLM techniques are set to use $V = U = 4$ or 16 and the number of possible phase factors are selected uniformly from $b^{(v)} = \pm 1$ and $a_i^{(u)} \in \{\pm 1, \pm j\}$, $i \in \{0, 1, \cdots, N-1\}$, respectively.

The TWTA and SSPA are modelled as described in (2.13), for the distortion met-

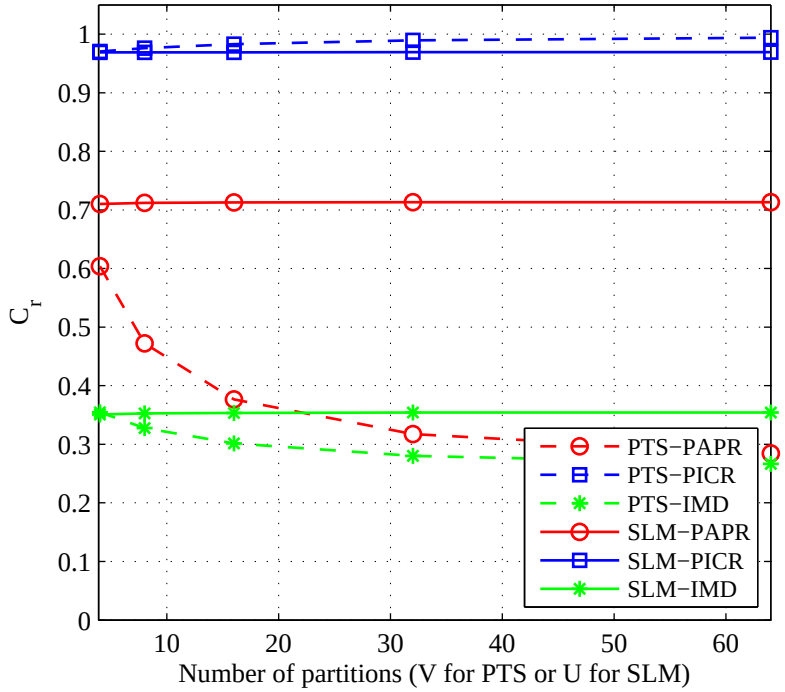

(a) TWTA case

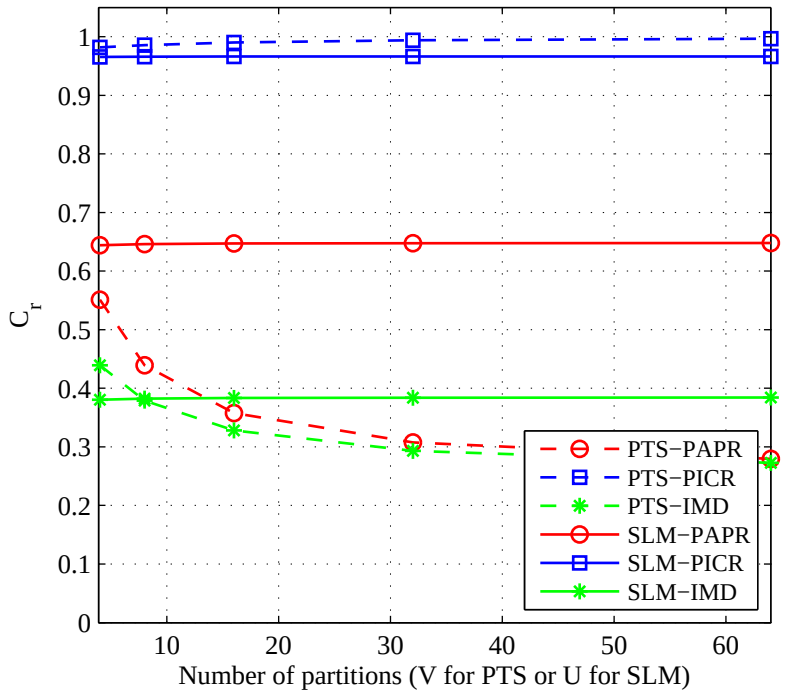

(b) SSPA case

Figure 5.7: Relative complexity for the PTS and SLM techniques based on the PAPR, IMD and PICR criteria.

rics calculation. Furthermore, memoryless models were used for the implementation of the OFDM signal transmission. In addition to the HPA nonlinearity, the channel adds zero mean AWGN with a variance of σ_η^2. For coherent demodulation, perfect knowledge of the phase coefficients for the PTS and SLM techniques at the receiver side is assumed. Moreover, for the TWTA case, the phase shift β in (5.5) is compensated properly at the receiver side through channel estimation. Consequently, the complex phase shift estimation illustrated in Section 2.5 is not required.

5.6.1 Power spectrum performance

Fig 5.8 depicts the out-of-band power produced by either the TWTA or the SSPA only case, using both the PTS-PAPR and the PTS-DSR schemes, utilising $V = 4$ and $N = 128$. It is clear from this figure that the PTS-DSR has slightly higher power spectral density than the HPA only case. However, the out-of-band power produced by the PTS-PAPR reduction technique is a little lower than that produced by the HPA only case.

5.6.2 CCDF performance

5.6.2.1 CCDF performance of PAPR

The CCDF is widely used to assess the performance of PAPR reduction techniques. Fig. 5.9 depicts the CCDF of PAPR for PTS-OFDM and SLM-OFDM systems based on the DSR, PICR, IMD and PAPR criteria. It can be observed that high CCDF values of PAPR in systems based on DSR reduction occur with lower probabilities than the corresponding values in systems based on the PICR or IMD reduction. For example, when $V/U = 4$ the PAPR value corresponding to a CCDF value of 10^{-4} for PTS-DSR and SLM-DSR is approximately 0.6 and 1 dB, respectively, compared to the OFDM systems without PAPR reduction. However, for $V/U = 16$, the PAPR value corresponding to a CCDF value for the DSR-reduction criterion is approximately 1.3 and 1.4 dB better than those of the OFDM systems without PAPR reduction. Furthermore, when using this V/U value with PTS-PAPR and SLM-PAPR, the reduction is approximately 2.4 and 2.6 dB better than the PTS-DSR and the SLM-DSR schemes, respectively.

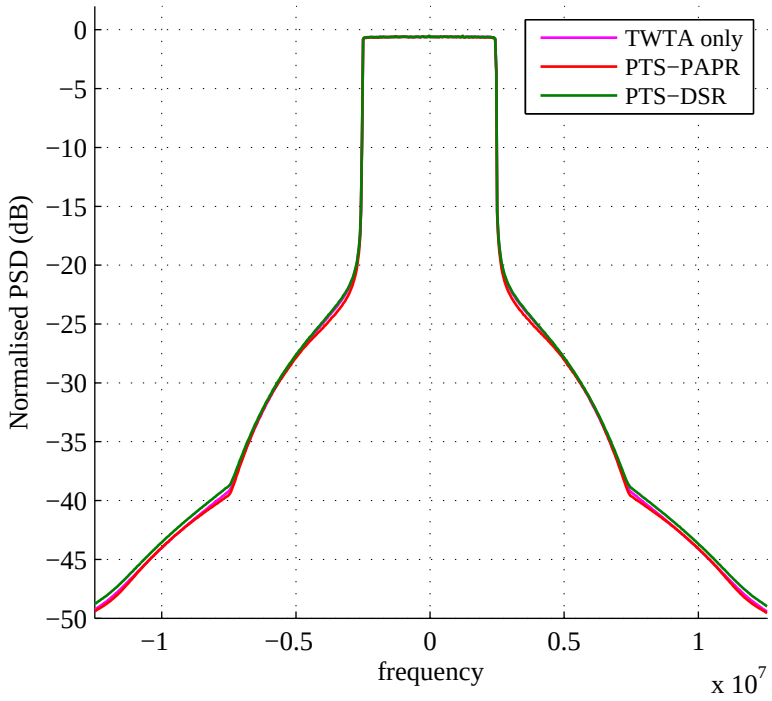

(a) TWTA with OBO = 5 dB

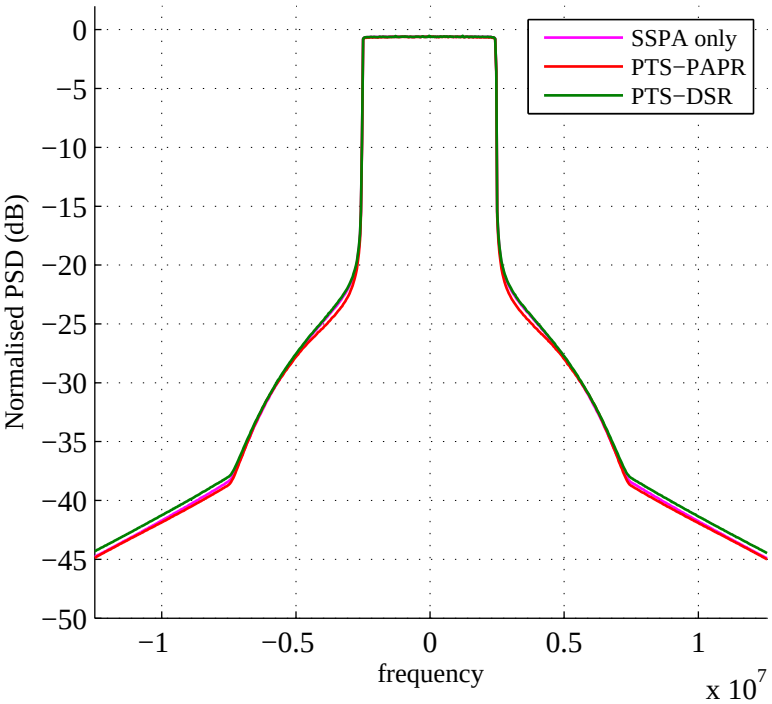

(b) SSPA with OBO = 3.5 dB

Figure 5.8: The out-of-band power spectrum plot of OFDM signal with and without PAPR reduction.

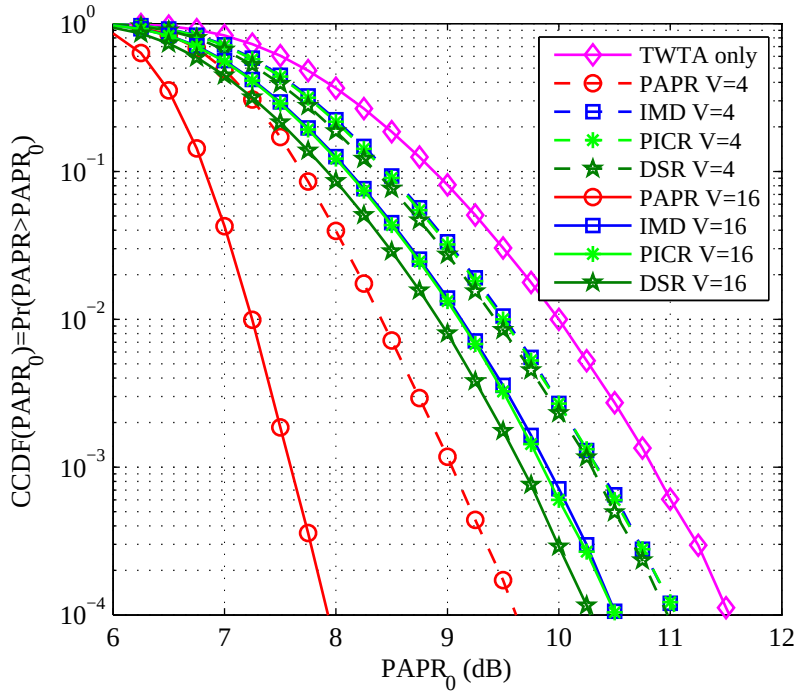

(a) PTS-based scheme

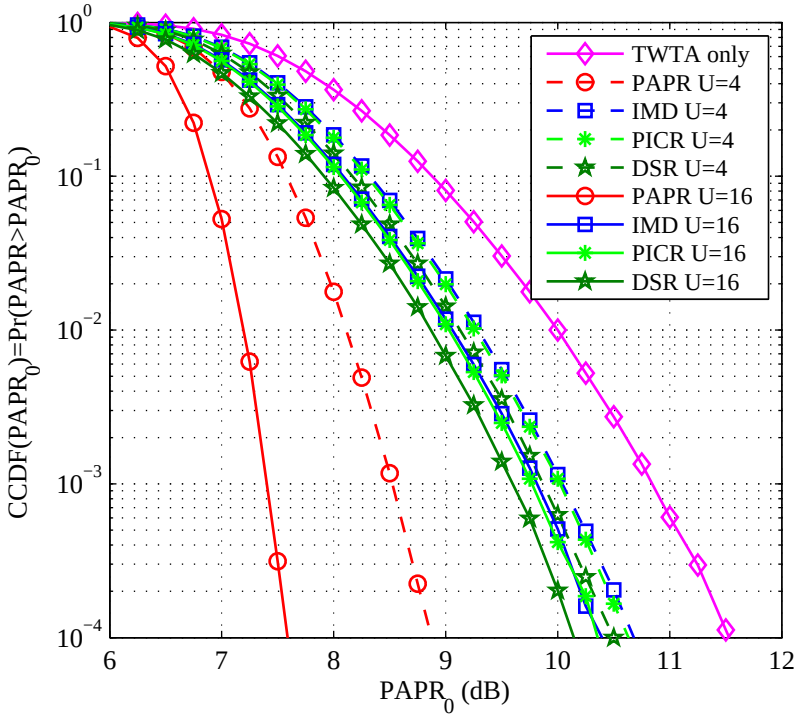

(b) SLM-based scheme

Figure 5.9: CCDF of the PAPR for OFDM systems based on the DSR, PICR, IMD and PAPR reduction criteria for different partitions.

5.6.2.2 CCDF performance of DSR

In this section, the CCDF of the DSR is utilised, which is defined as the probability that the DSR is greater than a reference value denoted as DSR_0. Fig. 5.10 depicts the CCDF of the DSR for an OFDM system using either the PTS or the SLM scheme for different partitions based on various reduction criteria utilising the TWTA model. Compared to the PTS-PAPR technique, the proposed DSR criterion provided an extra improvement of approximately 0.8 and 1.3 dB at CCDF of 10^{-4} for $V = 4$ and $V = 16$, respectively as shown in Fig. 5.10(a). It is worth mentioning that for different number of partitions the PTS-PICR and PTS-IMD have marginally lower DSR than PTS-PAPR. However, the PTS-DSR has the lowest DSR for different partitions. A similar CCDF pattern is shown in Fig. 5.10(b) for an OFDM system using the SLM scheme. From this figure, it is apparent that the SLM-DSR can achieve a reduction in CCDF of approximately 0.8 and 1.1 dB, respectively, compared to the SLM-PAPR for $U = 4$ and $U = 16$.

The CCDF of the DSR for the OFDM system using either the PTS or the SLM schemes is depicted in Fig. 5.11 for different partitions based on the DSR, PICR, IMD and PAPR reduction criteria, utilising the SSPA model. Fig. 5.11(a) shows that the proposed DSR criterion can achieve an extra improvement of approximately 0.9 and 1.7 dB for $V = 4$ and $V = 16$, respectively, in comparison to the PTS-PAPR technique. Furthermore, using the SLM scheme, a similar CCDF trend is shown in Fig. 5.11(b). It can be seen from this figure that the SLM-DSR can improve the CCDF performance by 0.9 and 1.6 dB, respectively, compared to the SLM-PAPR for $U = 4$ and $U = 16$.

5.6.3 BER performance

In this chapter, the BER performance is assessed over an AWGN, wideband satellite and frequency-selective multipath fading channels.

5.6.3.1 BER performance over an AWGN channel

The BER is one of the most significant criteria to assess the performance of communication systems. The BER performance of the proposed DSR and the other considered schemes is presented in Fig. 5.12 in the presence of the TWTA nonlinearity, based on either the PTS or the SLM scheme, respectively, for 16-QAM

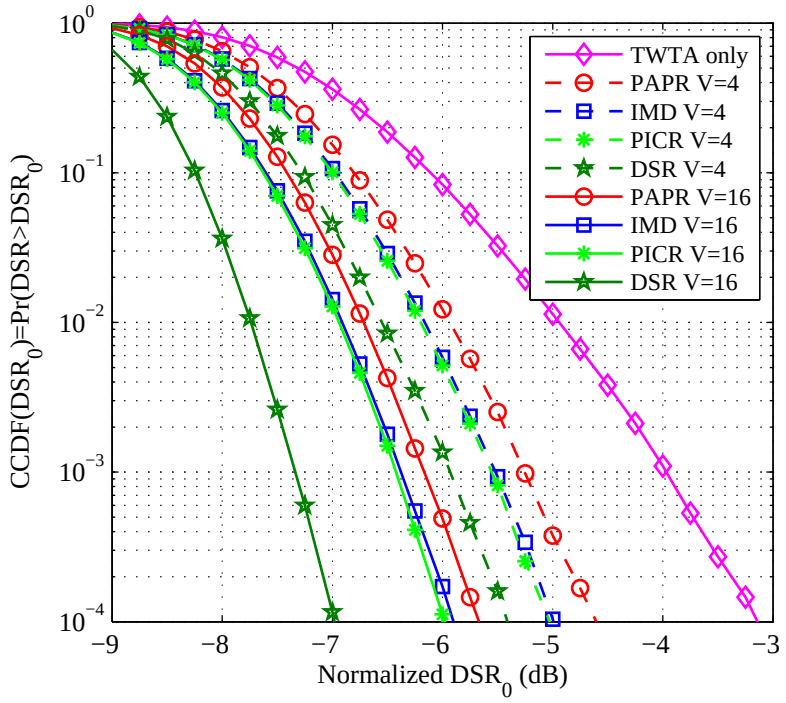

(a) PTS-based scheme

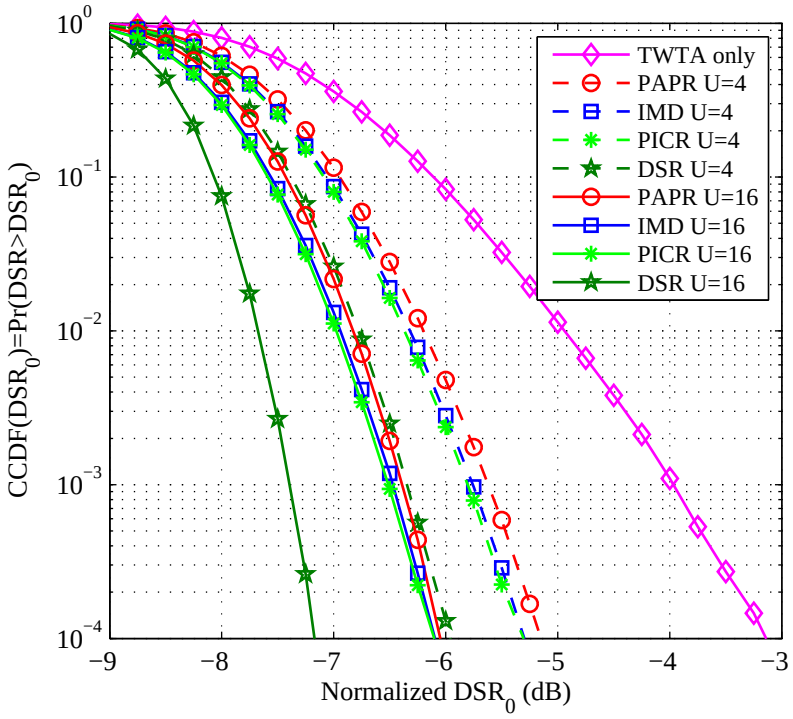

(b) SLM-based scheme

Figure 5.10: CCDF of the DSR for OFDM systems based on the DSR, PICR, IMD and PAPR reduction criteria for different partitions using the TWTA with OBO = 5 dB.

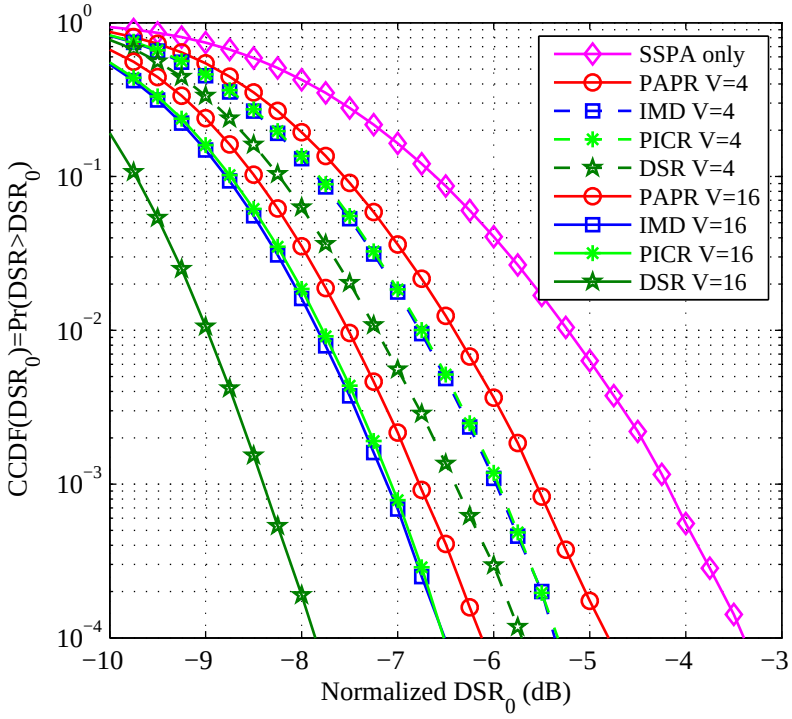

(a) PTS-based scheme

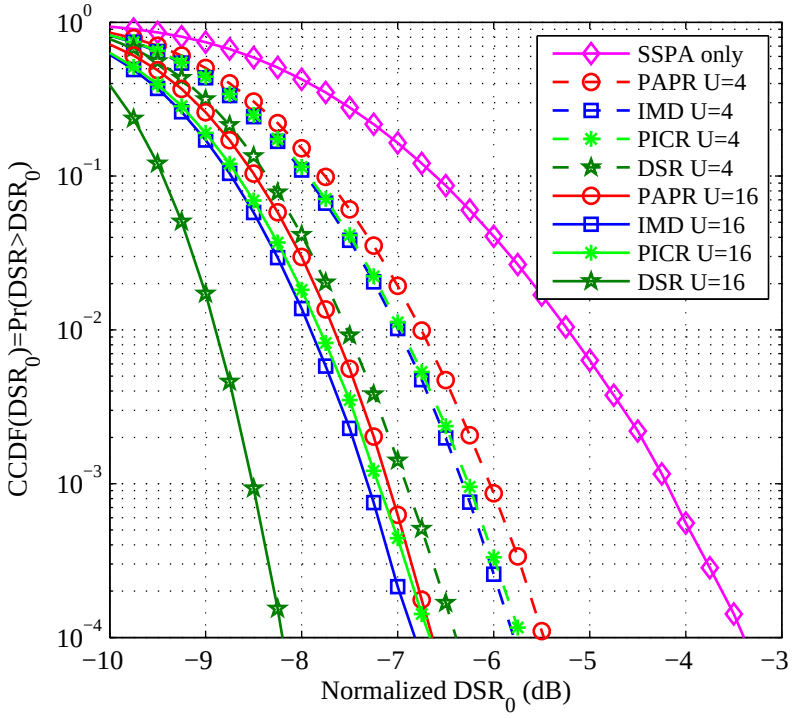

(b) SLM-based scheme

Figure 5.11: CCDF of the DSR for OFDM systems based on the DSR, PICR, IMD and PAPR reduction criteria for different partitions using the SSPA with OBO = 3.5 dB.

OFDM systems. It can be noted from Figs. 5.12(a) and 5.12(b), at a BER of 10^{-4} that the PTS-DSR and SLM-DSR managed to reduce the required SNR by approximately 4.3 and 3.5 dB, respectively, compared to the PTS-PAPR and SLM-PAPR for $V/U = 16$. This phenomenon is due to the fact that minimising the DSR level produced by the TWTA nonlinearity can provide superior indication of ICI, and hence, offer better BER performance when compared to other approaches, which are optimised in order to reduce the PAPR.

Fig. 5.13 depicts the BER systems based on the DSR, PICR, IMD and PAPR reduction criteria in the presence of the SSPA nonlinearity and AWGN for 16-QAM constellation. The most significant aspect in this figure is that for both the PTS-DSR and the SLM-DSR schemes, for $V/U = 16$ eliminate the error floor that is caused by the ICI. Furthermore, the SSPA is less sensitive than the TWTA due to the ICI effect, and hence, the error floor appears only at very low BERs.

The BER performance of the proposed DSR and PAPR schemes in the presence of the TWTA nonlinearity, based on either the PTS or the SLM scheme, for $V/U = 16$ is shown in Fig. 5.14 for the HM constellation. It can be noted that the PTS-DSR scheme can achieve an improvement of approximately 2.3 dB and 1.9 dB, respectively, at 10^{-4} BER for EL and BL. However, the proposed SLM-DSR scheme can accomplish an improvement of 3.5 dB and 1.5 dB, respectively, in BER performance. It is apparent that the proposed DSR metric can give an accurate indication of the interference generated by the TWTA and HM.

Fig. 5.15 depicts the BER systems based on either the PTS or the SLM scheme, for $V/U = 16$, in the presence of the SSPA nonlinearity and AWGN for the HM constellation. The PTS-DSR scheme can accomplish an improvement approximately 2.3 dB and 1.6 dB, respectively, for EL and BL. The proposed SLM-DSR, however, achieves an improvement that is only 0.3 dB lower in BER performance, than that of the PTS-DSR scheme for both layers.

Figs. 5.16 and 5.17 depict the BER performance for the same schemes mentioned above, utilising either the TWTA or the SSPA with a QPSK constellation, based on either the PTS or the SLM schemes, respectively. It can be seen from Fig. 5.16, that the PTS-DSR and SLM-DSR schemes, with $V/U = 16$, can achieve an improvement 1.8 and 1.4 dB, respectively, compared to the PTS-PAPR and SLM-PAPR schemes. However, when the SSPA is utilised, the PTS-DSR and SLM-DSR schemes, with $V/U = 16$, can achieve a 1.1 and 0.8 dB improvement in BER performance, respec-

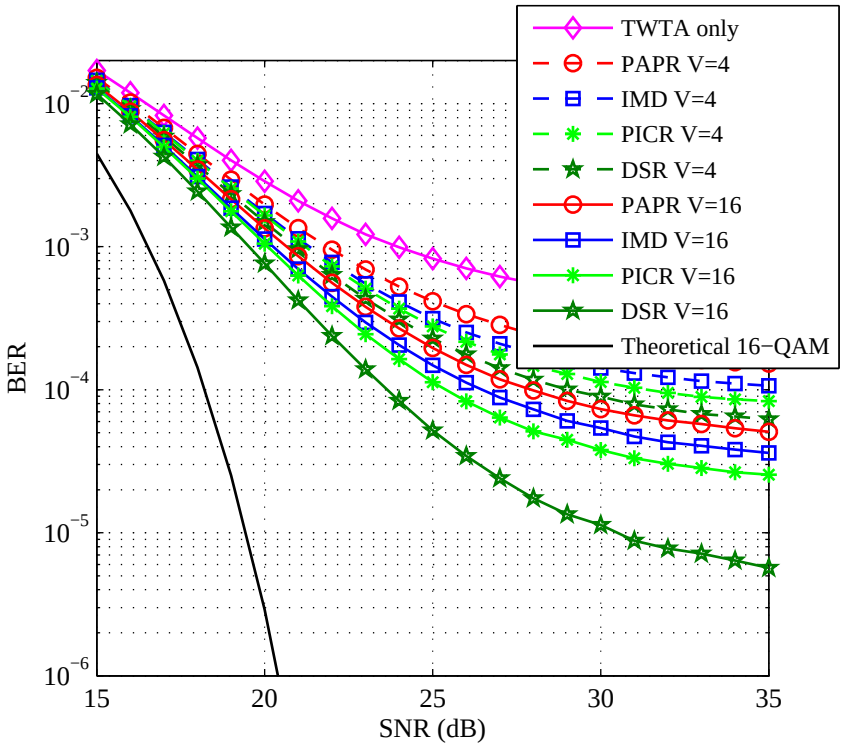

(a) PTS-based scheme

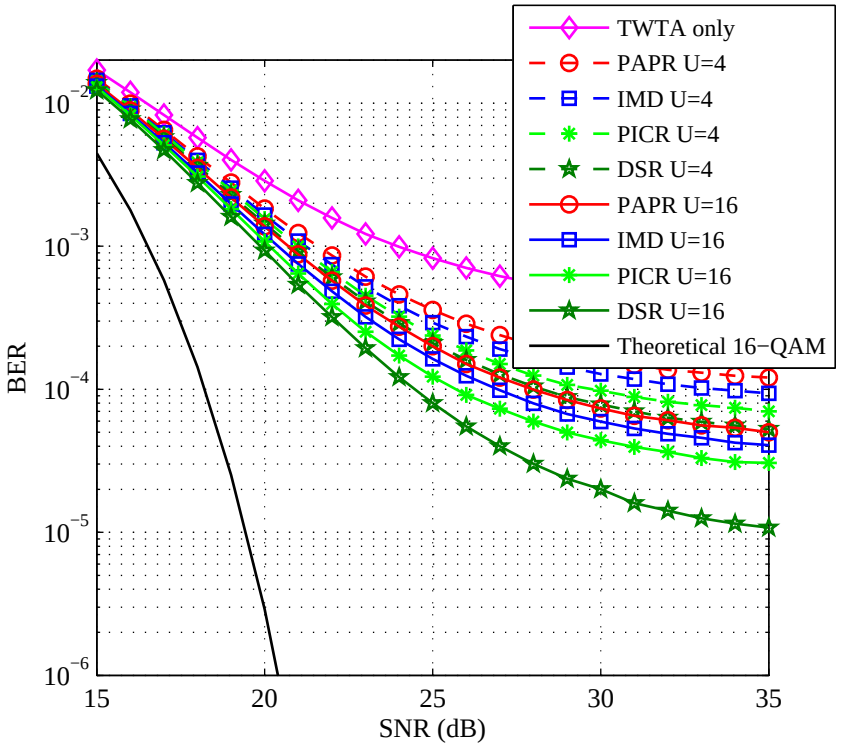

(b) SLM-based scheme

Figure 5.12: BER versus SNR for systems based on the DSR, PICR, IMD and PAPR reduction criteria in the presence of the TWTA nonlinearity and AWGN for 16-QAM constellation.

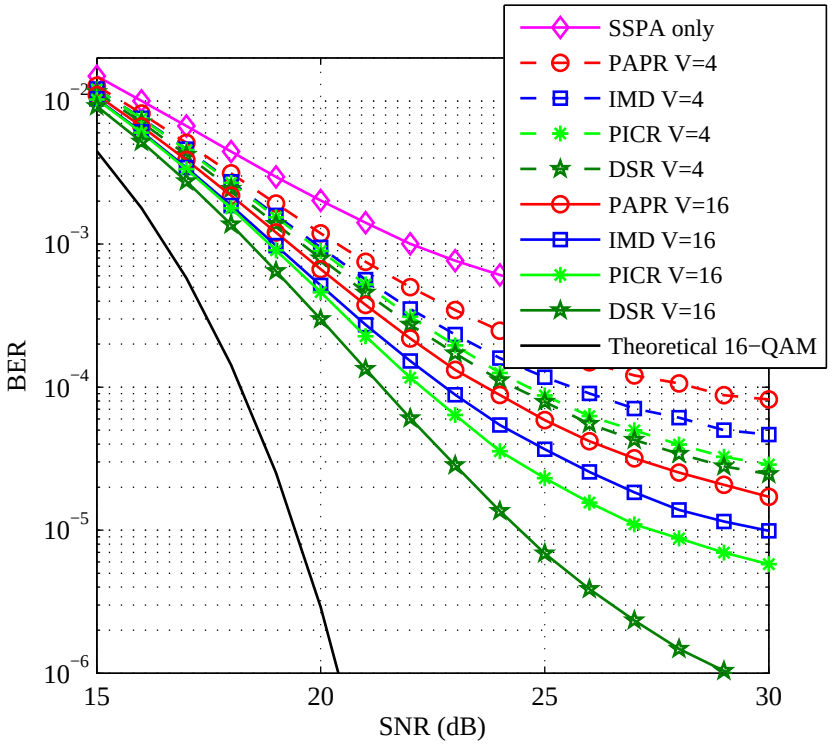

(a) PTS-based scheme

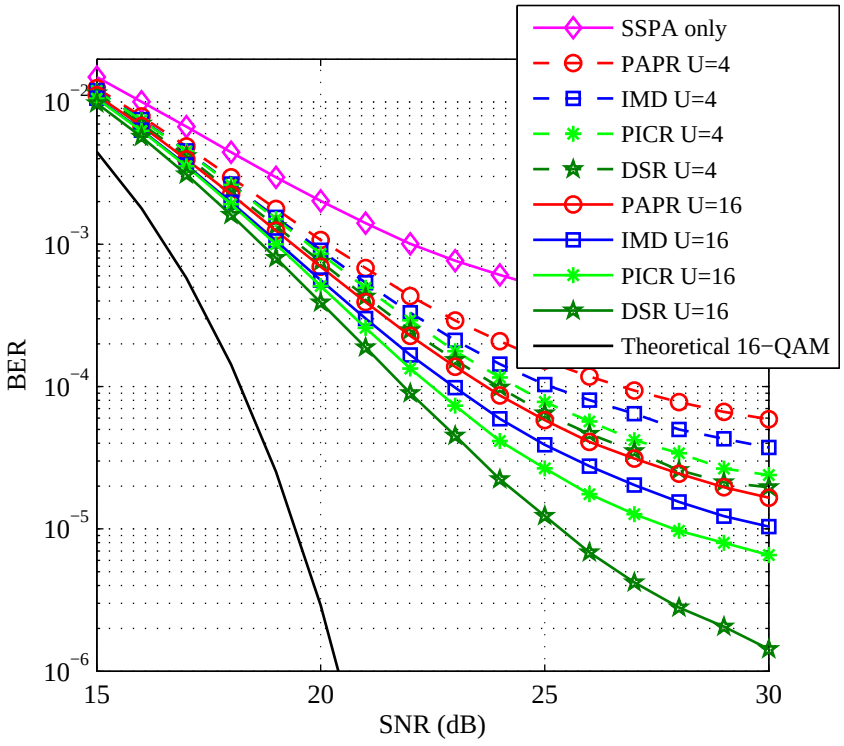

(b) SLM-based scheme

Figure 5.13: BER versus SNR for systems based on the DSR, PICR, IMD and PAPR reduction criteria in the presence of the SSPA nonlinearity and AWGN for 16-QAM constellation.

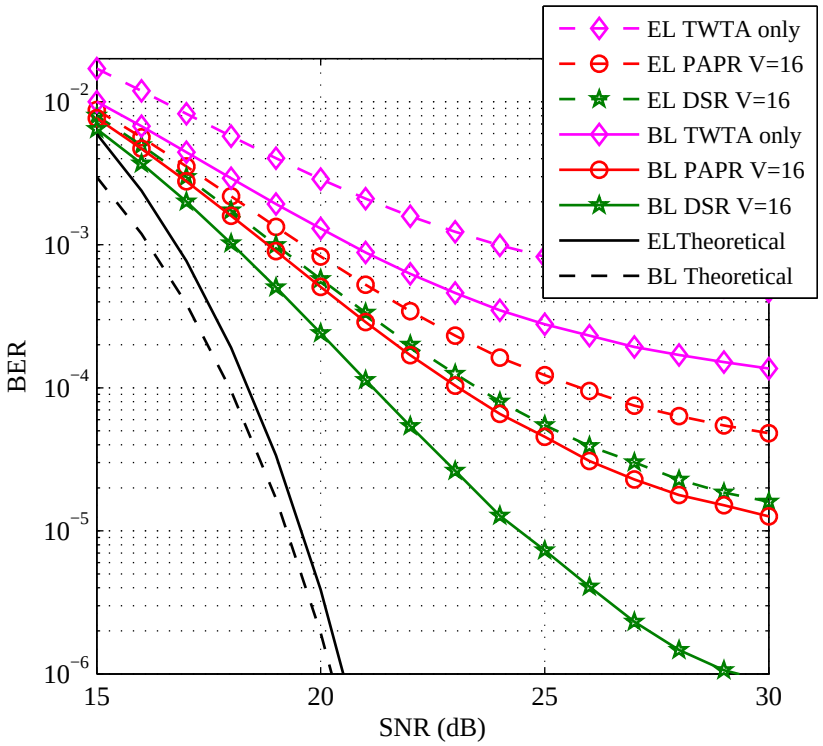

(a) PTS-based scheme

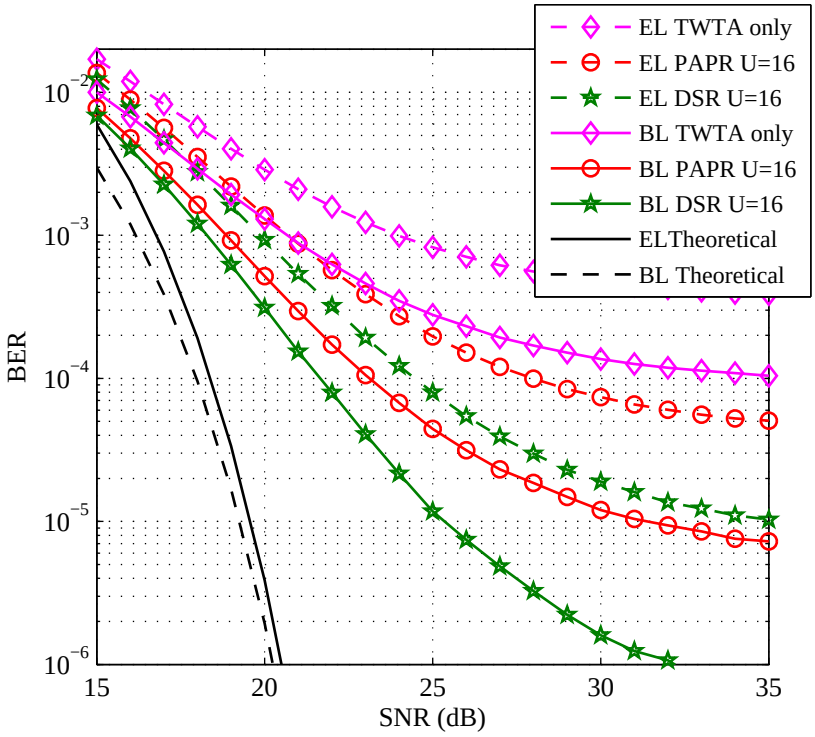

(b) SLM-based scheme

Figure 5.14: BER versus SNR for systems based on the DSR and PAPR reduction criteria in the presence of the TWTA nonlinearity and AWGN for the HM constellation.

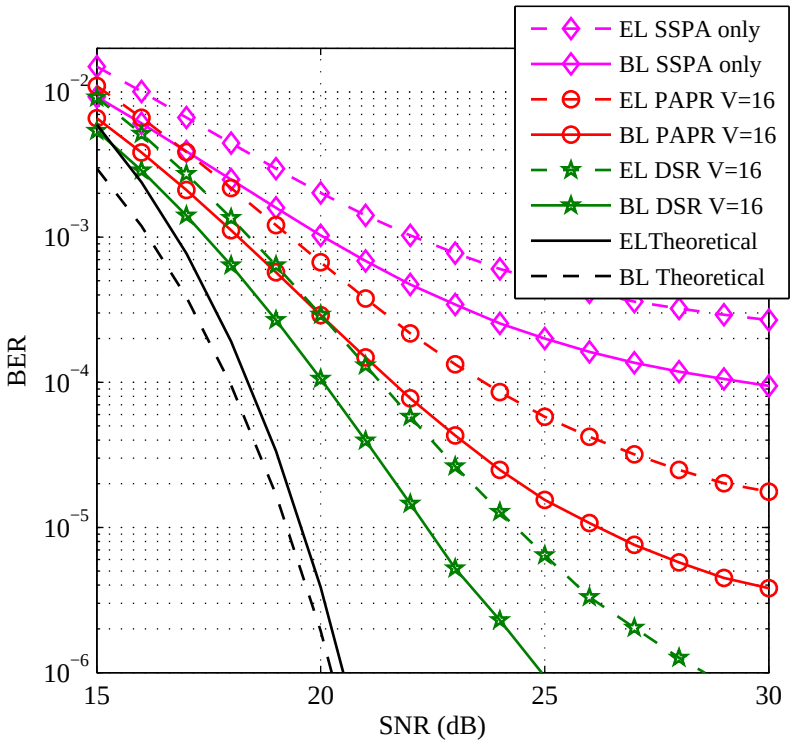

(a) PTS-based scheme

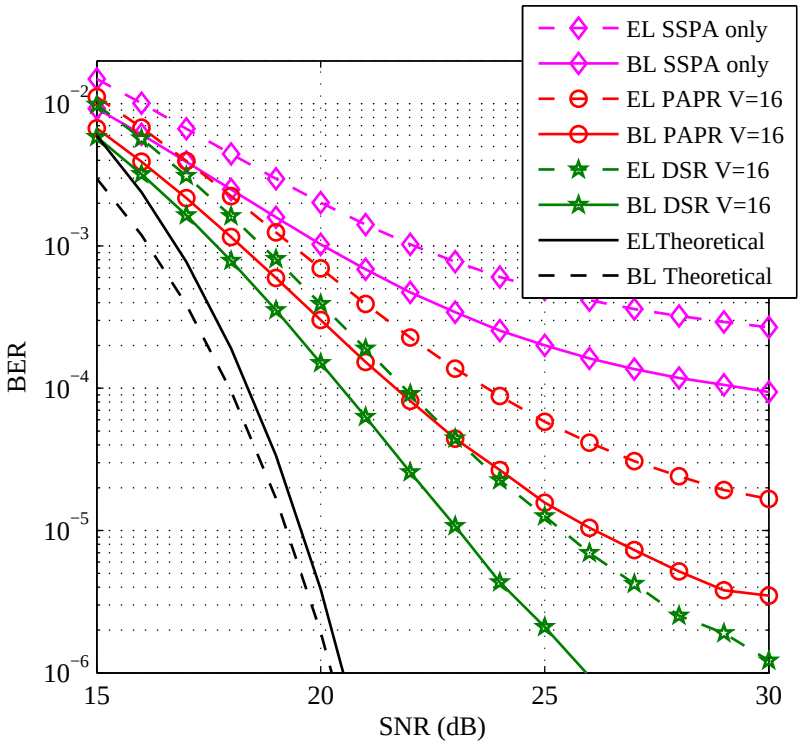

(b) SLM-based scheme

Figure 5.15: BER versus SNR for systems based on the DSR and PAPR reduction criteria in the presence of the SSPA nonlinearity and AWGN for the HM constellation.

tively, as shown in Fig. 5.17.

It can be observed from Figs. 5.12, 5.14 and 5.16 that the BER for all techniques still suffer from error floors that appear at high SNRs, which are due to the nonlinear effect of the TWTA. However, the error floor levels depend on the efficiency of the particular technique used. For the DSR case, the error floor levels were much lower than those of the other considered techniques. Complete elimination of the error floors requires a large number of partitions or high OBOs. Alternatively, low-level error floors can be eliminated more efficiently by using error control coding techniques.

5.6.3.2 BER performance in mobile satellite channel

The multipath fading channels are quite important for wireless applications. However, the DSR is computed at the transmitter side with the assumption that no channel information is available at the transmitter, which is the case in most practical scenarios. Consequently, the proposed technique should be applied to both AWGN and multipath fading channels without any change.

The proposed system is simulated in the wideband satellite mobile channel, in order to observe its performance under practical channel degradations. The BER performance for a 16-QAM modulation scheme in the presence of the TWTA nonlinearity and wideband channel with elevation angle, $\theta \leq 45$, is depicted in Fig. 5.18. A similar trend of the BER performance is achieved for the mobile satellite fading channel apart from an extra impairment approximately 2.5 dB, owing to multipath fading.

5.6.3.3 BER performance in multipath fading channel using a practical SSPA model

The BER performance for 16-QAM modulation scheme over a frequency-selective multipath fading channel and practical SSPA model is presented in Fig. 5.20, for the PTS and SLM schemes. The fading channel consists of 5 multipath components with delays of [0, 1, 2, 3, 4] samples, an average gain of [0.35, 0.25, 0.18, 0.13, 0.09], and the mean square delay spread $\sigma^2(\tau) = 1.74$ [104]. The channel frequency response is shown in Fig. 5.19. Moreover, the transmission SSPA parameters are selected to match the practical WiMax *SSPA 2.30-2.40-400* amplifier, described in

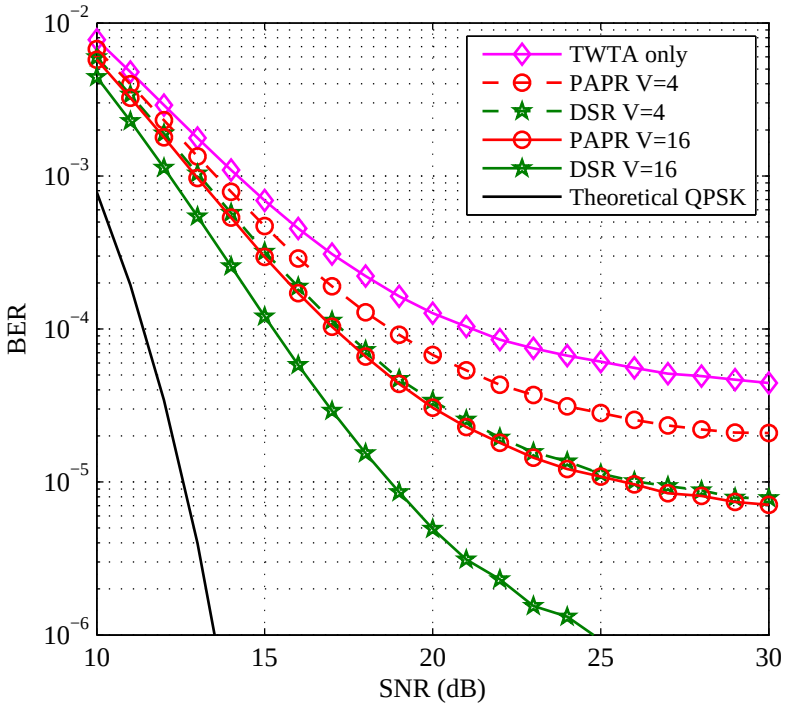

(a) PTS-based scheme

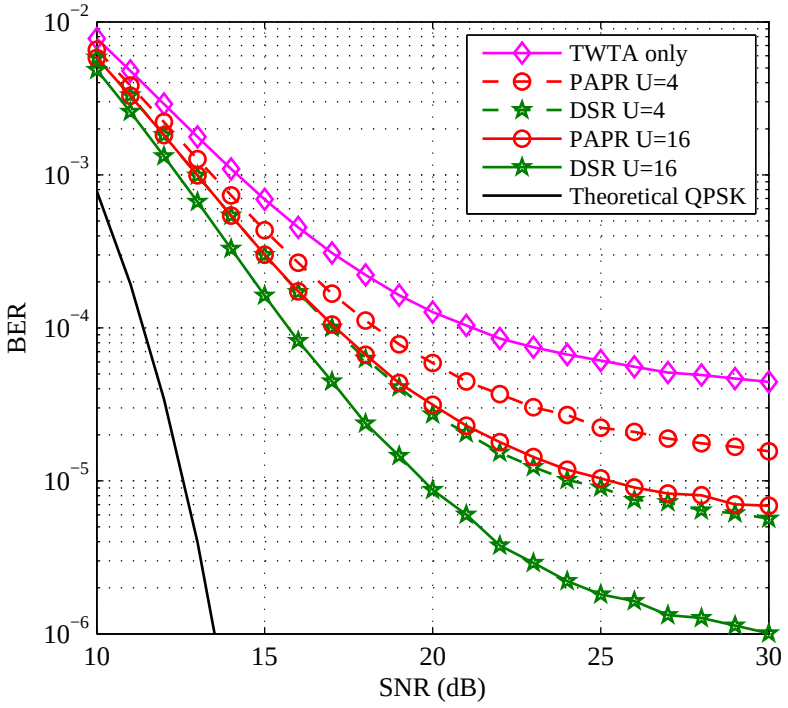

(b) SLM-based scheme

Figure 5.16: BER versus SNR for systems based on the DSR and PAPR reduction criteria in the presence of the TWTA nonlinearity and AWGN for the QPSK constellation.

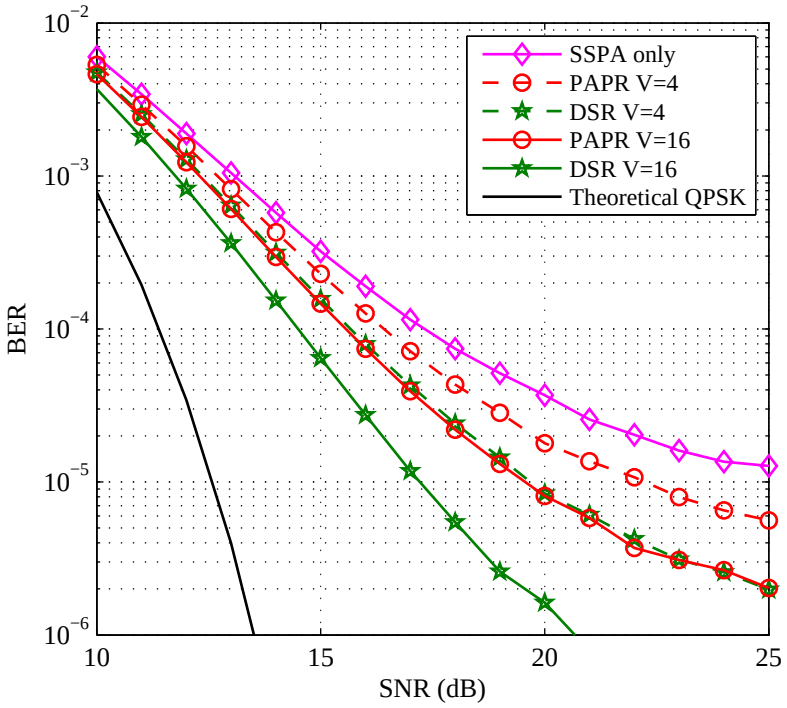

(a) PTS-based scheme

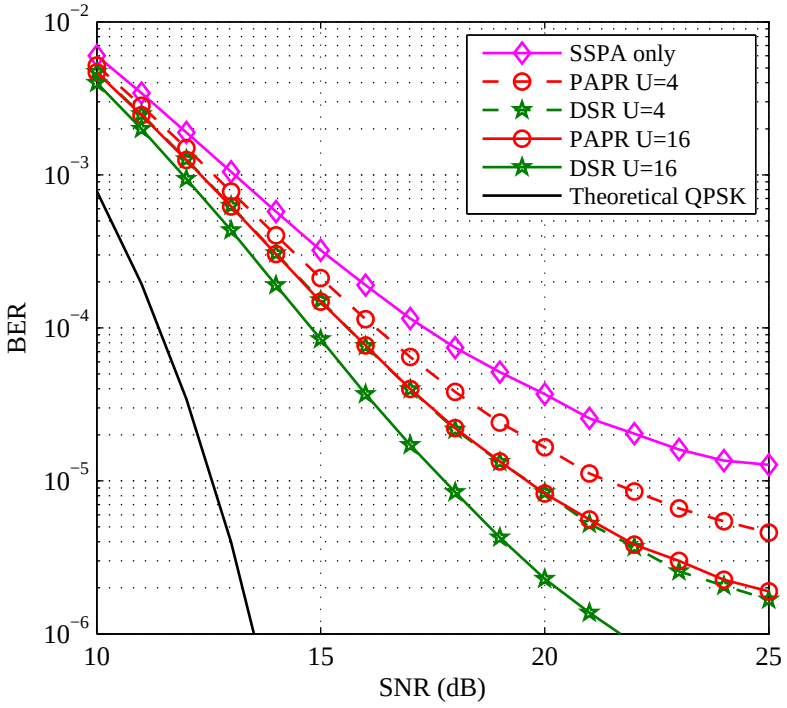

(b) SLM-based scheme

Figure 5.17: BER versus SNR for systems based on the DSR and PAPR reduction criteria in the presence of the SSPA nonlinearity and AWGN for the QPSK constellation.

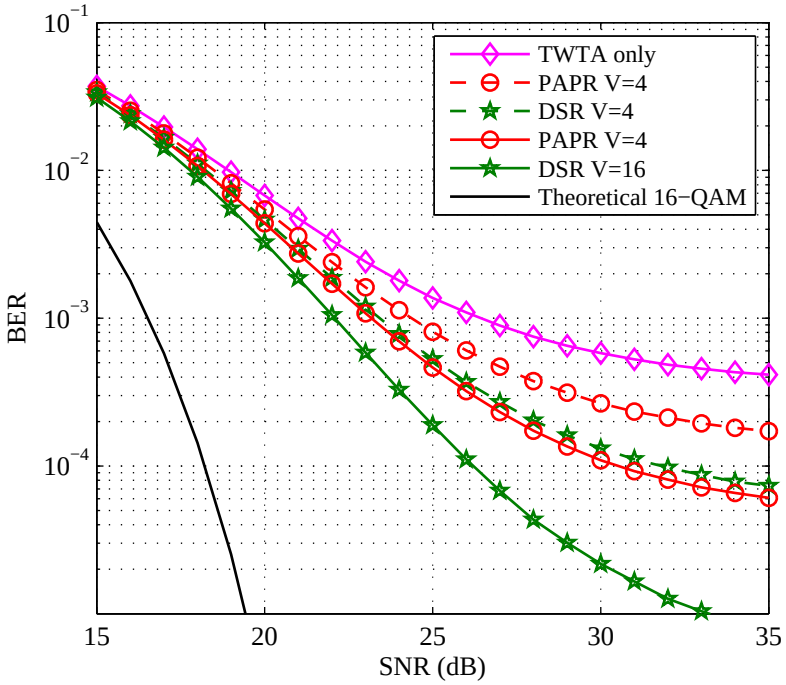

(a) PTS-based scheme

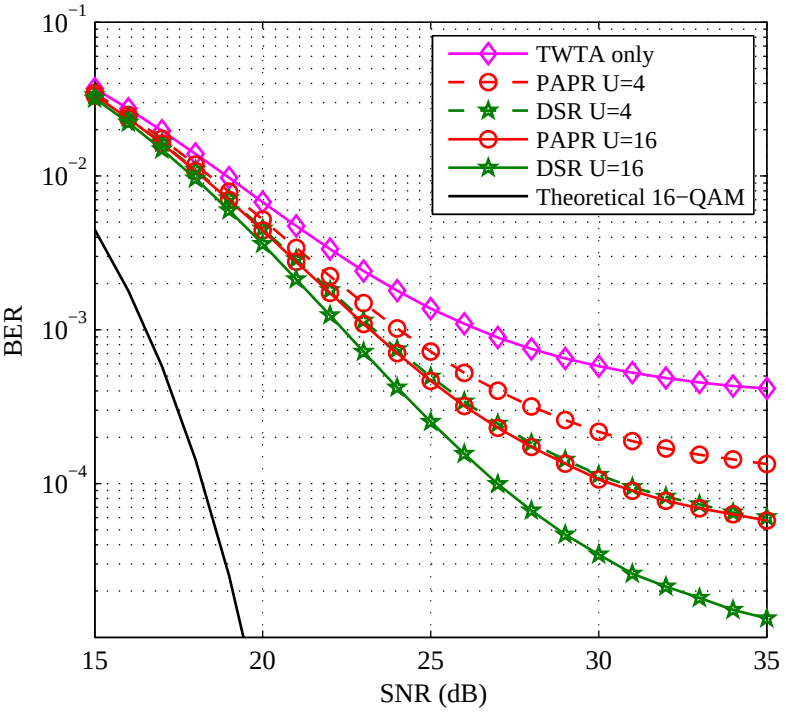

(b) SLM-based scheme

Figure 5.18: BER versus SNR for systems based on the DSR and PAPR reduction criteria in the presence of the TWTA nonlinearity and wideband satellite mobile channel, $\theta \leq 45$, for the 16-QAM constellation.

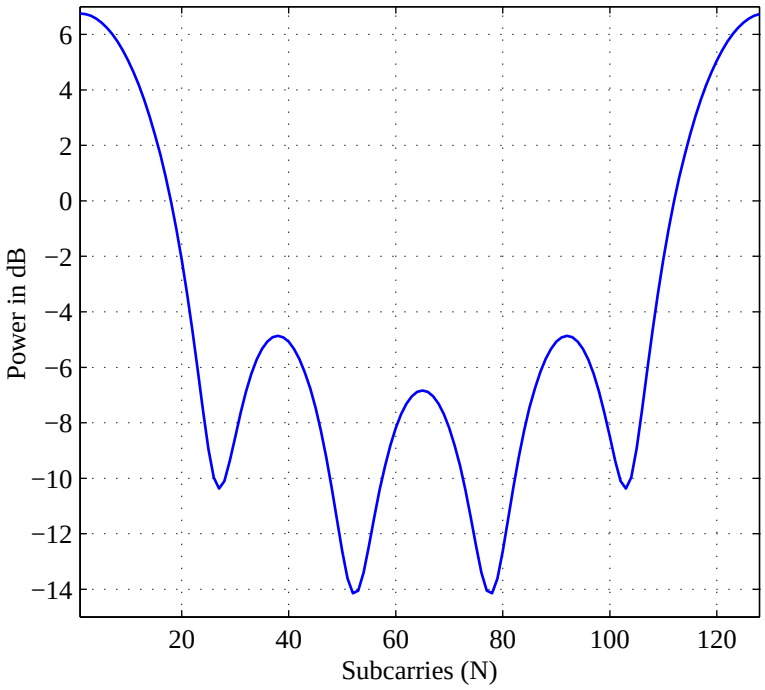

Figure 5.19: Frequency response of frequency-selective multipath fading channel

[105]. The parameters for this amplifier for the Rapp and polynomial models, are found using curve fitting techniques, where $p = 3.2676$, $\alpha_1 = 1$ and $\alpha_3 = -0.1787$ for OBO = 3.5 dB. As it can be observed from Fig. 5.20, the performance trend is sustained where the DSR outperforms the other considered techniques, irrespective of the channel model. Furthermore, the results obtained for the practical SSPA model, confirm that using the simple polynomial model to predict the DSR provides sufficient accuracy.

5.7 Chapter Summary

The present study confirms previous findings (the key idea of the PAPR reduction is to achieve an improvement in the BER performance) and contributes additional evidence that support the new metrics to reduce the BER. One of the more significant findings is that minimising the PAPR does not necessarily minimise the distortion produced by the nonlinearity of the HPA, and hence, it does not necessarily minimise the BER.

Table 5.2 summarises the performance and complexity of the proposed PTS-DSR and SLM-DSR scheme over the PAPR criterion, using either the TWTA or the

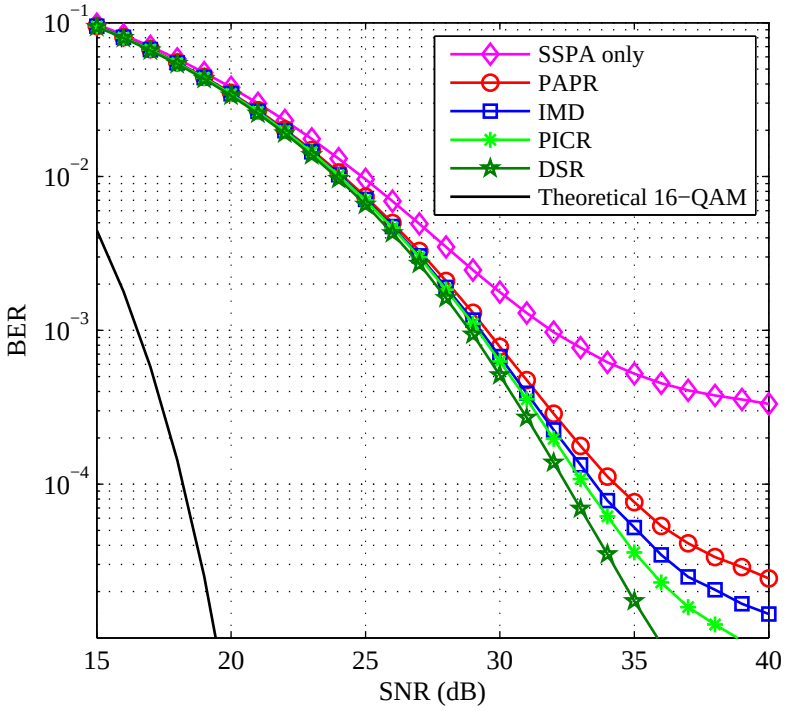

(a) PTS-based scheme

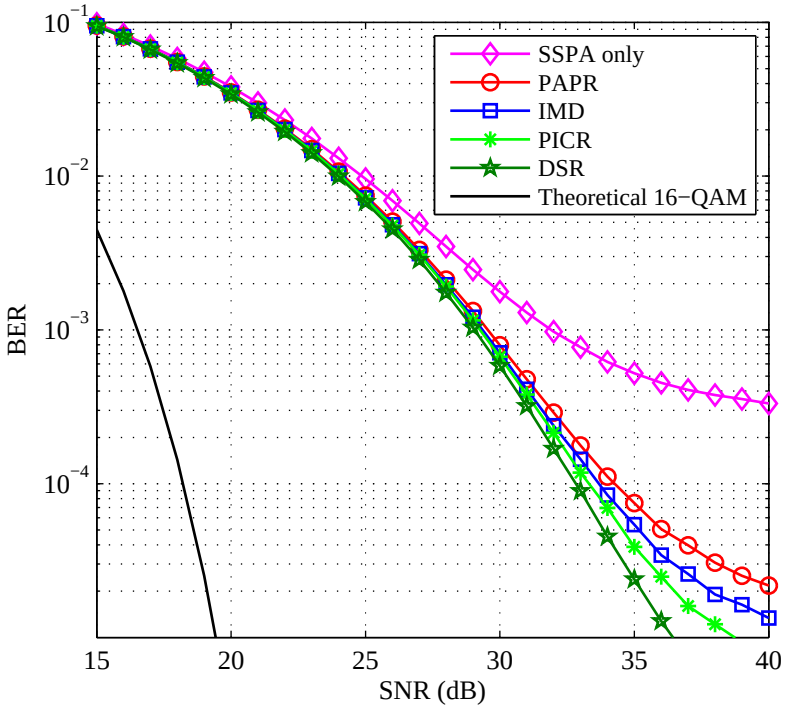

(b) SLM-based scheme

Figure 5.20: BER versus SNR for systems based on the DSR and PAPR reduction criteria in the presence of the practical SSPA nonlinearity and frequency-selective multipath fading channel for 16-QAM constellation, $V/U = 16$.

Table 5.2: The overall comparison of the proposed schemes over the PAPR-based technique for $V/U = 16$.

Proposed Technique	HPA Model	C_r in %	DSR Reduction in dB	Conste-llation	OBO in dB	SNR Improvement in dB
PTS-DSR	TWTA	38	1.3	16-QAM QPSK	5 0	4.3 1.8
	SSPA	36	1.7	16-QAM QPSK	3.5 0	1.7 No error floor 1.1 No error floor
SLM-DSR	TWTA	71	1.1	16-QAM QPSK	5 0	3.5 1.4
	SSPA	65	1.6	16-QAM QPSK	3.5 0	1.4 No error floor 0.8 No error floor

SSPA with a 16-QAM constellation. This table shows that the proposed schemes using SSPA can eliminate the error floor. Furthermore, a reduction in DSR by approximately 1.7 dB is accomplished. In addition, these schemes can reduce the relative complexity by 36% and 65% for the PTS and SLM schemes, respectively. The results of the proposed scheme using the TWTA are as follows: 38% and 71% reduction in C_r, and 1.3 and 1.1 dB reduction in DSR for PTS-DSR and SLM-DSR, respectively. For the TWTA case, the proposed systems can achieve an improvement of 4.3 and 3.5 dB in BER performance, respectively.

5.8 Conclusion

This chapter presented efficient techniques to improve the BER performance degradation due to the nonlinear characteristics of HPAs that are utilised in OFDM-based systems. The proposed techniques demonstrate that using less-direct PAPR indicators can provide better performance when combined with distortionless techniques, such as the PTS and SLM techniques. Therefore, the proposed technique is optimised to combat the consequences of the high PAPR, rather than reducing the PAPR itself. The proposed techniques are based on using the distortion level to select the optimal PTS and SLM system parameters. Simulation results have demonstrated that minimising the amplifier distortion provides a significant BER reduction in comparison to other techniques, which are optimised to reduce the PAPR. Moreover, the proposed techniques offer a complexity reduction of approximately 60%, for particular OFDM and HPA settings.

Chapter 6

Efficient ICI Reduction Techniques for OFDM Systems Distorted by Amplifier Nonlinearity and Frequency Offset

Multi-carrier systems are significantly affected by the ICI produced by both HPA and CFO. To reduce the ICI, we use the proposed metric, DSR, with the PTS and SLM schemes used for PAPR reduction, which is more constructive than the conventional PAPR metric. Simulation results have confirmed that the BER improvement of ~ 10.6 dB using the SSPA at BER $\sim 10^{-4}$ can be achieved when the proposed technique is compared to the standard PTS utilising 16 partitions. Moreover, complexity analysis demonstrates that the proposed system offers a significant complexity reduction of approximately 60% when compared to the well-known techniques. Finally, a closed form solution for ESNR is derived, and consequently, the accurate BER is calculated theoretically. An accepted accuracy of the BER between simulation and analytical calculation is achieved.

6.1 Carrier Frequency Offset Issue

6.1.1 Effect of CFO on system performance

Frequency offsets occur due to a mismatch between the transmitter and the receiver frequency of the local oscillators and/or Doppler shift of the channel, owing to rela-

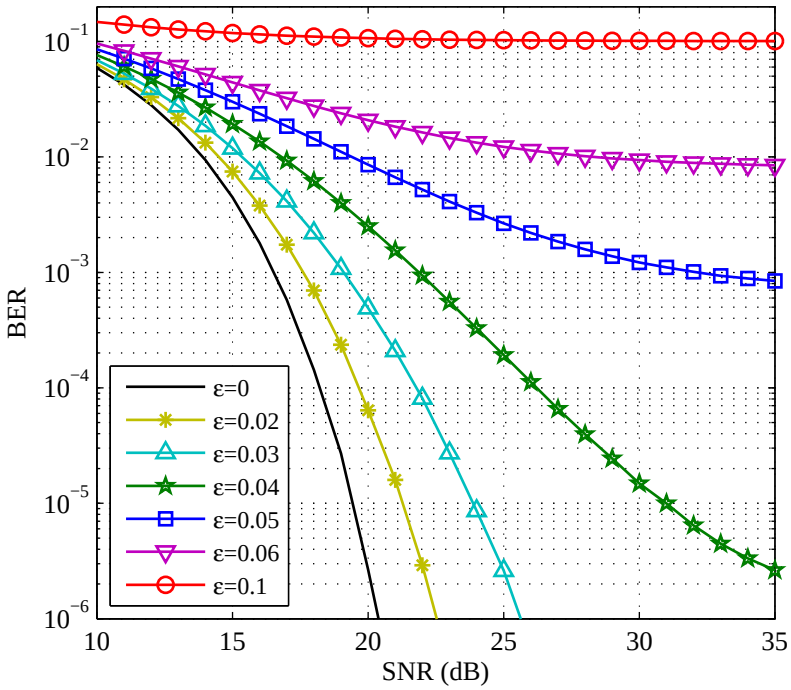

Figure 6.1: BER versus SNR for OFDM systems with various ε values using 16-QAM modulation.

tive motion between the transmitter and the receiver. Consequently, substantial ICI is introduced due to the overlapping in power spectrum between adjacent SCs. As a result, the BER degrades significantly. For example, in higher modulation schemes such as 64-QAM, a small CFO may degrade the system performance severely. The sensitivity to the frequency offset is commonly cited as a main OFDM drawback [4].

The carrier frequency offset, $\Delta\varepsilon$, gives an additional phase factor of $\mathrm{e}^{j2\pi\Delta\varepsilon t} = \mathrm{e}^{j2\pi\varepsilon ft} = \mathrm{e}^{j2\pi\varepsilon n/N}$ to the received signal, where f is the SC spacing, ε is the normalised CFO by f and $n = 0, 1, \cdots, N-1$ [106]. The normalised CFO can be classified into two main parts: integer and decimal (coarse and fine). The former part is a multiple of the SC spacing that causes a shift in the SC indices. A circular shift of the transmitted symbols is caused due to the integer part; however, the orthogonality of the SCs is not destroyed. The latter part on the other hand, which is less than half of the SC spacing, may cause ICI, due to the loss of orthogonality among the SCs [24].

Fig. 6.1 depicts the BER performance for OFDM systems with various ε values using 16-QAM modulation. It is clear from this figure utilising $\varepsilon \geq 0.05$, that the system BER is degraded severely and BER $= 10^{-4}$ cannot be achieved for these values of ε, even for high SNRs.

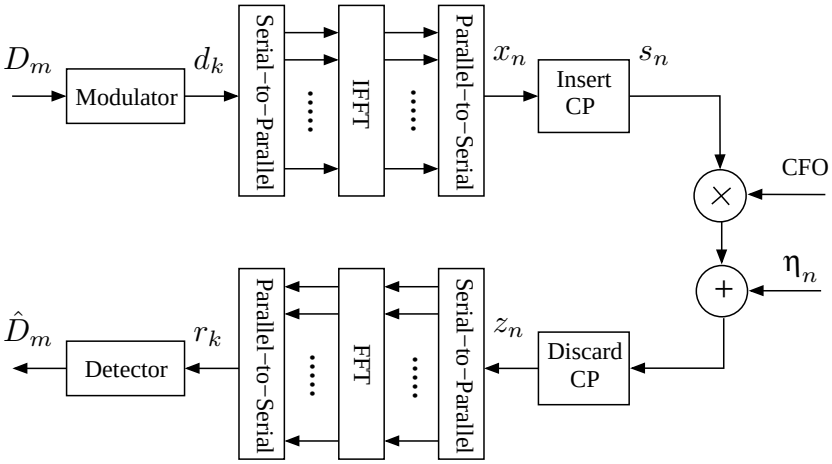

Figure 6.2: Block diagram of an OFDM system in the presence of the CFO.

6.1.2 CFO compensation

CFO compensation can be divided into three categories. Firstly, coarse decimal CFO estimation and correction which is performed in time-domain, i.e. before the FFT, to reduce the ICI effect on the estimation of the second category. The integer part which is the second category, can be estimated in the frequency-domain (after the FFT) to perform the correct indices of the SCs. Finally, the fine decimal frequency offset, $|\varepsilon| < 0.5$, is estimated and adjusted in frequency-domain [106].

In literature referring to the carrier frequency offsets in OFDM systems, several schemes have been proposed to combat these effects. These schemes can be categorised as: ICI self-cancellation scheme [107], time-domain windowing on the transmitted signals [108], time-domain equalisation [109] and statistical schemes for estimation and compensation of the ICI [110]. However, low bandwidth efficiency is achieved in approaches which adopt a long cyclic prefix [106].

6.1.3 Analysis of ICI due to CFO

Fig. 6.2 depicts the frequency offset model as a multiplicative vector presented in the channel of OFDM systems. The discrete-time complex-baseband OFDM signal after the IFFT block the transmitter can be represented as

$$x_n = \frac{1}{\sqrt{N}} \sum_{l=0}^{N-1} d_l \mathrm{e}^{j2\pi ln/N}. \;\; n = 0, 1, \cdots, N-1. \tag{6.1}$$

After parallel-to-serial conversion and CP insertion, the samples of the OFDM symbol s_n are perturbed by the CFO and the AWGN to construct the received signal

$$z_n = s_n e^{j2\pi\varepsilon n/N} + \eta_n. \tag{6.2}$$

At the receiver side, after removing the CP, the received signal samples are serial-to-parallel converted and applied to the FFT in order to produce the decision variables r_k, which can be expressed as

$$r_k = \frac{1}{\sqrt{N}} \sum_{n=0}^{N-1} z_n \, \mathrm{e}^{-j2\pi kn/N}. \;\; k = 0, 1, \cdots, N-1. \tag{6.3}$$

By substituting (6.2) and (6.1) in (6.3), r_k will be

$$r_k = \frac{1}{\sqrt{N}} \sum_{n=0}^{N-1} \left[\left[\frac{1}{\sqrt{N}} \sum_{l=0}^{N-1} d_l \mathrm{e}^{j2\pi ln/N} \right] \mathrm{e}^{j2\pi\varepsilon n/N} + \eta_n \right] \mathrm{e}^{-j2\pi kn/N}, \tag{6.4}$$

and subsequently

$$r_k = \frac{1}{N} \sum_{n=0}^{N-1} \sum_{l=0}^{N-1} d_l \mathrm{e}^{j2\pi(\varepsilon+l-k)n/N} + \omega_k, \tag{6.5}$$

where ω_k is the FFT of η_n. The first term in (6.5) can be expanded for $l = k$ and $l \neq k$, therefore, r_k can be rewritten as

$$r_k = \underbrace{d_k \frac{1}{N} \sum_{n=0}^{N-1} \mathrm{e}^{j2\pi\varepsilon n/N}}_{\text{Useful Signal}} + \underbrace{\frac{1}{N} \sum_{n=0}^{N-1} \sum_{\substack{l=0 \\ l\neq k}}^{N-1} d_l \mathrm{e}^{j2\pi(\varepsilon+l-k)n/N}}_{\text{ICI}} + \omega_k. \tag{6.6}$$

By using the geometric series property $\sum_{n=0}^{N-1} q^n = \dfrac{1-q^N}{1-q}$, r_k can be expressed as

$$\begin{aligned} r_k = & \underbrace{d_k \frac{\sin(\pi\varepsilon)}{N \sin\left(\dfrac{\pi\varepsilon}{N}\right)} \mathrm{e}^{j\pi\varepsilon(N-1)/N}}_{\text{Useful Signal}} \\ & + \underbrace{\sum_{\substack{l=0 \\ l\neq k}}^{N-1} d_l \frac{\sin(\pi(\varepsilon+l-k))}{N \sin\left(\dfrac{\pi(\varepsilon+l-k)}{N}\right)} \mathrm{e}^{j\pi(\varepsilon+l-k)(N-1)/N}}_{\text{ICI}} + \omega_k. \end{aligned} \tag{6.7}$$

It can be noted from (6.7) that the ICI term is a function of the data sequence d_k for $k = 0, \cdots, N-1$ and ε. Finally, r_k can be written in compact form as [101]

$$r_k = d_k\beta_0 + \sum_{\substack{l=0 \\ l\neq k}}^{N-1} d_l\beta_{l-k} + \omega_k, \quad \text{for} \quad k = 0, 1, \cdots, N-1. \tag{6.8}$$

where β_0 represents the complex phase shift given by

$$\beta_0 = \frac{\sin(\pi\varepsilon)}{N\sin\left(\frac{\pi\varepsilon}{N}\right)} \mathrm{e}^{j\pi\varepsilon(N-1)/N}, \tag{6.9}$$

and β_{l-k} is the nonlinear noise component owing to the CFO that can be described as

$$\beta_{l-k} = \frac{\sin(\pi(\varepsilon + l - k))}{N\sin\left(\frac{\pi(\varepsilon + l - k)}{N}\right)} \mathrm{e}^{j\pi(\varepsilon+l-k)(N-1)/N}. \tag{6.10}$$

The effect of ICI on the received signal is analysed for OFDM systems with $N = 32$ SCs using two values of ε, 0.2 and 0.4. Furthermore, $l = 0$ is considered, i.e., the SC with index 0 of the received signal is analysed. Fig. 6.3 shows the ICI coefficients, $|\beta_{l-k}|$, for all SC indices. It is clear from this figure that for larger ε values, the amplitude of the useful signal term, $|\beta_0|$, decreases, whereas the amplitude of the ICI terms increases.

6.2 PAPR Reduction Techniques to Reduce ICI Generated by the CFO

In addition to their role in PAPR reduction, it is interesting to note that the PTS and SLM can be used to reduce the influence of CFOs, i.e. ICI, in OFDM systems [101]. These techniques were developed by noting the correlation between the ICI and the data structure. For example, if all of the SCs in a given OFDM symbol are equal, the ICI becomes zero, even if the CFO is not zero. The authors in [101] introduced PICR, the definition of which is analogous to the PAPR metric. The PICR was used in combination with PTS and SLM schemes to reduce the ICI generated by the CFO. However, the PICR can be estimated at the transmitter side on the basis of worst-case CFO (ε_{wc}) values, where $\varepsilon_{wc} > 0$. Consequently, $|\varepsilon|$ should be less than ε_{wc} to assess the BER performance of the PICR-based scheme [101].

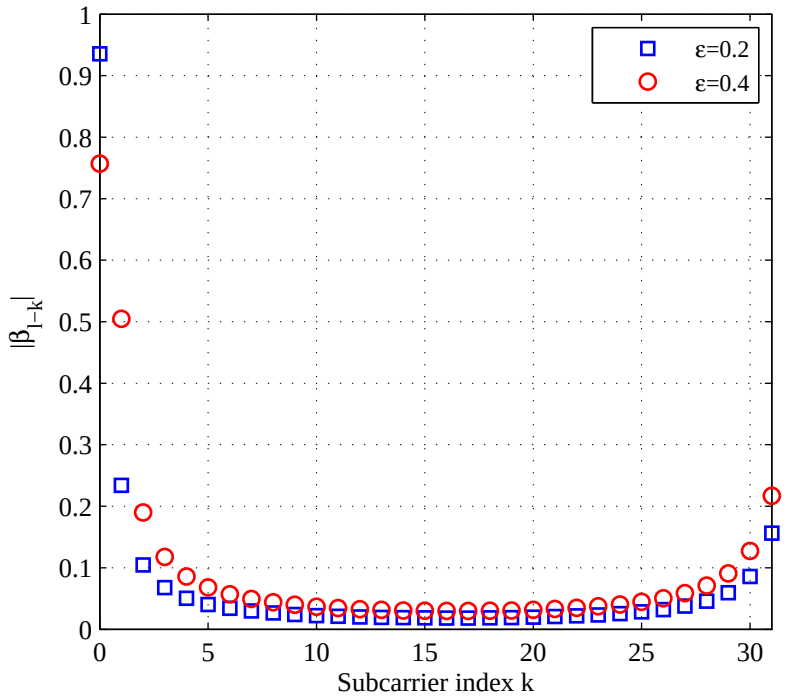

Figure 6.3: ICI coefficients for an OFDM system with $N = 32$ SCs.

6.3 ICI Analysis due to HPA Nonlinearity and CFO

Fig. 6.4 depicts a block diagram of OFDM system in the presence of a HPA and CFO. The effect of the nonlinearity on the signal quality can be evaluated by first computing the FFT after the HPA output and adding the CFO, except that the AWGN is set to zero since the computations are carried out at the transmitter side. By substituting (2.13) into (6.3), r_k can be expressed as

$$r_k = \frac{1}{\sqrt{N}} \sum_{n=0}^{N-1} \alpha_1 x_n \mathrm{e}^{j2\pi(\varepsilon-k)n/N} + \frac{1}{\sqrt{N}} \sum_{n=0}^{N-1} \alpha_3 |x_n|^2 x_n \mathrm{e}^{j2\pi(\varepsilon-k)n/N}. \tag{6.11}$$

Substituting (6.1) into (6.11), r_k can be rewritten as

$$\begin{aligned} r_k \;=\; & \frac{1}{\sqrt{N}} \sum_{n=0}^{N-1} \alpha_1 \left[\frac{1}{\sqrt{N}} \sum_{l=0}^{N-1} d_l \mathrm{e}^{j2\pi ln/N} \right] \mathrm{e}^{j2\pi(\varepsilon-k)n/N} \\ & + \frac{1}{\sqrt{N}} \sum_{n=0}^{N-1} \alpha_3 |x_n|^2 \left[\frac{1}{\sqrt{N}} \sum_{l=0}^{N-1} d_l \mathrm{e}^{j2\pi ln/N} \right] \mathrm{e}^{j2\pi(\varepsilon-k)n/N}, \end{aligned} \tag{6.12}$$

and after some mathematical manipulations, r_k can be expressed as

$$\begin{aligned} r_k &= d_k \left[\alpha_1 + \frac{\alpha_3}{\mathrm{IBO}_l}\right] \frac{\sin(\pi\varepsilon)}{N \sin\left(\frac{\pi\varepsilon}{N}\right)} \mathrm{e}^{j\pi\varepsilon(1-1/N)} \\ &\quad + \frac{\alpha_1}{N} \sum_{\substack{l=0 \\ l\neq k}}^{N-1} d_l \sum_{n=0}^{N-1} \mathrm{e}^{j2\pi(\varepsilon+l-k)n/N} \\ &\quad + \frac{\alpha_3}{N} \sum_{\substack{l=0 \\ l\neq k}}^{N-1} d_l \sum_{n=0}^{N-1} |x_n|^2 \mathrm{e}^{j2\pi(\varepsilon+l-k)n/N}. \end{aligned} \tag{6.13}$$

Finally, r_k can be presented in a similar compact form as shown in (5.4), where β is a combination of (5.5) and (6.9) that can be given by

$$\beta = \left[\alpha_1 + \frac{\alpha_3}{\mathrm{IBO}_l}\right] \frac{\sin(\pi\varepsilon)}{N \sin\left(\frac{\pi\varepsilon}{N}\right)} \mathrm{e}^{j\pi\varepsilon(1-1/N)}, \tag{6.14}$$

and ψ_k is the nonlinear ICI component which can be described as

$$\begin{aligned} \psi_k &= \frac{\alpha_1}{N} \sum_{\substack{l=0 \\ l\neq k}}^{N-1} d_l \sum_{n=0}^{N-1} \mathrm{e}^{j2\pi(\varepsilon+l-k)n/N} \\ &\quad + \frac{\alpha_3}{N} \sum_{\substack{l=0 \\ l\neq k}}^{N-1} d_l \sum_{n=0}^{N-1} |x_n|^2 \mathrm{e}^{j2\pi(\varepsilon+l-k)n/N}. \end{aligned} \tag{6.15}$$

Therefore, the metrics IMD, PICR and DSR investigated in Chapter 5 can be exploited to minimise the distortion for OFDM systems perturbed by amplifier nonlinearity and CFO.

6.3.1 Proposed ICI reduction using PTS scheme

In this section, the DSR and PICR criteria for both PTS and SLM techniques are introduced. Fig. 6.5 depicts the block diagram of PTS combined with DSR/PICR in the presence of HPA nonlinearity and CFO. In this technique, similar equation forms of $x_n^{(v)}$ and x_n can be obtained as shown in (5.12) and (3.9), respectively. The frequency-domain symbol, r_k, on the k-th SC after the polynomial model, CFO

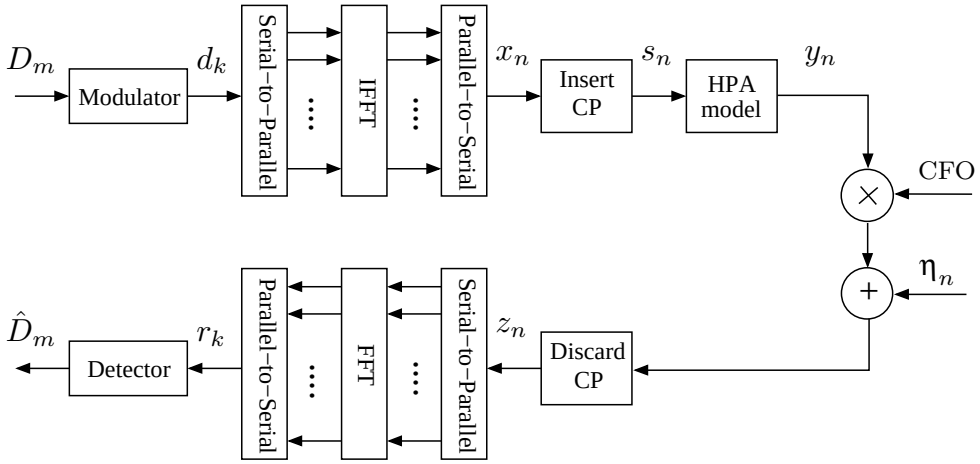

Figure 6.4: Block diagram of an OFDM system in the presence of the HPA and CFO.

effect and FFT blocks, can be written as

$$\begin{aligned} r_k = &\sum_{v=1}^{V} d_k^{(v)} b^{(v)} \left[\frac{\alpha_1}{N} \sum_{n=0}^{N-1} \mathrm{e}^{j2\pi\varepsilon n/N} + \frac{\alpha_3}{N} \sum_{n=0}^{N-1} |x_n|^2 \mathrm{e}^{j2\pi\varepsilon n/N} \right] \\ &+ \frac{\alpha_1}{N} \sum_{v=1}^{V} b^{(v)} \sum_{\substack{l=0 \\ l\neq k}}^{N-1} d_l^{(v)} \left[\sum_{n=0}^{N-1} \mathrm{e}^{j2\pi(\varepsilon+l-k)n/N} \right] \\ &+ \frac{\alpha_3}{N} \sum_{v=1}^{V} b^{(v)} \sum_{\substack{l=0 \\ l\neq k}}^{N-1} d_l^{(v)} \left[\sum_{n=0}^{N-1} |x_n|^2 \mathrm{e}^{j2\pi(\varepsilon+l-k)n/N} \right]. \end{aligned} \tag{6.16}$$

Similar forms for r_k and $\psi_{k,PTS}$ are presented in (5.14) and (5.15), respectively, where the complex phase shift β is identical to (6.14) and the term $\psi_k^{(v)}$ is given by

$$\psi_k^{(v)} = \frac{\alpha_1}{N} \sum_{\substack{l=0 \\ l\neq k}}^{N-1} d_l^{(v)} \sum_{n=0}^{N-1} \mathrm{e}^{j2\pi(\varepsilon+l-k)n/N} + \frac{\alpha_3}{N} \sum_{\substack{l=0 \\ l\neq k}}^{N-1} d_l^{(v)} \sum_{n=0}^{N-1} |x_n|^2 \mathrm{e}^{j2\pi(\varepsilon+l-k)n/N}. \tag{6.17}$$

Finally, the $\overline{\mathrm{DSR}}_{PTS}$ can be obtained from (5.17).

6.3.2 Proposed ICI reduction using SLM scheme

The block diagram of the SLM-based distortion sensing method is shown in Fig. 6.6 in the presence of HPA nonlinearity and CFO. Similar equations of $\mathbf{d}^{(u)}$ and $x_n^{(u)}$ can be obtained from (3.10) and (5.18), respectively. Therefore, the frequency-domain symbol on the k-th SC after the polynomial model, CFO effect and FFT blocks, can

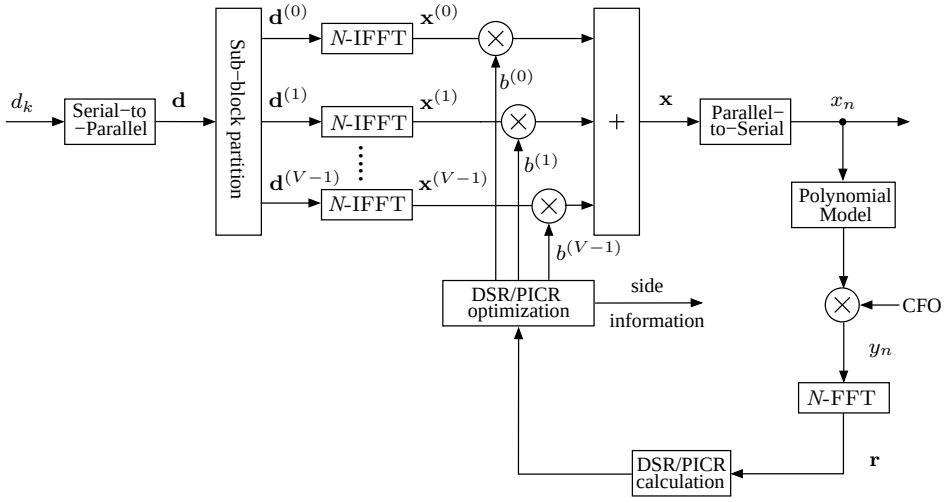

Figure 6.5: Block diagram of the proposed PTS scheme based on distortion sensing.

be expressed as

$$\begin{aligned} r_k^{(u)} =& d_k a_k^{(u)} \left[\frac{\alpha_1}{N} \sum_{n=0}^{N-1} \mathrm{e}^{j2\pi\varepsilon n/N} + \frac{\alpha_3}{N} \sum_{n=0}^{N-1} |x_n|^2 \mathrm{e}^{j2\pi\varepsilon n/N} \right] \\ &+ \frac{\alpha_1}{N} a_k^{(u)} \sum_{\substack{l=0 \\ l\neq k}}^{N-1} d_l \sum_{n=0}^{N-1} \mathrm{e}^{j2\pi(\varepsilon+l-k)n/N} \\ &+ \frac{\alpha_3}{N} a_k^{(u)} \sum_{\substack{l=0 \\ l\neq k}}^{N-1} d_l \sum_{n=0}^{N-1} |x_n|^2 \mathrm{e}^{j2\pi(\varepsilon+l-k)n/N}. \end{aligned} \tag{6.18}$$

A similar form for $r_k^{(u)}$ is presented in (5.20), where the complex phase shift β is identical to (6.14) and the term $\psi_{k,SLM}^{(u)}$ is given by

$$\psi_{k,SLM}^{(u)} = \frac{\alpha_1}{N} a_k^{(u)} \sum_{\substack{l=0 \\ l\neq k}}^{N-1} d_l \sum_{n=0}^{N-1} \mathrm{e}^{j2\pi(\varepsilon+l-k)n/N} + \frac{\alpha_3}{N} a_k^{(u)} \sum_{\substack{l=0 \\ l\neq k}}^{N-1} d_l \sum_{n=0}^{N-1} |x_n|^2 \mathrm{e}^{j2\pi(\varepsilon+l-k)n/N}. \tag{6.19}$$

Finally, the branch with the minimum $\overline{\mathrm{DSR}}_{SLM}$ obtained in (5.22) is selected for transmission.

6.4 Accurate BER Calculation

The authors in [16] derived analytical formulae for the complex phase shift and nonlinear noise term for OFDM signals passed through nonlinear polynomial models distortion. Consequently, using these formulae, an accurate theoretical form of ESNR and therefore probability of error was calculated theoretically. For a com-

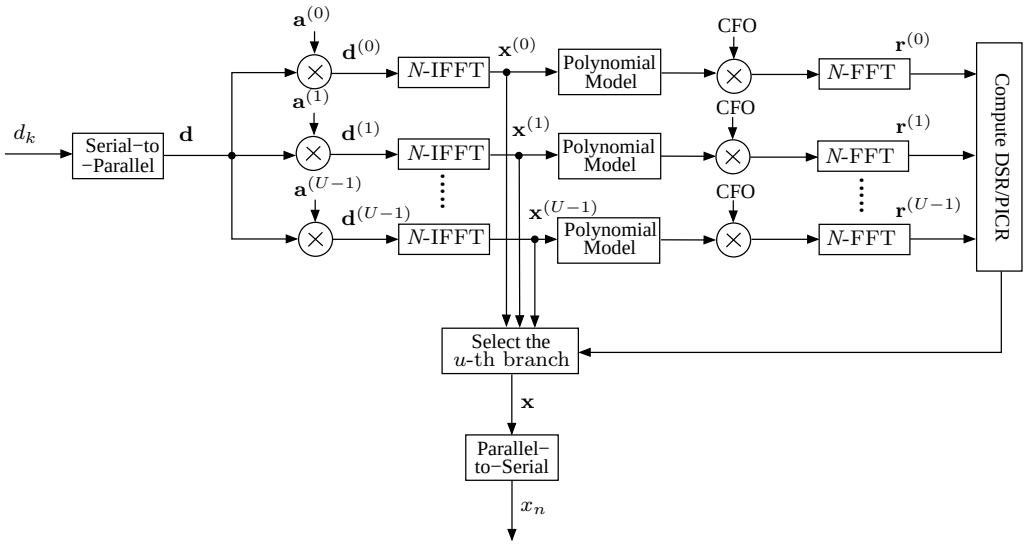

Figure 6.6: Block diagram of the proposed SLM scheme based on distortion sensing.

parison between the theoretical and simulated results, an accepted accuracy of the analysis was introduced. In addition, an accurate estimation of the output SNR for OFDM systems affected by the CFOs was derived in [110]. To avoid performing enormous simulations, an accurate BER formula for the OFDM signals perturbed by the amplifier nonlinearity and CFO is derived in this section.

By adding the AWGN to (5.4), r_k can be re-written as

$$r_k = \beta d_k + \psi_k + \omega_k. \tag{6.20}$$

The effective SNR (ESNR) of r_k for each SC can be computed as [16]

$$\text{ESNR} = \frac{P|\beta|^2}{\sigma_\eta^2 + \sigma_{ICI}^2}, \tag{6.21}$$

where the variance of the ICI is denoted as σ_{ICI}^2. From (6.13), the variance of the useful signal can be estimated as

$$E\{|\beta d_k|^2\} = P\left|\alpha_1 + \frac{\alpha_3}{\text{IBO}_l}\right|^2 \left[\frac{\sin(\pi\varepsilon)}{\pi\varepsilon}\right]^2, \tag{6.22}$$

where $N \sin\left(\frac{\pi\varepsilon}{N}\right) \simeq \pi\varepsilon$ for large values of N. The data symbols are random variables, d_k for $k = 0, \cdots, N-1$, are uncorrelated and have zero mean, $E\{d_k\} = 0$, and variance P, $E\{|d_k|^2\} = P$. As seen from (6.15) the interference component consists

of two terms. The ICI of the first term can be simplified as

$$\psi_k = \alpha_1 \sum_{\substack{l=0 \\ l\neq k}}^{N-1} d_l \frac{\sin(\pi(\varepsilon+l-k))}{N\sin\left(\frac{\pi(\varepsilon+l-k)}{N}\right)} \mathrm{e}^{j\pi(\varepsilon+l-k)(1-1/N)}, \tag{6.23}$$

therefore, the variance of ICI for the first term can be calculated as

$$E\{|\psi_k|^2\} = |\alpha_1|^2 \sum_{\substack{l=0 \\ l\neq k}}^{N-1} |d_l|^2 \left[\frac{\sin(\pi(\varepsilon+l-k))}{N\sin\left(\frac{\pi(\varepsilon+l-k)}{N}\right)}\right]^2. \tag{6.24}$$

The ICI for the first term can be evaluated in general by using a single case where $k = 0$ in (6.24), which produces

$$\sigma^2_{ICI_1} = E\{|\psi_0|^2\} = |\alpha_1|^2 P \sum_{l=1}^{N-1} \left[\frac{\sin(\pi(\varepsilon+l))}{\pi(\varepsilon+l)}\right]^2. \tag{6.25}$$

The variance of ICI for the second term, $\sigma^2_{ICI_2}$, can be derived by focusing on d_0, therefore, ψ_0 can be expressed as

$$\psi_0 = \frac{\alpha_3}{N} \sum_{l=1}^{N-1} d_l \sum_{n=0}^{N-1} |x_n|^2 \mathrm{e}^{j2\pi(\varepsilon+l)n/N}. \tag{6.26}$$

After some mathematical manipulations similar to those presented in [111] and which are shown in Appendix B, the variance of the ICI for the second term can be expressed as

$$\sigma^2_{ICI_2} = E\{|\psi_0|^2\} = \frac{|\alpha_3|^2 P}{\mathrm{IBO}_l^2}\left(\frac{3N^2-5N+2}{N^2}\right). \tag{6.27}$$

It can be noted from (6.27) that $\sigma^2_{ICI_2}$ is dependent only on the amplifiers' parameters and the number of SCs.

Finally, the ESNR for each SC can be calculated by substituting (6.22), (6.25) and (6.27) into (6.21)

$$\mathrm{ESNR} = \frac{\mathrm{SNR}\left|\alpha_1 + \frac{\alpha_3}{\mathrm{IBO}_l}\right|^2 \left[\frac{\sin(\pi\varepsilon)}{\pi\varepsilon}\right]^2}{\mathrm{SNR}\left[|\alpha_1|^2 \sum_{l=1}^{N-1}\left[\frac{\sin(\pi(\varepsilon+l))}{\pi(\varepsilon+l)}\right]^2 + \frac{|\alpha_3|^2}{\mathrm{IBO}_l^2}\left(\frac{3N^2-5N+2}{N^2}\right)\right] + 1}, \tag{6.28}$$

where $\mathrm{SNR} = P/\sigma^2_\eta$. At the output of demodulator, the BER for each SC for

M-QAM system can be estimated as [112]

$$\text{BER} \approx \frac{2}{m}\left(\frac{\sqrt{M}-1}{\sqrt{M}}\right)\text{erfc}\left(\sqrt{\frac{3\text{ESNR}}{2(M-1)}}\right). \tag{6.29}$$

The theoretical variances of the ICI and useful signals are depicted in Figs. 6.7, 6.8, 6.9 and 6.10 respectively, for 16-QAM-OFDM systems in the presence of the TWTA and SSPA nonlinearity using $N = 128$ at SNR = 20 dB, versus IBO in dB for various values of ε and for different IBOs versus ε. The coefficients used for TWTA polynomial model are $\alpha_1 = 0.9920+j0.0340$ and $\alpha_3 = -0.9100+j0.5755$, whereas the coefficients used for the SSPA polynomial model are $\alpha_1 = 1$ and $\alpha_3 = -0.132$. It can be noted from Figs. 6.7 and 6.9 that the variance of the ICI decreases exponentially, while the variance of the useful signal increases by increasing the IBO. Furthermore, higher values of the variance of ICI are shown for lower IBOs. In addition, the σ^2_{ICI} in the TWTA case is higher than in the SSPA case for different ε values, i.e. the BER degrades drastically. In contrast, different patterns are shown when increasing the CFO with constant IBO. It is clear from Figs. 6.8 and 6.10 that to minimise ESNR, the IBO should be increased while ε is decreased.

The simulation of BER is completed by transmitting the OFDM signals passing through the nonlinear amplifier 3^{rd} order polynomial model and adding the effects of the CFO and AWGN channel. The complex phase shift compensation at the receiver via channel estimation before detection of the OFDM data symbol is achieved by using (6.14). In contrast, the theoretical BER is evaluated using (6.29). Figs. 6.11 and 6.12 depict the BER in the presence of the amplifier nonlinearity, CFO and AWGN channel, for various values of OBO and CFO, respectively. An accepted agreement of the BER is achieved when the simulation is compared with the theoretical estimation, especially for various values of OBOs.

6.5 Computational Complexity

The computational complexity of the proposed PTS and SLM schemes based on distortion sensing is calculated in an analogous manner to that in chapter 5. The CFO effect can be added to the HPA output which requires N CMs. Therefore, $\mathcal{I}N$ and UN CMs are added for the proposed PTS and SLM schemes shown in Figs. 6.5 and 6.6, respectively. Consequently, the equations shown in Table 5.1 for

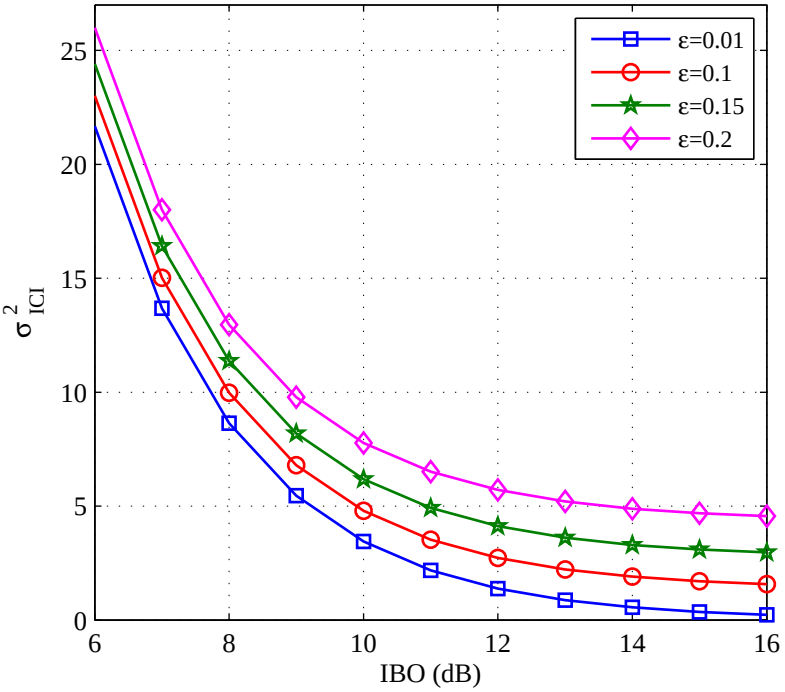

(a) Various ε

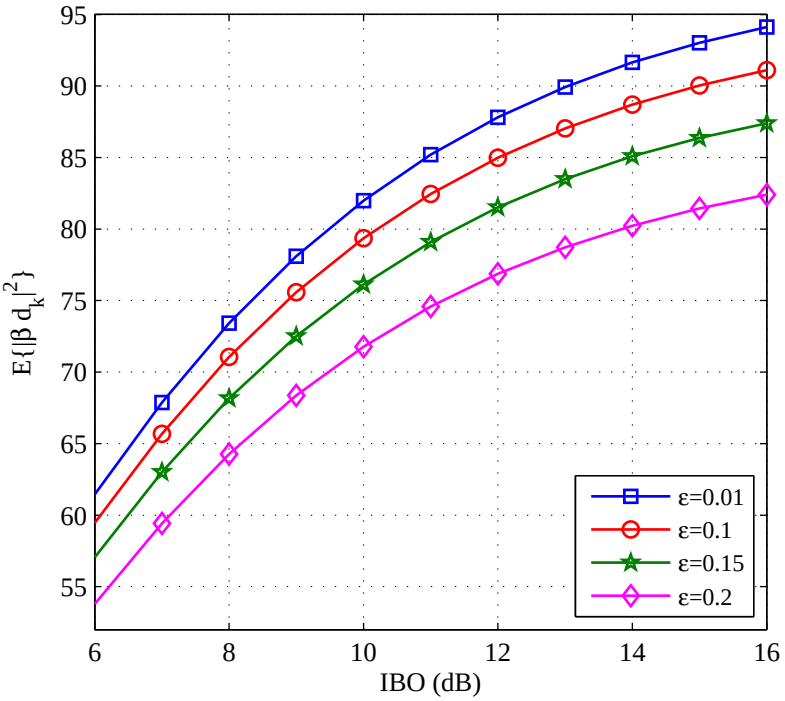

(b) Various ε

Figure 6.7: Theoretical variance versus IBO for 16-QAM-OFDM systems in the presence of the TWTA nonlinearity using $N = 128$ at SNR = 20 dB.

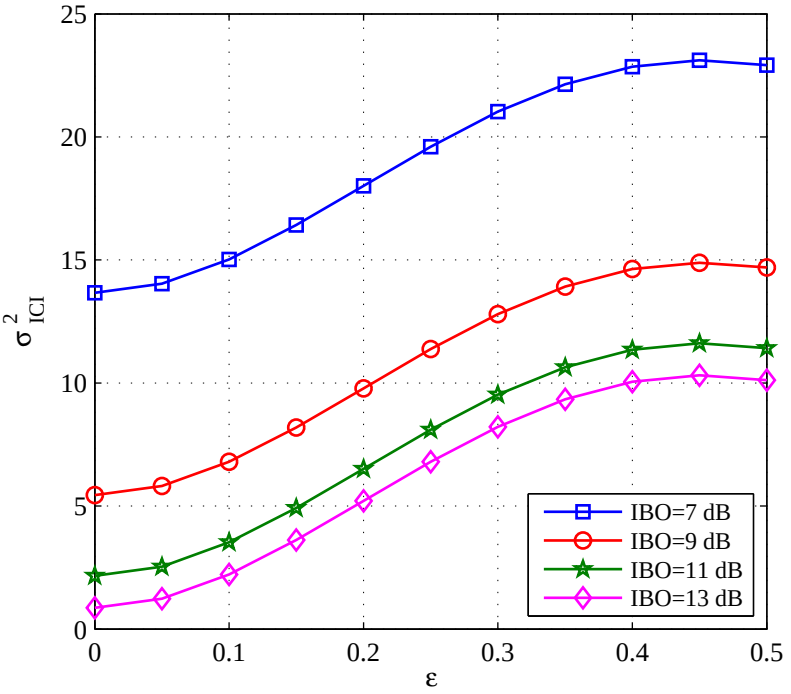

(a) Various IBO

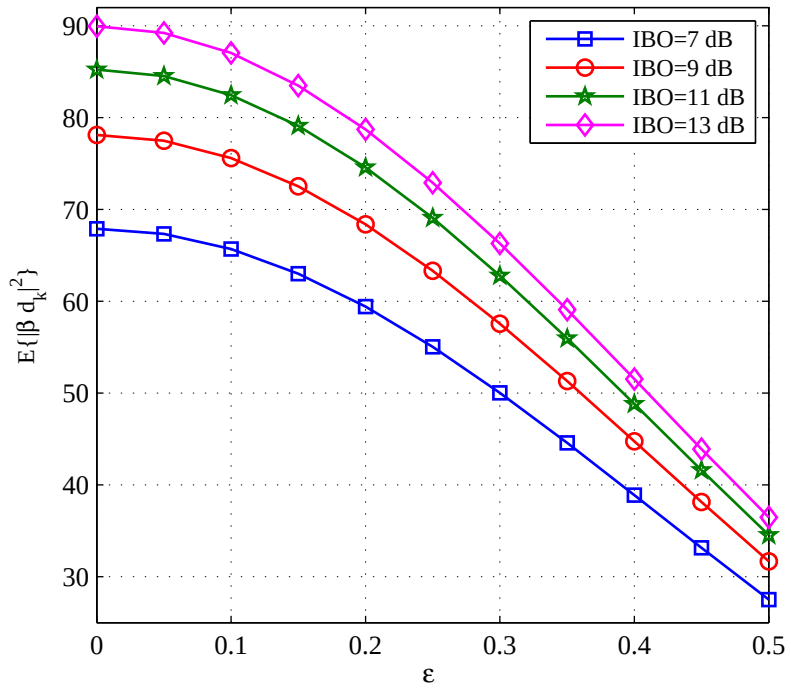

(b) Various IBO

Figure 6.8: Theoretical variance versus ε for 16-QAM-OFDM systems in the presence of the TWTA nonlinearity using $N = 128$ at SNR = 20 dB.

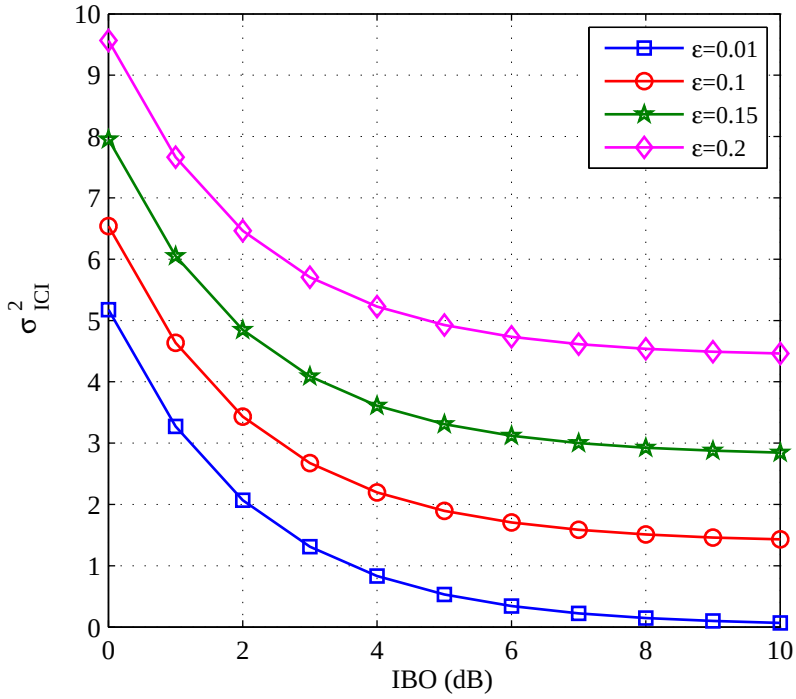

(a) Various ε

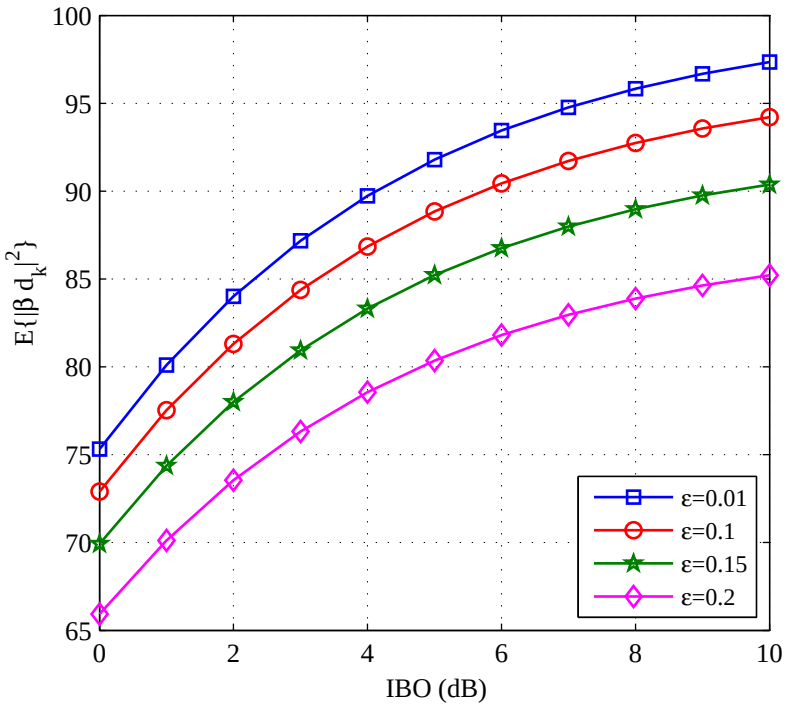

(b) Various ε

Figure 6.9: Theoretical variance versus IBO for 16-QAM-OFDM systems in the presence of the SSPA nonlinearity using $N = 128$ at SNR $= 20$ dB.

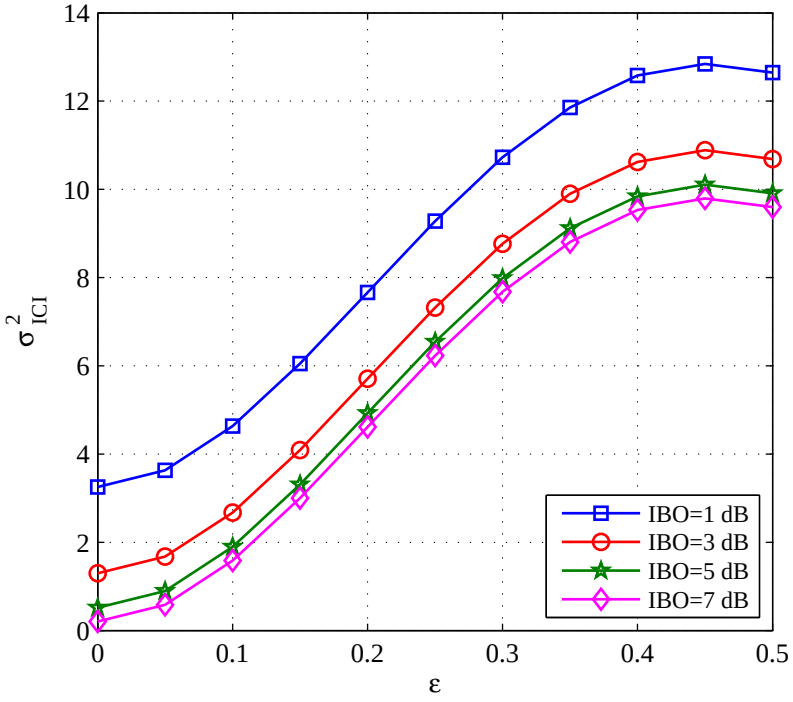

(a) Various IBO

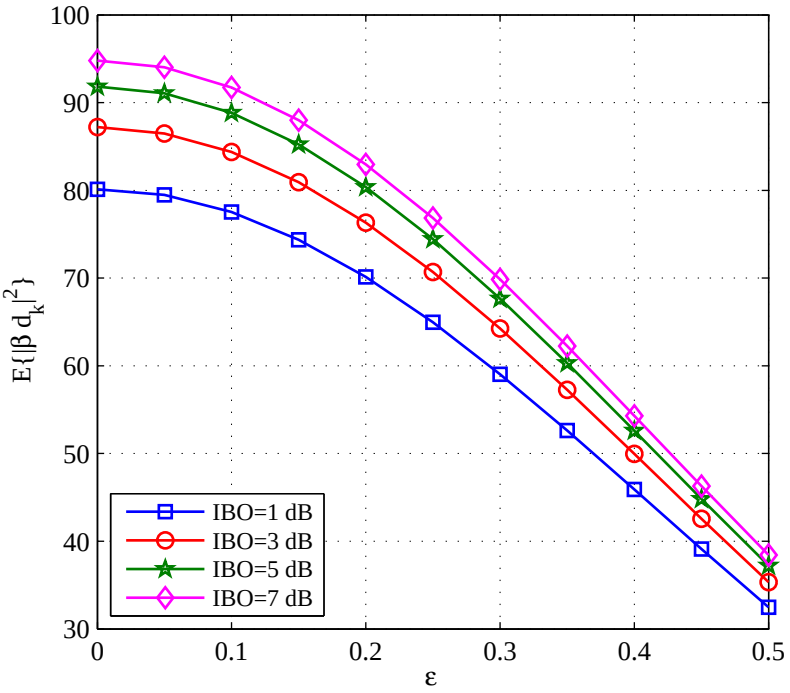

(b) Various IBO

Figure 6.10: Theoretical variance versus ε for 16-QAM-OFDM systems in the presence of the SSPA nonlinearity using $N = 128$ at SNR $= 20$ dB.

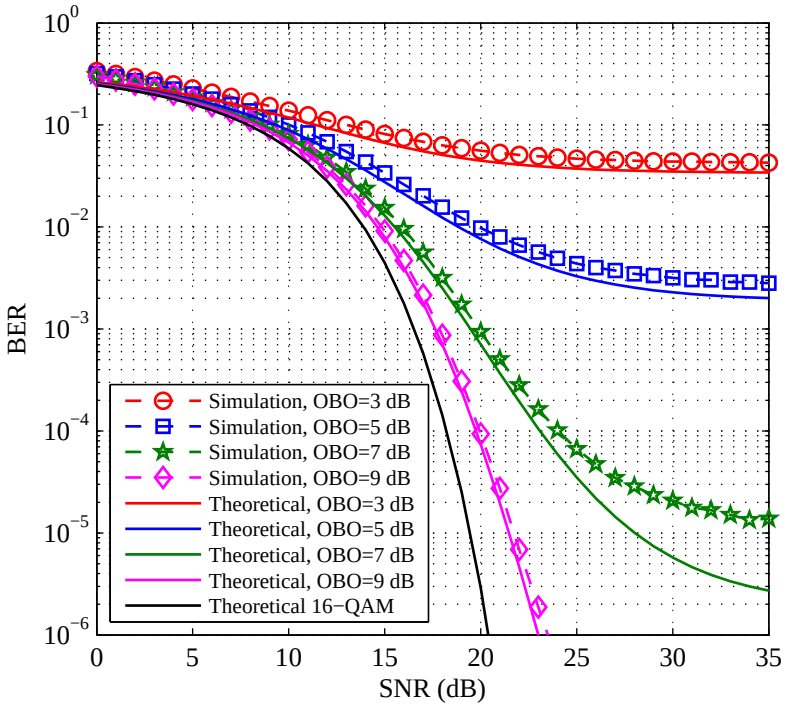

(a) TWTA case

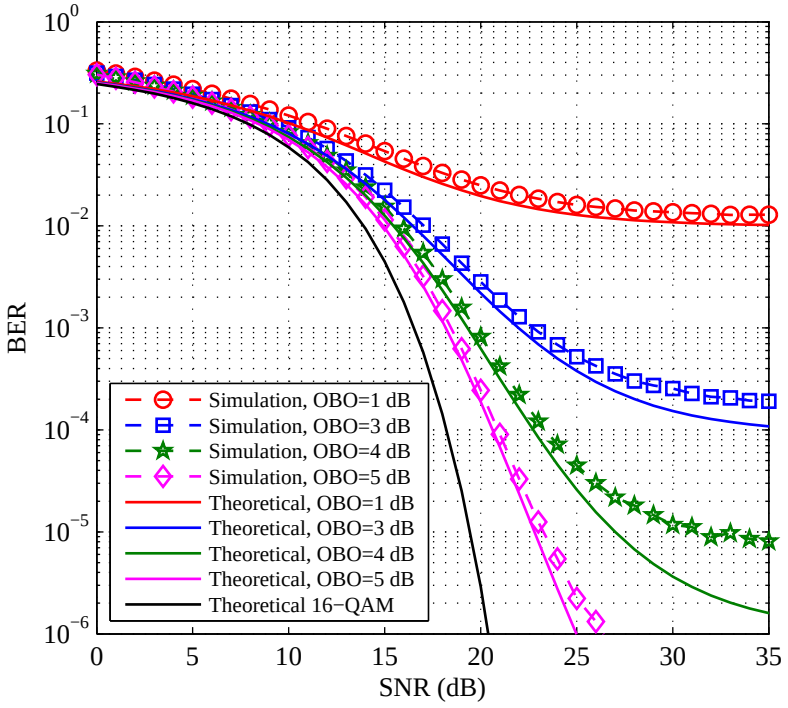

(b) SSPA case

Figure 6.11: Theoretical and simulation BER versus SNR for 16-QAM-OFDM systems in the presence of the amplifier nonlinearity using various values of OBOs and a CFO with $\varepsilon = 0$.

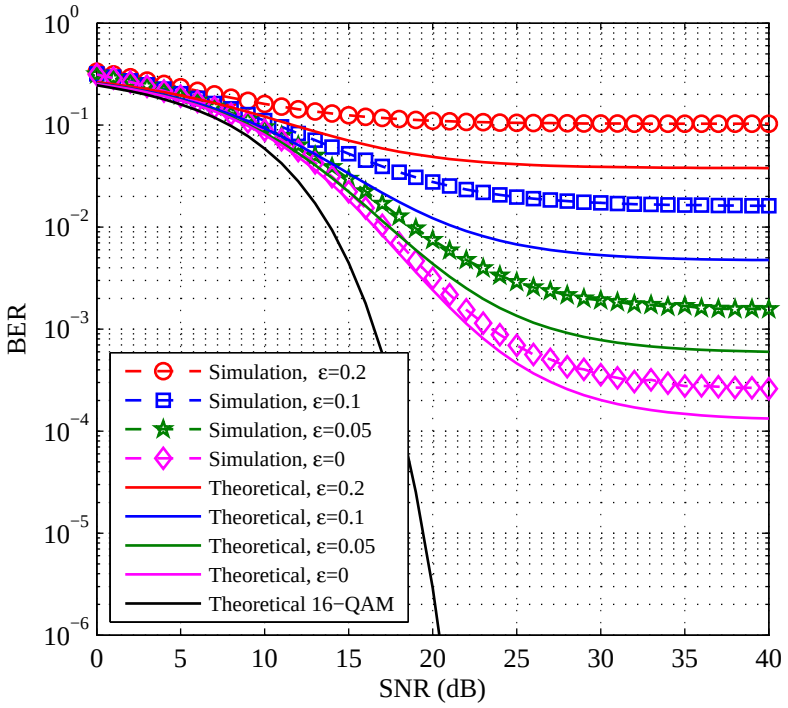

(a) TWTA with OBO = 6 dB

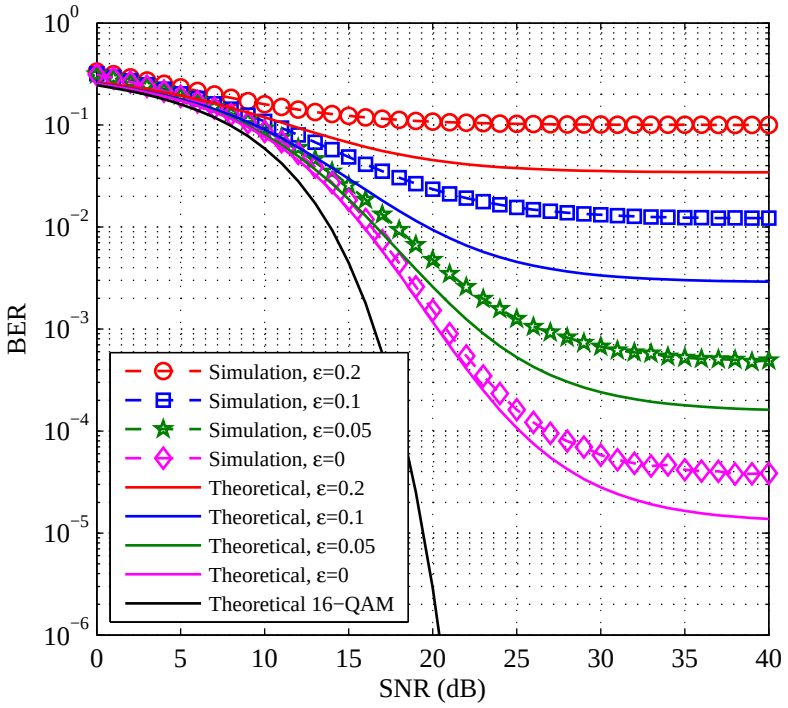

(b) SSPA with OBO = 3.5 dB

Figure 6.12: Theoretical and simulation BER versus SNR for 16-QAM-OFDM systems in the presence of the amplifier nonlinearity using various values of ε.

$A_{PTS-DSR}$, $M_{PTS-DSR}$, $A_{SLM-DSR}$ and $M_{SLM-DSR}$ can be modified. For example, given that $N = 128$, $V = U = 4$, $g = 4$, $f_a = 65\%$, $f_m = 75\%$ and $\mathcal{J} = V + 1$, the relative complexity using either the TWTA or the SSPA model will be increased by approximately 4% for both PTS-PAPR and SLM-PAPR techniques compared to the OFDM systems that are not affected by the CFO.

The C_r versus the number of SCs N for the PTS and SLM techniques based on the PAPR, IMD and PICR criteria using $V = U = 4$ is given in Fig. 6.13. The curves shown in the figure demonstrate that C_r is almost independent of N, particularly for $N \geq 256$ for both TWTA and SSPA cases. The C_r for the PAPR drops significantly to $\sim 73\%$ and 63.5% for the SLM and PTS, respectively using the TWTA, with $C_r \sim 67\%$ and 58.5% for the SLM and PTS respectively, using the SSPA. It is clear from this figure that the major reduction was recorded in the IMD case, and in contrast, the PICR has a slightly higher complexity than the DSR.

The relative complexity as a function of V and U for $N = 128$ SCs is presented in Fig. 6.14. Similar to the results in Fig. 6.13, it is apparent that C_r is almost independent of the values of V/U except for the PTS-PAPR and PTS-IMD, where C_r decreases substantially to less than 30% by increasing V/U to 64 for both the TWTA and SSPA cases. Consequently, using the DSR with the PTS at high V/U values becomes more attractive as the complexity reduction is more than 70%.

6.6 Numerical Results

Monte Carlo simulations are used to assess the performance of the proposed system and other conventional PAPR reduction techniques. The simulation results are obtained using 10^5 OFDM blocks generated using $N = 128$. Different Gray coded symbol constellations are used. Various partitions, $\{V, U\} = 4$ or 16, for the PTS and SLM techniques are also used. The number of possible phase factors are selected uniformly from $b^{(v)} = \pm 1$ and $a_i^{(u)} \in \{\pm 1, \pm j\}$, $i \in \{0, 1, \cdots, N-1\}$ for the IPTS and CSLM, respectively .

Two models of the TWTA and SSPA are used: polynomial and memoryless. The polynomial model is used for the distortion metrics calculation, while the memoryless is used for the implementation of the OFDM signal transmission. The coefficients used for the TWTA polynomial model are $\alpha_1 = 0.9920 + j0.0340$ and $\alpha_3 = -0.9100 + j0.5755$, whereas the coefficients used for the SSPA polynomial

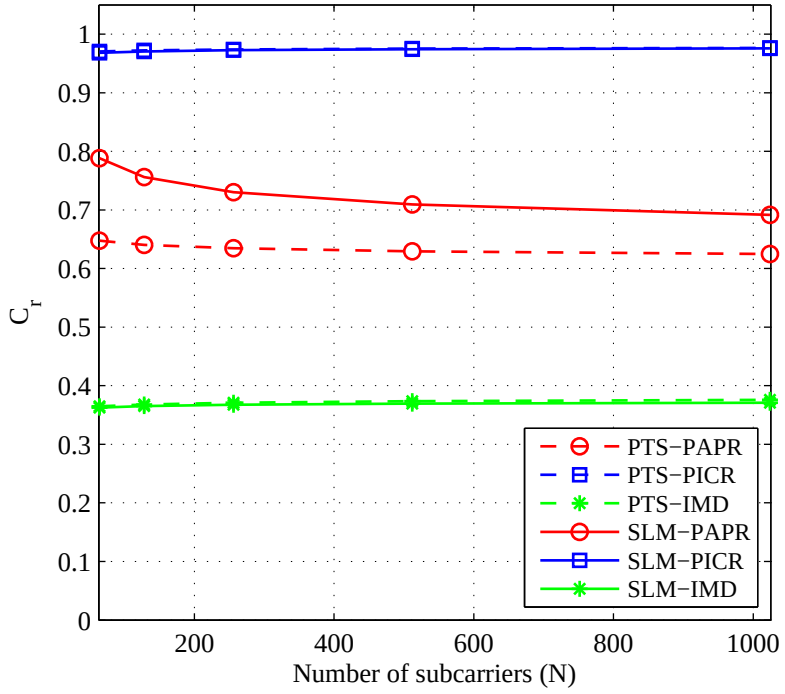

(a) TWTA case

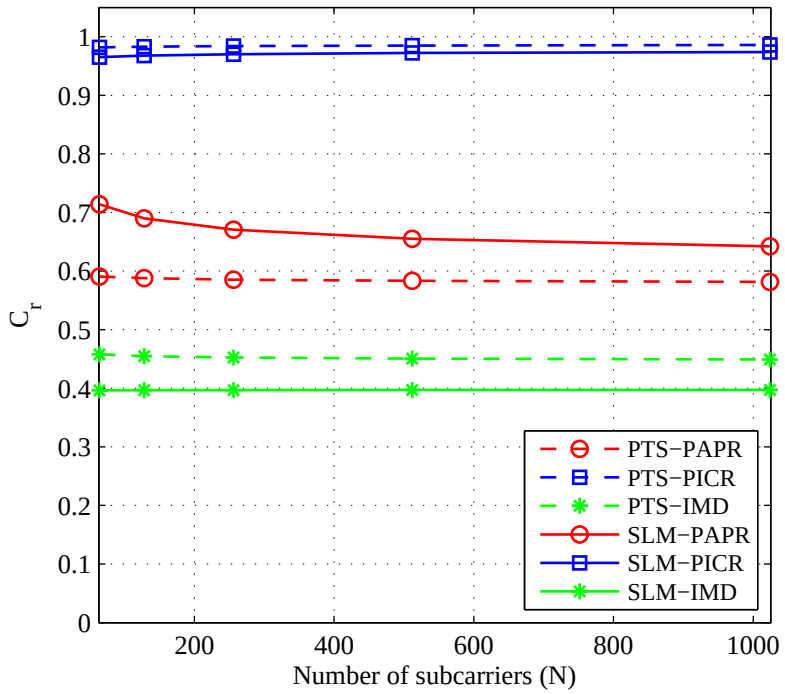

(b) SSPA case

Figure 6.13: Relative complexity for the PTS and SLM techniques based on the PAPR, IMD and PICR criteria for different N.

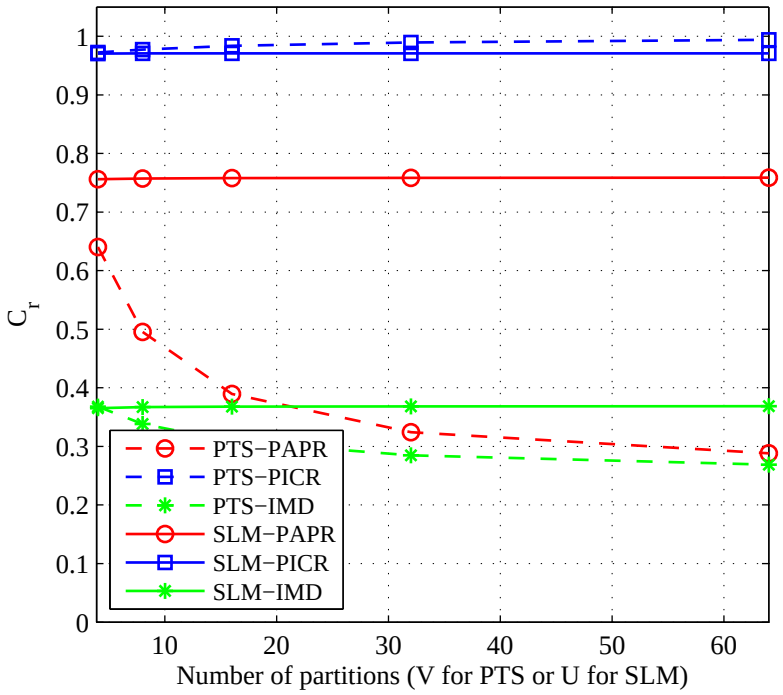

(a) TWTA case

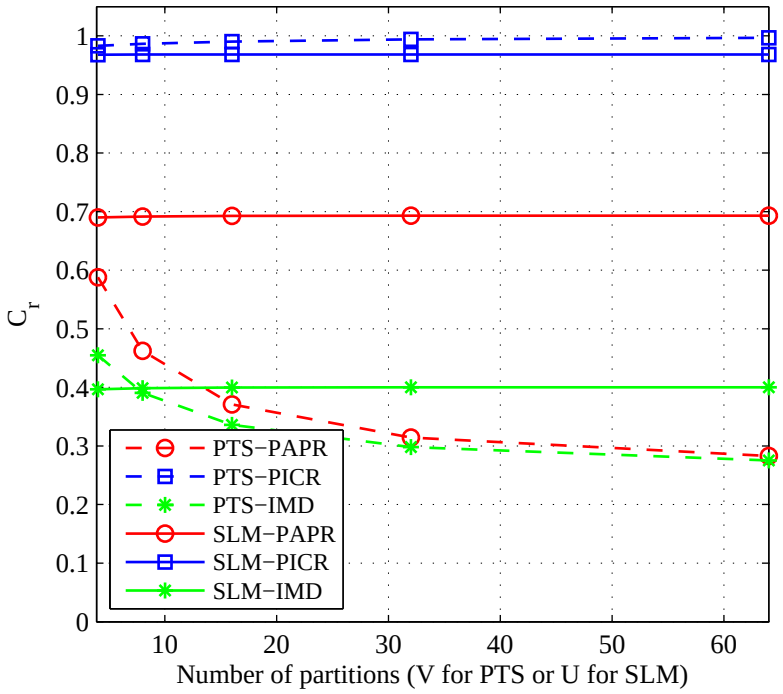

(b) SSPA case

Figure 6.14: Relative complexity for the PTS and SLM techniques based on the PAPR, IMD and PICR criteria for different V/U.

model are $\alpha_1 = 1$ and $\alpha_3 = -0.132$. The CFO and AWGN channel effects are added to the nonlinearity of the HPA. Perfect knowledge of the phase coefficients for the PTS and SLM techniques at the receiver side is assumed for coherent demodulation. It is worth noting that the demodulation process is performed based on the assumption of perfect symbol timing, carrier frequency and phase synchronisation.

6.6.1 CCDF performance of the DSR

The CCDF of the DSR for the 16-QAM-OFDM system using the PTS and SLM schemes, based on various reduction criteria in the presence of the TWTA nonlinearity with OBO = 5 and CFO with $\varepsilon_{wc} = 0.02$ and $|\varepsilon| = 0.01$, is depicted in Fig. 6.15. The distortion metrics can be estimated at the transmitter side on the basis of (ε_{wc}) values of the CFO. It is worth mentioning that the PTS-PICR and PTS-IMD have marginally lower DSR than the PTS-PAPR; on the other hand, the PTS-DSR has the lowest ICI for different number of partitions. The proposed PTS-DSR provided an improvement of approximately 0.8 and 1.3 dB at CCDF of 10^{-4} for $V = 4$ and $V = 16$, respectively, compared to the PTS-PAPR technique as shown in Fig. 6.15(a). A similar CCDF pattern is shown in Fig. 6.15(b) for an OFDM system using the SLM scheme. It is clear that the SLM-DSR can achieve approximately 0.8 and 1.1 dB reduction in CCDF, respectively, compared to the SLM-PAPR for $U = 4$ and $U = 16$.

Fig. 6.16 depicts the CCDF of the DSR for the OFDM system using the PTS and SLM schemes for different partitions based on the DSR, PICR, IMD and PAPR reduction criteria utilising the SSPA model with OBO = 3 and CFO with $\varepsilon_{wc} = 0.02$ and $|\varepsilon| = 0.01$. The proposed DSR criterion can achieve an improvement of approximately 0.8 and 1.5 dB for $V = 4$ and $V = 16$, respectively, compared to the PTS-PAPR technique as shown in Fig. 6.16(a). Furthermore, a similar CCDF trend is shown in Fig. 6.16(b) using the SLM scheme. Compared to the SLM-PAPR for $U = 4$ and $U = 16$, the SLM-DSR can improve the CCDF performance by 0.9 and 1.4 dB, respectively.

6.6.2 BER performance

The BER performance is assessed in this chapter over AWGN, wideband satellite and frequency-selective multipath fading channels.

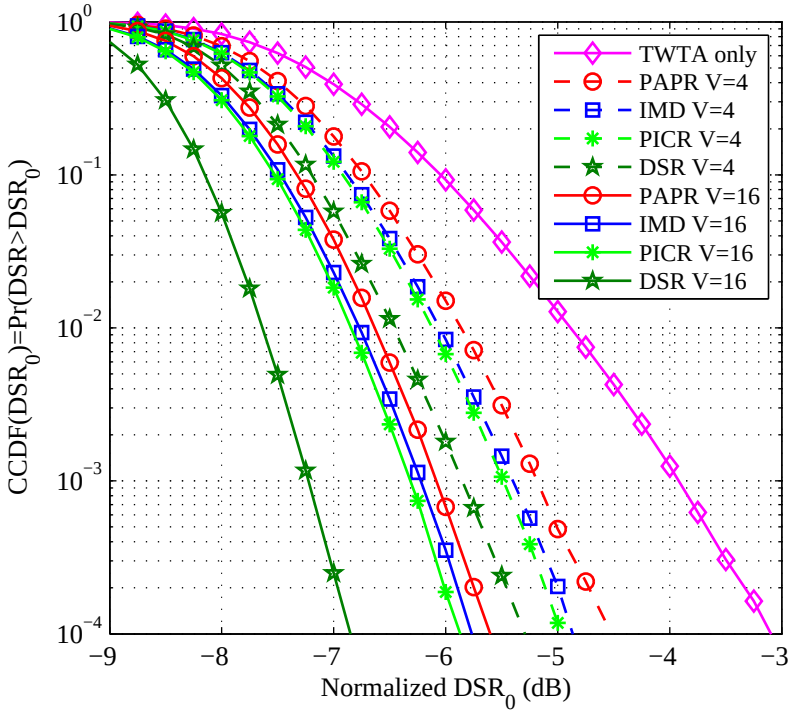

(a) PTS-based scheme

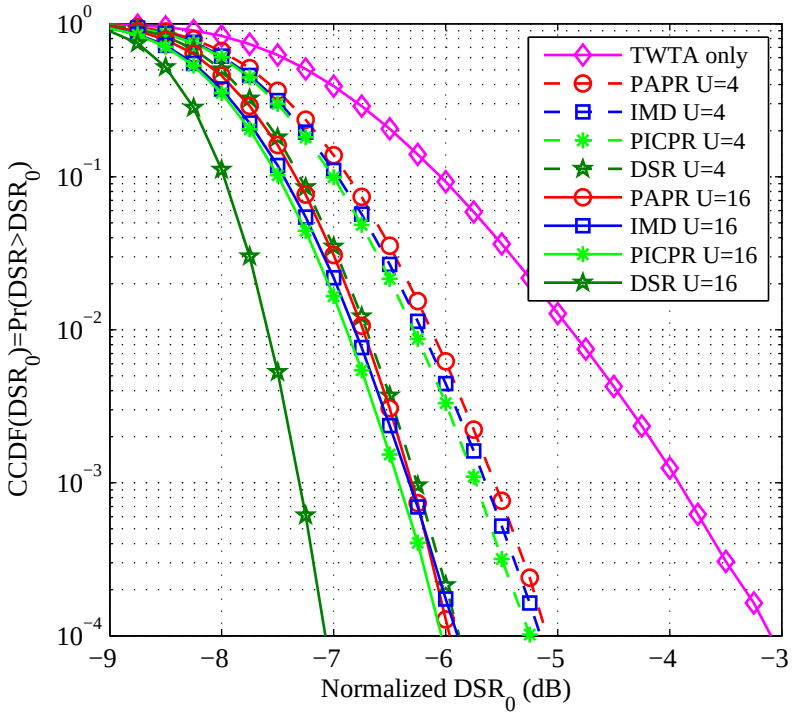

(b) SLM-based scheme

Figure 6.15: CCDF of the DSR for OFDM systems based on the DSR, PICR, IMD and PAPR reduction criteria for 4 and 16 partitions in the presence of the TWTA nonlinearity and CFO.

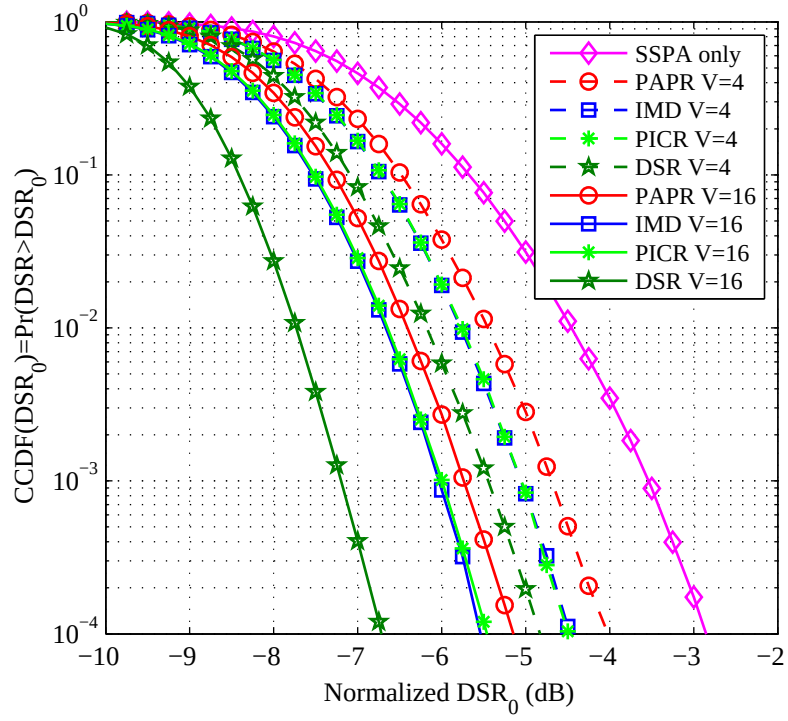

(a) PTS-based scheme

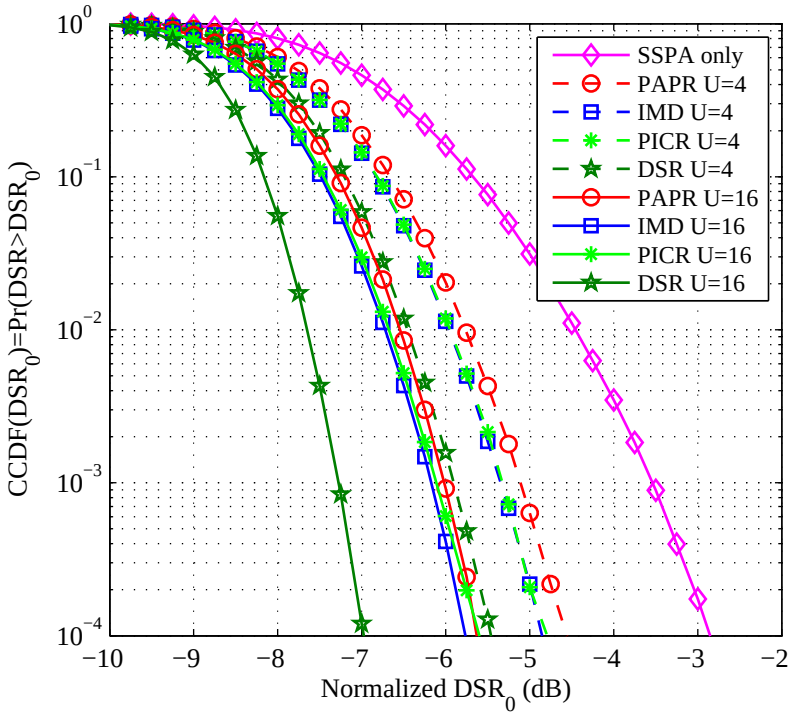

(b) SLM-based scheme

Figure 6.16: CCDF of the DSR for OFDM systems based on the DSR, PICR, IMD and PAPR reduction criteria for 4 and 16 partitions in the presence of the SSPA nonlinearity and CFO.

6.6.2.1 BER performance over an AWGN channel

Fig. 6.17 presents the BER performance of the DSR, PICR, IMD and PAPR reduction criteria in the presence of the TWTA nonlinearity with OBO = 5 and CFO with $\varepsilon_{wc} = 0.02$ and $|\varepsilon| = 0.01$ based on the PTS and SLM schemes for 16-QAM-OFDM systems. The PTS-DSR and SLM-DSR managed to reduce the required SNR approximately 5.9 and 4.7 dB, respectively, compared to the PTS-PAPR and SLM-PAPR for $V/U = 16$ at a BER of 10^{-4} as can be noted from Figs. 6.17(a) and 6.17(b). While, Fig. 6.18 depicts the BER systems based on the proposed DSR and the other considered schemes in the presence of the SSPA nonlinearity with OBO = 3, CFO with $\varepsilon_{wc} = 0.02$ and $|\varepsilon| = 0.01$ and AWGN for 16-QAM-OFDM systems. The main considerable achievement in this figure is the PTS-DSR and SLM-DSR for $V/U = 16$ can accomplish BER significant improvement approximately 10.6 and 8.3 dB, respectively, compared to the PTS-PAPR and SLM-PAPR. It is clear from Figs. 6.17 and 6.18 that the PTS-based systems can achieve superior improvement in the performance than the SLM-based systems especially for $V/U = 16$ partitions.

The BER performance of the proposed DSR and PAPR schemes is presented in Fig. 6.19 in the presence of the TWTA nonlinearity with OBO = 0 and CFO with $\varepsilon_{wc} = 0.08$ and $|\varepsilon| = 0.075$ based on the PTS and SLM schemes for QPSK-OFDM systems. As can be noted from this figure, the PTS-DSR and SLM-DSR managed to reduce the required SNR approximately 6.6 and 5.5 dB, respectively, compared to the PTS-PAPR and SLM-PAPR for $V/U = 16$. Furthermore, the DSR metric with $V/U = 4$ can achieve approximately similar performance than the PAPR with $V/U = 16$. Whereas, Fig. 6.20 depicts the BER performance for systems based on the DSR and PAPR reduction criteria in the presence of the SSPA nonlinearity with OBO = 0, CFO with $\varepsilon_{wc} = 0.15$ and $|\varepsilon| = 0.1$ and AWGN for QPSK-OFDM systems. Compared to the PTS-PAPR and SLM-PAPR for $V/U = 16$, the PTS-DSR and SLM-DSR can accomplish BER improvement approximately 4.2 and 3.1 dB, respectively. It can be noted that the QPSK-OFDM systems using the SSPA with same OBO can manage to deal with higher values of ε compared to that use the TWTA, due to the amount of ICI generated by the SSPA is less, and hence, the impairment in the BER performance is less.

The BER performance of the proposed DSR and PAPR schemes in the presence

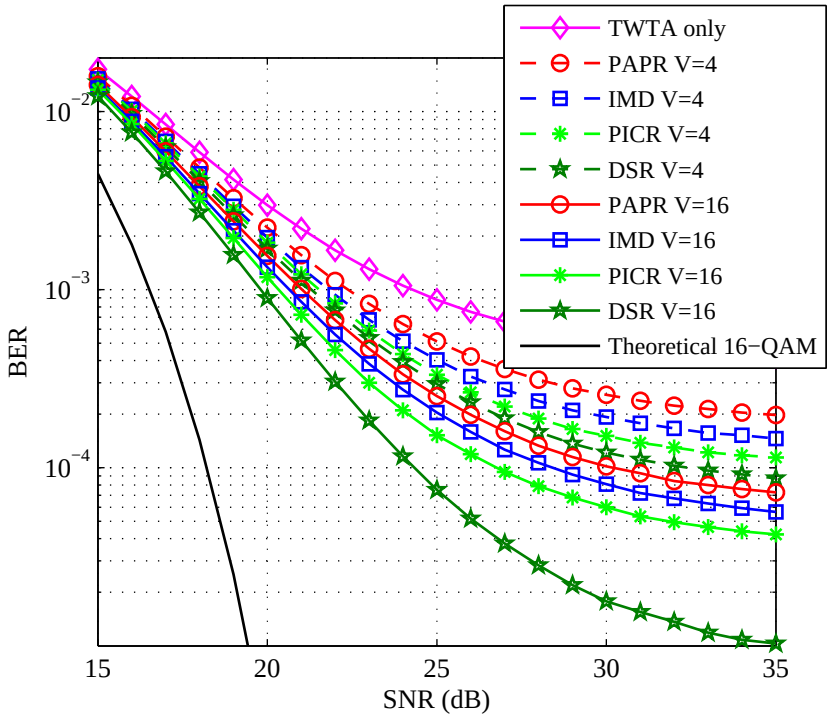

(a) PTS-based scheme

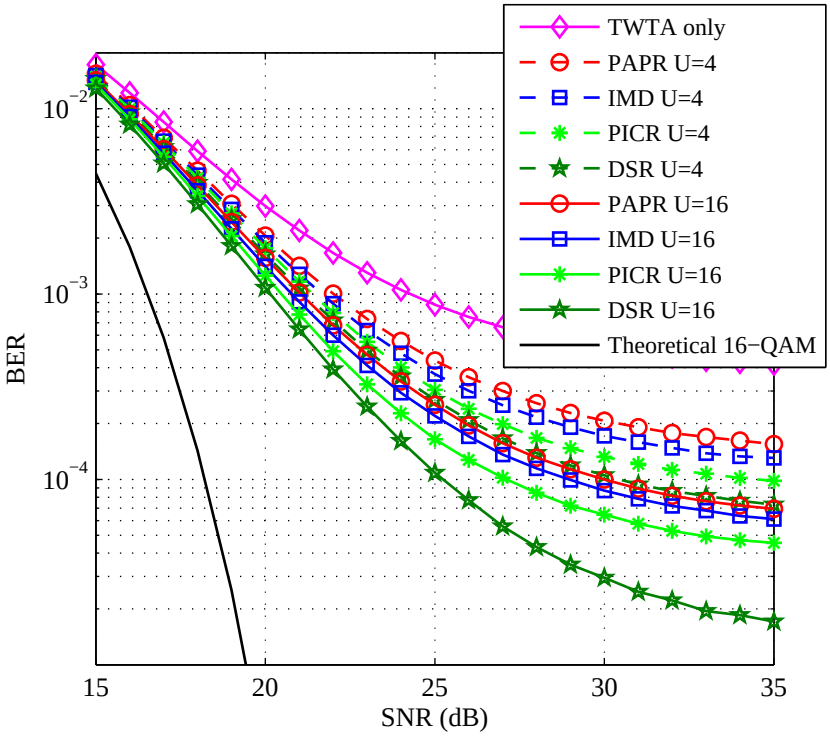

(b) SLM-based scheme

Figure 6.17: BER versus SNR for systems based on the DSR, PICR, IMD and PAPR reduction criteria in the presence of the TWTA nonlinearity, CFO and AWGN for 16-QAM constellation.

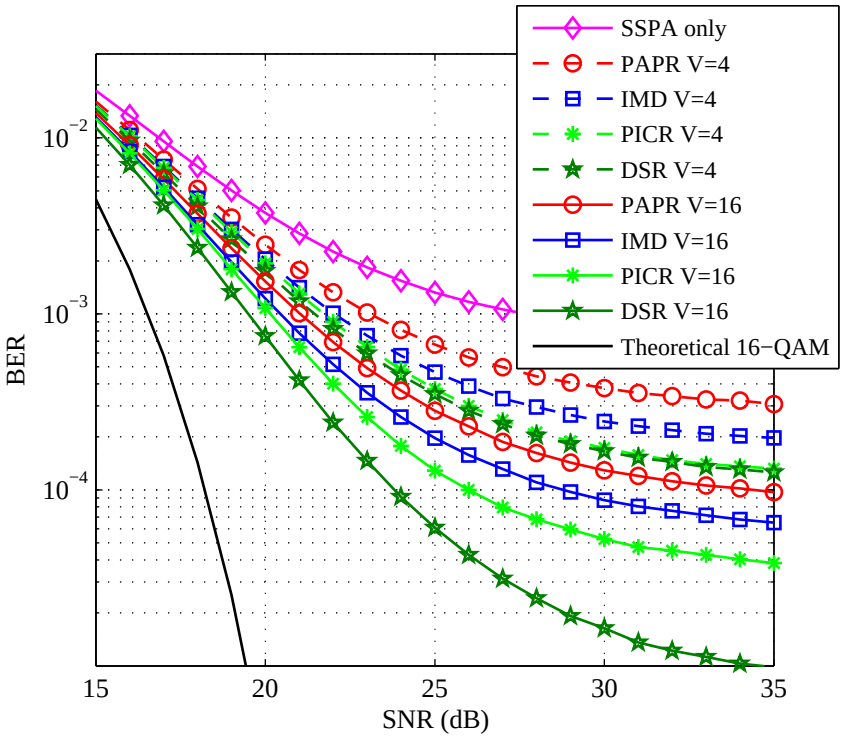

(a) PTS-based scheme

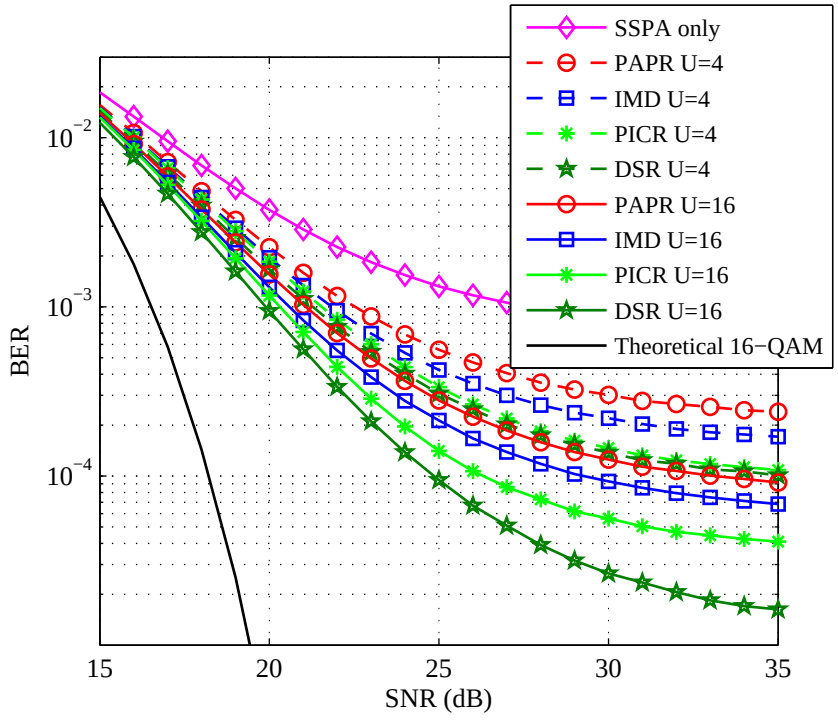

(b) SLM-based scheme

Figure 6.18: BER versus SNR for systems based on the DSR, PICR, IMD and PAPR reduction criteria in the presence of the SSPA nonlinearity, CFO and AWGN for 16-QAM constellation.

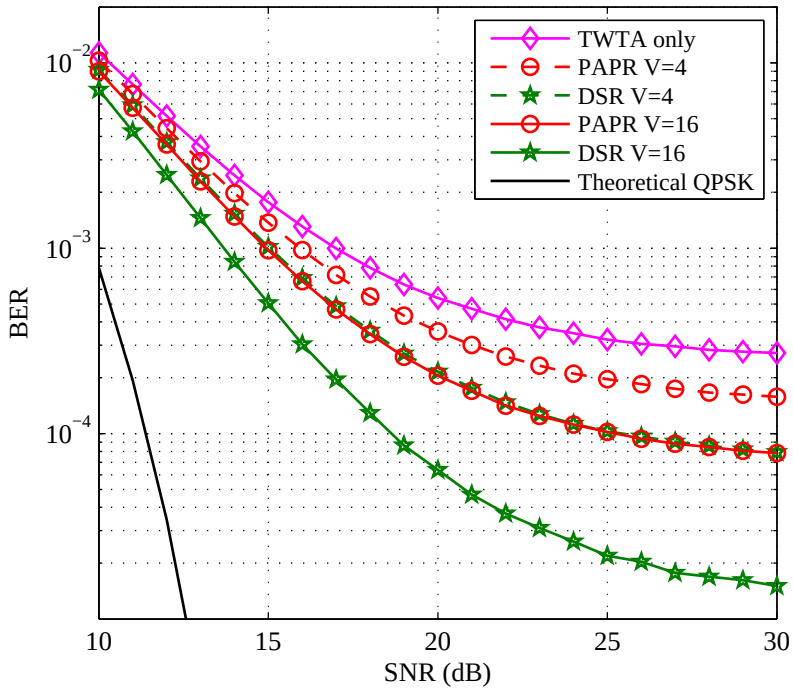

(a) PTS-based scheme

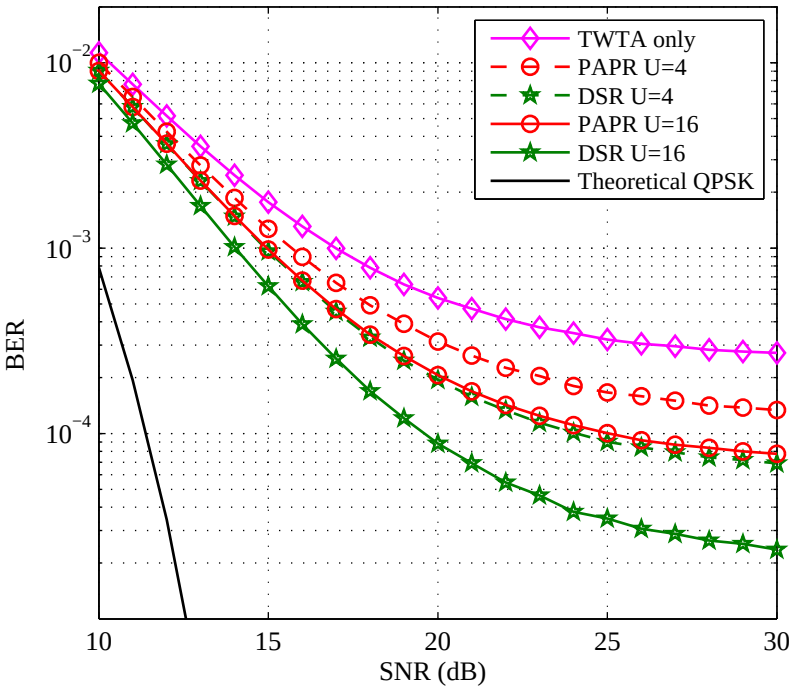

(b) SLM-based scheme

Figure 6.19: BER versus SNR for systems based on the DSR and PAPR reduction criteria in the presence of the TWTA nonlinearity, CFO and AWGN for QPSK constellation.

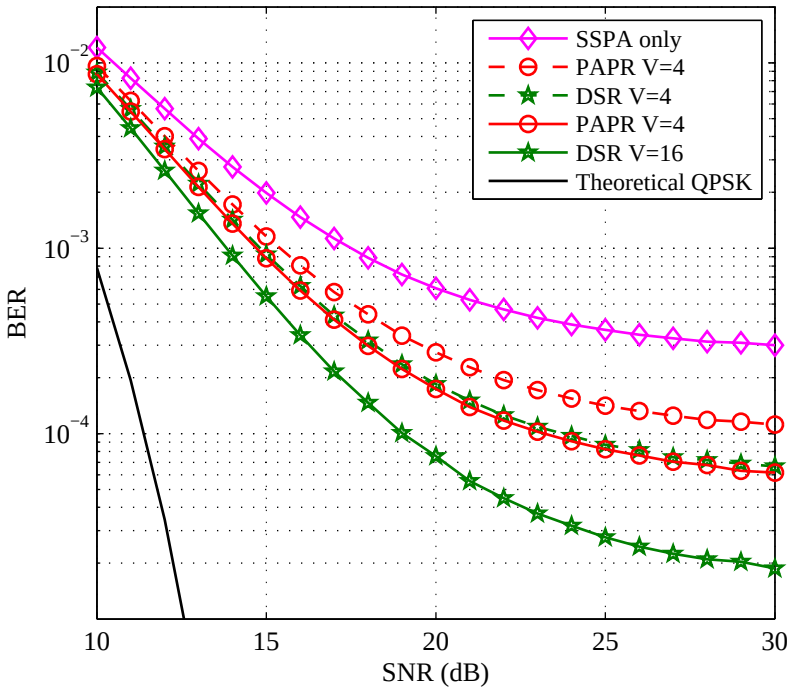

(a) PTS-based scheme

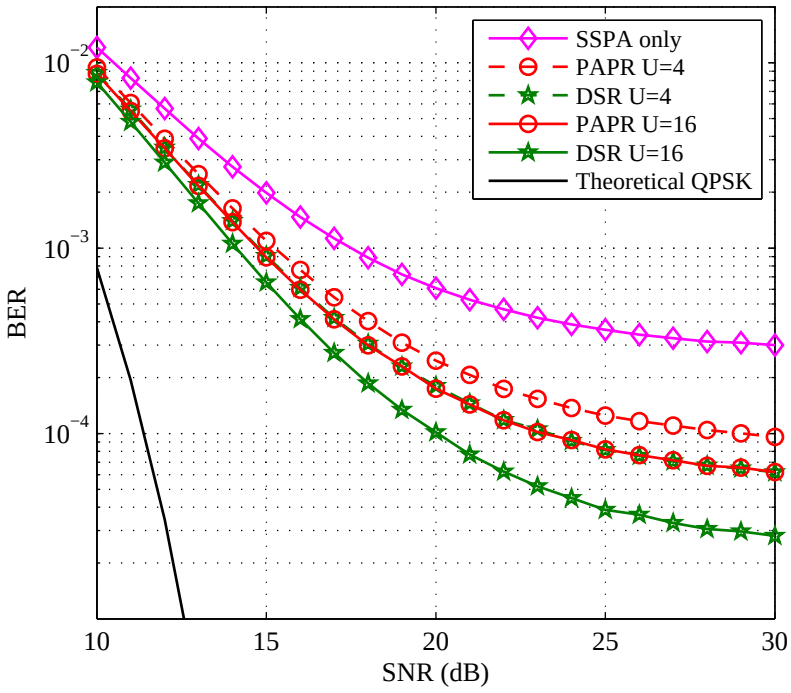

(b) SLM-based scheme

Figure 6.20: BER versus SNR for systems based on the DSR and PAPR reduction criteria in the presence of the SSPA nonlinearity, CFO and AWGN for QPSK constellation.

of the TWTA nonlinearity with OBO = 5 and CFO with $\varepsilon_{wc} = 0.02$ and $|\varepsilon| = 0.01$ based on the PTS and SLM schemes for $V/U = 16$ using HM constellation is shown in Fig. 6.21. It can be noted that the scheme PTS-DSR can achieve an improvement approximately 5.9 and 2.2 dB for EL and BL, respectively. Whereas, the proposed SLM-DSR can accomplish lower improvement of 4.7 and 1.7 dB, respectively. An accurate indication for the interference generated by the TWTA and CFO can be given using the proposed DSR metric. Fig. 6.22 depicts the BER systems based on the PTS and SLM schemes, $V/U = 16$, in the presence of the SSPA nonlinearity with OBO = 3 and CFO with $\varepsilon_{wc} = 0.02$ and $|\varepsilon| = 0.01$ for HM constellation. Compared to the PTS-PAPR and SLM-PAPR, the proposed PTS-DSR and SLM-DSR schemes can achieve an improvement approximately 3.3 and 2.7 dB, respectively, for BL.

6.6.2.2 BER performance in mobile satellite channel

The proposed system in the wideband satellite mobile channel is examined in order to observe its performance under practical channel degradations. Fig. 6.23 depicts the BER performance for a 16-QAM modulation scheme in the presence of the TWTA nonlinearity, CFO and wideband channel with elevation angle, $\theta \leq 45$. It can be noted from this figure that the PTS-DSR managed to reduce the required SNR by approximately 5.7 dB compared to the PTS-PAPR when $V = 16$, while the SLM-DSR can achieve a BER performance of approximately 1 dB below that of the PTS-DSR.

6.6.2.3 BER performance in multipath fading channel using a practical SSPA model

The BER performance for a 16-QAM modulation scheme over a frequency-selective multipath fading channel and practical SSPA model is presented in Fig. 6.24 for the PTS and SLM schemes. Similar parameters are used to those in Chapter 5 for the fading channel and the SSPA, except that $\alpha_3 = -0.1768$ for OBO = 3 dB, and CFO with $\varepsilon_{wc} = 0.02$ and $|\varepsilon| = 0.01$, are applied. As it can be observed from this figure, the performance patterns are similar; however, the DSR outperforms the other considered techniques, irrespective of the channel model.

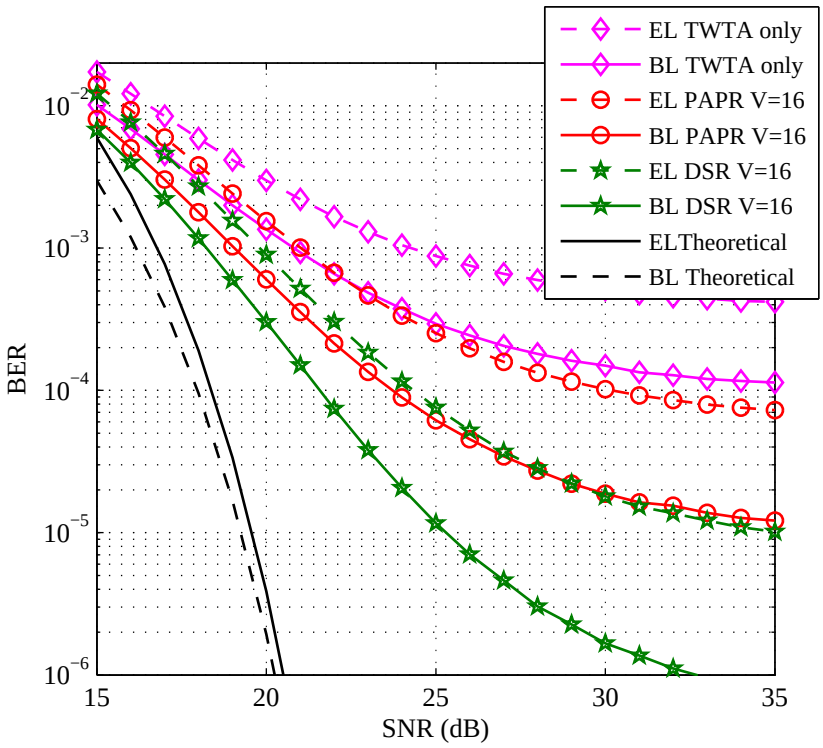

(a) PTS-based scheme

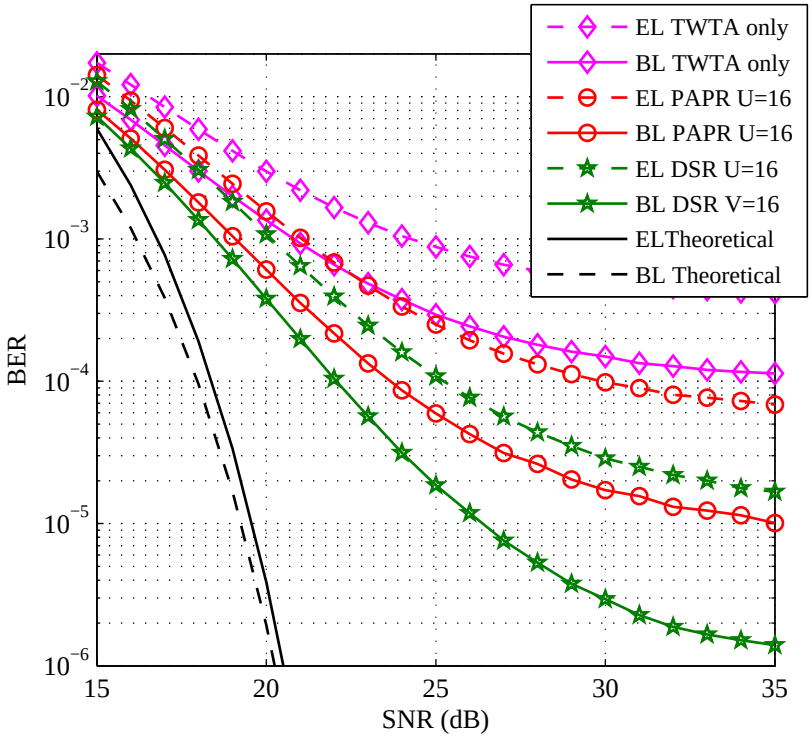

(b) SLM-based scheme

Figure 6.21: BER versus SNR for systems based on the DSR and PAPR reduction criteria in the presence of the TWTA nonlinearity, CFO and AWGN for HM constellation.

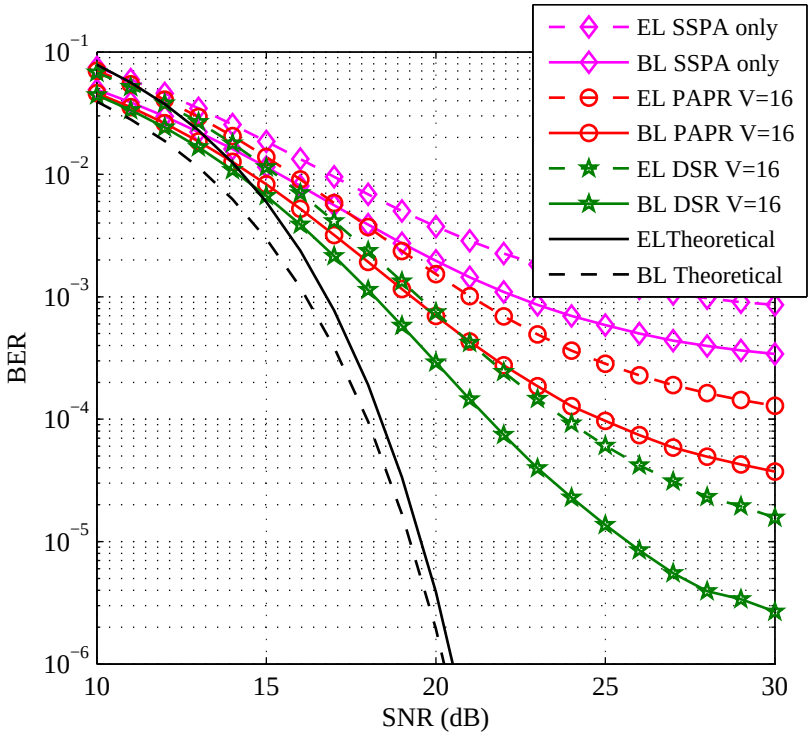

(a) PTS-based scheme

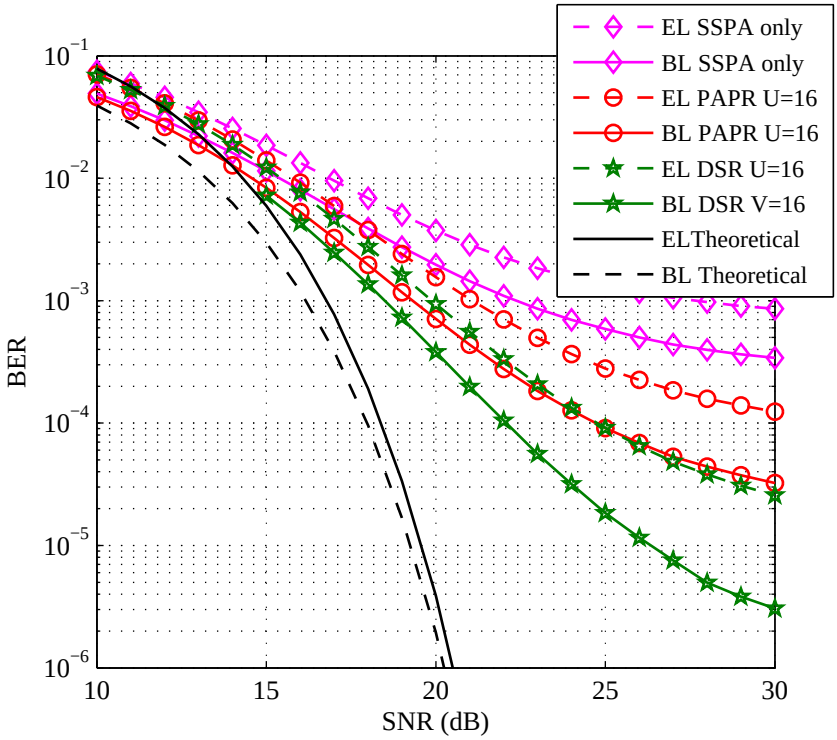

(b) SLM-based scheme

Figure 6.22: BER versus SNR for systems based on the DSR and PAPR reduction criteria in the presence of the SSPA nonlinearity, CFO and AWGN for HM constellation.

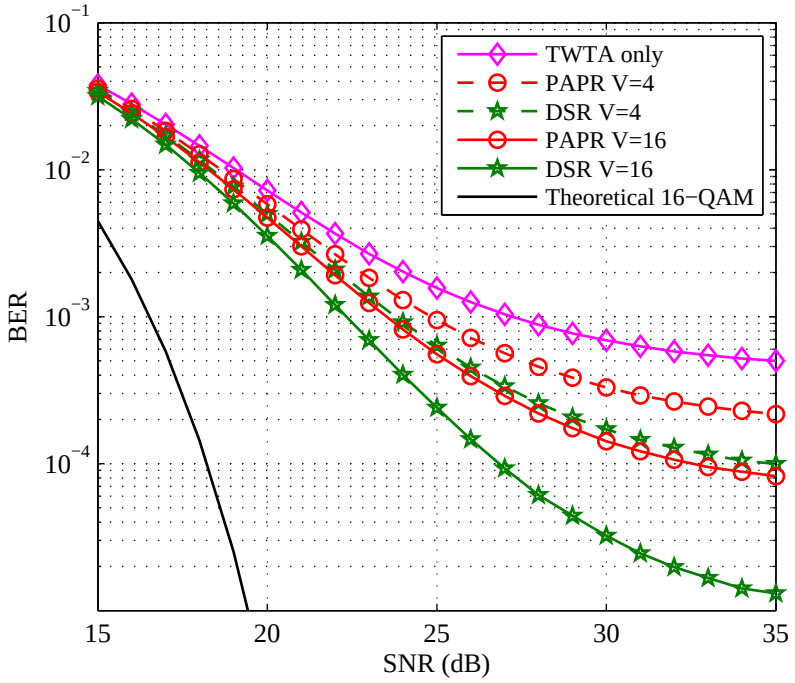

(a) PTS-based scheme

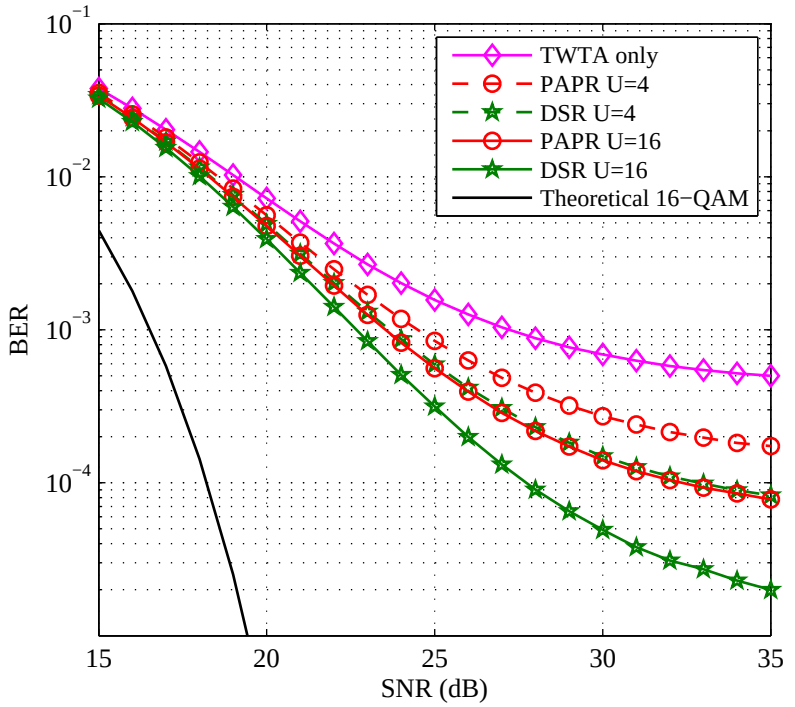

(b) SLM-based scheme

Figure 6.23: BER versus SNR for systems based on the DSR and PAPR reduction criteria in the presence of the TWTA nonlinearity, CFO and wideband satellite mobile channel, $\theta \leq 45$, for 16-QAM constellation.

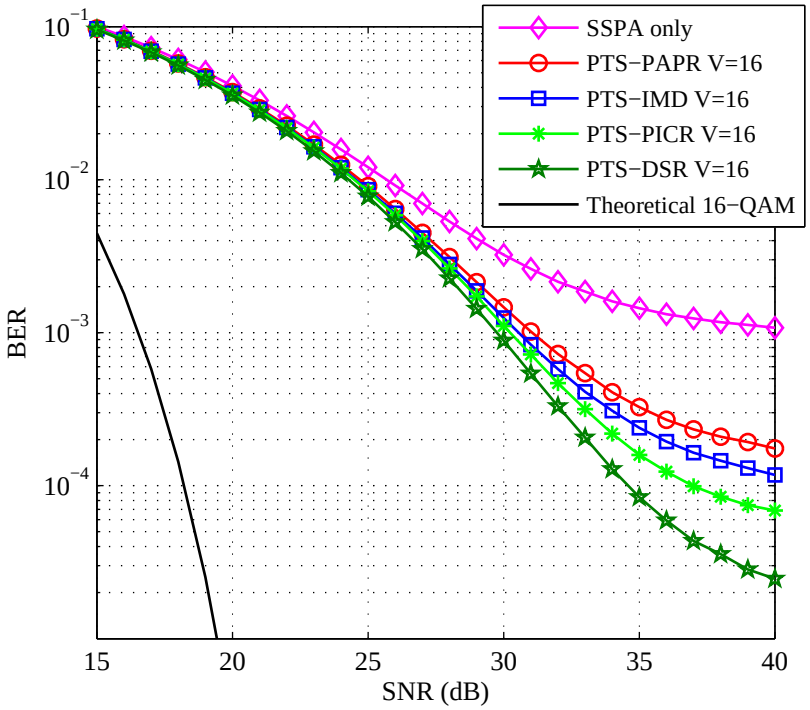

(a) PTS-based scheme

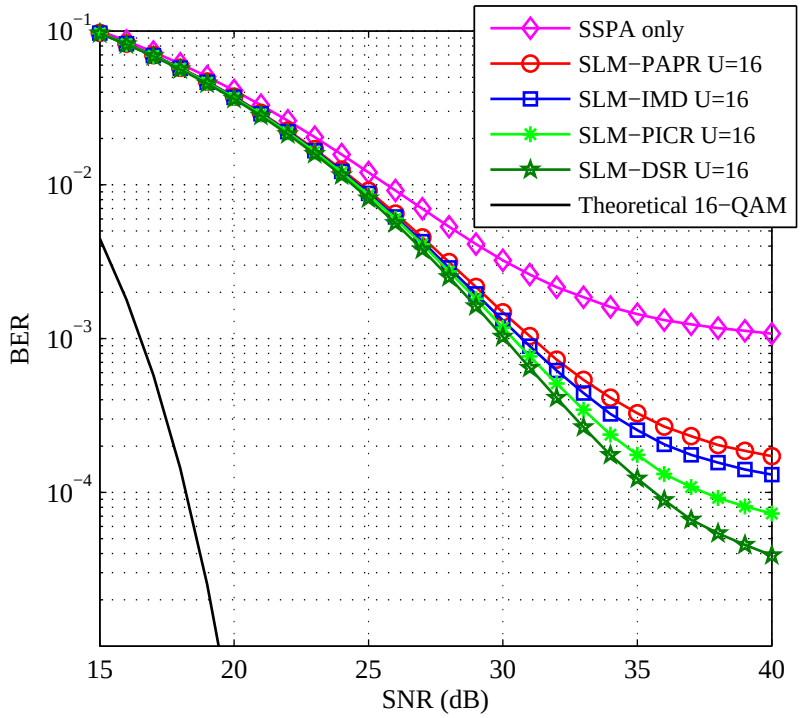

(b) SLM-based scheme

Figure 6.24: BER versus SNR for systems based on the DSR and PAPR reduction criteria in the presence of the practical SSPA nonlinearity, CFO and frequency-selective multipath fading channel for a 16-QAM constellation, $V/U = 16$.

Table 6.1: The overall comparison of the proposed schemes over the PAPR-based technique for $V/U = 16$.

Proposed Technique	HPA Model	C_r in %	DSR Reduction in dB	Conste-llation	OBO in dB	CFO ε	SNR Improvement in dB
PTS-DSR	TWTA	39	1.3	16-QAM	5	0.01	5.9
				QPSK	0	0.075	6.6
	SSPA	37	1.5	16-QAM	3	0.01	10.6
				QPSK	0	0.1	4.2
SLM-DSR	TWTA	75	1.1	16-QAM	5	0.01	4.7
				QPSK	0	0.075	5.5
	SSPA	69	1.4	16-QAM	3	0.01	8.3
				QPSK	0	0.1	3.1

6.7 Chapter Summary

Table 6.1 summarises the performance and complexity of the proposed PTS-DSR and SLM-DSR schemes over the PAPR criterion, in the presence of either the TWTA or the SSPA and CFO using 16-QAM or QPSK constellation. This table shows that the proposed schemes using the SSPA can achieve a DSR reduction by approximately 1.5 dB. In addition, the highest reduction in BER is achieved when the SSPA and 16-QAM modulation scheme is used, that is 10.6 and 8.3 dB for the PTS-DSR and SLM-DSR, respectively. Furthermore, the QPSK-based systems using the SSPA can manage higher values of ε compared to those that use the TWTA, as the amount of ICI generated by the SSPA is less, which can reduce the impairment in the BER performance.

6.8 Conclusion

This chapter presented efficient techniques to reduce the BER degraded by the HPA and CFO utilised in OFDM-based systems. The proposed techniques are based on measuring the distortion produced by the amplifier and CFO, which is more accurate than the PAPR as the distortion is not taken into account for the PAPR calculation and the PAPR metric is estimated before the amplifier. Also in this chapter, a closed form solution for the BER is derived theoretically and an accepted agreement of the BER is achieved when the simulation is compared with the analytical calculation.

Chapter 7

Low-Complexity Approaches for Nonlinear OFDM Transmission using Maximum Cross Correlation

This chapter presents efficient approaches to reduce the impact of nonlinear power amplifiers on the BER of OFDM systems. The proposed approaches are based on the well-established PAPR reduction schemes, a power amplifier model and a simple single point cross correlator. Unlike the conventional schemes, the optimum phase sequence in the proposed approaches is selected by maximising the correlation between the input and output of the power amplifier model. Simulation results have confirmed that the BER using the proposed approaches is almost identical to the state-of-the-art while the complexity is reduced by more than 80% for particular system configurations.

7.1 Introduction

In the literature, enormous research reports considered the problem of PAPR inherent in OFDM signals. Two particular approaches that received remarkable attention are the PTS and SLM. However, while these approaches have exceptional PAPR reduction capability, they suffer from high computational complexity. The conventional approaches are based on computing the PAPR for different preselected phase sequences, then the sequence that minimises the PAPR is selected for transmission. The receiver should be informed about the selected sequence, which is typically per-

formed by sending side information. The PTS and SLM high complexity is mainly treated by using efficient search processes to select the optimum phase sequence, or by using various optimisation metrics to select the corresponding phase sequence. Examples for some common optimisation metrics are the MSE [3], IMD [68], DSR [100] and PICR [101]. In addition to the complexity reduction, adopting a particular optimisation metric would have high impact on the system BER.

Based on a particular optimisation metric, PTS and SLM-based techniques can be categorised as time-domain or frequency-domain systems. In time-domain systems, the optimisation metric is computed after the IFFT directly, while computing the optimisation metric in frequency-domain systems is performed after passing the IFFT output through a nonlinear model followed by a FFT to extract the frequency-domain symbols contaminated by ICI. Then, the FFT output is used to compute the optimisation metric [68] and [101]. Generally speaking, frequency-domain techniques are more hardware complex due to the additional FFT operation, which has to be repeated for several iterations. However, such techniques offer better BER reduction due to the fact that they are designed to minimise the ICI, and hence the BER will be minimised.

As hinted in the above discussion, several techniques aim at reducing the BER by minimising the ICI that results from the HPA nonlinearity. Alternatively, the authors in [3] proposed a new PTS based on minimising the MSE between the input and output signals of the HPA. Therefore, the MSE is used to measure the distortion caused by the HPA and the transmission sequence is selected to minimise the MSE. The main limitation of this approach is the high complexity due to the tapping of the HPA output and the nonlinear adaptive estimator used to estimate the HPA characteristics.

This chapter presents new approaches to reduce the BER degradation of OFDM systems due to the nonlinear characteristics of the HPA. The general structure of the proposed approaches is similar to the conventional PTS and SLM techniques, except that the transmission phase sequence is selected to maximise the cross correlation between the input and output of the nonlinear HPA model. The proposed approaches are highly efficient because they do not require an FFT after the nonlinear HPA model, nor they require accurate knowledge of the HPA characteristics. In addition to the significant complexity reduction, the achieved BER of the proposed approaches is equivalent to the state-of-the-art.

7.2 Proposed Approaches using PTS and SLM Schemes

Figs. 7.1 and 7.2 depict the block diagram of the proposed PTS and SLM approaches, respectively. Similar equation forms, mentioned in chapter 3, to the conventional PTS and SLM can be obtained for the proposed approaches. The effect of the HPA on the transmitted signal can be estimated by applying $\mathbf{x}$ to the polynomial model

$$y_n \approx \alpha_1 x_n + \alpha_3 |x_n|^2 x_n. \tag{7.1}$$

Intuitively speaking, if the HPA has pure linear characteristic curve, or the maximum signal level is less than the saturation point of the amplifier, then the input and output of the HPA will be identical, i.e. $\mathbf{x} = \mathbf{y}$, otherwise $\mathbf{x} \neq \mathbf{y}$. Consequently, this section proposes new PTS and SLM systems based on selecting a phase sequence that maximises the similarity between $\mathbf{x}$ and $\mathbf{y}$ using the cross correlation as an optimisation metric. However, there is no need to implement a complete cross correlator because it is obvious that the maximum correlation occurs when there is no shift between the two signals. The single point cross correlation can be expressed as

$$R_{xy}^{(0)} = \sum_{n=0}^{N-1} x_n y_n^* = \alpha_1 \sum_{n=0}^{N-1} |x_n|^2 + \alpha_3 \sum_{n=0}^{N-1} |x_n|^4. \tag{7.2}$$

Since most practical HPAs exhibit compressive nonlinearity, then $\alpha_3/\alpha_1 < 0$ [68]. Moreover, without loss of generality, we can select $\alpha_1 > 0$ since it represents the amplifier gain, thus $\alpha_3 < 0$. Consequently, the first term in (7.2) is fixed and the second term is negative and proportional to $|x_n|^4$. Therefore, R_{xy} is maximum when $\mathbf{x} = \mathbf{y}$.

In a similar fashion to conventional PTS, the correlation function R_{xy} will be computed for all possible phase sequences. The selected phase sequence for transmission is

$$\mathbf{b} = \arg \max_{\mathbf{b}^{(i)}} \{R_{xy}^{(0)}\}, \tag{7.3}$$

where $\mathbf{b}^{(i)} = [b_0^{(i)}, b_1^{(i)}, \cdots, b_{V-1}^{(i)}]$ and $0 \leq i \leq 2^{V-1}$. However, for the proposed SLM approach, the correlation function can be computed for all possible phase sequences.

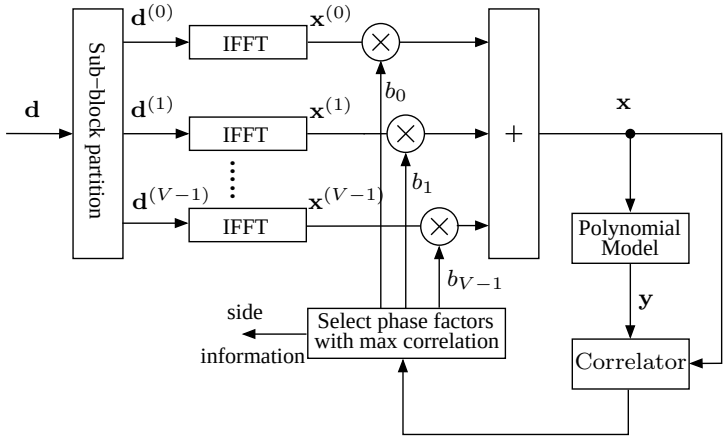

Figure 7.1: Block diagram of the proposed PTS approach based on correlation metric.

The transmitted phase sequence can be represented as

$$\mathbf{a} = \arg\max_{\mathbf{a}^{(u)}} \{R_{xy}^{(0)}\}, \tag{7.4}$$

where $\mathbf{a}^{(u)} = [a_0^{(u)}, a_1^{(u)}, \cdots, a_{N-1}^{(u)}]$ and $u = 0, 1, \cdots, U-1$. Therefore, the proposed approaches indirectly reduce the signal distortion by maximising the similarity between the input and output signals of the HPA.

7.3 Computational Complexity

To simplify the complexity comparison among various techniques we adopt the BER as a performance metric and an oversampling factor $L = 1$ for all techniques. The computational complexity is assessed in terms of the number of RMs and RAs. Since all systems are PTS and SLM-based with the same L value, then their complexity is equivalent except for the computation of the optimisation metric. For the PTS-based schemes, the computational complexity of all considered systems can be compared based on the complexity of computing the optimisation metric, which can be described as follows:

- $R_{xy}^{(0)}$: The computational complexity of the correlation metric can be computed directly from (7.2), which gives after some straight forward computations $RA_{CORR} = 3N$, $RM_{CORR} = 3N+4$ for the TWTA case and $RA_{CORR} = 3N-1$, $RM_{CORR} = 3N + 1$ for the SSPA case.

- DSR: $12N$ RMs and $6N$ RAs for the TWTA model, and $6N$ RMs and $3N$

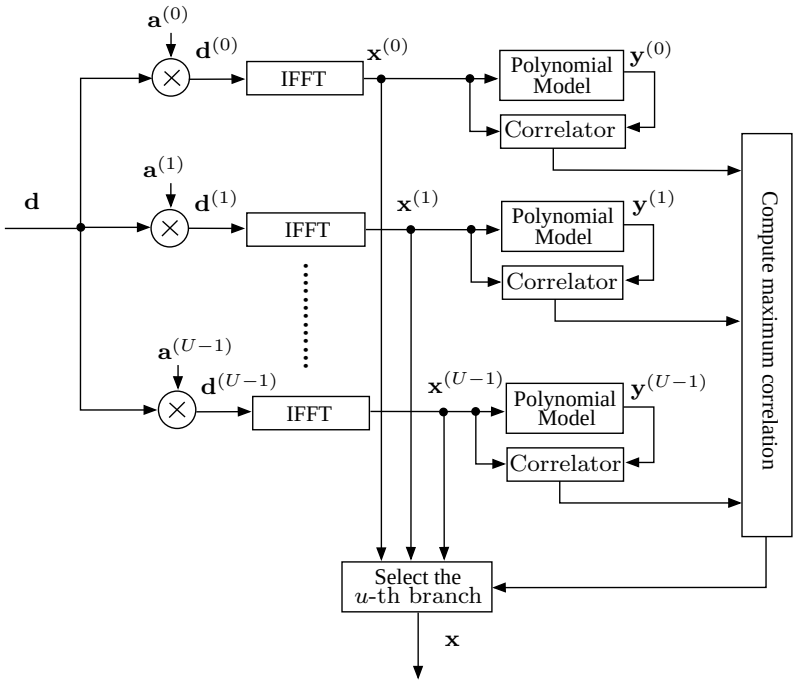

Figure 7.2: Block diagram of the proposed SLM approach based on correlation metric.

RAs for the SSPA model are required to compute the output of polynomial model. $0.5N\log_2 N$ CMs and $N\log_2 N$ CAs are required for the N-point FFT. $10N$ RMs, $7N$ RAs for the TWTA model, and $8N$ RMs, $5N$ RAs for the SSPA model are required to calculate the DSR metric. Therefore, $RA_{DSR} = N(13 + 3\log_2 N)$, $RM_{DSR} = 2N(11 + 2\log_2 N)$ are required for the TWTA case and $RA_{DSR} = 2N(7 + \log_2 N)$, $RM_{DSR} = N(8 + 3\log_2 N)$ are required for the SSPA case.

- MSE: Given that the MSE is used as an optimisation metric instead of the cross correlator in Fig. 7.1, then $MSE = \sum_{n=0}^{N-1} |x_n - y_n|^2$. Substituting y_n by the right side of (7.1) and simplifying the result yields $MSE = \alpha_3^2 \sum_{n=0}^{N-1} |x_n|^6$. Consequently, $RA_{MSE} = 2N - 1$, $RM_{MSE} = 4N + 2$ for the TWTA case and $RA_{MSE} = 2N - 1$, $RM_{MSE} = 4N + 1$ for the SSPA case.

In comparison to the PTS systems, it is interesting to note that the complexity equations for SLM-based systems are similar, while the iteration is U for the proposed SLM-CORR systems, instead of $\mathcal{I}$ in the proposed PTS-CORR systems. Table 7.1 summarises the complexity of the DSR, MSE and correlation metrics for the PTS-based systems.

Table 7.1: Computational complexity for the PTS-DSR, PTS-MSE and PTS-CORR algorithms.

Proposed Technique	HPA Model	RAs	RMs
PTS-CORR	TWTA	$3N\mathcal{I}$	$(3N+4)\mathcal{I}$
	SSPA	$(3N+1)\mathcal{I}$	$(3N-1)\mathcal{I}$
PTS-DSR	TWTA	$N(13+3\log_2 N)\mathcal{I}$	$2N(11+2\log_2 N)\mathcal{I}$
	SSPA	$2N(7+\log_2 N)\mathcal{I}$	$N(8+3\log_2 N)\mathcal{I}$
PTS-MSE	TWTA	$(2N-1)\mathcal{I}$	$(4N+2)\mathcal{I}$
	SSPA	$(2N-1)\mathcal{I}$	$(4N+1)\mathcal{I}$

It can be noted from Table 7.1 that the CORR scheme using SSPA model offers a substantial complexity reduction of about 80% and 90% in terms of the required RAs and RMs, respectively, when compared to the DSR for $N = 128$. The MSE requires about 33% less RAs than the CORR scheme, however it requires about 33% more RMs. Therefore, the MSE has a non negligible additional complexity over the proposed scheme since the complexity of multiplication is considerably higher than the addition.

7.4 Numerical Results

Monte Carlo simulation is used to assess the BER performance of the PTS-CORR and compare it to the standard PAPR-PTS and PTS-DSR. The simulation results are obtained using 10^5 OFDM blocks generated using $N = 128$ SCs. The data symbols are selected uniformly from a Gray coded 16-QAM symbol constellation. The number of partitions V used is either 4 or 16. Instead of searching for the optimum phase sequence $\mathbf{b}$ among 2^V possible sequences, we limit the search space to only V different sequences with the elements of each sequence is selected uniformly from $\{0, \pi\}$. For coherent demodulation, we assume perfect knowledge of the phase sequence and the channel state information at the receiver side.

The SSPA model described in (2.10) is used to represent the transmission HPA, while the model given in (7.1) is used for the DSR and correlation metrics calculation. This is necessary to model the difference between the practical HPA and the mathematical model used to compute $R_{xy}^{(0)}$. The transmission SSPA parameters are selected to match the practical SSPA amplifier described in [105]. This amplifier is used for WiMAX in the frequency range 2.3 to 2.5 GHz. The amplifier parameters

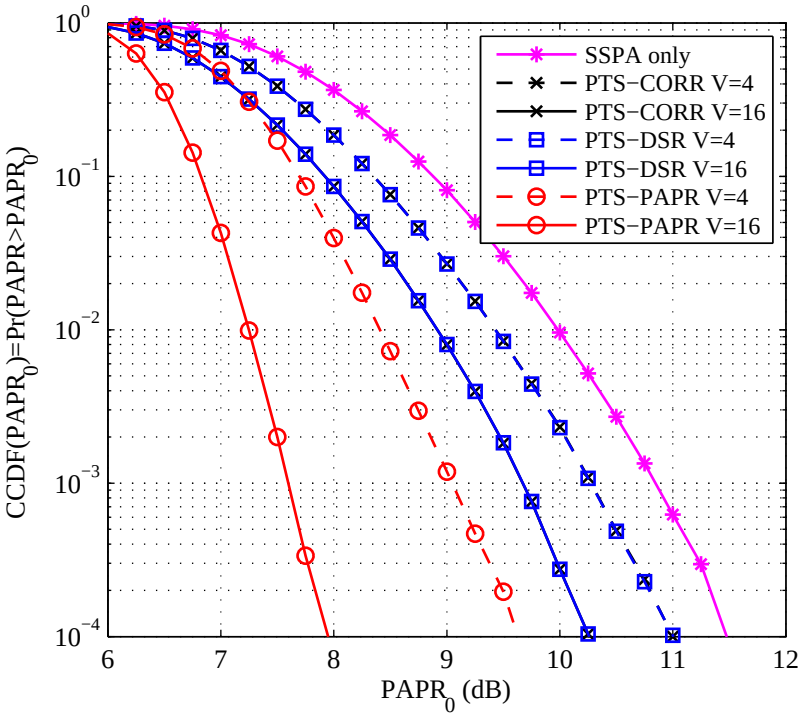

Figure 7.3: CCDF of the PAPR for OFDM systems based on the PAPR, DSR and proposed approach for different partitions.

for both models are computed using curve fitting methods for OBO = 3 dB, where $A_{sat} = 3.286$, $\alpha_1 = 1$ and $\alpha_3 = -0.1769$.

Fig. 7.3 depicts the CCDF of PAPR for PTS-OFDM systems. It can be observed that high CCDF values of PAPR in systems based on DSR reduction occur with similar probabilities to the corresponding values in systems based on the correlation approach. For example, when $V = 16$, the PAPR value corresponding to a CCDF value for the DSR-reduction criterion is approximately 1.3 dB better than those of the OFDM systems without PAPR reduction. Furthermore, when using this V value with PTS-PAPR, the reduction is approximately 2.4 dB better than the PTS-DSR scheme.

The BER performance of the proposed and the other considered schemes is presented in Fig 7.4 for an AWGN channel using $V = 4$ and 16. As it can be noted from this figure, the proposed PTS-CORR BER is equivalent to the BER of the PTS-DSR for both values of V, while the BER of the PTS-PAPR was significantly higher. Moreover, simulation results have confirmed that the BER using the MSE are roughly identical to the DSR and CORR results. Therefore, tapping the HPA output and estimating its characteristics accurately did not have any noticeable impact on the BER while the complexity will be increased substantially.

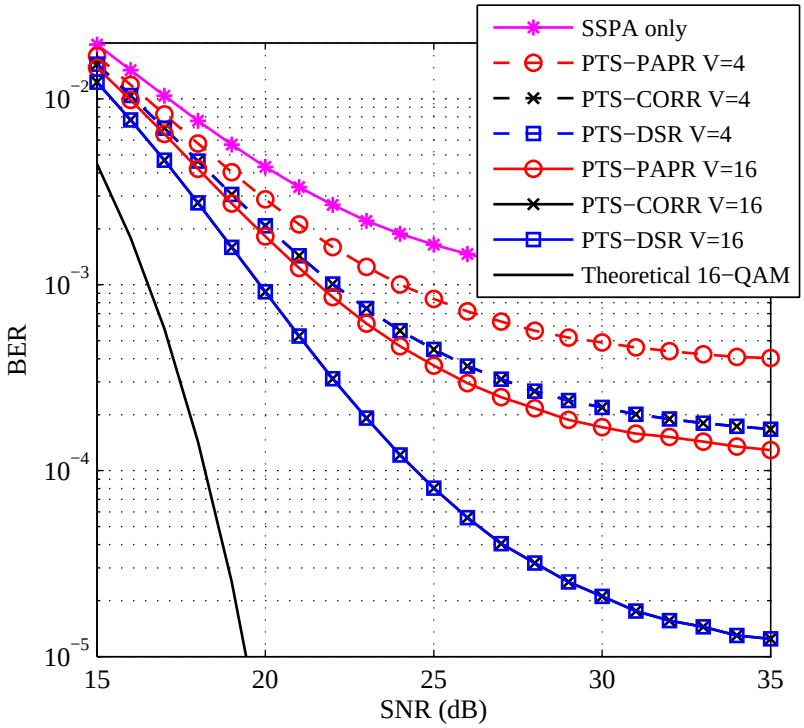

Figure 7.4: BER of the PAPR, DSR and proposed approach over an AWGN channels using $V = 4$ and 16.

The BER performance of the PTS-CORR in frequency-selective multipath fading channels is presented in Fig 7.5. The considered fading channel consists of 5 multipath components with delays of [0, 1, 2, 3, 4] samples, an average gain of [0.35, 0.25, 0.18, 0.13, 0.09] and the mean square delay spread $\sigma^2(\tau) = 1.74$ [104]. The results presented in Fig 7.5 clearly demonstrate that the BER performance trend in fading channels follows that in AWGN channel where the correlation approach outperforms the PAPR technique and matches the DSR.

7.5 Conclusion

This chapter presented new low-complexity approaches to reduce the BER performance degradation caused by the nonlinear characteristics of the HPA utilised in OFDM-based systems. The proposed approaches are based on maximising the correlation between the input and output of the HPA. Complexity analyses have demonstrated that the proposed approaches offer approximately 90% complexity reduction in terms of the number of multiplications and approximately 80% in terms of the number of additions as compared to the state-of-the-art. Furthermore, the gained complexity reduction was achieved without any noticeable BER penalty.

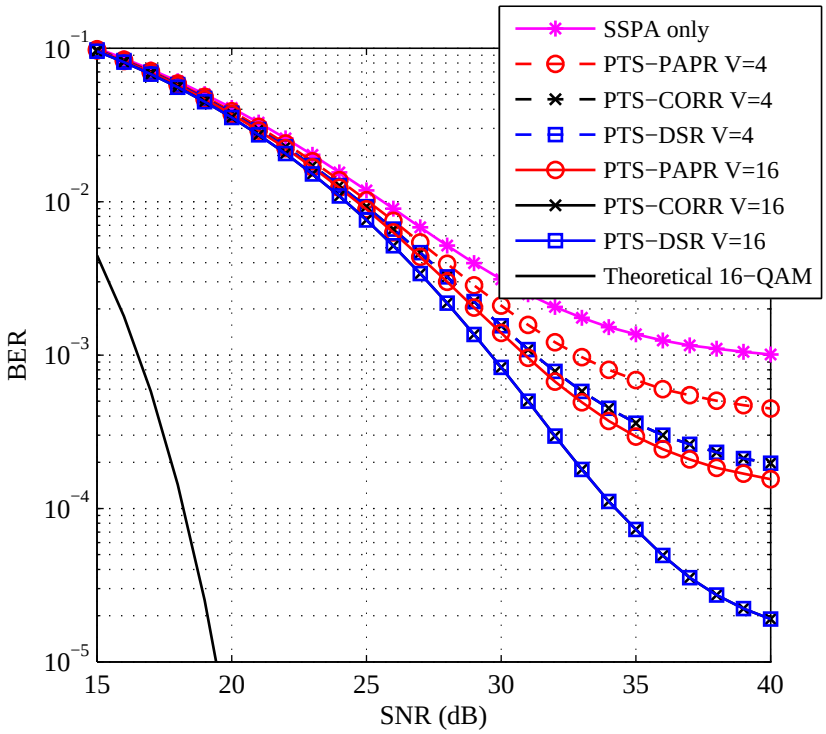

Figure 7.5: BER of the PAPR, DSR and the proposed system in multipath fading channels using $V = 4$ and 16.

Chapter 8

Conclusion and Future Work

M-QAM based OFDM has become the *de facto* standard for satellite communication systems deployed in the 3G systems, this combination has also become a robust candidate for the 4G wireless transmission systems. This modulation scheme can be utilised for high bit rate multimedia applications, however, other limitations such as the PAPR may reduce the gain that can be achieved by using OFDM due to the use of HPAs. The nonlinearity of the amplifier causes loss of orthogonality among the SCs, and hence, ICI is introduced in the transmitted signal. The ICI power is proportional to the amplitude of the signal at the amplifier input and it may cause considerable BER degradation.

The motivation behind this thesis was to reduce the ICI produced by the HPA by applying state-of-the-art PAPR techniques; whilst paying particular attention to the inherent increase in computational complexity. Therefore, three factors were taken into account, system computational complexity, HPA efficiency and BER performance, and a number of methods were proposed to achieve low computational complexity, low error rate and high amplifier power efficiency.

In the first contribution, new LC-IPTS and SLC-IPTS schemes were developed that employed only two IFFTs and circulant transform matrices, in order to reduce the complexity and improve the system performance. Furthermore, the overall computational complexity for the proposed schemes was derived and formulated. The simulation results showed that the proposed odd-case LC-IPTS can reduce the complexity and improve the system performance. Moreover, the proposed odd-case SLC-IPTS can reduce both the computational complexity and the number of SI bits, albeit at the cost of a less reduction in PAPR and BER performance.

In the second (main) contribution, efficient techniques to reduce the BER of the OFDM signals transmitted over nonlinear HPA were proposed. The proposed techniques were based on predicting the distortion power that an HPA would generate due to the nonlinear characteristics of such devices. In a fashion similar to SLM or PTS schemes, the predicted distortion was used to select a set of phases that minimise the actual HPA distortion and consequently the BER. Moreover, the proposed techniques offered a complexity reduction for particular OFDM and HPA settings compared to other techniques, which are optimised to reduce the PAPR.

In the third contribution, the effect of the CFO was added to the proposed techniques based on predicting the distortion introduced by HPA nonlinearity. Simulation results have confirmed that an improvement in BER can be achieved when the proposed techniques are compared to the standard PAPR techniques. Moreover, complexity analysis demonstrated that the proposed systems offer a significant complexity reduction. Finally, a closed form for ESNR was derived and consequently the accurate BER was calculated theoretically. An accepted accuracy of the BER between simulation and analytical calculation was achieved.

Finally, in the fourth contribution, new approaches were proposed to reduce the complexity of the proposed techniques that are based on predicting the distortion. In the proposed approaches, the transmitted phase vector was selected to maximise the cross correlation between the input and output of the nonlinear HPA model. Complexity analyses demonstrated that the proposed approaches can achieve a significant reduction compared to the current leading techniques proposed in the main contribution. Furthermore, the gained complexity reduction was achieved without any noticeable BER degradation.

Future Work

The ICI minimisation based on PAPR reduction techniques that can achieve significant improvement in BER performance for OFDM systems even now faces many challenges. Several topics for future investigation can be suggested. These are:

- Extension of the schemes carried out in this thesis to manage M-PSK-OFDM, M-QAM-OFDM and higher-order HM-OFDM systems. Investigation of higher-order modulation schemes is worthwhile as several practical systems such as

DVB-T2 and DVB-S2 use OFDM signals with higher-order modulation.

- In the standard OFDM, the same modulation technique is utilised on all types of sub-channels. Nevertheless, severely faded sub-channels can deteriorate the BER. Adaptive modulation is one method to improve the performance, where the transmission of higher-order modulation schemes are used for high SNR OFDM sub-channels, and the transmission of lower-order modulation schemes are used for low SNR OFDM sub-channels. On the other hand, the entire transmitted power is allocated differently due to different OFDM sub-channels, depending on their existing SNR. It is well known that the allocation process can be interfered by the amplifier nonlinearity due to different OFDM sub-channels, causing different nonlinear distortion levels. Clearly, the development of robust allocation algorithms is a valuable topic. As a result, an investigation of the relation between nonlinearity and adaptive OFDM systems should be carried out.

- The effect of the maximum Doppler shift, f_d, is not taken into account in this study based on the assumption of perfect phase synchronisation. A range of user speeds could be included for comparative investigation. Moreover, other factors can be considered in order to obtain a wide image of OFDM system performance.

- The effects of nonlinear distortion for the uncoded OFDM were studied. Extension of the techniques utilised in this thesis can be applied to multi-path fading channels with coded OFDM schemes.

- An accurate BER formula for the distorted OFDM signals using the HPA nonlinearity and CFO was derived in AWGN channel. The effects of frequency-selective fading channels should be added and theoretical analysis needs to be studied.

- Some issues in this thesis require a deeper analysis; it would be beneficial to explore the effect of receiving the SI imperfectly and to confirm that their influence is minimal. Furthermore, embedding the SI in our proposed techniques requires further investigation.

- Future work should consider other diversity techniques such as multiple-input

multiple-output (MIMO) systems in order to improve the performance and increase the diversity. Compared to single-input single-output (SISO) systems, the improvement achieved in the system diversity is relative to the minimum number of transmit and receive antennas. The PAPR is one drawback of MIMO-OFDM systems; therefore, it would be interesting to implement our proposed techniques in mobile wireless systems that might offer further improvement to the BER performance.

- Recently, non-uniform 16-QAM and HM constellations have received enormous attention for several applications such as multimedia transmission. Furthermore, these constellations have been the existent standard for the DVB-T. In the same symbol, various levels of bit protection can be adjusted by altering the effective distances between the symbols; this is the main property of non-uniform constellations. For that reason, non-uniform constellations are an attractive topic to investigate with the proposed techniques for future work.

- The proposed schemes may be implemented in hardware by emulating external field programmable gate array (FPGA) and digital signal processing (DSP) units. Consequently, the realisation of efficient and consistent hardware techniques can be achieved with lower cost platforms.

Appendix A

Circulant Matrix Vectors

As an example $\mathbf{b} = [1, -1, 1, 1]$, the circulant matrix for this odd-case (1) vector can be described as

$$\mathbf{T}_r = 0.5 \times \begin{bmatrix}
1 & 0 & 0 & 0 & -j & 0 & 0 & 0 & 1 & 0 & 0 & 0 & j & 0 & 0 & 0 \\
0 & 1 & 0 & 0 & 0 & -j & 0 & 0 & 0 & 1 & 0 & 0 & 0 & j & 0 & 0 \\
0 & 0 & 1 & 0 & 0 & 0 & -j & 0 & 0 & 0 & 1 & 0 & 0 & 0 & j & 0 \\
0 & 0 & 0 & 1 & 0 & 0 & 0 & -j & 0 & 0 & 0 & 1 & 0 & 0 & 0 & j \\
j & 0 & 0 & 0 & 1 & 0 & 0 & 0 & -j & 0 & 0 & 0 & 1 & 0 & 0 & 0 \\
0 & j & 0 & 0 & 0 & 1 & 0 & 0 & 0 & -j & 0 & 0 & 0 & 1 & 0 & 0 \\
0 & 0 & j & 0 & 0 & 0 & 1 & 0 & 0 & 0 & -j & 0 & 0 & 0 & 1 & 0 \\
0 & 0 & 0 & j & 0 & 0 & 0 & 1 & 0 & 0 & 0 & -j & 0 & 0 & 0 & 1 \\
1 & 0 & 0 & 0 & j & 0 & 0 & 0 & 1 & 0 & 0 & 0 & -j & 0 & 0 & 0 \\
0 & 1 & 0 & 0 & 0 & j & 0 & 0 & 0 & 1 & 0 & 0 & 0 & -j & 0 & 0 \\
0 & 0 & 1 & 0 & 0 & 0 & j & 0 & 0 & 0 & 1 & 0 & 0 & 0 & -j & 0 \\
0 & 0 & 0 & 1 & 0 & 0 & 0 & j & 0 & 0 & 0 & 1 & 0 & 0 & 0 & -j \\
-j & 0 & 0 & 0 & 1 & 0 & 0 & 0 & j & 0 & 0 & 0 & 1 & 0 & 0 & 0 \\
0 & -j & 0 & 0 & 0 & 1 & 0 & 0 & 0 & j & 0 & 0 & 0 & 1 & 0 & 0 \\
0 & 0 & -j & 0 & 0 & 0 & 1 & 0 & 0 & 0 & j & 0 & 0 & 0 & 1 & 0 \\
0 & 0 & 0 & -j & 0 & 0 & 0 & 1 & 0 & 0 & 0 & j & 0 & 0 & 0 & 1
\end{bmatrix}. \tag{A.1}$$

It is clear from (A.1) that $\mathbf{T}_r$ has VLN non-zero elements. For odd-case (2) vector, $\mathbf{b} = [-1, 1, -1, -1]$, the circulant matrix can be explained as

$$\mathbf{T}_r = 0.5 \times \begin{bmatrix}
-1 & 0 & 0 & 0 & j & 0 & 0 & 0 & -1 & 0 & 0 & 0 & j & 0 & 0 & 0 \\
0 & -1 & 0 & 0 & 0 & j & 0 & 0 & 0 & -1 & 0 & 0 & 0 & j & 0 & 0 \\
0 & 0 & -1 & 0 & 0 & 0 & j & 0 & 0 & 0 & -1 & 0 & 0 & 0 & j & 0 \\
0 & 0 & 0 & -1 & 0 & 0 & 0 & j & 0 & 0 & 0 & -1 & 0 & 0 & 0 & j \\
j & 0 & 0 & 0 & -1 & 0 & 0 & 0 & j & 0 & 0 & 0 & -1 & 0 & 0 & 0 \\
0 & j & 0 & 0 & 0 & -1 & 0 & 0 & 0 & j & 0 & 0 & 0 & -1 & 0 & 0 \\
0 & 0 & j & 0 & 0 & 0 & -1 & 0 & 0 & 0 & j & 0 & 0 & 0 & -1 & 0 \\
0 & 0 & 0 & j & 0 & 0 & 0 & -1 & 0 & 0 & 0 & j & 0 & 0 & 0 & -1 \\
-1 & 0 & 0 & 0 & j & 0 & 0 & 0 & -1 & 0 & 0 & 0 & j & 0 & 0 & 0 \\
0 & -1 & 0 & 0 & 0 & j & 0 & 0 & 0 & -1 & 0 & 0 & 0 & j & 0 & 0 \\
0 & 0 & -1 & 0 & 0 & 0 & j & 0 & 0 & 0 & -1 & 0 & 0 & 0 & j & 0 \\
0 & 0 & 0 & -1 & 0 & 0 & 0 & j & 0 & 0 & 0 & -1 & 0 & 0 & 0 & j \\
j & 0 & 0 & 0 & -1 & 0 & 0 & 0 & j & 0 & 0 & 0 & -1 & 0 & 0 & 0 \\
0 & j & 0 & 0 & 0 & -1 & 0 & 0 & 0 & j & 0 & 0 & 0 & -1 & 0 & 0 \\
0 & 0 & j & 0 & 0 & 0 & -1 & 0 & 0 & 0 & j & 0 & 0 & 0 & -1 & 0 \\
0 & 0 & 0 & j & 0 & 0 & 0 & -1 & 0 & 0 & 0 & j & 0 & 0 & 0 & -1
\end{bmatrix}. \tag{A.2}$$

Similar to (A.1) the $\mathbf{T}_r$ has VLN non-zero elements. The circulant matrix for an even-case (1) vector, $\mathbf{b} = [-1, -1, 1, 1]$, can be expressed as

$$\mathbf{T}_r = 0.5 \times \begin{bmatrix}
0 & 0 & 0 & 0 & -1-j & 0 & 0 & 0 & 0 & 0 & 0 & 0 & -1+j & 0 & 0 & 0 \\
0 & 0 & 0 & 0 & 0 & -1-j & 0 & 0 & 0 & 0 & 0 & 0 & 0 & -1+j & 0 & 0 \\
0 & 0 & 0 & 0 & 0 & 0 & -1-j & 0 & 0 & 0 & 0 & 0 & 0 & 0 & -1+j & 0 \\
0 & 0 & 0 & 0 & 0 & 0 & 0 & -1-j & 0 & 0 & 0 & 0 & 0 & 0 & 0 & -1+j \\
-1+j & 0 & 0 & 0 & 0 & 0 & 0 & 0 & -1-j & 0 & 0 & 0 & 0 & 0 & 0 & 0 \\
0 & -1+j & 0 & 0 & 0 & 0 & 0 & 0 & 0 & -1-j & 0 & 0 & 0 & 0 & 0 & 0 \\
0 & 0 & -1+j & 0 & 0 & 0 & 0 & 0 & 0 & 0 & -1-j & 0 & 0 & 0 & 0 & 0 \\
0 & 0 & 0 & -1+j & 0 & 0 & 0 & 0 & 0 & 0 & 0 & -1-j & 0 & 0 & 0 & 0 \\
0 & 0 & 0 & 0 & -1+j & 0 & 0 & 0 & 0 & 0 & 0 & 0 & -1-j & 0 & 0 & 0 \\
0 & 0 & 0 & 0 & 0 & -1+j & 0 & 0 & 0 & 0 & 0 & 0 & 0 & -1-j & 0 & 0 \\
0 & 0 & 0 & 0 & 0 & 0 & -1+j & 0 & 0 & 0 & 0 & 0 & 0 & 0 & -1-j & 0 \\
0 & 0 & 0 & 0 & 0 & 0 & 0 & -1+j & 0 & 0 & 0 & 0 & 0 & 0 & 0 & -1-j \\
-1-j & 0 & 0 & 0 & 0 & 0 & 0 & 0 & -1+j & 0 & 0 & 0 & 0 & 0 & 0 & 0 \\
0 & -1-j & 0 & 0 & 0 & 0 & 0 & 0 & 0 & -1+j & 0 & 0 & 0 & 0 & 0 & 0 \\
0 & 0 & -1-j & 0 & 0 & 0 & 0 & 0 & 0 & 0 & -1+j & 0 & 0 & 0 & 0 & 0 \\
0 & 0 & 0 & -1-j & 0 & 0 & 0 & 0 & 0 & 0 & 0 & -1+j & 0 & 0 & 0 & 0
\end{bmatrix}. \tag{A.3}$$

As can be seen from (A.3) the $\mathbf{T}_r$ has $VLN/2$ non-zero elements. Finally, The circulant matrix for an even-case (2) vector, $\mathbf{b} = [-1, 1, -1, 1]$, can be illustrated as

$$\mathbf{T}_r = 0.5 \times \begin{bmatrix}
0 & 0 & 0 & 0 & 0 & 0 & 0 & 0 & -1 & 0 & 0 & 0 & 0 & 0 & 0 & 0 \\
0 & 0 & 0 & 0 & 0 & 0 & 0 & 0 & 0 & -1 & 0 & 0 & 0 & 0 & 0 & 0 \\
0 & 0 & 0 & 0 & 0 & 0 & 0 & 0 & 0 & 0 & -1 & 0 & 0 & 0 & 0 & 0 \\
0 & 0 & 0 & 0 & 0 & 0 & 0 & 0 & 0 & 0 & 0 & -1 & 0 & 0 & 0 & 0 \\
0 & 0 & 0 & 0 & 0 & 0 & 0 & 0 & 0 & 0 & 0 & 0 & -1 & 0 & 0 & 0 \\
0 & 0 & 0 & 0 & 0 & 0 & 0 & 0 & 0 & 0 & 0 & 0 & 0 & -1 & 0 & 0 \\
0 & 0 & 0 & 0 & 0 & 0 & 0 & 0 & 0 & 0 & 0 & 0 & 0 & 0 & -1 & 0 \\
0 & 0 & 0 & 0 & 0 & 0 & 0 & 0 & 0 & 0 & 0 & 0 & 0 & 0 & 0 & -1 \\
-1 & 0 & 0 & 0 & 0 & 0 & 0 & 0 & 0 & 0 & 0 & 0 & 0 & 0 & 0 & 0 \\
0 & -1 & 0 & 0 & 0 & 0 & 0 & 0 & 0 & 0 & 0 & 0 & 0 & 0 & 0 & 0 \\
0 & 0 & -1 & 0 & 0 & 0 & 0 & 0 & 0 & 0 & 0 & 0 & 0 & 0 & 0 & 0 \\
0 & 0 & 0 & -1 & 0 & 0 & 0 & 0 & 0 & 0 & 0 & 0 & 0 & 0 & 0 & 0 \\
0 & 0 & 0 & 0 & -1 & 0 & 0 & 0 & 0 & 0 & 0 & 0 & 0 & 0 & 0 & 0 \\
0 & 0 & 0 & 0 & 0 & -1 & 0 & 0 & 0 & 0 & 0 & 0 & 0 & 0 & 0 & 0 \\
0 & 0 & 0 & 0 & 0 & 0 & -1 & 0 & 0 & 0 & 0 & 0 & 0 & 0 & 0 & 0 \\
0 & 0 & 0 & 0 & 0 & 0 & 0 & -1 & 0 & 0 & 0 & 0 & 0 & 0 & 0 & 0
\end{bmatrix}. \tag{A.4}$$

We can see from (A.4) that the $\mathbf{T}_r$ has LN non-zero elements.

Appendix B

Variance of Nonlinear Noise

We will derive $\sigma^2_{ICI_2}$ by consternating on d_0, therefore, ψ_0 in (6.26) can be expressed as

$$\psi_0 = \sum_{l=1}^{N-1} Q_l, \tag{B.1}$$

where

$$Q_l = \frac{\alpha_3}{N} d_l \sum_{n=0}^{N-1} |x_n|^2 \mathrm{e}^{j2\pi(\varepsilon+l)n/N}. \tag{B.2}$$

The variance of Q_l is given by

$$\begin{aligned}
\sigma^2_{Q_l} &= E\left\{Q_l \cdot Q_l^*\right\} \\
&= \frac{|\alpha_3|^2 P}{N^2} E\left\{\sum_{n=0}^{N-1} |x_n|^2 \mathrm{e}^{j2\pi(\varepsilon+l)n/N} \sum_{m=0}^{N-1} |x_m|^2 \mathrm{e}^{-j2\pi(\varepsilon+l)m/N}\right\} \\
&= \frac{|\alpha_3|^2 P}{N^2} E\left\{\sum_{n=0}^{N-1}\sum_{m=0}^{N-1} |x_n|^2 |x_m|^2 \mathrm{e}^{j2\pi l(n-m)/N}\right\} \\
&= \frac{|\alpha_3|^2 P}{N^2} E\left\{\sum_{n=0}^{N-1}\sum_{m=0}^{N-1} \left(\frac{1}{N^2}\sum_{u=0}^{N-1}\sum_{v=0}^{N-1} d_u d_v^* \mathrm{e}^{j2\pi(u-v)n/N}\right)\right. \\
&\qquad \left.\left(\frac{1}{N^2}\sum_{\acute{u}=0}^{N-1}\sum_{\acute{v}=0}^{N-1} d_{\acute{u}} d_{\acute{v}}^* \mathrm{e}^{j2\pi(\acute{u}-\acute{v})m/N}\right) \mathrm{e}^{j2\pi l(n-m)/N}\right\} \\
&= \frac{|\alpha_3|^2 P}{N^6} E\left\{\sum_{n=0}^{N-1}\sum_{m=0}^{N-1}\sum_{u=0}^{N-1}\sum_{v=0}^{N-1}\sum_{\acute{u}=0}^{N-1}\sum_{\acute{v}=0}^{N-1} d_u d_v^* d_{\acute{u}} d_{\acute{v}}^* \mathrm{e}^{j2\pi(l(n-m)+(u-v)n+(\acute{u}-\acute{v})m)/N}\right\} \\
&= \begin{cases} \dfrac{|\alpha_3|^2 (N+2) P^3}{N^4} & \text{when } n=m, u=v, \acute{u}=\acute{v} \\ 0 & \text{otherwise.} \end{cases}
\end{aligned} \tag{B.3}$$

The variance of nonlinear noise can be given by

$$\sigma^2_{ICI_2} = E\left\{|\psi_0|^2\right\} - \left(E\left\{\psi_0\right\}\right)^2, \tag{B.4}$$

where $\left(E\left\{\psi_0\right\}\right)^2 = 0$ while $E\left\{Q_l\right\} = 0$. Therefore,

$$\begin{aligned}
\sigma^2_{ICI_2} &= E\left\{|\psi_0|^2\right\} \\
&= E\left\{\sum_{l=1}^{N-1} Q_l \sum_{t=1}^{N-1} Q_t^*\right\} \\
&= E\left\{Q_1 \cdot Q_1^* + Q_2 \cdot Q_2^* + \cdots + Q_{N-1} \cdot Q_{N-1}^*\right. \\
&\quad + Q_1 \cdot Q_2^* + Q_1 \cdot Q_3^* + \cdots + Q_1 \cdot Q_{N-1}^* \\
&\quad + Q_2 \cdot Q_3^* + Q_2 \cdot Q_4^* + \cdots + Q_2 \cdot Q_{N-1}^* \\
&\quad \left. + \cdots + Q_{N-2} \cdot Q_{N-1}^*\right\} \\
&= (N-1)\sigma^2_{Q_l} + (N-1)(N-2)C_{lt},
\end{aligned} \tag{B.5}$$

where $E\{x+y\} = E\{x\} + E\{y\}$ [113] and C_{lt} is the covariance that can be written as

$$\begin{aligned}
C_{lt} &= E\left\{Q_l \cdot Q_t^*\right\} \\
&= \frac{|\alpha_3|^2}{N^2} E\left\{\sum_{n=0}^{N-1} d_l |x_n|^2 \mathrm{e}^{j2\pi(\varepsilon+l)n/N} \sum_{m=0}^{N-1} d_t^* |x_m|^2 \mathrm{e}^{-j2\pi(\varepsilon+t)m/N}\right\} \\
&= \frac{|\alpha_3|^2}{N^2} E\left\{d_l d_t^* \sum_{n=0}^{N-1}\sum_{m=0}^{N-1}\left(\frac{1}{N^2}\sum_{u=0}^{N-1}\sum_{v=0}^{N-1} d_u d_v^* \mathrm{e}^{j2\pi(u-v)n/N}\right)\right. \\
&\qquad \left.\left(\frac{1}{N^2}\sum_{\acute{u}=0}^{N-1}\sum_{\acute{v}=0}^{N-1} d_{\acute{u}} d_{\acute{v}}^* \mathrm{e}^{j2\pi(\acute{u}-\acute{v})m/N}\right)\mathrm{e}^{j2\pi l(n-m)/N}\right\} \\
&= \frac{|\alpha_3|^2}{N^6} E\left\{\sum_{n=0}^{N-1}\sum_{m=0}^{N-1}\sum_{u=0}^{N-1}\sum_{v=0}^{N-1}\sum_{\acute{u}=0}^{N-1}\sum_{\acute{v}=0}^{N-1} d_l d_t^* d_u d_v^* d_{\acute{u}} d_{\acute{v}}^* \mathrm{e}^{j2\pi(l(n-m)+(u-v)n+(\acute{u}-\acute{v})m)/N}\right\} \\
&= \begin{cases} \dfrac{2|\alpha_3|^2 P^3}{N^4} & \text{when } n=m, v=l, u=t, \acute{u}=\acute{v} \\ 0 & \text{otherwise.} \end{cases}
\end{aligned} \tag{B.6}$$

By substituting (B.3) and (B.6) into (B.5) we obtain

$$\begin{aligned}\sigma^2_{ICI_2} &= \frac{(N-1)(N+2)|\alpha_3|^2P^3}{N^4} + \frac{2(N-1)(N-2)|\alpha_3|^2P^3}{N^4} \\ &= \frac{|\alpha_3|^2P}{\mathrm{IBO}_l^2}\left(\frac{3N^2-5N+2}{N^2}\right).\end{aligned} \tag{B.7}$$

References

[1] M. Ibnkahla, Q. M. Rahman, A. I. Sulayman, H. A. Al-Asady, J. Yuan, and A. Safwat, "High-speed satellite mobile communications: Technologies and challenges," *Proc. IEEE*, vol. 92, no. 2, pp. 312–339, Feb. 2004.

[2] ETSI EN 302 583 V1.1.0, "Digital video broadcasting (DVB); framing structure, channel coding and modulation for satellite services to handheld devices (SH) below 3 GHz," *European Standard (Telecommunications series)*, Jan. 2008.

[3] D. H. Park and H. K. Song, "A new PAPR reduction technique of OFDM system with nonlinear high power amplifier," *IEEE Trans. Comput.*, vol. 53, no. 2, pp. 327–332, May 2007.

[4] R. V. Nee and R. Prasad, *OFDM for wireless multimedia Communications.* Boston London: Artech House, 2000.

[5] J. G. Proakis, *Digital Communications.* New York: McGraw-Hill: 4th edition, 2001.

[6] ETSI TR 101 190 V1.3.1, "Digital video broadcasting (DVB); implementation guidelines for DVB terrestrial services; transmission aspects," *European Standard (Telecommunications series)*, Oct. 2008.

[7] H. Jiang and P. A. Wilford, "A hierarchical modulation for upgrading digital broadcast systems," *IEEE Trans. Broadcast.*, vol. 51, no. 2, pp. 223–229, June 2005.

[8] S. H. Choi, C. I. Oh, D. G. Oh, and D. I. Chang, "Analysis of demmapping for hierarchical 16QAM," *Int. Symp. on Communications and Information Technologies*, pp. 653–656, Sep. 2006.

[9] S. Plass, A. Dammann, S. Kaiser, and K. Fazel, *Multi-carrier systems and solutions 2009*. Herrsching Germany: Springer, 2006.

[10] S. Wang, S. Kwon, and B. K. Yi, "On enhancing hierarchical modulation," *Int. Symp. on Broadband Multimedia Systems and Broadcasting*, pp. 1–6, 2008.

[11] S. Wang and B. K. Yi, "Optimizing enhanced hierarchical modulations," *IEEE Global Telecommunications Conf.*, pp. 1–5, 2008.

[12] R. T. Juang, P. Ting, K. Y. Lin, H. P. Lin, and D. B. Lin, "Enhanced hierarchical modulation with interference cancellation for OFDM systems," *20th IEEE Int. Symp. on Personal, Indoor and Mobile Radio Communications*, pp. 217–220, 2009.

[13] R. T. Juang, P. Ting, H. P. Lin, and D. B. Lin, "Link adaptation based on repetition coding for mobile worldwide interoperability for microwave access systems," *IET Commun.*, vol. 4, Iss. 9, pp. 1039–1048, 2010.

[14] A. A. M. Saleh, "Frequency-independent and frequency-dependent nonlinear models of TWT amplifiers," *IEEE Trans. Commun.*, vol. 29, no. 11, pp. 1715–1720, Nov. 1981.

[15] C. Rapp, "Effects of HPA-nonlinearity on a 4-DPSK/OFDM-signal for a digital sound broadcasting signal," *2nd European Conf. on Satellite Communications*, pp. 179–184, Oct. 1991.

[16] V. A. Bohara and S. H. Ting, "Theoretical analysis of OFDM signals in nonlinear polynomial models," *6th IEEE Int. Conf. on Information, Communications and Signal Processing*, pp. 1–5, Dec. 2007.

[17] G. Santella and F. Mazzenga, "A hybrid analytical-simulation procedure for performance evaluation in M-QAM-OFDM schemes in presence of nonlinear distortions," *IEEE Trans. Veh. Technol.*, vol. 47, no. 1, pp. 142–151, Feb. 1998.

[18] B. Ai, Z. Yang, C. Pan, T. Zhang, and J. Ge, "Effects of PAPR reduction on HPA predistortion," *IEEE Trans. Consum. Electron.*, vol. 51, no. 4, pp. 1143–1147, Nov. 2005.

[19] ETSI TS 101 475 V1.1.1, "Broadband radio access networks (BRAN); HIPERLAN type 2; physical (PHY) layer," *European Standard (Telecommunications series)*, 2000-04.

[20] S. C. Thompson, J. G. Proakis, and J. R. Zeidler, "The effectiveness of signal clipping for PAPR and total degradation reduction in OFDM systems," *IEEE Global Telecommunications Conf.*, pp. 2807–2811, 2005.

[21] R. E. Sheriff and Y. F. Hu, *Mobile Satellite Communication Networks*. West Sussex England: John Wiley and Sons Ltd, 2001.

[22] S. R. Saunders and A. A. Zavala, *Antennas and Propagation for Wireless Communication Systems*. West Sussex England: John Wiley and Sons Ltd, 2007.

[23] M. S. Karaliopoulos and F. N. Pavlidou, "Modelling the land mobile satellite channel: a review," *IEEE J. Elect. and Commun. Eng.*, pp. 235–247, Oct. 1999.

[24] M. Ibnkahla, *Signal processing for mobile communications handbook*. Washington D.C.: CRC Press, 2005.

[25] A. Jahn, H. Bischl, and G. Heiss, "Channel characterisation for spread spectrum satellite communications," *4th IEEE Int. Symp. on Spread Spectrum Techniques and Applications Proceedings*, vol. 3, pp. 1221–1226, 1996.

[26] M. A. N. Parks, S. R. Saunders, and B. G. Evans, "Wideband characterisation and modelling of the mobile satellite propagation channel at L- and S-Bands," *10th IEEE Int. Conf. on Antennas and Propagation*, pp. 239–243, Apr. 1997.

[27] I. Ali, P. G. Bonanni, N. Al-Dhahir, and J. E. Hershey, *Doppler applications in LEO satellite communication systems*. Dordrecht: Kluwer Academic Publishers, 2002.

[28] P. Banelli, G. Baruffa, and S. Cacopardi, "Effects of HPA non linearity on frequency multiplexed OFDM signals," *IEEE Trans. Broadcast.*, vol. 47, no. 2, pp. 123–136, June 2001.

[29] S. H. Han and J. H. Lee, "An overview of peak-to-average power ratio reduction techniques for multicarrier transmission," *IEEE Trans. Wireless Commun.*, pp. 56–65, Apr. 2005.

[30] T. Jiang and Y. Wu, "An overview: Peak-to-average power ratio reduction techniques for OFDM signals," *IEEE Trans. Broadcast.*, vol. 54, no. 2, pp. 257–268, June 2008.

[31] C. Tellambura, "Computation of the continuous-time PAR of an OFDM signal with BPSK subcarriers," *IEEE Commun. Lett.*, vol. 5, no. 5, pp. 185–187, May 2001.

[32] S. Hara and R. Prasad, *Multicarrier Techniques for 4G Mobile Communications*. Boston London: Artech House, 2003.

[33] H. Ochiai and H. Imai, "Performance of the deliberate clipping with adaptive symbol selection for strictly band-limited OFDM systems," *IEEE J. Sel. Areas Commun.*, vol. 18, no. 11, pp. 2270–2277, Nov. 2000.

[34] X. Li and L. J. Cimini, "Effects of clipping and filtering on the performance of OFDM," *IEEE Commun. Lett.*, vol. 2, no. 5, pp. 131–133, May 1998.

[35] A. E. Jones, T. A. Wilkinson, and S. K. Barton, "Block coding scheme for reduction of peak to mean envelope power ratio of multicarrier transmission schemes," *IEEE Elect. Lett.*, vol. 30, no. 25, pp. 2098–2099, Dec. 1994.

[36] H. Nikookar and K. S. Lidsheim, "Random phase updating algorithm for OFDM transmission with low PAPR," *IEEE Trans. Broadcast.*, vol. 48, no. 2, pp. 123–128, June 2002.

[37] X. Huang, J. Lu, J. Zheng, K. B. Letaief, and J. Gu, "Companding transform for reduction in peak-to-average power ratio of OFDM signals," *IEEE Trans. Wireless Commun.*, vol. 3, no. 6, pp. 2030–2039, Nov. 2004.

[38] J. Tellado, *Peak to Average Power Ratio Reduction for Multicarrier Modulation*. Stanford: PhD thesis, 1999.

[39] Y. J. Kou, W. S. Lu, and A. Antoniou, "A new peak-to-average power-ratio reduction algorithm for OFDM systems via constellation extension," *IEEE Trans. Wireless Commun.*, vol. 6, no. 5, pp. 1823–1832, May 2007.

[40] S. H. Muller and J. B. Huber, "OFDM with reduced peak-to-average power ratio by optimum combination of partial transmit sequences," *IEEE Elect. Lett.*, vol. 33, no. 5, pp. 368–369, Feb. 1997.

[41] A. D. S. Jayalath and C. Tellambura, "Reducing the peak-to-average power ratio of orthogonal frequency division multiplexing signal through bit or symbol interleaving," *IEEE Elect. Lett.*, vol. 36, no. 13, pp. 1161–1163, June 2000.

[42] A. E. Jones and T. A. Wilkinson, "Combined coding for error control and increased robustness to system nonlinearities in OFDM," *46th IEEE Vehicular Technology Conf.*, vol. 2, pp. 904–908, 1996.

[43] J. A. Davis and J. Jedwab, "Peak-to-mean power control in OFDM, Golay complementary sequences, and Reed-Muller codes," *IEEE Trans. Inf. Theory*, vol. 45, no. 7, pp. 2397–2417, Nov. 1999.

[44] K. G. Paterson, "Generalized Reed-Muller codes and power control in OFDM modulation," *IEEE Trans. Inf. Theory*, vol. 46, no. 1, pp. 104–120, Jan. 2000.

[45] T. Jiang, Y. Yang, and Y. H. Song, "Exponential companding technique for PAPR reduction in OFDM systems," *IEEE Trans. Broadcast.*, vol. 51, no. 2, pp. 244–248, June 2005.

[46] D. Wulich, "Definition of efficient PAPR in OFDM," *IEEE Commun. Lett.*, vol. 9, no. 9, pp. 832–834, Sep. 2005.

[47] S. G. Kang, J. G. Kim, and E. K. Joo, "A novel subblock partition scheme for partial transmit sequence OFDM," *IEEE Trans. Broadcast.*, vol. 45, no. 3, pp. 333–338, June 1999.

[48] L. J. Cimini and N. R. Sollenberger, "Peak-to-average power ratio reduction of an OFDM signal using partial transmit sequences," *IEEE Commun. Lett.*, vol. 4, no. 3, pp. 86–88, Mar. 2000.

[49] A. D. S. Jayalath and C. Tellambura, "Adaptive PTS approach for reduction of peak-to-average power ratio of OFDM signal," *IEEE Elect. Lett.*, vol. 36, no. 14, pp. 1226–1228, July 2000.

[50] ——, "The use of interleaving to reduce the peak-to-average power ratio of an OFDM signal," *IEEE Global Telecommunications Conf.*, vol. 1, pp. 82–86, 2000.

[51] W. S. Ho, A. S. Madhukumar, and F. Chin, "Peak-to-average power reduction using partial transmit sequences: A suboptimal approach based on dual layered phase sequencing," *IEEE Trans. Broadcast.*, vol. 49, no. 2, pp. 225–231, June 2003.

[52] O. J. Kwon and Y. H. Ha, "Multi-carrier PAP reduction method using suboptimal PTS with threshold," *IEEE Trans. Broadcast.*, vol. 49, no. 2, pp. 232–236, June 2003.

[53] L. Yang, R. S. Chen, Y. M. Siu, and K. K. Soo, "PAPR reduction of an OFDM signal by use of PTS with low computational complexity," *IEEE Trans. Broadcast.*, vol. 52, no. 1, pp. 83–86, Mar. 2006.

[54] P. Boonsrimuang, K. Mori, T. Paungma, and H. Kobayashi, "Proposal of improved PTS method for OFDM signal," *18th IEEE Int. Symp. on Personal, Indoor and Mobile Radio Communications*, pp. 1–5, 2007.

[55] S. J. Ku, C. L. Wang, and C. H. Chen, "A reduced-complexity PTS-based PAPR reduction scheme for OFDM systems," *IEEE Trans. Wireless Commun.*, vol. 9, no. 8, pp. 2455–2460, Aug. 2010.

[56] J. Hou, J. Ge, and J. Li, "Peak-to-average power ratio reduction of OFDM signals using PTS scheme with low computational complexityy," *IEEE Trans. Broadcast.*, vol. 57, no. 1, pp. 143–148, Mar. 2011.

[57] P. Foomooljareon, W. A. C. Fernando, and K. M. Ahmed, "PAPR reduction of OFDM systems using input sequence envelope scaling," *57th IEEE Vehicular Technology Conf.*, vol. 2, pp. 1243–1247, 2003.

[58] Y. R. Tsai and S. J. Huang, "PTS with non-uniform phase factors for PAPR reduction in OFDM systems," *IEEE Commun. Lett.*, vol. 12, no. 1, pp. 20–22, Jan. 2008.

[59] N. T. Hieu, S. W. Kim, and H. G. Ryu, "PAPR reduction of the low complexity phase weighting method in OFDM communication system," *IEEE Trans. Consum. Electron.*, vol. 51, no. 3, pp. 776–782, Aug. 2005.

[60] D. W. Lim, S. J. Heo, J. S. No, and H. Chung, "A new PTS OFDM scheme with low complexity for PAPR reduction," *IEEE Trans. Broadcast.*, vol. 52, no. 1, pp. 77–82, Mar. 2006.

[61] A. Ghassemi and T. A. Gulliver, "A low-complexity PTS-based radix FFT method for PAPR reduction in OFDM systems," *IEEE Trans. Signal Process.*, vol. 56, no. 3, pp. 1161–1166, Mar. 2008.

[62] S. S. Kim, M. J. Kim, and T. A. Gulliver, "A new PTS for PAPR reduction by local search in GA," *Int. Joint Conf. on Neural Networks*, pp. 2370–2373, July 2006.

[63] H. L. Hung, Y. F. Huang, C. M. Yeh, and T. H. Tan, "Performance of particle swarm optimization techniques on PAPR reduction for OFDM systems," *IEEE Int. Conf. on Systems, Man and Cybernetics*, pp. 2390–2395, 2008.

[64] T. T. Nguyen and L. Lampe, "On partial transmit sequences for PAR reduction in OFDM systems," *IEEE Trans. Wireless Commun.*, vol. 7, no. 2, pp. 746–755, Feb. 2008.

[65] J. C. Chen, "Partial transmit sequences for peak-to-average power ratio reduction of OFDM signals," *IEEE Signal Process. Lett.*, vol. 16, no. 6, pp. 545–548, June 2009.

[66] Y. Wang, W. Chen, and C. Tellambura, "A PAPR reduction method based on artificial bee colony algorithm for OFDM signals," *IEEE Trans. Wireless Commun.*, vol. 9, no. 10, pp. 2994–2999, Oct. 2010.

[67] X. Lei, Y. Tang, S. Li, and Y. Li, "A minimum clipping power loss scheme for mitigating the clipping noise in OFDM," *IEEE Global Telecommunications Conf.*, vol. 1, pp. 6–9, 2003.

[68] M. R. D. Rodrigues and I. J. Wassell, "IMD reduction with SLM and PTS to improve the error-probability performance of nonlinearly distorted OFDM signals," *IEEE Trans. Veh. Technol.*, vol. 55, no. 2, pp. 537–548, Mar. 2006.

[69] L. J. Cimini and N. R. Sollenberger, "Peak-to-average power ratio reduction of an OFDM signal using partial transmit sequences with embedded side information," *IEEE Global Telecommunications Conf.*, vol. 2, pp. 746–750, Nov. 2000.

[70] C. C. Feng, C. Y. Wang, C. Y. Lin, and Y. H. Hung, "Protection and transmission of side information for peak-to-average power ratio reduction of an OFDM signal using partial transmit sequences," *58th IEEE Vehicular Technology Conf.*, vol. 4, pp. 2461–2465, Oct. 2003.

[71] A. D. S. Jayalath and C. Tellambura, "Side information in PAR reduced PTS-OFDM signals," *14th IEEE Int. Symp. on Personal, Indoor and Mobile Radio Communications*, vol. 1, pp. 226–230, Sep. 2003.

[72] ——, "SLM and PTS peak-power reduction of OFDM signals without side information," *IEEE Trans. Wireless Commun.*, vol. 4 no. 5, pp. 2006–2013, Sep. 2005.

[73] T. Giannopoulos and V. Paliouras, "A low-complexity PTS-based PAPR reduction technique for OFDM signals without transmission of side information," *IEEE Workshop on Signal Processing Systems Design and Implementation*, pp. 434–439, Oct. 2006.

[74] H. G. Ryu, S. A. Kim, and C. X. Wang, "A side information embedded PTS scheme in the OFDM communication system," *IEEE Pacific Rim Conf. on Communications, Computers and Signal Processing*, pp. 300–303, Aug. 2007.

[75] Y. Zhou and T. Jiang, "A novel multi-points square mapping combined with PTS to reduce PAPR of OFDM signals without side information," *IEEE Trans. Broadcast.*, vol. 55, no. 4, pp. 831–835, Dec. 2009.

[76] L. Guan, T. Jiang, D. Qu, and Y. Zhou, "Joint channel estimation and PTS to reduce peak-to-average-power radio in OFDM systems without side information," *IEEE Signal Process. Lett.*, vol. 17, no. 10, pp. 883–886, Oct. 2010.

[77] H. Kim, E. Hong, C. Ahn, and D. Har, "A pilot symbol pattern enabling data recovery without side information in PTS-based OFDM systems," *IEEE Trans. Broadcast.*, vol. 57, no. 2, pp. 307–312, June 2011.

[78] L. Yang, K. K. Soo, S. Q. Li, and Y. M. Siu, "PAPR reduction using low complexity PTS to construct of OFDM signals without side information," *IEEE Trans. Broadcast.*, vol. 57, no. 2, pp. 284–290, June 2011.

[79] R. W. Bauml, R. F. H. Fischer, and J. B. Huber, "Reducing the peak-to-average power ratio of multicarrier modulation by selected mapping," *IEEE Elect. Lett.*, vol. 32, no. 22, pp. 2056–2057, Oct. 1996.

[80] C. L. Wang and Y. Ouyang, "Low-complexity selected mapping schemes for peak-to-average power ratio reduction in OFDM systems," *IEEE Trans. Signal Process.*, vol. 53, no. 12, pp. 4652–4660, Dec. 2005.

[81] C. L. Wang and S. J. Ku, "Novel conversion matrices for simplifying the IFFT computation of an SLM-based PAPR reduction scheme for OFDM systems," *IEEE Trans. Commun.*, vol. 57, no. 7, pp. 1903–1907, July 2009.

[82] D. W. Lim, J. S. No, C. W. Lim, and H. Chung, "A new SLM OFDM scheme with low complexity for PAPR reduction," *IEEE Signal Process. Lett.*, vol. 12, no. 2, pp. 93–96, Feb. 2005.

[83] S. J. Heo, H. S. Noh, J. S. No, and D. J. Shin, "A modified SLM scheme with low complexity for PAPR reduction of OFDM systems," *IEEE Trans. Broadcast.*, vol. 53, no. 4, pp. 804–808, Dec. 2007.

[84] E. Alsusa and L. Yang, "Low-complexity post-IFFT PAPR reduction technique for OFDM systems," *IEEE Elect. Lett.*, vol. 42, no. 19, pp. 1123–1124, Sep. 2006.

[85] L. Yang, K. K. Soo, Y. M. Siu, and S. Q. Li, "A low complexity selected mapping scheme by use of time domain sequence superposition technique for PAPR reduction in OFDM system," *IEEE Trans. Broadcast.*, vol. 54, no. 4, pp. 821–824, Dec. 2008.

[86] A. Ghassemi and T. A. Gulliver, "Partial selective mapping OFDM with low complexity IFFTs," *IEEE Commun. Lett.*, vol. 12, no. 1, pp. 4–6, Jan. 2008.

[87] C. P. Li, S. H. Wang, and C. L. Wang, "Novel low-complexity SLM schemes for PAPR reduction in OFDM systems," *IEEE Trans. Signal Process.*, vol. 58, no. 5, pp. 2916–2921, May 2010.

[88] M. Breiling, S. H. Muller, and J. B. Huber, "SLM peak-power reduction without explicit side information," *IEEE Commun. Lett.*, vol. 5, no. 6, pp. 239–241, June 2001.

[89] N. Chen and G. T. Zhou, "Peak-to-average power ratio reduction in OFDM with blind selected pilot tone modulation," *IEEE Trans. Wireless Commun.*, vol. 5, no. 8, pp. 2210–2216, Aug. 2006.

[90] E. Alsusa and L. Yang, "Redundancy-free and BER-maintained selective mapping with partial phase-randomising sequences for peak-to-average power ratio reduction in OFDM systems," *IET Commun.*, vol. 2, no. 1, pp. 66–74, Jan. 2008.

[91] S. Y. L. Goff, B. K. Khoo, C. C. Tsimenidis, and B. S. Sharif, "A novel selected mapping technique for PAPR reduction in OFDM systems," *IEEE Trans. Commun.*, vol. 56, no. 11, pp. 1775–1779, Nov. 2008.

[92] C. L. Wang, M. Y. Hsu, and Y. Ouyang, "Low-complexity peak-to-average power ratio reduction technique for OFDM systems," *IEEE Global Telecommunications Conf.*, pp. 2375–2379, Dec. 2003.

[93] H. G. Ryu and K. J. Youn, "A new PAPR reduction scheme: SPW (subblock phase weighting)," *IEEE Trans. Consum. Electron.*, vol. 48, no. 1, pp. 81–89, Feb. 2002.

[94] Q. Wen, Y. Xiao, P. Cheng, C. Zhang, and S. Li, "S-PTS for PAPR reduction in OFDM systems," *4th IEEE Conf. on Wireless Communications, Networking and Mobile Computing*, pp. 1–4, Oct. 2008.

[95] R. Baxley and G. Zhou, "Comparing selected mapping and partial transmit sequence for PAR reduction," *IEEE Trans. Broadcast.*, vol. 53, no. 4, pp. 797–803, Dec. 2007.

[96] M. Rumney, *LTE and the Evolution to 4G Wireless: Design and Measurement Challenges.* Agilent Technologies Publication, 2009.

[97] DVB:, "Frame structure channel coding and modulation for a second generation digital terrestrial television broadcasting system (DVB-T2)," June 2008.

[98] IEEE 802.16-2009, "IEEE standard for local and metropolitan area networks part 16: Air interface for broadband wireless access systems," 2009.

[99] ETSI EN 302 307 V1.1.2, "Digital video broadcasting (DVB); second generation framing structure, channel coding and modulation systems for broadcasting, interactive services, news gathering and other broadband satellite applications," 2006.

[100] A. Behravan and T. Eriksson, "PAPR and other measures for OFDM systems with nonlinearity," *5th Int. Symp. on Wireless Personal Multimedia Communications*, vol. 1, pp. 149–153, 2002.

[101] K. Sathananthan and C. Tellambura, "Partial transmit sequence and selected mapping schemes to reduce ICI in OFDM systems," *IEEE Commun. Lett.*, vol. 6, no. 8, pp. 313–315, Aug. 2002.

[102] G. Karam and H. Sari, "Analysis of predistortion, equalization and ISI cancellation techniques in digital radio systems with nonlinear transmit amplifiers," *IEEE Trans. Commun.*, vol. 37, no. 12, pp. 1245–1253, Dec. 1989.

[103] R. Baxley and G. Zhou, "Computational complexity analysis of FFT pruning a Markov modeling approach," *12th Digital Signal Processing Workshop - 4th Signal Processing Education Workshop*, pp. 535–539, Sep. 2006.

[104] A. Al-Dweik, A. Hazmi, B. Sharif, and C. Tsimenidis, "Novel multiple-access interference reduction technique for multiuser FH-OFDM networks," *IEEE Int. Conf. on Communication Systems*, pp. 488–492, 2010.

[105] Aethercomm, "Wimax - revolutionizing the art of linear HPA's," *http://www.aethercomm.com/products/29*, Oct. 2007.

[106] B. Ai, Z. Yang, C. Pan, J. Ge, Y. Wang, and Z. Lu, "On the synchronization techniques for wireless OFDM systems," *IEEE Trans. Broadcast.*, vol. 52, no. 2, pp. 236–244, June 2006.

[107] Y. Zhao and S. Haggman, "Intercarrier interference self-cancellation scheme for OFDM mobile communication systems," *IEEE Trans. Commun.*, vol. 49, no. 7, pp. 1185–1191, Jul. 2001.

[108] C. Muschallik, "Improving an OFDM reception using an adaptive Nyquist windowing," *IEEE Trans. Consum. Electron.*, vol. 42, no. 3, pp. 259–269, Aug. 1996.

[109] N. Al-Dhahir and J. M. Cioffi, "Optimum finite-length equalization for multicarrier transceivers," *IEEE Trans. Commun.*, vol. 44, no. 1, pp. 65–64, Jan. 1996.

[110] P. H. Moose, "A technique for orthogonal frequency division multiplexing frequency offset correction," *IEEE Trans. Commun.*, vol. 42, no. 10, pp. 2908–2914, Oct. 1994.

[111] V. Bohara and S. H. Ting, "Analytical performance of orthogonal frequency division multiplexing systems impaired by a non-linear high-power amplifier with memory," *IET Commun.*, vol. 3, no. 10, pp. 1659–1666, 2009.

[112] S. Haykin, *Communication Systems*. Wiley: 4th edition, 2000.

[113] A. Papoulis, *Probability, Random Variables and Stochastic Processes*. McGraw-Hill: 3rd edition, 1991.